

# Full Explanatory Supplement

2 January 2013

# Main Page

---

**Very important information for new users: READ ME FIRST.**

**Very important information for all users: News.**

If you are reading the printed version of this ES wiki, the online version can be found at the URL:

[http://www.sciops.esa.int/wikiSI/planckpla/index.php?title=Main\\_Page&instance=Planck\\_PLA\\_ES](http://www.sciops.esa.int/wikiSI/planckpla/index.php?title=Main_Page&instance=Planck_PLA_ES) <sup>[1]</sup>.

For help with editing the Explanatory Supplement consult the User's Guide <sup>[2]</sup> for a detailed User Guide of the MediaWiki software or the Explanatory Supplement Help page for the guidelines on editing the ES.

A set of *books* (a collection of pages that can easily be printed together as a pdf file) can be found here. We also have a page explaining how to create your own book.

**PDF Book:** A book with the full contents can be found here and a pdf version updated weekly can be found here:.

## Explanatory supplement

By Planck Collaboration

The Explanatory Supplement is a reference text to the public data delivered from the operations of the European Space Agency's Planck satellite during its mission.

1. The Planck mission
    1. Mission overview (Dupac)
  2. The satellite
    1. Overview (Leonardi)
    2. The service module (Leonardi)
    3. Common cryogenics (Mendes)
      1. Thermal Design (Mendes)
      2. Passive cooling
      3. Sorption Cooler
      4. Qualification and performance
    4. Instruments
      1. HFI design, qualification, and performance (Lamarre/Pajot)
      2. LFI design, qualification, and performance (Gregorio)
    5. The telescope (Leonardi)
    6. Others
      1. The standard radiation environment monitor (Mendes)
      2. The fiber optic gyro unit (Leonardi)
  3. Ground Segment and Operations
    1. Ground segment overview (Dupac)
    2. Contingencies (Leonardi)
    3. Operational history (Leonardi)
    4. Survey scanning and performance (Dupac)
    5. Thermal environment (Leonardi)
    6. Radiation environment (Mendes)
    7. Pointing performance (Dupac)
-

4. Data processing
  1. Data flow overview (Leonardi)
  2. On-board processing
  3. MOC processing (Leonardi)
  4. HFI Data Processing: THIS IS CURRENTLY TERSE, since it will be populated with some of the content of the HFI DPC paper and co-papers being written. (Bouchet)
    1. Pre-processing (Vibert)
    2. TOI processing (Desert)
    3. Detectors pointing & beam (Crill/Jones/Jaffe)
    4. Map-making (Perdereau)
    5. Power Spectra (Bouchet)
    6. HFI internal overall validation (Ganga)
    7. Summary of HFI data characteristics & the RIMO content (Bouchet)
5. LFI data processing: Introduction (Zacchei)
  1. Pre-processing (Frailis)
    1. Overview
    2. The LFI scientific telemetry
    3. From packets to raw TOIs
    4. On-board time reconstruction
  2. TOI processing (Mennella)
    1. *To be completed*
    2. ADC Correction (Galeotta/Watson)
    3. Spikes Removal (Tavagnacco)
    4. Gaps Filling (Galeotta/Polenta)
    5. Gain Modulation Factor
    6. Diode Combination
    7. Planet Flagging
    8. Photometric calibration (Galeotta)
    9. Noise estimation (Maino)
      1. Overview
      2. Operations
      3. Fitting Pipeline
      4. The final noise parameters
  3. Detector Pointing (Maris/Galeotta)
    1. Wobble Angle
    2. Stellar Aberration
  4. Beams (Sandri/Villa)
    1. Main Beams and Focal Plane calibration
    2. Effective beams
  5. Map-making (Keihanen)
    1. *To be completed*
    2. Noise Covariance Matrix (Anna-Stiina Suur-Uski)
    3. Half-ring jackknife Noise Maps (Jussi Valiviita)
    4. Noise Montecarlo Simulation (Hannu Kurki-Suonio)
  6. LFI internal overall validation (Maino)

7. LFI specific L3 activities: masks, MCQA, etc
  1. power spectra: intra-frequency checks & aggregation, LFI specific checks, ...)
  2. Band pass information
  3. Polarisation information
8. Summary of LFI data characteristics & the RIMO content
6. HFI/LFI joint data processing
  1. Compact Source catalogues ([Ashdown/Nuevo/Caniego](#))
  2. CMB map cleaning from Foreground emissions ([Ashdown/Baccigalupi](#))
  3. CMB Power spectra and Planck likelihood code CLIK([Bouchet/Natoli](#))
  4. Simulations ([bouchet](#))
7. Scientific analyses products ([bouchet](#))]
8. PSO processing ([Mendes](#))
5. Planck Legacy Archvie
  1. Overview ([Dupac](#))
  2. Planck legacy archive contents
    1. Mission science products
      1. Overview
      2. Timelines
        1. Semi-raw signal timelines
        2. Cleaned and calibrated signal timelines
        3. Pointing timelines
        4. FITS file structure
    3. Single detector maps
      1. Single detector maps
      2. FITS file structure
    4. Frequency Maps
      1. Introduction
      2. Types of maps
      3. List of products
      4. FITS file structure
    5. Astrophysical component maps
      1. CMB maps
      2. Synchrotron and free-free maps
      3. Anomalous emission maps
      4. Dust opacity map and model
      5. CO emission maps
      6. Other maps (CO, CIB, etc.)
    6. Catalogues
      1. Early Release Compact Source Catalogue
      2. Planck Catalogues of Compact Sources
      3. SZ Cluster Catalogue (basic + cosmology)
      4. High-z source Catalogue
      5. Catalogue of Cold Cores
    7. Angular power spectra
    8. Planck Likelihood Code



9. The RIMO
  1. Overview
  2. Detector-level data
  3. Map-level data
  4. Band transmissions
  5. Detector noise spectra
  6. Beam Window Functions
2. Additional Science products
  1. Data products
    1. Specially processed maps
    2. Additional catalogues
    3. Additional angular power spectra
    4. The Planck Sky Model
  2. Ancillary data
    1. Scientific data used to generate Planck products
    2. Simulation data
  3. Mission history
    1. Survey history data (Dupac)
    2. Satellite history data (Dupac)
  4. Payload design, performance and calibration data
    1. Instrument performance
    2. Telescope
    3. Thermal and cooler system
    4. Fiber optic gyro (Leonardi)
    5. Space radiation environment monitor (Mendes)
  5. Software utilities
    1. Unpack and display (ESA)
    2. Unit conversion and Color correction (DPC)
    3. Print and plot (ESA)
    4. Analysis (ESA)
    5. Format conversion (ESA)
6. Appendix
  1. Acronym list
7. References

## References

- [1] [http://www.sciops.esa.int/wikiSI/planckpla/index.php?title=Main\\_Page&instance=Planck\\_PLA\\_ES](http://www.sciops.esa.int/wikiSI/planckpla/index.php?title=Main_Page&instance=Planck_PLA_ES)  
[2] <http://meta.wikimedia.org/wiki/Help:Contents>
-

# The Planck Mission

## Mission overview

### Introduction

Planck is a space telescope of the European Space Agency designed to answer key cosmological questions. Its main goal is to determine the geometry and content of the Universe, and which theories describing the birth and evolution of the Universe are correct. To achieve this ambitious objective, it observed the Cosmic Microwave Background radiation (CMB), emitted about 14 billion years ago, just over 300,000 years after the Big Bang. Today the CMB permeates the Universe and is observed to have an average temperature of 2.7 K. Small deviations from this average value (the so-called anisotropies), observable at angular scales larger than  $\sim 5$  arcminutes, encode a wealth of information on the properties of the Universe in its infancy. The objective of Planck is to measure these properties with an unprecedented accuracy and level of detail.

As with all ESA scientific missions, Planck was developed in a partnership with the European scientific community. Two consortia of scientific institutes, each led by a Principal Investigator, developed and delivered to ESA two instruments designed specifically for Planck. Each of these instruments targets a specific number of wavelength bands within the range in which the CMB is observable. Together, the two instruments are capable of collecting data of a quality adequate to measure the CMB signal and distinguish it from other confusing sources. A large telescope collects the light from the sky and deliver it to the instruments for measurement and analysis.

The reflectors of the Planck telescope were developed and delivered to ESA by a Danish consortium of institutes. ESA retains overall management of the project, develops and procures the spacecraft, integrates the instruments into the spacecraft, and launches and operates it. Planck was launched on May 14th 2009 on an Ariane 5 rocket together with the Herschel Space Observatory. After launch, they were both placed into orbits around the L2 Lagrange of the Sun-Earth system, located about 1.5 million km from the Earth. From that far vantage point, Planck swept the sky regularly in large swaths, and covered it fully about six times. Each of the two instrument consortia operated their respective instrument and processed all the data into usable scientific products. At the end of the mission the consortia delivered the final products to ESA, which archives them and distributes them to the community.



## Early operations and transfer to orbit

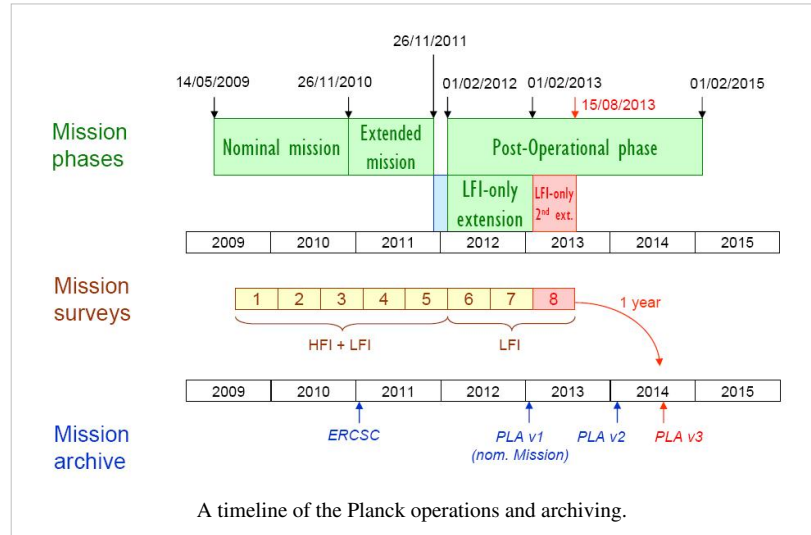
Planck was launched from the Centre Spatial Guyanais in Kourou (French Guyana) on 14 May 2009 at its nominal lift-off time of 13:12 UT, on an Ariane 5 ECA rocket of Arianespace2. ESA's Herschel observatory was launched on the same rocket. At 13:37:55 UT, Herschel was released from the rocket at an altitude of 1200 km; Planck followed suit at 13:40:25UT. The separation attitudes of both satellites were within 0.1 deg.

of prediction. The Ariane rocket placed Planck with excellent accuracy (semimajor axis within 1.6 % of prediction), on a trajectory towards the second Lagrangian point of the Earth-Sun system (L2) . The orbit describes a Lissajous trajectory around L2 with a ~6 month period that avoids crossing the Earth penumbra for at least 4 years.

After release from the rocket, three large manoeuvres were carried out to place Planck in its intended final orbit. Once in its final orbit, very small manoeuvres are required at approximately monthly intervals (1 ms–1 per year) to keep Planck from drifting away from its intended path around L2. The attitude manoeuvres required to follow the scanning strategy require about 2.6 ms–1 per year. Overall, the excellent performance of launch and orbit manoeuvres will lead to a large amount (~160 kg, or ~40% of initial tank loading) of fuel remaining on board at end of mission operations.

Planck started cooling down radiatively shortly after launch. Heaters were activated to hold the focal plane at 250 K, which was reached around 5 h after launch. The valve opening the exhaust piping of the dilution cooler was activated at 03:30 UT, and the 4He-JT cooler compressors were turned on at low stroke at 05:20 UT. After these essential operations were completed, on the second day after launch, the focal plane temperature was allowed to descend to 170 K for out-gassing and decontamination of the telescope and focal plane.

## Commissioning and initial science operations



The Herschel and Planck spacecrafts in the launch vehicle configuration.

## Commissioning

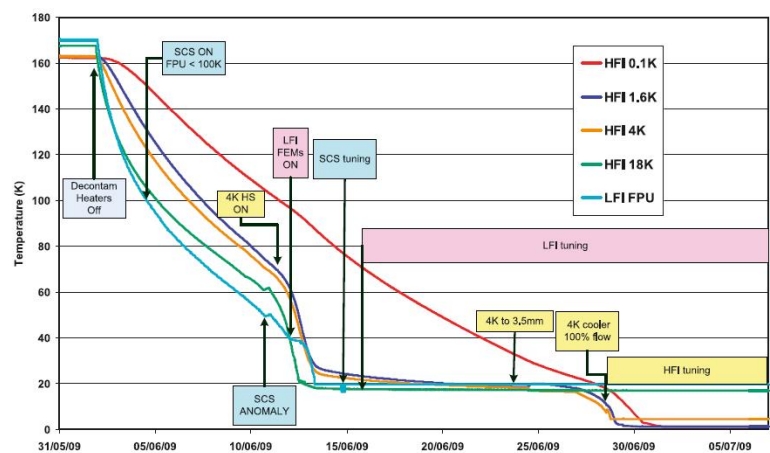
The first period of operations focussed on commissioning activities, i.e., functional check-out procedures of all sub-systems and instruments of the Planck spacecraft in preparation for running science operations related to calibration and performance verification of the payload. Planning for commissioning operations was driven by the telescope decontamination period of 2 weeks and the subsequent cryogenic cool-down of the payload and instruments. The overall duration of the cool-down was approximately 2 months, including the decontamination period. The commissioning activities were executed very smoothly and all sub-systems were found to be in good health. The commissioning activities were formally completed at the time when the HFI bolometer stage reached its target temperature of 100 mK, on 3 July 2009 at 01:00 UT. At this time all the critical resource budgets (power, fuel, lifetime, etc.) were found to contain very significant margins with respect to the original specification.



The Herschel and Planck launch by an Ariane 5 ECA rocket.

## Calibration and performance verification

Calibration and performance verification (CPV) activities started during the cool-down period and continued until the end of August 2009. On completion of all the planned activities, it was concluded that the two instruments were fully tuned and ready for routine operations. No further parameter tuning was expected to be needed, except for the sorption cooler, which requires a weekly change in



Schematics of the cool-down sequence, from Planck Coll. 2011, A&A 536, A1.

operational parameters. The scientific performance parameters of both instruments was in most respects as had been measured on the ground before launch. The only significant exception was that, due to the high level of Galactic cosmic rays, the bolometers of HFI were detecting a higher number of glitches than expected, causing a modest (~10%) level of systematic effects on their noise properties. The satellite did not introduce any major systematic effects into the science data. In particular, the telemetry transponder did not result in radio-frequency interference, which implies that the data acquired during visibility periods is useable for science.

## First-Light Survey

The First Light Survey (FLS) was the last major activity planned before the start of routine surveying of the sky. It was conceived as a two-week period during which Planck would be fully tuned up and operated as if it was in its routine phase. This stable period could have resulted in the identification of further tuning activities required to optimise the performance of Planck in the long-duration surveys to come. The FLS was conducted between 13 and 27 August, and in fact led to the conclusion that the Planck payload was operating stably and optimally, and required no further tuning of its instruments. Therefore the period of the FLS was accepted as a valid part of the first Planck

survey.

## Routine operations phase

The routine operations phase of Planck is characterised by continuous and stable scanning of the sky and data acquisition by LFI and HFI. It started with the FLS on 13 August of 2009, at 14:15 UT.

The Planck satellite generates (and stores on-board) data continuously at the following typical rates: 21 kilobit s<sup>-1</sup> (kbps) of house-keeping (HK) data from all on-board sources, 44 kbps of LFI science data and 72 kbps of HFI science data. The data are brought to ground in a daily pass of approximately 3 h duration. Besides the data downloads, the passes also acquire realtime HK and a 20 min period of real-time science (used to monitor instrument performance during the pass). Planck utilises the two ESA deep-space ground stations in New Norcia (Australia) and Cebreros (Spain), usually the former. Scheduling of the daily telecommunication period is quite stable, with small perturbations due to the need to coordinate the use of the antenna with other ESA satellites (in particular Herschel). At the ground station the telemetry is received by redundant chains of front-end/back-end equipment. The data flows to the mission operations control centre (MOC) located at ESOC in Darmstadt (Germany), where it is processed by redundant mission control software (MCS) installations and made available to the science ground segment. To reduce bandwidth requirements between the station and ESOC only one set of science telemetry is usually transferred. Software is run post-pass to check the completeness of the data. This software check is also used to build a catalogue of data completeness, which is used by the science ground segment to control its own data transfer process. Where gaps are detected, attempts to fill them are made as an offline activity (normally next working day), the first step being to attempt to reflow the relevant data from station. Early in the mission these gaps were more frequent, with some hundreds of packets affected per week (impact on data return of order 50 ppm) due principally to a combination of software problems with the data ingestion and distribution in the MCS, and imperfect behaviour of the software gap check. Software updates implemented during the mission have improved the situation such that gaps are much rarer, with a total impact on data return well below 1 ppm. Redump of data from the spacecraft is attempted when there have been losses in the space link. This has only been necessary on three occasions. In each case the spacecraft redump has successfully recovered all the data.

All the data downloaded from the satellite, and processed products such as filtered attitude information, are made available each day for retrieval from the MOC by the LFI and HFI Data Processing Centres (DPCs).

The scanning strategy is the following: the spin axis follows a cycloidal path on the sky by step-wise displacements of 2 arcmin approximately every 50 min. The dwell time (i.e., the duration of stable data acquisition at each pointing) has varied sinusoidally by a factor of  $\sim 2$ . Planck's scanning strategy results in significantly inhomogeneous depth of integration time across the sky; the areas near the ecliptic poles are observed with greater depth than all others.

The scanning strategy for the second year of Routine Operations (i.e., Surveys 3 and 4) is exactly the same as for the first year, except that all pointings are shifted by 1 arcmin along the cross-scanning direction, in order to provide finer sky sampling for the highest frequency detectors when combining two years of observations.

Orbit maintenance manoeuvres were carried out at approximately monthly intervals<sup>6</sup>. Although the manoeuvres only required a few minutes, preparations, post-manoeuve massproperty calibration, and re-entry into scientific slewing mode increased the overhead to several hours. The manoeuvres were carried out without disturbing the path of the spin axis from its nominal scanning law. The dwell times of pointings before and after the execution of the manoeuvre were reduced to allow all pre-planned pointings to be carried out.

While the Planck detectors are scanning the sky, they also naturally observe celestial calibrators. The main objects used for this purpose are the Crab Nebula, and the bright planets Mars, Jupiter and Saturn.

## Payload performance

The main achievements in terms of payload performance are the following:

- the angular resolution measured on planets is within a few per cent of that predicted on the ground
- the instantaneous sensitivity of the Planck LFI and HFI channels is estimated to be approximately 10% larger than that measured on the ground and extrapolated to launch conditions
- the photometric calibration uncertainty quoted is conservatively based on the current knowledge of systematic effects and data processing pipelines. There is no reason to believe that the mission goals (1% in CMB channels and 3% at the highest frequencies) will not be reached for all Planck channels in due time.

## References

A complete overview of the Planck mission and its science programme can be found in the so-called Blue Book : [http://www.sciops.esa.int/SA/PLANCK/docs/Bluebook-ESA-SCI%282005%291\\_V2.pdf](http://www.sciops.esa.int/SA/PLANCK/docs/Bluebook-ESA-SCI%282005%291_V2.pdf)

More details on the Planck mission performance can be found in Planck coll. 2011, A&A 536, A1.

A complete list of Planck publications can be found here [1].

## References

[1] [http://www.sciops.esa.int/index.php?project=PLANCK&page=Planck\\_Published\\_Papers](http://www.sciops.esa.int/index.php?project=PLANCK&page=Planck_Published_Papers)

# The Satellite

## Overview

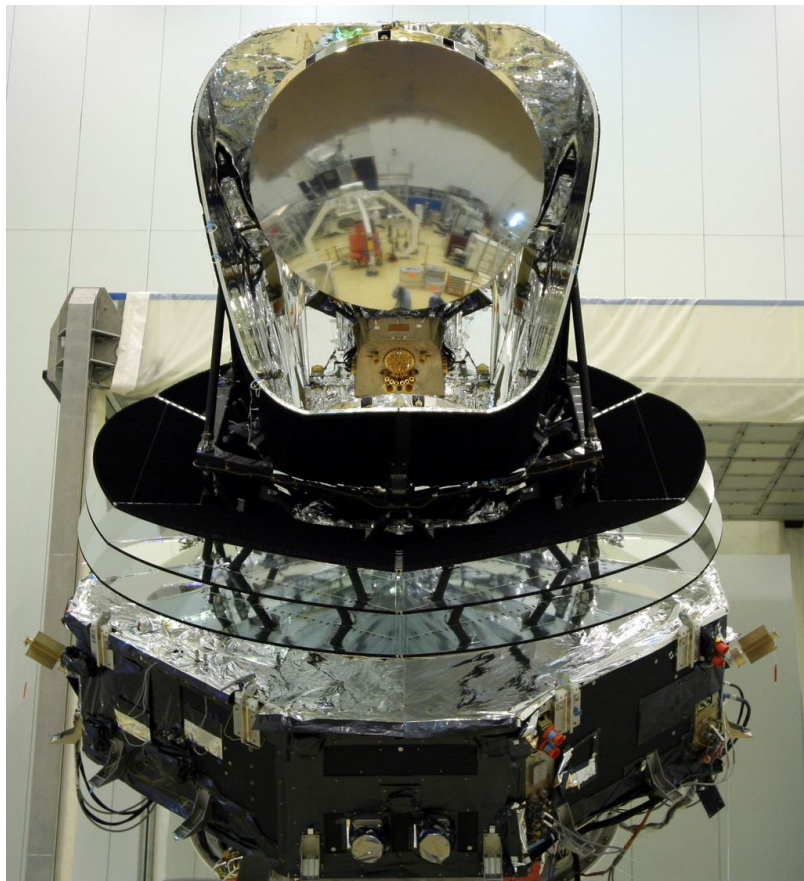
The Planck satellite was designed, built and tested around two major modules:

- **The payload module** containing an off-axis telescope with a projected diameter of 1.5m, focussing radiation from the sky onto a focal plane shared by detectors of the LFI and HFI, operating at 20K and 0.1K respectively; a telescope baffle that simultaneously provides stray-light shielding and radiative cooling; and three conical “V-groove” baffles that provide thermal and radiative insulation between the warm service module and the cold telescope and instruments.
- **The service module** containing all the warm electronics servicing instruments and satellite; and the solar panel providing electrical power. It also contains the cryocoolers, the main on-board computer, the telecommand receivers and telemetry transmitters, and the attitude control system with its sensors and actuators. The most relevant technical characteristics of the Planck spacecraft are detailed in the Table below.

Table. Planck satellite characteristics.

<b>Diameter</b>	4.2 m	Defined by the solar array
<b>Height</b>	4.2 m	
<b>Total mass at launch</b>	1912 kg	Fuel mass = 385 kg at launch; He mass = 7.7 kg
<b>Electrical power demand (avg)</b>	1300 W	Instrument part: 685 W (Beginning of Life), 780 W (End of Life)
<b>Minimum operational lifetime</b>	18 months	Planck operated for 32 months with both instruments; the LFI continues surveying the sky
<b>Spin rate</b>	1 rpm	$\sim 0.6$ arcmin/sec (changes due to manoeuvres); stability during inertial pointing $\sim 6.5 \times 10^{-5}$ rpm/h
<b>Max angle of spin axis to Sun</b>	10 deg	To maintain the payload in the shade; default angle is 7.5 deg
<b>Max angle of spin axis to Earth</b>	15 deg	To allow communication to Earth
<b>Angle between spin axis and telescope boresight</b>	85 deg	Max extent of FOV $\sim 8$ deg
<b>On-board data storage capacity</b>	32 Gbit	Two redundant units (only one is operational at any time)
<b>Data transmission rate to ground (max)</b>	1.5 Mbps	Within 15 deg of Earth, using a 35 m ground antenna
<b>Daily contact period</b>	3 h	The effective real-time science data acquisition bandwidth is 130 kbps





**The fully assembled Planck satellite a few days before integration into the Ariane 5 rocket. Herschel is visible by reflection on the primary reflector.**

For more information, see Tauber et al. 2010, A&A 520, A1.



# The service module

---

The SVM provides the various equipment and instruments housed in it with suitable mechanical and thermal environments during launch and orbit. It is formed by an octagonal box, built around a conical tube, which supports the following subsystems intervening in flight operations:

- Command and Data Management.
- Attitude Control and Measurement.
- Power Control.
- Reaction Control.
- Telemetry, Tracking and Command.
- Thermal Control.

The SVM contains all the warm satellite and payload electronic units, with the only exception of the box containing JFETs for impedance-matching to the HFI bolometers, which is mounted on the primary reflector support panel, to allow the operation of the JFETs at an optimal temperature of  $\sim 130$  K. The service module holds:

- Main computer
- Attitude control computer
- Data processing units
- Star trackers
- LFI electronics
- Dilution control unit
- HFI readout electronics
- 4K compressors
- Helium tanks: 36000 litres of  $^4\text{He}$ , and 12000 litres of  $^3\text{He}$  gas are stored in four high-pressure tanks.
- Sorption cooler radiator
- Sorption cooler electronics
- Sorption compressors (2 redundant units)
- Hydrazine tanks
- Medium-gain antenna
- Telemetry subsystem.

For more information, see Tauber et al. 2010, A&A 520.

# Common cryogenics

---

## Thermal design

---

(Note: Adapted from Tauber et al. 2010, A&A 520, A1 and Ade et al. 2011, A&A 536)

This is a test

### Introduction

The performance of the Planck instruments in space is enabled by their low operating temperatures, 20 K for LFI and 0.1 K for HFI, achieved through a combination of passive radiative cooling and three active mechanical coolers. The scientific requirement for very broad frequency coverage led to two detector technologies with widely different temperature and cooling needs. Active coolers could satisfy these needs; a helium cryostat, as used by previous cryogenic space missions (IRAS, COBE, ISO, Spitzer, AKARI), could not. Radiative cooling is provided by three V-groove radiators and a large telescope baffle. The active coolers are a hydrogen sorption cooler (<20 K), a  $^4\text{He}$  Joule-Thomson cooler (4.7 K), and a  $^3\text{He}$ - $^4\text{He}$  dilution cooler (1.4 K and 0.1 K). The flight system was at ambient temperature at launch and cooled in space to operating conditions. The HFI bolometer plate reached 93 mK on 3 July 2009, 50 days after launch. The solar panel always faces the Sun, shadowing the rest of Planck, and operates at a mean temperature of 384 K. At the other end of the spacecraft, the telescope baffle operates at 42.3 K and the telescope primary mirror operates at 35.9 K. The temperatures of key parts of the instruments are stabilized by both active and passive methods. Temperature fluctuations are driven by changes in the distance from the Sun, sorption cooler cycling and fluctuations in gas-liquid flow, and fluctuations in cosmic ray flux on the dilution and bolometer plates. These fluctuations do not compromise the science data.

The contrast between the high power dissipation in the warm service module ( $\sim 1000$  W at 300 K) and that at the coldest spot in the satellite ( $\sim 100$  nW at 0.1 K) are testimony to the extraordinary efficiency of the complex thermal system which has to achieve such disparate ends simultaneously while preserving a very high level of stability at the cold end.

### Passive cooling

The telescope baffle and V-groove shields (see Figs.) are key parts of the passive thermal system. The baffle (which also acts as a stray-light shield) is a high-efficiency radiator consisting of  $\sim 14$  m<sup>2</sup> of open aluminium honeycomb coated with black cryogenic paint; the effective emissivity of this combination is very high (>0.9). The **V-grooves** are a set of three conical shields with an angle of 5° between adjacent shields; the surfaces (approx 10 m<sup>2</sup> on each side) are specular (aluminum coating with an emissivity of  $\sim 0.045$ ) except for the outer ( $\sim 4.5$  m<sup>2</sup>) area of the topmost V-groove which has the same high-emissivity coating as the baffle. This geometry provides highly efficient radiative coupling to cold space, and a high degree of thermal and radiative isolation between the warm spacecraft bus and the cold telescope, baffle, and instruments. The cooling provided by the passive system leads to a temperature of 40-45 K for the telescope and baffle. Table 3 lists temperature ranges predicted in flight for various parts of the satellite, based on a thermo-mechanical model which has been correlated to test results; the uncertainty in the prediction for elements in the cold payload is of order (+0.5 K, -2 K).

A more detailed account of the passive cooling stage design can be found [here](#)

---

## Active cooling

The active refrigeration chain further reduces the detector temperatures to 20 K (LFI front-end low noise amplifiers) and 0.1 K (HFI bolometers) respectively. It is based on three distinct units working in series (see Fig. 7):

### The hydrogen sorption cooler

The hydrogen sorption cooler was designed and built expressly for Planck at NASA's Jet Propulsion Laboratory (USA) (Bhandari et al. 2004; Pearson et al. 2006); it directly cools the LFI low-noise amplifiers to their operating temperature while providing pre-cooling for the HFI cooler chain. The sorption cooler consists of two cold redundant units, each including a six-element sorption compressor and a Joule-Thomson (JT) expansion valve. Each element of the compressor is filled with hydride material (La Ni<sub>4.78</sub> Sn<sub>0.22</sub>) which alternately absorbs and releases hydrogen gas under control of a heat source. The cooler produces liquid hydrogen in two liquid-vapor heat-exchangers (LVHXS) whose temperatures are stabilized by hydrogen absorption into three compressor elements. LVHX1 provides pre-cooling for the HFI 4K cooler, while LVHX2 cools the LFI focal plane unit (FPU). The vapor pressure of the liquid hydrogen in the LVHXS is determined primarily by the absorption isotherms of the hydride material used in the compressor elements. Thus, the heat rejection temperature of the compressor elements determines the instrument temperatures. On the spacecraft the compressor rejects heat to a radiator to space with flight allowable temperatures between 262 and 282 K; the radiator is a single unit which couples the active and redundant sorption coolers via a network of heat pipes. The operating efficiency of the Planck sorption cooler depends on passive cooling by radiation to space, which is accomplished by heat exchange of the gas piping to the three V-groove radiators. The final V-groove is required to be between 45 and 60 K to provide the required cooling power for the two instruments. At the expected operating temperature of  $\sim 47$  K, with a working pressure of 3.2 MPa, the two sorption coolers produce the 990 mW of required cooling power for the two instruments, with a margin of  $\sim 100$  mW. The temperature in flight at the heat exchangers will be 17.5 K (LVHX1) and 19 K (LVHX2). LVHX2 is actively stabilised by a closed loop heat control; typical temperature fluctuation spectra are shown in Fig. 8.

The details of the design, calibration and operation of the sorption cooler can be found [here](#)

### The 4K cooler

The 4 K cooler is based on the closed circuit JT expansion of helium, driven by two mechanical compressors, one for the high pressure side and one for the low pressure side. A description of this system is given in Bradshaw et al. (1997). Similar compressors have already been used for active cooling at 70 K in space. The Planck 4 K cooler was initially developed under an ESA programme to provide 4 K cooling with reduced vibration for the FIRST (now Herschel) satellite. For this reason the two compressors are mounted in a back-to-back configuration, which cancels most of the momentum transfer to the spacecraft. Furthermore, force transducers placed between the two compressors provide an error signal which is used by the drive electronics servo system to control the motion profile of the pistons up to the 7th harmonic of the base compressor frequency ( $\sim 40$  Hz). The damping of vibration achieved by this system is more than two orders of magnitude at the base frequency and factors of a few at higher harmonics; the residual vibration levels will have a minor heating effect on the 100 mK stage, and negligible impact on the pointing. Pre-cooling of the helium is provided by the sorption cooler described above. The cold end of the cooler consists of a liquid helium reservoir located just behind the JT orifice. This cold tip is attached to the bottom of the 4 K box of the HFI FPU (see Fig. 7). It provides cooling for this screen and also pre-cooling for the gas in the dilution cooler pipe described later in this section. The margin between heat lift and heat load depends sensitively on the pre-cooling temperature provided by the sorption cooler at the LVHX1 interface. The temperature of LVHX1 is thus the most critical interface of the HFI cryogenic chain; system-level tests have shown that it is likely to be  $\sim 17.5$  K, about 2 K below the maximum requirement[\*]. At this pre-cooling temperature the heat load is 10.6 mW and the heat lift is 16.1 mW for a compressor stroke amplitude of 3.5 mm (the maximum is 4.4 mm). The heat load of the 4 K cooler onto the sorption cooler is only 30 mW, a very small amount with respect to

the heat lift of the sorption cooler (990 mW); thus there is little back reaction of the 4 K onto the sorption cooler.

Here you will find a more detailed overview of the 4K cooler.

### **The dilution cooler**

The dilution cooler consists of two cooling stages in series, using 36 000 litres of Helium 4 and 12 000 litres of Helium 3 gas stored on-board in 4 high-pressure tanks. The first stage is based on JT expansion, and produces cooling for the 1.6 K screen of the FPU and for pre-cooling of the second stage cooler. The latter is based on a dilution cooler principle working at zero-G, which was invented and tested by A. Benoît (Benoît et al. 1997), and developed into a space-qualified system by the Institut d'Astrophysique Spatiale (Orsay) and DTA Air Liquide (Grenoble), see Triqueneaux et al. (2006). The gas from the tanks (at 300 bars at the start of the mission) is brought down to 19 bars through a pressure regulator and the flow through the dilution is regulated by a set of discrete restrictions which can be switched by telecommand. The gas is vented to space after the dilution process[\*], and the cooler therefore has a lifetime limited by the gas supply. The dilution of the two helium isotopes provides the cooling of the bolometers to a temperature around 100 mK which is required to deliver a very high sensitivity for the channels near the peak of the CMB spectrum (noise equivalent power around  $10^{-17} \text{ W}/\sqrt{\text{Hz}}$ ), limited mostly by the background photon noise.

The details of design, calibration and operation of the dilution cooler can be found here

FIGURES STILL TO BE ADDED

## **Passive cooling**

---

## **Sorption cooler**

---

# Qualification and performance

---

## HFI design, qualification, and performance

---

THIS SECTION IS CURRENTLY IN A VERY PRELIMINARY FORM. It is intended to provide an overview of the instrument and of its different sub-systems. Two papers that include and detail this information are available: LAMARRE, Jean-Michel, PUGET, Jean-Loup et 93 co-auteurs, " Planck pre-launch status: The HFI instrument, from specification to actual performance", Astronomy and Astrophysics, Volume 520, id.A9 (20 pages, A&A Homepage), 09/2010. and Planck-HFI Core Team and 165 co-authors. " Planck early results. IV. First assessment of the High Frequency Instrument in-flight performance", Astronomy & Astrophysics, Volume 536, id.A4 (A&A Homepage) 12/2011." Additional detailed information potentially useful for the use of the HFI data will be included into this section or annexed to it.

### HFI high level description and Architecture

(Lamarre/Pajot)

The HFI instrument is designed around 52 bolometers. Twenty of the bolometers (spider-web bolometers or SWBs) are sensitive to total power, and the remaining 32 units are arranged in pairs of orthogonally-oriented polarisation-sensitive bolometers (PSBs). All bolometers are operated at a temperature of  $\sim 0.1$  K by mean of a space qualified dilution cooler coupled with a high precision temperature control system. A 4He-JT provides an active cooling for 4 K stages using vibration controlled mechanical compressors to prevent excessive warming of the 100 mK stage and minimize microphonic effects in the bolometers. Bolometers and sensitive thermometers are read using AC-bias scheme through JFET amplifiers operated at  $\sim 130$  K that provide high sensitivity and low frequency stability. The HFI covers six bands centred at 100, 143, 217, 353, 545 and 857 GHz, thanks to a thermo-optical design consisting of three corrugated horns and a set of compact reflective filters and lenses at cryogenic temperatures.

The whole satellite is organized to provide thermal transitions between its warm part exposed to the sun and earth radiation, and the focal plane instruments that include the cold receivers (Sections XXX1 and XXX2). The various parts of the HFI are distributed among three different stages of the satellite in order to provide each sub-system an optimal operating temperature. The "warm" parts, including nearly all the electronics and the sources of fluids of the 4K and 0.1K coolers, are attached and thermally linked to the service module of the satellite. The first stage of the preamplifiers is attached to the back of the passively cooled telescope structure. The focal plane unit is attached to the 20K stage cooled by the sorption cooler. This is detailed in (XXX2).

The telescope and horns selects the geometrical origin of photons. They provide a high transmission efficiency to photons inside the main beam, while photons coming from the intermediate and far-side lobes have very low probability of being detected. This essential characteristics is known by a complex process mixing ground measurements of components (horns, reflectors), modelling the shape of the far side lobes, and measuring in-flight bright sources, especially planets.

The filters and bolometers define the spectral responses and absolute optical efficiency, that will be known mostly from ground based measurements

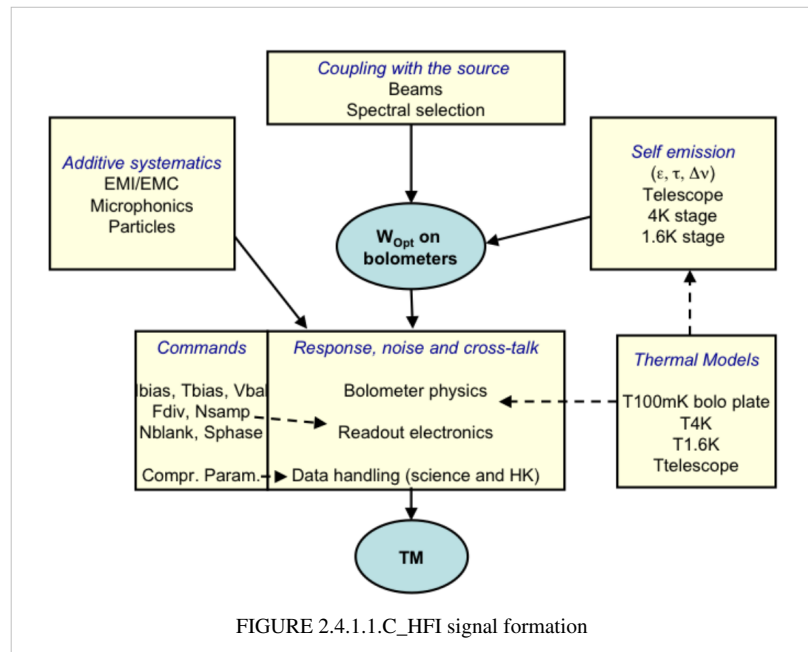
performed at component, sub-system and system levels reported in this document. The relations between spectral response and geometrical response will also be addressed.

Photons absorbed by a bolometer include the thermal radiation emitted by the various optical devices: telescope, horns and filters. They are transformed in heat that propagates to the bolometer thermometer and influence its temperature which is itself measured by the readout electronics. Temperatures of all these items must stable enough not to contaminate the scientific signal delivered by the bolometers. How this stability is reached is described in section 2.4.1\_cryogeny.

The bolometer temperature depends also on the temperature of the bolometer plate, on the intensity of the biasing current and on any spurious inputs, such as cosmic rays and mechanical vibrations. Such systematics are included in the list of section 2.4.1.\_systematics.

Since the bolometer thermometer is part of an active circuitry that also heats it, the response of this system is complex and has to be considered as a whole. In addition, due to the modulation of the bias current and to the sampling of the data, a complex time response is expected, which modifies the beam shape resulting from the scanning of point sources. Section 2.4.1.\_time response is dedicated to the description of the time response.

Figure 2.4.1.1\_HFI signal formation: Logic of the formation of the signal in HFI. This is an idealized description of the physics that takes place in the instrument. The optical power that is absorbed by the bolometers comes from the observed sky and from the instrument itself. The bolometers and readout electronics, acting as a single and complex chain, transform this optical power in data that is compressed and transmitted for science data reduction.



## Cryogenics

(F .Pajot)

### Dilution

The HFI 3He-4He dilution cooler produces temperatures of 0.1 K for the bolometers through the dilution of 3He into 4He and 1.4 K through JT expansion of the 3He and 4He mixture. The dilution cooler is described in detail in section 2.3.3 of early paper II <sup>[1]</sup>.

The dilution was operated with flows set to the minimum available values, and provided a total lifetime of 30.5 months, exceeding the nominal lifetime of 16 months by 14.5 months. The dilution stage was stabilized by a PID control with a regulating power between 20 and 30 nW providing a temperature close to 101 mK. The bolometer plate was stabilized at 102.8 mK with about 5 nW dissipated by PID regulation. The cooling power values were in very good agreement with those obtained during the ground tests and calibration. However, the cosmic particles interactions with the 100 mK stages induced temperature fluctuations and glitches on the thermometers measurements. The baseline correction of the bolometers signals from the 100 mK bolometer stage temperatures fluctuations is described in the TOI processing section.

At very low frequency, below 1 mHz, the temperature fluctuations are very well correlated with the high energy particles hit rate, as measured by the on-board monitor. At frequencies in the 10 mHz to 1 Hz range, single events inducing a global or partial temperature change of the bolometer plate are observed.

The 1.4K stage is very stable and given the very low coupling coefficients between the 1.4K optical components and the detectors no effect can be measured on the signal.

Detailed thermal analysis of the in-flight stability of the dilution cooler can be found in section 5.4 of early paper II <sup>[2]</sup>.

### 4K J-T cooler

The HFI 4K J-T cooler produces a temperature of 4K for the HFI 4K stage and optics and the precooling of the dilution gases. Full description of the 4K cooler can be found in in section 2.3.2 of early paper II <sup>[1]</sup>.

The 4K cooler was operated without interruption during all the survey phase of the mission. It is still in operation as it also provides the cooling of the optical reference loads of the LFI. The 4K PID stabilizing the temperature of the HFI optics is regulated at 4.81 K using a power around 1.8 mW.

The 4K J-T cooler compressors amplitude was set to 3450 micrometers during the CPV, and was maintained to this value during all the mission. Its cooling power is very stable and gives enough margin to cancel out the fluctuations induced by the sorption cooler fluctuations and adjustments. Following the unexpected shutdown of the compressors during CPV, their operation was nominal during all the rest of the mission.

Details on the in-flight performance of the 4K J-T cooler can be found in in section 5.3 of early paper II <sup>[3]</sup>.

## Cold optics

(Lamarre)

### Horns, lenses

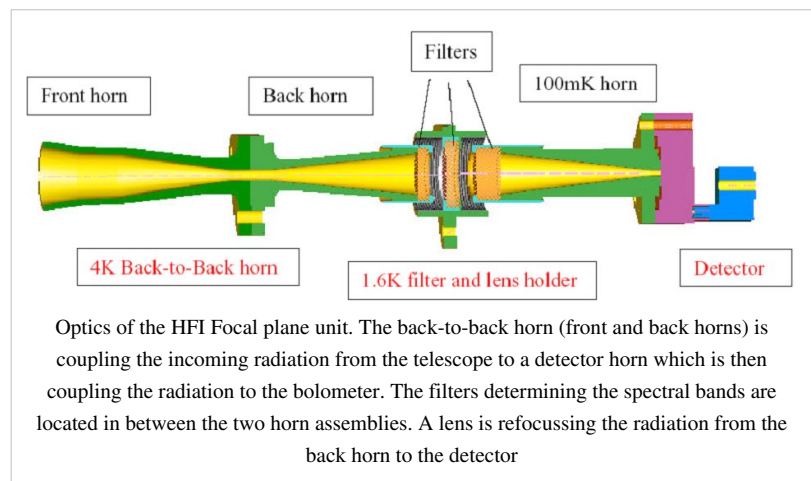
links to Peter's paper

#### Feed horns beams (sub-system level)

In order to meet with straylight, beam shapes and filtering requirements, a design using feedhorn coupled detectors has been chosen, with a triple horn configuration (see Figure 3.1.1). A detailed description of the HFI optical design and beam performances is given in Maffei et al.(2009) and Ade et al.(2009).

#### Single-moded horns patterns

The spectral and geometrical properties of the horns have been characterized individually. The measured beam pattern of a typical front horn is compared with the prediction from the design (figure 3.1.2). The fit is excellent down to very low levels, which validates the logics that prevailed for characterizing the horns: modelling and optimizing the horns before implementation. Validating the model with a complete measurement of the beam intensity patterns.



For the single-moded horns, a method has been developed to use the measured intensities, together with the phase information from modeling to derive “worst-case” horn beam patterns that can be used in GRASP simulations of the telescope beams (phase information is mandatory). Worst-case beam patterns have been computed for all single-moded HFI horn types. A .pdf file (IAS-FN-WCB-001-03022009) detailing the algorithm can be found on the optics ftp site at [ctwg1.planck.fr](http://ctwg1.planck.fr), in the following directory: /File\_Exchange\_Box\_GOPT/Files\_from\_FN/Worst\_case\_beams”

As an example, in Figure 3.1.3, we show the difference in encircled powers at constant isolevel intervals for the HFI 143\_1a channel main beam using both the model and worst-case horns.



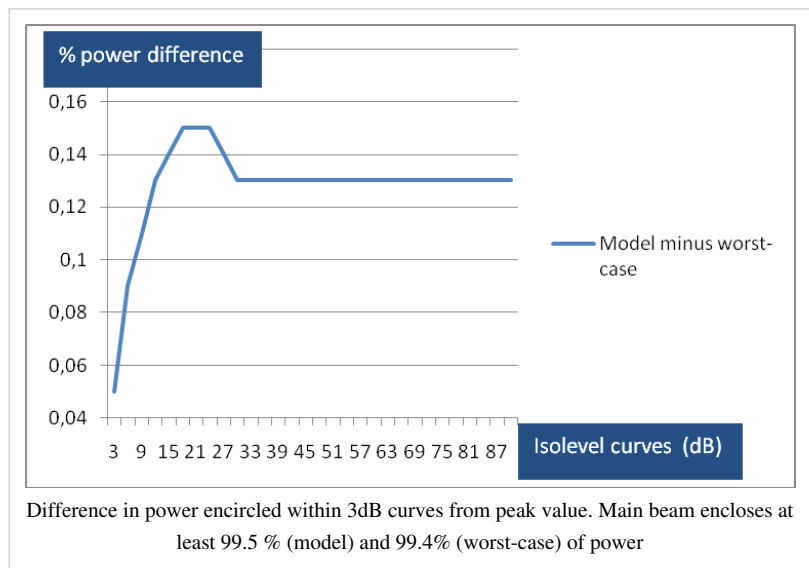
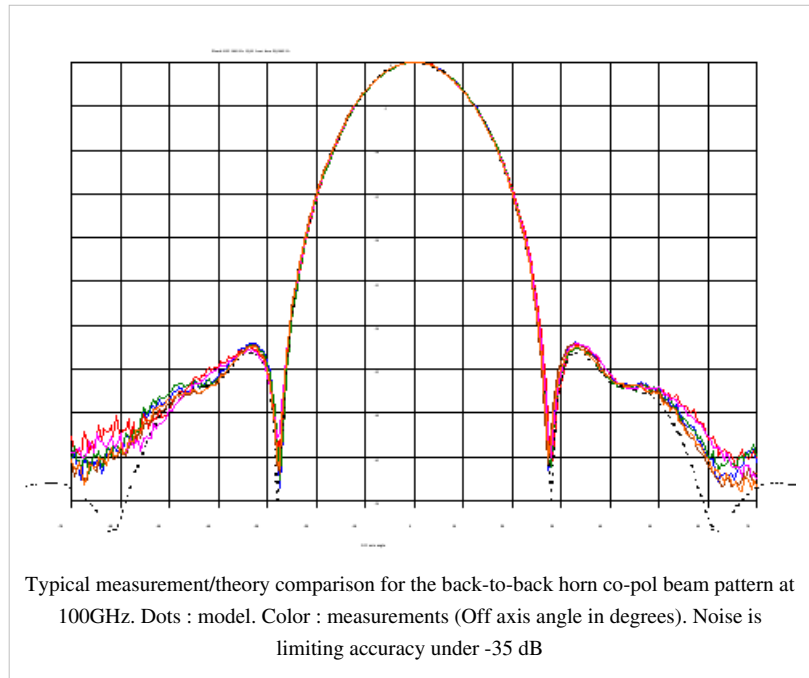
### Ideal Multi-moded horns simulations

In the high frequency 545GHz and 857GHz Planck pixels both the back-to-back (BTB) horn and the detector horn have overmoded waveguide filters. The waveguide-horn structures are modelled using the scattering matrix approach used for the single-moded-CMB-channel horns, with the inclusion of modes of azimuthal orders,  $n = 0, 1, 2, 3$  and 4. We assume reciprocity, and that the cavity plus cavity horn and filter behaves like a black-body: since the waveguide filter in the detector horn is wider than that of the BTB, it is reasonable to assume that any mode that can propagate through the BTB filter also propagates through the detector horn filter from the cavity. Thus, as far as the beam patterns are concerned the BTB is effectively coupled to a black body cavity also and all modes are excited at the back end of the BTB horn. Thus, all waveguide modes are equally excited in power but are also independent of each other so there is no phase relationship between them. Many of these modes may contribute independently (i.e. incoherently) to the beam on the sky. All coherent aperture fields have to be independently propagated through the PLANCK telescope.

From the S21 transmission scattering matrix for the whole BTB we recover the group of true independent hybrid fields that are transmitted by the waveguide filter and horn at the aperture of the BTB. These hybrid fields propagate independently through the telescope and onto the sky at a single frequency. The beam pattern for the band is obtained by adding the filter transmission weighted coherent fields in quadrature across the band (Microwave Horns and Feeds A. David Olver, Institution of Electrical Engineers) ("Shaped Corrugated horns for Cosmic Microwave Background Anisotropy Measurements" B. Maffei, P.A.R. Ade, C.E. Tucker, E. Wakui, R.J. Wylde, J.A. Murphy, R.M. Colgan, Int Jour Infrared & Millimeter waves, 21, (12) 2023-2033, December 2000).

Far field patterns of horns and comparison with test data:

The far-field patterns of the horns (which illuminate the Planck mirrors) have been simulated and are shown in figure 3.1.4a for a few spot frequencies across the 857 GHz band. Note that the edge taper is approx -30dB at 25 degrees as required at the centre of the band. Superimposed is the broadband measurement made at Cardiff (see below) which



clearly looks narrower than the majority of the spot frequency measurements and requires explanation. The measured far field beam patterns across the band are narrower than the predicted far field beams right across the band. The simulated beams are too wide suggesting missing higher order modes, either due to attenuation between the cavity and the BTB, or to the experimental setup. Away from the band centre the theoretical beams also appear to be too wide, indicating missing modes (see figure 3.1.4b).

Grouping contributions according to azimuthal order and overlaying the measurement data to investigate missing field distributions, modes of order 2 and higher appear to be absent. The beam containing modes of azimuthal orders  $n = 0$  and 1 appears to fit the measured beams reasonably. Adding modes with azimuthal order  $n = 2$  gives a simulated beam that is too wide, suggesting that these modes are absent from the measured BTB front aperture field.

## filters, band

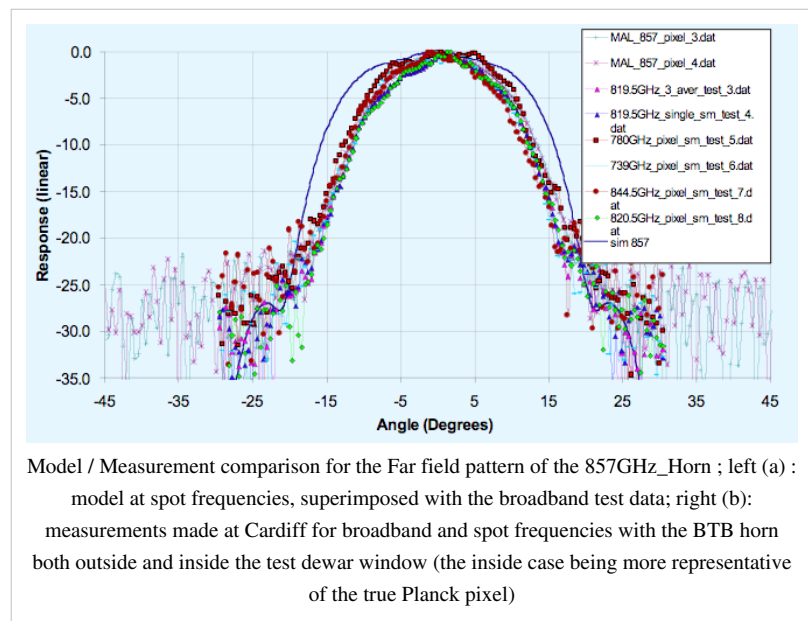
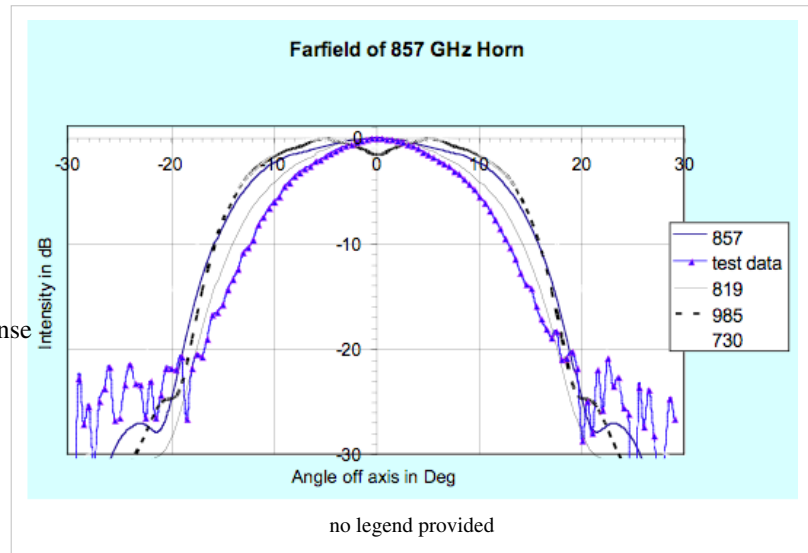
Includes Locke's very detailed document.

Raw inclusion of Locke Spencer section following JML instructions (22-oct2012) [http://www.sciops.esa.int/wiki/SI/planckpla/index.php?title=HFI\\_Detector\\_Spectral\\_Response](http://www.sciops.esa.int/wiki/SI/planckpla/index.php?title=HFI_Detector_Spectral_Response)

## Abstract

This section is comprised of excerpts from the *HFI - Spectral Calibration report of the IAS measurements, v3.00*, an internal report describing detailed pre-flight ground based measurements of the HFI focal plane. The experimental setup, data collection, and related data processing are described. The official version of the HFI detector spectral transmission profiles is available within the HFI instrument model and the RIMO files in the Planck Legacy archive [ref.] . This data is comprised of broadband Fourier transform spectrometer (FTS) measurements conducted with the HFI focal plane assembly as described above, and includes a waveguide model for the low frequency spectral region, and component-level filter

spectra for the remaining out of band spectral regions. Specific attention is given to in-band and near-band spectral regions surrounding CO rotational transitions in order to support the CO extraction component separation effort [ref.] . The spectral transmission profiles are evaluated with parameters such as cut-on, cut-off, centre frequency, effective frequency (including spectral index), and band-width are provided in the analysis. Further evaluation yields



band-average spectra ( [ref.] ) and unit conversion / colour correction coefficients ( [ref.] ) and software routines ( [ref.] ).

## Objectives

The main goal of the spectral transmission tests of the HFI instrument is to measure the spectral response of all HFI detectors to a known source of EM radiation individually. This was determined by measuring the interferometric output of all detection channels for radiation propagated through a continuously scanned polarising fourier transform spectrometer (FTS). The required accuracy to which the spectral transmission is to be recovered is 1 % (see §Req.).

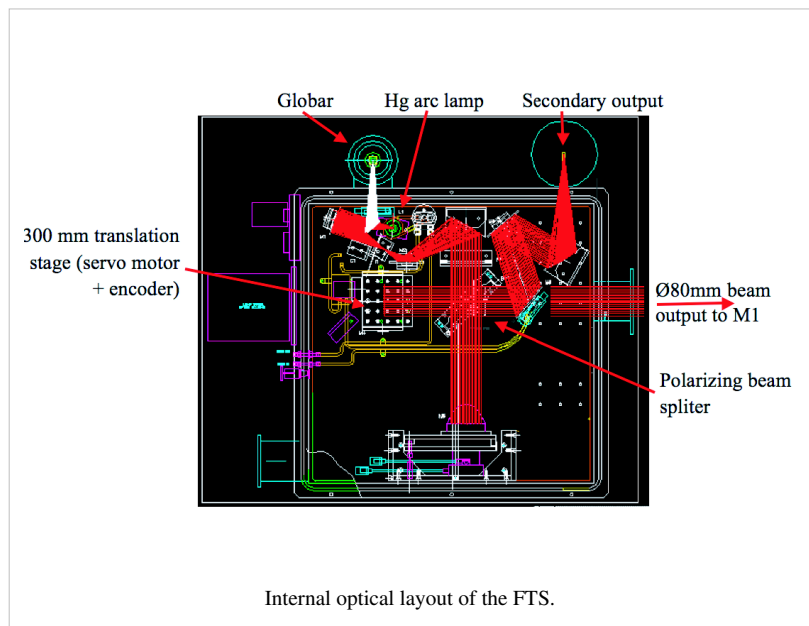
It is important to note that the absolute spectral calibration cannot be achieved solely from the analysis of the FTS data because of uncertainties in the coupling efficiency of the FTS source through the FTS, input optics, and integrating sphere. The relative FTS measurements must be combined with the optical efficiency tests which used internal black-body sources (EFF Test – see §EFF).

## Description of setup

A brief description of the optical setup used for the spectral characterisation of the HFI instrument performed at the FPU level in the Saturne calibration facility at IAS is provided here. Further details are available from the pre-launch calibration papers . The spectrometer configuration is based on a polarizing Fourier transform interferometer, feeding an integrating sphere inside the Saturne tank (Figs. [fig:Optical-layout-of] & [fig:Top-view-of]). The output of the integrating sphere is conjugated by a mirror with the focal plane of the HFI. Therefore data are acquired simultaneously on all pixels while the moveable mirror in the external FTS is scanned.

An external light source system (ELS, see Fig.[fig:FTS/ELS-assembly-with]) is provided in addition to the FTS for time constant measurements. Selection between the FTS and the ELS is done by the M1 flip mirror.

The polarising FTS was provided by Sciencetech Inc. (Canada) under contract with IAS and ESA (Fig.[fig:Internal-optical-layout]). The source can be selected from either a Hg vapour arc lamp or a globar. The 300 mm translation stage allows symmetric interferograms with a maximum theoretical (unapodized) Instrument Line Shape (ILS)



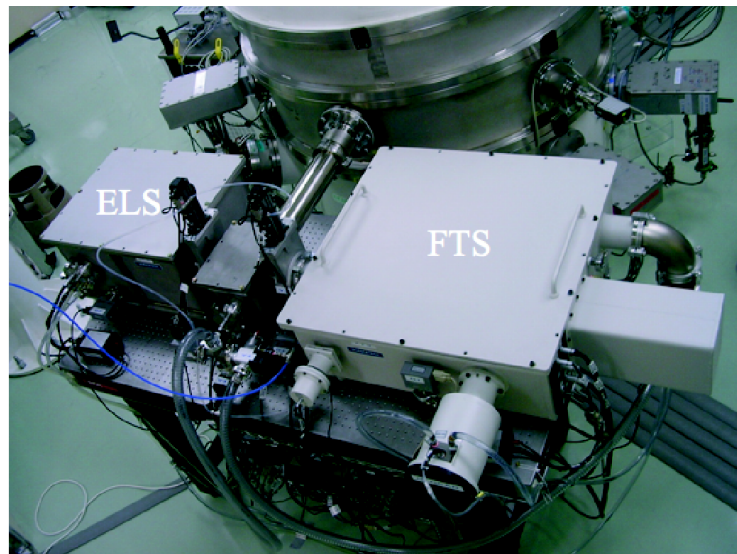
Internal optical layout of the FTS.

Full-Width-at-Half-Maximum (FWHM) resolution of  $0.020 \text{ cm}^{-1}$ . Filtering of short wavelength is done on the optical path entering the Saturne cryostat as follows:

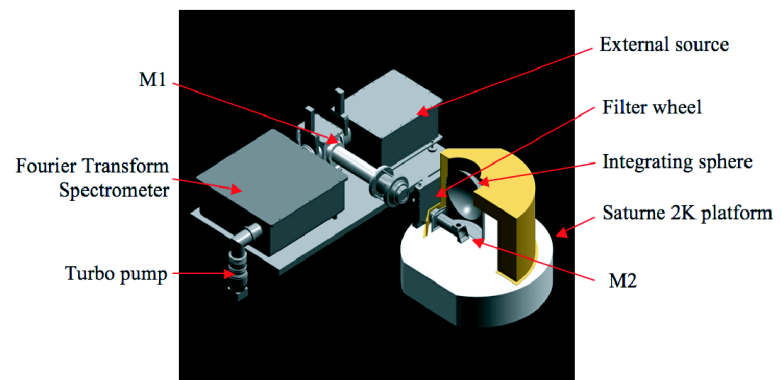
- Saturne vacuum window is polyethylene (6mm thick)
- 1<sup>st</sup> thermal filter at 300K
- 2<sup>nd</sup> thermal filter at 77K

- $46\text{ cm}^{-1}$  filter at 77K
- $3^{\text{rd}}$  thermal filter at 20K
- filter wheel at 2K (Fig. [fig:2K-filter-wheel]) with selection of: open, closed,  $35\text{ cm}^{-1}$  or  $10\text{ cm}^{-1}$  filter

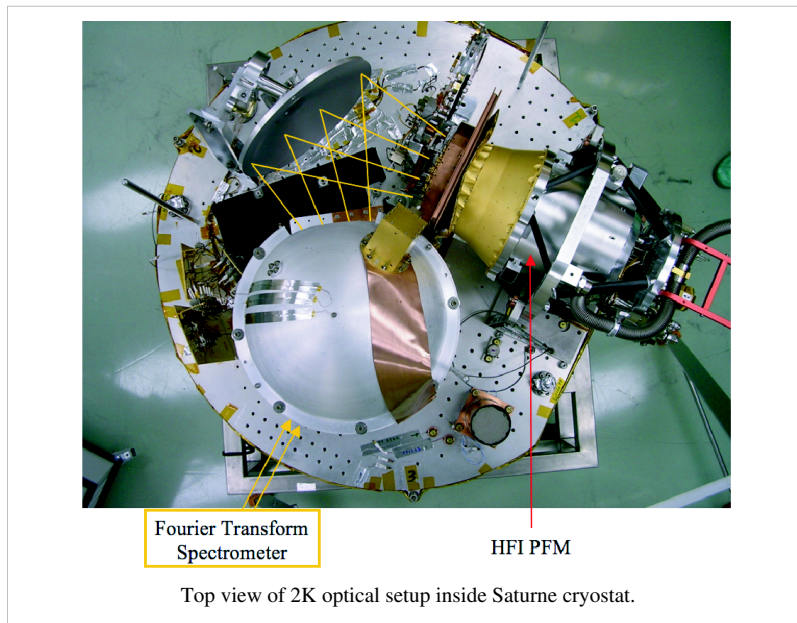
FIXME: typo in figure



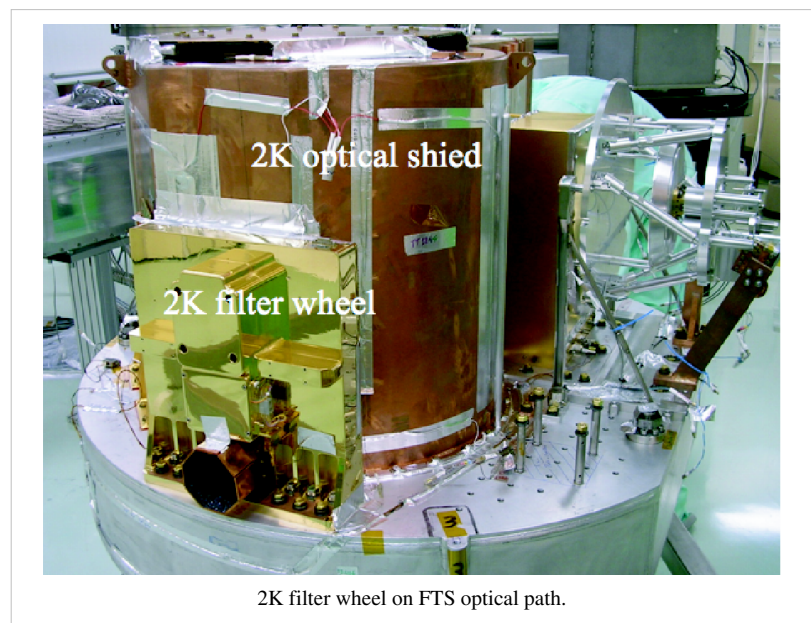
FTS/ELS assembly with Saturne cryostat.



Optical layout of the FTS with respect to the Saturne cryostat.



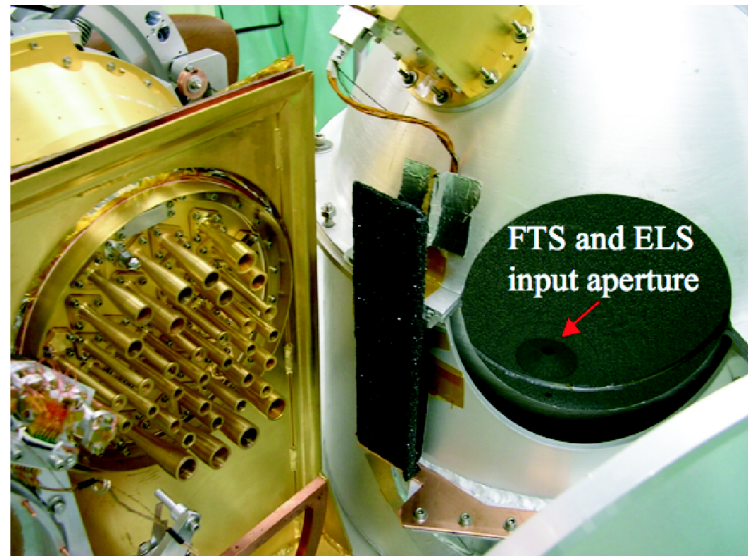
FIXME: typo in figure





The optical flux from the FTS enters the integrating sphere through an 8mm diameter hole at its bottom (Fig. [fig:FTS-input-aperture]), which is the conjugate of the M1 mirror by M2.

During scanning, encoder pulses from the translation stage are time stamped with a clock synchronized with the HFI signal acquisition clock (itself provided by the spacecraft simulator used during the calibration). In a similar way, a mechanical ZPD (Zero Path Difference) signal is stamped and stored in the database. After verification, the scanning speed was found to be sufficiently stable to be



Saturne integrating sphere and HFI focal plane.

assumed as constant along the section of the interferogram needed for spectral processing. Therefore the data processing described below does not use the reference signal but relies instead on the data acquisition time line to derive the optical path difference.

To provide a reference monitor for the interferometric flux, a dedicated bolometer is used within the integrating sphere. The flux recorded by this detector is directly related to the flux received by the HFI detectors on the focal plane which is coupled directly to the sphere output hole via mirror M1. The reference bolometer was provided by the team of N. Coron at IAS and has a predetermined absolute calibration between the flux measured and its output signal. It is fed by a modified Winston horn from Infrared Lab. Inc. (USA) and operated at 300 mK using a  $^3\text{He}$  fridge (Torre-Chanin). The reference spectra acquired during the calibration run with this bolometer are used to identify standing wave features in the FTS source and path (lamp, windows,...) and to check the shape of the source spectrum. The diffraction losses at low frequencies due to the horn exit aperture diameter (2.6 mm) is a limitation taken into account in the data processing of the low frequency channels of HFI.

## Data Collection

To allow for data sets that have the same instrumental effects the bulk of the sequences have been performed with the same parameters. Also, separate single tests have been performed in different configurations to understand instrument systematics. The following is a list of the sequences adopted for the final spectral calibration data.

- **Max OPD:** The Maximum Optical Path Difference adopted during FTS testing is 30 cm. This relates to a nominal maximum resolution for the spectra of  $\simeq 0.02 \text{ cm}^{-1}$ . This maximum resolution may then be deteriorated by the actual sample of data selected and by the apodization of the data (see §[sec:apod]).
- **Speed:** The Speed of the scanning FTS is set to  $0.1 \text{ cm/s}$  for all of the data. The sampling of the data given by the acquisition frequency allows knowledge of the spectrum up to  $\simeq 430 \text{ cm}^{-1}$ . This is well above the optical filter cut-off frequency, so aliasing is not a concern. The independent filter measurements used in the spectral transmission outside of the optical pass-band (see §[sec:filter]) have a Nyquist frequency of  $600 \text{ cm}^{-1}$ .
- **Source:** two sources were used in separate measurements. The mercury arc lamp as the main source for the final data and also a GLOBAL source to study any systematic effect present in the different measurements. (Although ratio with reference bolometer should remove such artifacts.) The spectra used to generate the Spectral Transmission data products in the IMO all originated from the mercury arc lamp as the optical source.
- **Spectral range:** The spectral range of the radiation entering the Saturne cryostat is given by a fixed  $46 \text{ cm}^{-1}$  LPE filter and a rotating filter wheel with the following positions (1- Open (no added filtering), 2- Dark (no radiation

allowed), 3- LPE =  $10 \text{ cm}^{-1}$ , 4- LPE =  $36 \text{ cm}^{-1}$ ). The last two positions have been adopted for the final data of the three low channels (100, 143, 217 GHz) and the higher three spectral channels (353, 545, 857 GHz), respectively.

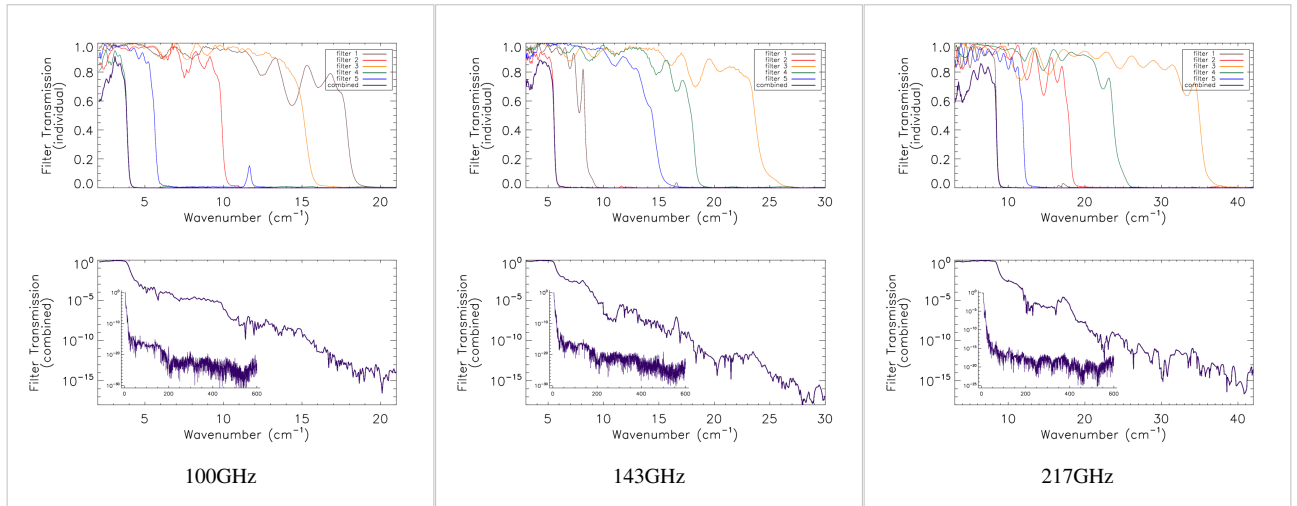
## Additional Experiments

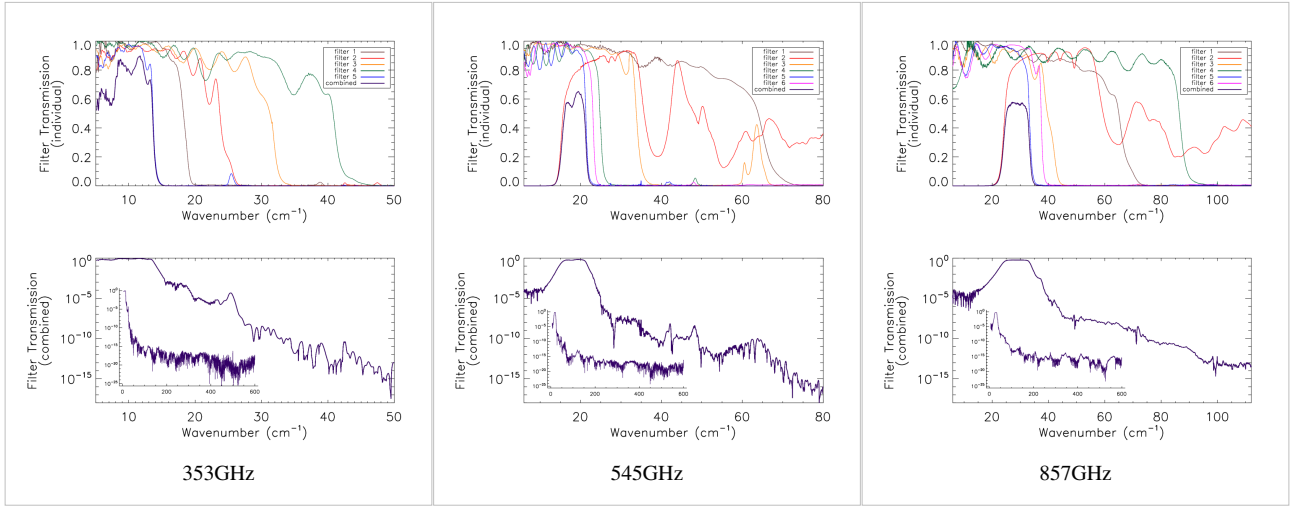
There were two significant additional tests that are used in the derivation of the HFI detector spectral transmission profiles beyond the scope of the IAS HFI FTS measurements. Additional filter measurements were recorded in the AIG test facility at Cardiff during filter stack production. These measurements are used to extend the IAS FTS spectral measurements beyond the HFI spectral passband. The EFF tests are used to obtain optical efficiency parameters for each detector. These parameters, when combined with the respective normalized spectral transmission profiles, provide an estimate of the absolute spectral transmission. The EFF tests are discussed briefly in §EFF, with greater detail provided by A. Catalano . The filter measurements are described in §filter below.

## Filter Measurements

Prior to the IAS measurements with the integrated HFI detectors and filter stacks, FTS measurements of the individual filters comprising the filter stacks for each band were conducted at Cardiff. As will be discussed in §[sec:OOB], the independent measure of the filter stack transmission is used for a portion of the HFI detector spectral transmission for regions of the spectrum where it is deemed to be of better quality than the IAS FTS measurements (i.e. for frequencies outside of the band edge filter cut-off(s)). The filter stacks for each of the frequency bands are comprised of 5 filters. There is an additional low frequency cut-on filter for the 545 and 857 GHz bands as the waveguide cut-on is too low. Figures [fig:Filt100] – [fig:Filt857] show the individual filter transmission measurements as well as the combined filter stack product.

Combined (bottom) and individual (top) filter transmission measurements for the 5 filters within the HFI band filter stacks (6 for 545 and 857 GHz).





The uncertainty on the combined filter transmission measurement is determined as follows. Let  $f_i(\sigma)$  represent the individual filter transmission. The standard deviation of all values of  $f_i(\sigma)$  below a threshold of 0.001 is used as an approximate uncertainty for each individual filter measurement, i.e.  $s_i$ . The individual uncertainty estimates are combined to provide an estimate of the combined filter transmission spectral uncertainty through standard error propagation. For the combined filter transmission represented as  $F(\sigma)$ , the associated uncertainty estimate is given as

## Raw Data

Table 1 contains the details for the sets of data adopted for data analysis in the generation of the HFI detector spectral transmission profiles. The first two columns report the date and time of the starting point of the data set. The third column indicates the approximate scan length (in minutes). The fourth column is the maximum number of valid interferograms that are present in the data file. The column labeled RFP (Rotating Filter Wheel Position) indicates the filtering condition under which the data was taken: 1-Totally open (no filtering other than the ever present  $46 \text{ cm}^{-1}$  LPE; 2-Closed (no radiation is allowed to pass into the cryostat from the FTS); 3-  $10 \text{ cm}^{-1}$  LPE filter (for the low frequency channels); 4-  $36 \text{ cm}^{-1}$  LPE filter (for the high frequency channels). The column immediately following indicates, within a milliKelvin, the average reading of the bolometer plate thermometers during the scan time. The data sets with the RFP set to 3 were used for the lower frequency channels, i.e. the 100, 143, and 217 GHz bands. The data corresponding to an RFP of 4 were used for the higher frequency channels, i.e. the 353, 545, and 857 GHz bands. Table [tab:BrefData] indicates the data sets used to obtain the reference bolometer spectra. In most instances the data were acquired synchronously, however, there were cases when the HFI data was of good quality and the reference bolometer data was not, and vice-versa. The recorded data corresponding to the entries in Tables [tab:RawData] & [tab:BrefData] were used in the determination of the HFI spectral transmission profiles. There is also additional data that was recorded as part of the test campaign but not used in this specific work that is not listed here.



Date (DD/MM/YY)	Time	length (min)	#Ifgm.	RFP	Source	T(mK)
25/06/06	07:52	25	4	4	Hg	140
25/06/06	08:33	25	4	4	Hg	140
25/06/06	09:02	65	12	4	Hg	140
25/06/06	10:05	65	12	4	Hg	140
25/06/06	11:15	65	12	4	Hg	140
26/06/06	09:44	25	4	4	Hg	140
27/06/06	17:48	148	28	3	Hg	<130
27/06/06	20:20	335	50	3	Hg	<120
28/06/06	21:39	163	28	3	Hg	95
05/07/06	06:23	82	16	4	Hg	100

**Summary of recorded data used to generate the reference bolometer spectra.**

Date (DD/MM/YY)	Time	length (min)	#Ifgm.	RFP	Source
22/06/06	17:50	50	9	3	Hg
22/06/06	18:40	50	9	3	Hg
22/06/06	19:30	50	9	3	Hg
22/06/06	20:20	50	9	3	Hg
22/06/06	21:10	50	9	3	Hg
22/06/06	22:50	50	9	3	Hg
22/06/06	23:40	50	9	3	Hg
25/06/06	07:52	25	4	4	Hg
25/06/06	10:05	65	12	4	Hg
25/06/06	11:15	65	12	4	Hg
26/06/06	09:44	25	4	4	Hg
26/06/06	17:04	38	7	3	Hg
26/06/06	22:23	41	8	3	Hg
27/06/06	00:04	86	16	3	Hg
27/06/06	17:48	148	28	3	Hg
27/06/06	20:20	335	50	3	Hg
28/06/06	21:39	163	28	3	Hg
05/07/06	06:23	82	16	4	Hg

## Data Processing

<!-- [sec:DP] -->

Having identified the data sections that are of interest, here follows the data processing sequence used to obtain the resulting spectra. The processing steps taken are as follows:

1. Selection and extraction of time sampled data sets
2. Conversion of time sampled data to arrays of OPD sampled interferogram data sets
3. Fourier transformation and averaging of interferogram data sets
4. Discrimination of poor quality spectra by standard deviation comparison (see §[sec:FTavg])
5. Division of detector spectra by reference bolometer spectra to obtain normalized spectral transmission profiles
6. Combination of relative transmission spectra with filter measurements and waveguide models
7. Determination of optical efficiency through evaluation of normalized spectral transmission in the context of the EFF experiments
8. Addition of over-sampled data into spectrum for the CO transition regions (see §[sec:CO])
9. Identification of common frequency sampling per channel and interpolation of spectra onto the common sampling

### Selection and extraction of data sets

The selected arrays of data are imported into a KST client from the QLA server

```
plck-op-3.ias.u-psud.fr
```

and subsequently exported as text files. Separate files are generated for the various bolometer signals and sample times for each detector. The exported text files were transferred from the remote IAS machines to the dedicated Planck computer at Cardiff,

```
planck01.astro.cf.ac.uk,
```

for further processing and analysis. A sample bolometer signal timeline is shown in Fig. [fig:BolSig].

The bolometer signal is stored within the initial database in several formats: raw ADU, signal voltage, resistance, current, temperature, total power, electrical power, and radiant power, all of which may be exported to a KST session as a function of sample time. Although all of the above formats originated from the recorded detector ADU signal and instrument model parameters, it was not possible to trace these refined database vectors to the specific bolometer parameters used in their conversion. Also exported from a KST session were the set balance voltages and bias currents for each detector so that a bolometer model using the current IMO parameters (IMO ver. 2\_50) could be applied to the raw data as well. The motivation for the application of a bolometer model to the data was to reduce the in-band effects of detector nonlinearities as evidence of detector operation in a non-linear regime was identified within the raw data.

For the interferograms within each of the data sets in the above tables (Tab. [tab:RawData] & [tab:BrefData]), a coarse estimate of the temporal location of each position of Zero Optical-Path Difference (ZPD) was determined using the characteristic local maxima associated with a broad-band fringe for detectors with good S/N. This coarse ZPD location was then used as a starting point to identify a unique ZPD location within each interferogram through the fitting of a low order polynomial to the ZPD fringe.

The interferogram boundaries are determined as the mid-points between subsequent interferograms, less a small number of buffer points ( $\sim 10$ ) to ensure that the extracted interferograms include regions associated with the FTS stage travel having constant velocity while excluding the acceleration regions.

Visual verification of the extracted interferograms is performed to ensure that each ZPD was identified correctly and to remove any low-quality interferograms. The overlap of the extracted interferograms is also verified visually, with any anomalies either corrected (through a revised ZPD location) or removed. These interferograms are then saved to

separate files, to be combined as a large dataset further on in the processing.

Once interferograms have been extracted from each data set, they are combined into a single array for each detector. The Maximum Optical Path Difference (MPD) is determined for each interferogram, and the minimum for each detector within a combined data set is used to generate an evenly sampled Optical Path Difference (OPD) grid onto which each interferogram in the combined data is then interpolated. This ensures that each individual interferogram is sampled at ZPD and that each spectrum has identical frequency sampling and can thus be averaged together. An example of a combined interferogram data set is illustrated in Figure [fig:CombinedIFGMex] where the central portions of the recorded interferograms are shown. A similar plot for each HFI detector is included in the Appendices (see §[sec:allIFGMs]). The MPD value for each detector, and corresponding spectral resolution, is shown in Fig. [fig:MPD].

/figures/LSfigs/

### Fourier Transformation and Averaging of Interferogram Data Sets

In preparation for Fourier transformation, a low-order polynomial baseline removal is performed on the individual interferograms. Consequently, no information can be recovered from the spectrum below  $\sim 0.1 \text{ cm}^{-1}$ , but this is of no concern as this region of the spectrum is replaced by a waveguide fit in the final data product (see §[sec:WG]). An average interferogram is determined and used to identify glitches for removal from the interferogram data. If possible, the exponentially decaying tail of a glitch is identified, fit, removed, and replaced by the average of the remainder of the data set (which does not contain a glitch). If this is not possible then the entire interferogram is removed from the data set.

Although an average interferogram is determined, it is not directly used in obtaining the average spectrum. Once the data set has been deglitched, individual interferograms may be apodized (see §[sec:apod]), and then undergo Fourier transformation and phase correction. To allow phase correction to take place at the individual interferogram level, data averaging is then performed in the spectral domain. The uncertainty for every spectral data point is determined statistically through the standard deviation at a given frequency. A check for poor quality spectra is performed by comparing the overall standard deviation including and excluding any given spectrum. An example of the individual spectra and uncertainty for bc00 is shown in Fig. [fig:CombinedSpecEx]; similar plots for all of the detectors are shown in §[sec:allSpecs].

Table [tab:Igstats] contains information on the individual detector data sets for each of the HFI detectors. Columns three and four contain the number of interferograms and spectra, respectively, used in the generation of subsequent data. These numbers may disagree due to the discrimination of poor quality data discussed above. There will never be more spectra than interferograms for a given data set. The fifth column indicates the minimum MPD for the detector data set. The FTS Instrument Line Shape (ILS) Full-Width-at-Half-Maximum (FWHM) for the data set is provided in the sixth column. An estimate of the S/N is obtained using the average spectrum and its statistical uncertainty, averaged across the in-band region of the spectrum.

The averaged spectra are then normalized and divided by a (normalized) reference bolometer spectrum (see §[sec:setup] & §[sec:Bref]). This is done to remove spectral features from the data beyond those due to the HFI optics and detectors. The terminology ‘pre-ratio’ is used to refer to the spectra before division by the reference bolometer spectra.

### Properties of HFI Detector Spectra

Band (GHz)	bc	# Ifgm.	# Spec.	MPD (cm)	ILS FWHM <sub>(cm<sup>-1</sup>)</sub>	avg. S/N
100	00	96	93	29.648639	0.020355066	104.70555
100	01	96	95	29.648639	0.020355066	203.34226
100	20	96	96	29.649801	0.020354268	271.38262
100	21	95	94	29.650962	0.020353471	264.65385
100	40	96	94	29.652124	0.020352674	432.40921
100	41	96	96	29.652124	0.020352674	962.98064
100	80	95	95	29.650962	0.020353471	262.71036
100	81	96	96	29.650962	0.020353471	227.35782
143	02	96	95	29.652124	0.020352674	434.93136
143	03	96	96	29.652124	0.020352674	458.86741
143	10	95	95	29.652124	0.020352674	565.21311
143	30	92	92	29.653286	0.020351876	424.53824
143	31	92	92	29.652124	0.020352674	447.50343
143	42	92	92	29.652124	0.020352674	536.23423
143	50	96	96	29.652124	0.020352674	441.68983
143	51	96	96	29.652124	0.020352674	476.22684
143	60	96	96	29.652124	0.020352674	517.43269
143	70	95	94	29.652124	0.020352674	326.06542
143	82	96	96	29.652124	0.020352674	454.23293
143	83	96	96	29.652124	0.020352674	439.50612
217	04	96	96	29.652124	0.020352674	625.92713
217	11	96	96	29.652124	0.020352674	580.32904
217	12	67	67	29.663741	0.020344703	549.24264
217	22	96	96	29.652124	0.020352674	550.65242
217	43	95	95	29.652124	0.020352674	616.57750
217	44	96	96	29.652124	0.020352674	543.78288
217	52	95	94	29.652124	0.020352674	684.91039
217	61	92	92	29.652124	0.020352674	594.70296
217	62	95	95	29.652124	0.020352674	579.69385
217	71	96	96	29.652124	0.020352674	631.30065
217	72	96	96	29.652124	0.020352674	687.10844
217	84	92	92	29.652124	0.020352674	636.36790
353	05	55	55	29.651916	0.020352816	354.15815
353	13	57	57	29.651916	0.020352816	319.09858
353	23	55	55	29.651916	0.020352816	218.05772
353	24	64	64	29.651916	0.020352816	236.44464
353	32	56	56	29.651916	0.020352816	238.40018

353	33	55	55	29.651916	0.020352816	219.60443
353	45	64	64	29.653078	0.020352019	246.97889
353	53	57	57	29.651916	0.020352816	225.27621
353	54	57	57	29.651916	0.020352816	228.47058
353	63	57	56	29.651916	0.020352816	140.16991
353	64	55	55	29.651916	0.020352816	158.85037
353	85	57	57	29.653078	0.020352019	246.18460
545	14	63	63	29.654240	0.020351221	448.67624
545	34	64	64	29.654240	0.020351221	481.87111
545	55	57	57	29.654240	0.020351221	328.07835
545	73	57	57	29.654240	0.020351221	447.49901
857	25	64	64	29.653078	0.020352019	501.25106
857	35	64	64	29.654240	0.020351221	567.55125
857	65	42	42	29.653078	0.020352019	482.41906
857	74	64	64	29.654240	0.020351221	491.89133

### Apodization

Apodization of FTS interferograms results in reduced sidelobes of the FTS spectral ILS, at the cost of broadening the central feature of the ILS itself. Another perspective is that the interferogram is preferentially weighted at certain OPD regions (i.e. ZPD) over others prior to Fourier transformation. This also, ideally, results in an improvement in the spectral S/N for a broad-spectrum source, again at the cost of reduced spectral resolution. Figure [fig:apodKernel] illustrates a variety of interferogram apodization kernels that have been used in this work. The modified Norton-Beer 1.5 apodization function has been selected to be used for the final spectral transmission profile data set as it represents a good compromise between the desired ILS sidelobe reduction and improved S/N with marginal reduction in spectral resolution. Figure [fig:ApodCompare] illustrates the difference between apodizations on the same sample data.

### Reference Bolometer Spectra

The reference bolometer spectra are obtained in a fashion similar to that used for the HFI detectors. Wherever possible, the same data processing is applied to the reference bolometer data as was applied to the HFI detector data, including RFP setting, scan speed, scan length, source intensity, apodization, phase correction, etc. Table [tab:Brefstats] contains the reference bolometer data set properties corresponding those listed for the HFI detectors in Table [tab:Igstats]. Figures [fig:BrefL] - [fig:Bref857] illustrate the resultant spectra and S/N from the reference bolometer data sets. Figure [fig:SNall] compares the approximate S/N of the average spectrum for each detector against the reference bolometer average spectrum S/N over the same spectral region.

### Properties of Ref. Bolometer Spectra

Band (GHz)	RFP	# Ifgm.	# Spec.	MPD (cm)	ILS FWHM <sub>(cm<sup>-1</sup>)</sub>	avg. S/N
100	3	164	164	29.644698	0.020357772	11.478057
143	3	164	164	29.644698	0.020357772	37.361317
217	3	164	164	29.644698	0.020357772	126.14280
353	4	24	24	29.652306	0.020352549	136.06159
545	4	24	24	29.652306	0.020352549	314.58093
857	4	24	24	29.652306	0.020352549	388.23050

#### Out-of-Band Spectral Transmission Content

The HFI detector spectral transmission profiles have been extended beyond the optical pass-band of the detectors. This is done by using a combination of a waveguide model and external filter measurements for the out-of-band regions of the detector spectral response. An uncertainty estimate for these additional spectral regions is also provided, however, it should be noted that the spectral uncertainty for the waveguide and filter spectra are determined indirectly (as described above/below).

There is a transition from IAS FTS data to filter data for every band edge which is defined by an optical filter. For the 100, 143, 217, and 353 GHz bands this is the high frequency cut-off band edge. For the 545 and 857 GHz bands a separate filter is used to define each of the high and low frequency band edges. For the spectral regions outside of the HFI detector optical bands, first the IAS FTS data is used to qualitatively verify that there are no spectral leaks or features, and then the external filter measurements are grafted into the ratioed spectra where they better represent the relative spectral transmission. The spectral transmission profiles switch from the ratioed IAS FTS data to the filtered data as follows:

1. The normalized ratioed spectrum is scaled by the optical efficiency (see §[sec:EFF]) whereas the filter spectrum remains normalized. This results in a conservative over-estimation of the out-of-band transmission.
2. A lower threshold frequency,  $\nu_l$ , is defined for each band, below which the FTS data must be used.
3. An upper threshold frequency,  $\nu_u$ , is defined for each band, above which the filter data must be used. The  $\nu_u$  is defined to be twice the band cut-on frequency. This is done to avoid introducing any detector nonlinearity residuals into the final spectral transmission data products.
4. The region between the lower and upper threshold frequencies is defined as the transition region.
5. The transition point is defined as the first data point in the transition region where the ratioed FTS spectrum is greater in amplitude than the filter spectrum.
6. If no such transition point exists, the filter spectrum is temporarily scaled to be smaller until a transition point is identified, after which the filter spectrum is restored to its original amplitude. If the temporary filter data scaling becomes less than 0.01 then the upper threshold frequency is defined as the transition point.
7. The filter spectrum is used for the transmission profile for all frequencies greater than and equal to the transition frequency.
8. The above method resulted in a mild distortion to the spectrum within the transition region for the 143 and 857 GHz spectra. This was a result of nonlinearity features in the FTS spectra just before the transition region cut-off. In these cases, a comparison between the FTS data derivative and filter data derivative was used to determine the transition point, instead of using the spectral amplitudes.

Additionally, a similar technique is used, with decreasing frequency instead of increasing, for the 545 and 857 GHz bands with a filter-induced frequency cut-on. Figure [fig:OOBex] illustrates an example of both the FTS and filter spectra used in extending the transmission profiles beyond the HFI optical bands. Similar plots for every detector are shown in §[sec:stitch].

### Waveguide Model

A waveguide model is used to provide the data for the lowest frequency portion of the HFI detector spectral transmission. For the 100, 143, 217, and 353 GHz bands the waveguide model is transitioned (with increasing frequency) to the FTS ratioed spectra directly. There is an intermediate transition to the filter data, and then the ratioed spectra for the 545 and 857 GHz bands. For each detector, the waveguide transmission,  $W(\sigma)$ , is given by the following relation

where  $\sigma$  is the frequency in  $\text{cm}^{-1}$ ,  $r_w$  is the waveguide radius in cm,  $l_w$  is the waveguide length in cm, and  $C_{nm}$  is a waveguide specific constant; 1.841 for the TE<sub>11</sub>/TM<sub>11</sub>(HE<sub>11</sub>) hybrid mode in this case. Table [tab:WG] lists the waveguide radii and lengths resultant from the waveguide model fit to the ratioed spectra. As all of the feedhorns for a given band are meant to be identical (i.e. within mechanical manufacturing tolerances) the uncertainty of the waveguide transmission is estimated statistically using all of the waveguide models for each band. I.e. for  $n$  bands, the uncertainty at each spectral data point is determined by the standard deviation of  $n$  transmission values at that frequency. As a result of each detector in a given band having a unique cut-on frequency, this method begins to over-estimate the uncertainty for frequencies approaching the cut-on; for regions very near the waveguide cut-on, the uncertainty is extrapolated from the ratioed spectrum as a more accurate representation.

### Waveguide model parameters for the HFI detectors.

Band (GHz)	bc	Det.	$r^W(\text{mm})$	$l^W(\text{mm})$
100	00	1a	1.039705	1000
100	01	1b	1.038040	12.5813
100	20	2a	1.038375	14.3000
100	21	2b	1.041035	12.3750
100	40	3a	1.042370	12.9250
100	41	3b	1.042370	12.5125
100	80	4a	1.033050	13.2000
100	81	4b	1.033050	12.6500
143	02	1a	0.740345	9.4500
143	03	1b	0.737550	9.5625
143	10	5	0.736155	9.4500
143	30	2a	0.740345	9.4500
143	31	2b	0.739880	9.2250
143	42	6	0.741275	9.4500
143	50	3a	0.741275	9.4500
143	51	3b	0.741275	9.4500
143	60	7	0.729635	9.7875
143	70	8	0.739415	9.4500
143	82	4a	0.739415	9.4500
143	83	4b	0.738480	9.4500
217	04	1	0.4740750	7.8000
217	11	5a	0.4814250	7.8000
217	12	5b	0.4817310	8.0000
217	22	2	0.4749935	7.8000

217	43	6a	0.4832625	8.0000
217	44	6b	0.4832625	8.0000
217	52	3	0.4753000	8.0000
217	61	7a	0.4820375	8.0000
217	62	7b	0.4820375	8.0000
217	71	8a	0.4838750	8.0000
217	72	8b	0.4838750	1000
217	84	4	0.4740750	7.6000
353	05	1	0.2921850	6.47500
353	13	2	14300	7.00000
353	23	3a	0.2891650	7.70000
353	24	3b	3535	7.52500
353	32	4a	0.2869000	7.35000
353	33	4b	0.2870890	7.39375
353	45	7	0.2876550	6.12500
353	53	5a	0.2936950	7.35000
353	54	5b	0.2936950	7.61250
353	63	6a	0.2929400	6.73750
353	64	6b	0.2925625	6.62500
353	85	8	0.2889765	6.73750
545	14	1	1000	3.600
545	34	2	0.3865875	3.525
545	55	3	0.3800065	3.525
545	73	4	0.3787875	3.525
857	25	1	0.2985	2.4
857	35	2	0.2985	2.4
857	65	3	0.2985	2.4
857	74	4	0.2985	2.4

### Optical Efficiency

The EFF tests involved exposing the HFI detectors to a known blackbody source and observing the response. Sufficient details for the HFI detector spectral transmission profiles are provided here while full details of the EFF experiments and results are provided in a separate technical report . A blackbody source internal to the Saturne cryostat was set to a variety of temperatures (  $\sim 1 - 6$  K) and the bolometer detector response was recorded. A bolometer model was applied to the recorded response in order to obtain the radiative optical power absorbed by the detector, in units of W, i.e.  $P_{\text{abs}}(T_i)$  where  $T_i$  represents the blackbody source temperature. Using the measured source temperature, the theoretical radiative optical power incident on the detector is also calculated using the Planck function. The ratio of the received power and the theoretical power provides the optical efficiency term. To remove any offsets in the measurement, a ratio of differences between unique temperature settings is used. The measured absorbed optical power difference is given by



where  $T_j$  and  $T_i$  represent two unique source temperature settings. The theoretical incident power is determined using the HFI detector spectral transmission profiles. Let  $\tau(\nu)$  represent the normalized detector transmission spectrum (i.e. it has been ratioed and had the waveguide model and filter data appropriately grafted). The spectral transmission is scaled for  $\lambda^2$  throughput and then re-normalized as follows

where  $\text{Norm}(f(x))$  is the division of  $f(x)$  by its maximum value, and  $c$  is the speed of light. The normalized spectral transmission is then used with the Planck function at the temperature setting to determine the theoretical power,  $P_{\text{th}}(T_i)$ , as follows

where  $h$  is the Planck constant,  $k$  is the Boltzmann constant, the integration limits are given by  $\nu_1$  and  $\nu_2$ , and  $n_m$  is the expected mode content of the frequency band. Table [tab:modes] lists the  $n_m$  values used for each band. In this case the integration is performed over the range  $\nu \in [67 \text{ GHz}, 1142 \text{ GHz}]$ . The difference between the theoretical power loading is given by

which allows the optical efficiency term to be determined as follows

Thus, if  $\epsilon\tau'(\nu)$  were used in Equation [eq:EFFPth] in place of  $\tau'(\nu)$ , the resultant optical efficiency would be unity, indicating that the transmission losses have already been taken into account.

The uncertainty estimate of the optical efficiency is statistically based on the results from the multiple temperature settings used in the EFF test sequences.

### Mode Content for the HFI detector bands.

Band (GHz)	100	143	217	353	545	857
$n_m$	1	1	1	1	3.4	8.3

### CO interpolation

The IAS FTS/Saturne data taken with the HFI detectors is limited to a spectral resolution of  $\sim 0.017 \text{ cm}^{-1}$  ( $\sim 0.5 \text{ GHz}$ ) by the mechanical travel of the FTS translation stage. This corresponds to an unapodized FTS ILS FWHM of  $\sim 0.020 \text{ cm}^{-1}$  ( $\sim 0.61 \text{ GHz}$ ). The previous iteration of the spectral transmission (IMO ver. 2\_28), in addition to a triangular apodization kernel, has a factor of 3 sub-sampled spectral resolution to improve the signal-to-noise ratio (S/N) of the output spectra. In light of the CO contribution to the 100 GHz spectra, the spectral transmission has been reprocessed at the original full spectral resolution with a different apodization function which provides better noise reduction and less spectral resolution degradation, as discussed above.

In order to provide an improved estimate of the spectral transmission near the CO features, an interpolation of the spectra by a factor of  $\sim 10$  has been performed. This over-sampling was accomplished by zero-padding the FTS interferograms prior to Fourier transformation, and subsequently incorporated into the Nyquist-sampled spectral data near the CO transitions (see Table [tab:CO]). Although the data are presented at higher resolution, the resolution of independent data points is not improved, i.e. the ILS line-width remains the same. A flag column has been added to the spectral transmission profile data files to indicate whether a given data point originates from the actual data, or is a result of the ILS-based interpolation. The region of the over-sampled, interpolated, data has been extended to also include other CO isotopes; the COJ1-0 – J9-8 transitions should be oversampled for CO, C  $^{13}\text{O}$ , CO  $^{17}$ , and CO  $^{18}$ . The original data points within the over-sampled region have been preserved (i.e. every tenth data point – the data point that is not an interpolated one – is flagged with a zero rather than a one), as is indicated by the data flag, so a flag filter on the data will restore the independent data points easily. Figure [fig:COflag] illustrates the regions where the over-sampling has been incorporated into the spectral transmission profiles. An example of the over-sampled spectra is shown in Figure [fig:COzoom100] for the 100 GHz detectors. Examples for the other detector bands are shown in §[sec:COappend]

**Regions of HFI spectral transmission profiles near CO transitions.**

Band (GHz)	CO transition ( $J_{Upper} - J_{Lower}$ )	$\nu_o$ (GHz)	over-sampled region (GHz)
100	1 – 0	115.2712018	109.67 – 115.39
143	1 – 0	115.2712018	109.67 – 115.39
143	2 – 1	230.5380000	219.34 – 230.77
217	2 – 1	230.5380000	219.34 – 230.77
353	3 – 2	345.7959899	329.00 – 346.15
545	4 – 3	461.0407682	438.64 – 461.51
545	5 – 4	576.2679305	548.28 – 576.85
857	6 – 5	691.4730763	657.89 – 692.17
857	7 – 6	806.6518060	767.48 – 807.46
857	8 – 7	921.7997000	877.04 – 922.73
857	9 – 8	1036.9123930	986.57 – 1037.95

**Spectral transmission for CO transitions for HFI detectors.**

BC	Det.	CO transition ( $J_{Upper} - J_{Lower}$ )	Transmission	
100	00	1a	1 – 0	$0.1495 \pm 0.0054$
100	01	1b	1 – 0	$0.1812 \pm 0.0052$
100	20	2a	1 – 0	$0.2577 \pm 0.0119$
100	21	2b	1 – 0	$0.1944 \pm 0.0086$
100	40	3a	1 – 0	$0.2798 \pm 0.0133$
100	41	3b	1 – 0	$0.1660 \pm 0.0093$
100	80	4a	1 – 0	$0.2538 \pm 0.0114$
100	81	4b	1 – 0	$2173 \pm 0.0105$
217	04	1	2 – 1	$0.3781 \pm 0.0026$
217	11	5a	2 – 1	$0.4530 \pm 0.0029$
217	12	5b	2 – 1	$0.4174 \pm 0.0030$
217	22	2	2 – 1	$0.3773 \pm 0.0026$
217	43	6a	2 – 1	$0.3149 \pm 0.0023$
217	44	6b	2 – 1	$0.3609 \pm 0.0030$
217	52	3	2 – 1	$0.3924 \pm 0.0025$
217	61	7a	2 – 1	$0.3428 \pm 0.0022$
217	62	7b	2 – 1	$0.2770 \pm 0.0017$
217	71	8a	2 – 1	$0.4623 \pm 0.0031$
217	72	8b	2 – 1	$0.4340 \pm 0.0031$
217	84	4	2 – 1	$0.3506 \pm 0.0025$
05	1	3 – 2	$0.4487 \pm 0.0036$	
353	13	2	3 – 2	$0.5461 \pm 0.0044$
353	23	3a	3 – 2	$0.3443 \pm 0.0030$

353	24	3b	3 – 2	0.4706 ± 0.0037
353	32	4a	3 – 2	0.3099 ± 0.0024
353	33	4b	3 – 2	0.2801 ± 0.0027
353	45	7	3 – 2	0.2923 ± 0.0022
353	53	5a	3 – 2	0.3150 ± 0.0024
353	54	5b	3 – 2	0.3181 ± 0.0023
353	63	6a	3 – 2	0.2059 ± 0.0014
353	64	6b	3 – 2	0.2113 ± 0.0017
353	85	8	3 – 2	0.3509 ± 0.0028
545	14	1	4 – 3	0.0747 ± 0.0003
545	34	2	4 – 3	0.0731 ± 0.0003
545	55	3	4 – 3	0.0521 ± 0.0002
545	73	4	4 – 3	0.0473 ± 0.0002
545	14	1	5 – 4	0.3306 ± 0.0012
545	34	2	5 – 4	0.3183 ± 0.0011
545	55	3	5 – 4	0.2428 ± 0.0009
545	73	4	5 – 4	0.2597 ± 0.0009
857	25	1	6 – 5	0.0280 ± 0.0001
857	35	2	6 – 5	0.0241 ± 0.0001
857	65	3	6 – 5	0.0292 ± 0.0001
857	74	4	6 – 5	0.0159 ± 0.0001
857	25	1	7 – 6	0.1636 ± 0.0005
857	35	2	7 – 6	0.1427 ± 0.0004
857	65	3	7 – 6	2176 ± 0.0007
857	74	4	7 – 6	0.1168 ± 0.0003
857	25	1	8 – 7	0.2554 ± 0.0009
857	35	2	8 – 7	0.2218 ± 0.0007
857	65	3	8 – 7	0.2744 ± 0.0009
857	74	4	8 – 7	0.1119 ± 0.0004
857	25	1	9 – 8	0.0053 ± 0.0000
857	35	2	9 – 8	0.0060 ± 0.0000
857	65	3	9 – 8	0.0085 ± 0.0000
857	74	4	9 – 8	0.0001 ± 0.0000

## Conformity with requirements

The two defining requirements indicated in the HFI calibration plan are the acquisition of the spectral transmission of the single pixels with a prescribed accuracy and spectral resolution. The desired accuracy is 3% for the low frequency channels (CMB – 100, 143, and 217 GHz) and 1% for the high frequency channels (353, 545, 857 GHz). The spectral resolution requirement is for a resolution superior to  $0.1 \text{ cm}^{-1}$ .

The spectral resolution requirement has been exceeded by more than a factor of five. It is also possible to degrade the spectral resolution to the  $0.1 \text{ cm}^{-1}$  requirement to gain an improvement in the S/N.

No quantitative number is present on the document regarding the blocking of high frequency (near IR, visible, UV) radiation outside the range of the instrument. Checks in order to quantify the rejection have been performed at subsystem level and estimates of the out-of-band transmission profiles have been incorporated into the data products.

The requirement on the spectral transmission accuracy for the CMB channels is of 3%. There is also a requirement that the high frequency channels effective frequencies be known to within 1%; knowledge of the transmission to 1% accuracy should allow this.

Considering statistical fluctuations in the determination of the spectra, these goals have been achieved. There are, however, caveats regarding the nature of error bars when dealing with frequency space. The nature of uncertainties in spectra determination is less obvious than when dealing with timestream data. Systematic effects produced from instrumental setup, but also by data reduction can in some cases exceed the actual statistical oscillation in the determination of the final spectra. This is the case for the high-frequency data for instance where the statistical fluctuation of the different determinations of the spectra in some case are better than 1 part in  $10^3$ .

A second caveat regards the method of data analysis of the calibration test data, for which the ratio with the reference bolometer data (of which the relative error is a function of frequency) introduces an error that increase with wavelength. With the spectral resolution of the data provided being much higher than the stated  $0.1 \text{ cm}^{-1}$ , the transmission accuracy requirement is not met for the 100 GHz detectors. It is possible to degrade the spectral resolution to the  $0.1 \text{ cm}^{-1}$  level to allow the accuracy to achieve the required level, but the higher spectral resolution data has been provided to better assist with the CO contamination removal from the 100 GHz signal.

## Detection chain

(Francesco Piacentini)

### Bolometers

The heart of the HFI - the detectors - are bolometers, solid-state devices in which the incoming radiation dissipates its energy as heat that increases the temperature of a thermometer. The instrument Flight Model total number of bolometers is 52, split into 6 channels at central frequencies of 100, 143, 217, 353, 545, and 857GHz. Two extra bolometers not optically coupled to the telescope are added to the focal plane to monitor thermal noise (Dark Bolometers).

Thirty two of these bolometers are polarization sensitive allowing a map of the CMB polarisation to be built.

Bolometers consist of (i) an absorber that transforms the in-coming radiation into heat; (ii) a thermometer that is thermally linked to the absorber and measures the temperature changes; and (iii) a weak thermal link to a thermal sink, to which the bolometer is attached.

The detectors are semi-conducting NTD thermistor bolometers. There are two kinds of detector modules:

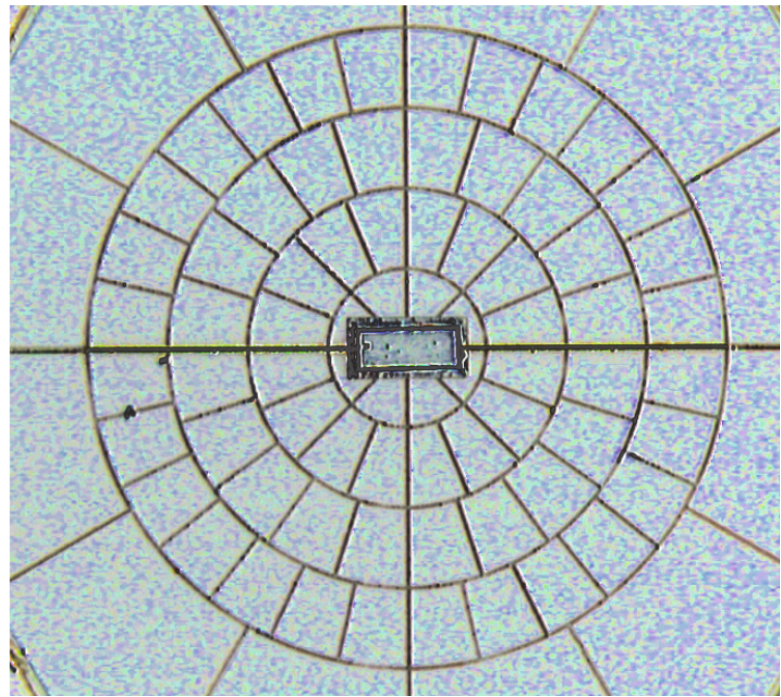
- SWB, spider web bolometers, are mounted on an absorbing spider-web of metallised silicon nitride
- PSB, polarization sensitive bolometers, are mounted on a parallel absorbing grid of metallised silicon nitride.

In the spider-web bolometers, or SWBs (Bock et al. 1995; Mouskops et al. 1997), the absorbers consist of metallic grids deposited on a Si<sub>3</sub>N<sub>4</sub> substrate in the shape of a spider web. The mesh design and the impedance of the

metallic layer are adjusted to match vacuum impedance and maximize the absorption of millimeter waves, while minimizing the cross section to particles. The absorber is designed to offer equal impedance to any linearly polarised radiation. Nevertheless, the thermometer and its electrical leads define a privileged orientation (Fig. SWB) that makes the SWBs slightly sensitive to polarisation, as detailed in (Rosset et al. 2010). The thermometers are made of neutron transmuted doped (NTD) germanium (Haller et al. 1996), chosen to have an impedance of about  $10\text{ M}\Omega$  at their operating temperature.

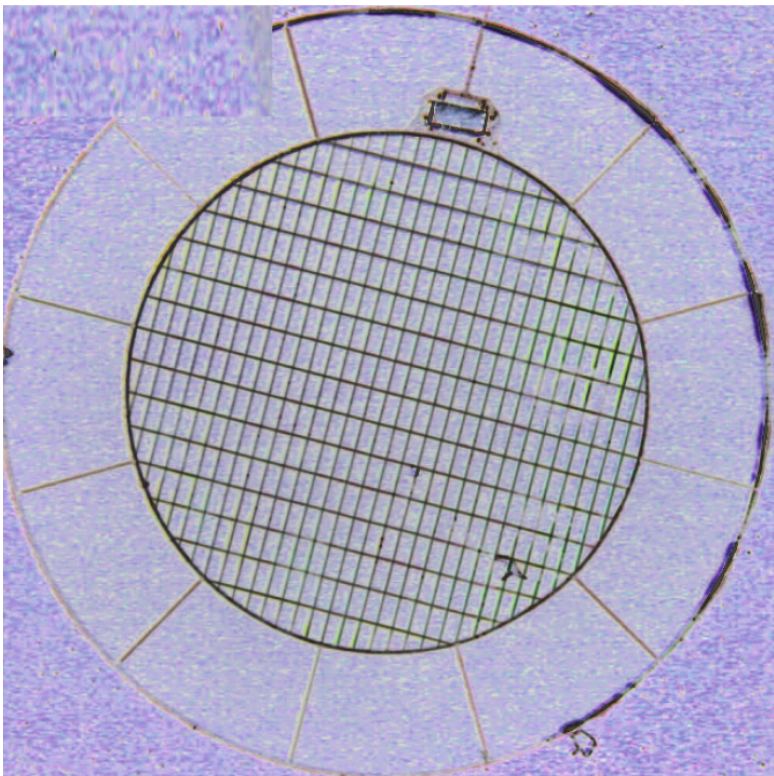
The absorber of PSBs is a rectangular grid (Fig. PSB) with metallization in one direction (Jones et al. 2003). Electrical fields parallel to this direction develop currents and then deposit some power in the grid, while perpendicular electrical fields propagate through the grid without significant interaction. A second PSB perpendicular to the first one absorbs the other polarisation. Such a PSB pair measures two polarisations of radiation collected by the same horns and filtered by the same devices, which minimises the systematic effects: differences between polarised beams collected by a given horn are typically less than  $-30\text{ dB}$  of the peak. The differences in the spectral responses of a PSB pair also proved to be a few percent in the worst case. Each pair of

PSBs sharing the same horn is able to measure the intensity Stokes parameter and the Q parameter associated with its local frame. An associated pair of PSBs rotated by  $45^\circ$  scans exactly the same line (if the geometrical alignment is perfect), providing the U Stokes parameter.



Picture of a spider web bolometer. This a 143 GHz module, The temperature sensor is at the center of the absorbing grid

The detectors operate at a temperature close to 100 mK, while the filters are distributed on the 100mK, 1.6 K, and 4 K stages in such a way that the heat load on the coldest stages is minimized to limit the heat load on the detectors and to decrease the heat lift requirement and thus enhance the mission lifetime. The self-emission of the 4K stage is minimised to limit the photon noise contribution on the detectors from the instrument. The HFI Focal Plane Unit accommodates sub-millimeter absorbing material in order to decrease the scattering inside it.



Picture of a polarization sensitive bolometer. This a 217 GHz module, The temperature sensor is at the an edge of the absorbing grid

Focal plane layout

The layout of the detectors in the focal plane is defined to cope with the scanning strategy. The HFI horns are positioned at the centre of the focal plane, where the optical quality is good enough for the high frequencies. The curvature of rows compensates for the distortion of images by the telescope. A pair of identical SWB will scan the same circle on the sky to provide additional redundancy. Similar horns feeding PSBs are also aligned so that two pairs of PSBs rotated by 45 ° with respect to each other scan the same line.

This will provide the Q and U Stokes parameters with minimal correction for the pointing (Rosset et al. 2010). Residual systematics will come from the differences between the beam shapes of the two horns. In all cases except for the 100 GHz horns, a measurement is also done by a pair of similar channels shifted by 1.25 arcminutes in the cross-scan direction, to ensure adequate sampling. In the figures focal plane layout is reported.

Table 1. The HFI receivers.

Band	$\nu_{center}$ [GHz]	Bandwidth [%]	Number of bolometers
100P .....	100	33	8
143P .....	143	32	8
143 .....	143	30	4
217P .....	217	29	8
217 .....	217	33	4
353P .....	353	29	8
353 .....	353	28	4
545 .....	545	31	4
857 .....	857	30	4

Notes. The “P” identifies the polarisation sensitive bolometers.

to be change into a real table



## Readout

The AC bias readout electronics of the HFI instrument (Gaertner et al. 1997) includes a number of original features proposed by several laboratories (CRTBT in Grenoble, CESR in Toulouse and IAS in Orsay), which were validated on the Diabolo experiment and on the balloon-borne Archeops experiment. It was developed for space by the CESR in Toulouse.

The particular features of the HFI AC bias readout are mainly

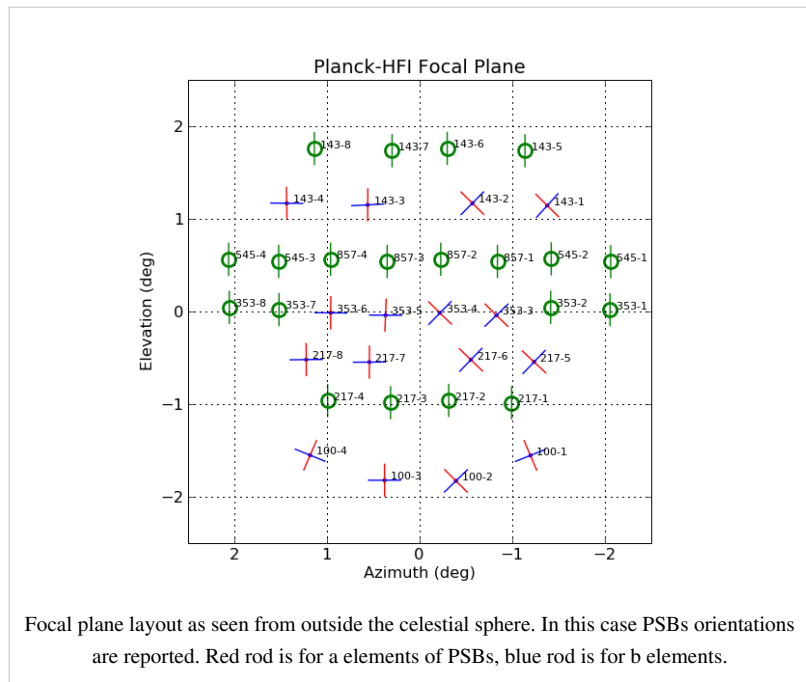
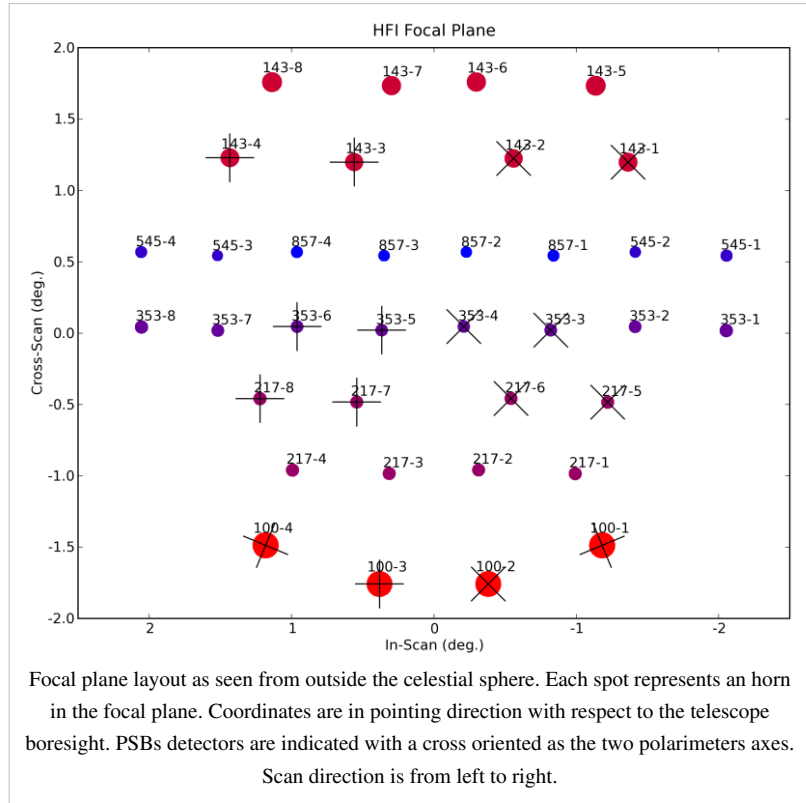
- i) that the cold load resistors were replaced by capacitors because they have no Johnson noise;
- ii) that the detectors are biased by applying a triangular voltage to the load capacitors

which produces a square current [I<sub>bias</sub>] in the capacitors, and a square voltage [T<sub>bias</sub>] that compensates for the stray capacitance of the wiring (producing a nearly square bias current into the bolometer);

- iii) that a square offset compensation signal is subtracted to the bolometric signal to minimise the amplitude of the signal that has to be amplified and digitized;
- iv) that the electronic scheme is symmetrical and uses a differential amplification scheme to optimize the immunity to electromagnetic interferences;
- v) and finally that every parameter of the REU can be set by commands, which

is made possible by using digital-to-analog and analog-to-digital converters extensively.

The readout electronics consist of 72 channels designed to perform low noise measurements of the impedance of 52 bolometers, two blind bolometers, 16 accurate low temperature thermometers, all in the 10 MΩ range, one resistor of 10 MΩ and one capacitor of 100 pF. The semiconductor bolometers and thermometers of Planck-HFI operate at



cryogenic temperature around 100 mK on the focal plane, with impedance of about 10 M $\Omega$  when biased at the optimal current. The readout electronics on the contrary have to operate at “room” temperature (300 K). The distance between the two extremities of the readout chain is about 10 m and could represent a point of extreme susceptibility to electromagnetic interference. The readout electronic chain was split into three boxes. These are the JFET box, located on the 50 K stage of the satellite at 2.2 m from the focal plane, the pre-amplifier unit (PAU), located 1.8m further at 300 K, and the REU, located on the opposite side of the satellite, 5 m away. Each of the three boxes (JFET, PAU and REU) consists of 12 belts of six channels. The first nine belts are dedicated to the bolometers, and the three last ones to the accurate thermometers, the resistor and the capacitor (see figure Organization of the HFI readout).

## Principles of the readout electronics.

See figure [Principles of readout electronics]. The bolometer is biased by a square wave AC current obtained by the differentiation of a triangular voltage through a load capacitance, in a completely differential architecture. The presence of the stray capacitance due to losses of charge in the wiring requires a correction of the shape of the square bias current by a transient voltage. Thus the bias voltage generation is controlled by the two parameters I-bias and T-bias that express the amplitude of the triangular and transient voltage. The compensation voltage added to the bolometric signal to optimize the dynamic of the chain is controlled by the V-bal parameter.

Parameters of the Readout Unit can be set to optimize the detectors performance.

The modulation frequency of the AC bias system,  $f_{\text{mod}}$  of the square bias current can be tuned from 70 Hz to 112 Hz by the telecommand parameters: Nsample, which defines the number of samples per half period of modulated signal, fdv which determines the sampling frequency of the ADC.

The optimal frequencies are around 90 Hz.

Each channel has its own settings for the following parameters: I-bias, amplitude of the triangular bias voltage;

T-bias, amplitude of the transient bias voltage;

V-bal, amplitude of the square compensation voltage;

G-amp, value of the programmable gain of the REU [1/3, 1, 3, 7.6];

N-blank, number of blanked samples at the beginning of halfperiod not taken into account during integration of the signal;

S-phase, phase shift when computing the integrated signal.

All these parameters influence the effective response of the detection chains, and were optimized during the calibration campaigns and confirmed during the calibration and performance verification (CPV) phase following the launch of Planck. The scientific signal is provided by the integral of the signal on each half-period, between limits fixed by the S-phase and N-blank parameters.

Nbelt / Nchannel	0	1	2	3	4	5
0	100-1a	100-1b	143-1a	143-1b	217-1	353-1
1	143-5	217-5a	217-5b	353-2	545-1	Dark 1
2	100-2a	100-2b	217-2	353-3a	353-3b	857-1
3	143-2a	143-2b	353-4a	353-4b	545-2	857-2
4	100-3a	100-3b	143-6	217-6a	217-6b	353-7
5	143-3a	143-3b	217-3	353-5a	353-5b	545-3
6	143-7	217-7a	217-7b	353-6a	353-6b	857-3
7	143-8	217-8a	217-8b	545-4	857-4	Dark 2
8	100-4a	100-4b	143-4a	143-4b	217-4	353-8
9	Ther_0.1K 1	Ther_PID2 N	Ther_PID1 N	Ther_PID1.6 N	Ther_1.6K 1	Ther_PID4 N
10	Resistor	Capa 2	Ther_0.1K 2	Ther_PID1.6 R	Ther_4KH 1	Ther_4KL 1
11	Ther_PID2 R	Ther_PID1 R	Ther_1.6K 2	Ther_PID4 R	Ther_4KH 2	Ther_4KL 2

Organization of the HFI readout. Each row represents a belt. Each belt has 6 channels. (to be change into a real table ?)



The interaction of modulated readout electronics with semiconductor bolometers is rather different from that of a classical DC bias readout (Jones 1953). The differences were seen during the calibration of the HFI, although the readout electronics was designed to mimic the operation of a DC biased bolometric system as far as possible. With the AC readout the maximum of responsivity is lower and is obtained for higher bias current in the bolometer with respect to the DC model. This is caused by the stray capacitance in the wiring which has negligible effects for a DC bias and a major effect for an AC bias. In our case, a stray capacitance of 150 pF induces increases of NEP ranging from 4% (857 GHz bolometers) to 10% (100 GHz bolometers) and also affects the HFI time response. Details of the effect of the HFI AC bias system into the time response of the detectors are discussed in the Time Response <sup>[4]</sup> Section.

## JFETs

Given the high impedance of the bolometers and the length of the connecting cables, it is essential that the impedance of the signal is lowered as close as possible to the detectors. In our system this is accomplished by means of JFET source followers, located in boxes connected to the 50 K stage. The JFET box has been designed, developed and tested in the Observational Cosmology group in the Physics Department of the University of Rome "La Sapienza" (Brienza D. et al 2006). There are two JFETs per channel, since the readout is fully differential, and they provide a current amplification of the signal while keeping the voltage amplification very close to unity.

Inside the box, the JFETs are mounted on a thermally insulated plate with an active temperature control to keep them at the optimal temperature of 110 K. With a dissipated power lower than 240 mW, mainly produced by the JFETs and the source resistors, we obtained a noise power spectral density of less than 3 nV Hz<sup>1/2</sup> for the frequency range of interest. This increases the total noise of all bolometer channels by less than 5%.

## Data compression

The output of the readout electronics unit (REU) consists of one value for each of the 72 science channels for each half-period of modulation. This number,  $S_{REU}$ , is the sum of the 40 16-bit ADC signal values obtained within the given half-period. The data processor unit (DPU) performs a lossy quantization of  $S_{REU}$ .

We define a compression slice of 254  $S_{REU}$  values, corresponding to about 1.4 s of observation for each detector and to a strip of sky about 8 degrees long. The mean  $\langle S_{REU} \rangle$  of the data within each compression slice is computed, and data are demodulated using this mean:

where  $1 < i < 254$  is the running index within the compression slice.

The mean  $\langle S_{demod} \rangle$  of the demodulated data  $S_{demod,i}$  is computed and subtracted, and the resulting data slice is quantized according to a step size  $Q$  that is fixed per detector:

This is the lossy part of the algorithm: the required compression factor, obtained through the tuning of the quantization step  $Q$ , adds a measure of noise to the data. Assuming Gaussian white noise with standard deviation  $\sigma$ , a quantization setting of  $\sigma/Q = 2$  adds 1% to the noise (Pajot et al. 2010; Pratt 1978). The value of  $\sigma$  was determined at the end of the CPV phase after subtraction of the signal from the timeline.

The two means  $\langle S_{REU} \rangle$  and  $\langle S_{demod} \rangle$  are computed as 32-bit words and sent through the telemetry, together with the  $S_{DPU,i}$  values. Variable-length encoding of the  $S_{DPU,i}$  values is performed on board, and the inverse decoding is applied on ground.

Optimal use of the bandpass available for the downlink (75 kb/s average for HFI science) was obtained initially by using a value of  $Q = \sigma/2.5$  for all bolometer signals. After 12 December 2009, only for the 857 GHz detectors, the value was reset to  $Q = \sigma/2.0$  to avoid data loss due to exceeding the limit of downlink rate.

## Time\_response

The HFI bolometers and readout electronics have a finite response time to changes in incident optical power. The bolometers are thermal detectors of radiation whose response time is determined by the thermal circuit defined by the heat capacity of the detector and thermal conductivity.

Due to Planck's nearly constant scan rate, the time response is degenerate with the optical beam. However, because of the long time scale effects present in the time response, the time response is deconvolved from the data in the processing of the HFI data (see TOI processing).

The time response of the HFI bolometers and readout electronics is modeled as a Fourier domain transfer function (called the LFER4 model) consisting of the product of an bolometer thermal response  $F(\omega)$  and an electronics response  $H'(\omega)$ .

## LFER4 model

If we write the input signal (power) on a bolometer as the bolometer physical impedance can be written as: where  $\omega$  is the angular frequency of the signal and  $F(\omega)$  is the complex intrinsic bolometer transfer function. For HFI the bolometer transfer function is modelled as the sum of 4 single pole low pass filters: The modulation of the signal is done with a square wave, written here as a composition of sine waves of decreasing amplitude: where we have used the Euler relation  $\sin x = (e^{ix} - e^{-ix})/2i$  and  $\omega_r$  is the angular frequency of the square wave. The modulation frequency is  $f_{mod} = \omega_r/2\pi$  and was set to  $f_{mod} = 90.18759\text{Hz}$  in flight. This signal is then filtered by the complex electronic transfer function  $H(\omega)$ . Setting:  $\omega_k^+ = \omega + (2k+1)\omega_r$ ,  $\omega_k^- = \omega - (2k+1)\omega_r$  we have: This signal is then sampled at high frequency ( $2f_{mod}NS$ ).  $NS$  is one of the parameters of the HFI electronics and corresponds to the number of high frequency samples in each modulation semi-period. In order to obtain an output signal sampled every  $\pi/\omega_r$  seconds, we must integrate on a semiperiod, as done in the HFI readout. To also include a time shift  $\Delta t$ , the integral is calculated between  $n\pi/\omega_r + \Delta t$  and  $(n+1)\pi/\omega_r + \Delta t$  (with  $T = 2\pi/\omega_r$  period of the modulation). The time shift  $\Delta t$  is encoded in the HFI electronics by the parameter  $S_{phase}$ , with the relation  $\Delta t = S_{phase}/NS/f_{mod}$ .

After integration, the  $n$ -sample of a bolometer can be written as where

The output signal in equation eqn:output can be demodulated (thus removing the  $(-1)^n$ ) and compared to the input signal in equation bol\_in. The overall transfer function is composed of the bolometer transfer function and the effective electronics transfer function,  $H'(\omega)$ :  $TF(\omega) = F(\omega)H'(\omega)$

The shape of  $H(\omega)$  is obtained combining low and high-pass filters with Sallen Key topologies (with their respective time constants) and accounting also for the stray capacitance low pass filter given by the bolometer impedance combined with the stray capacitance of the cables. The sequence of filters that define the electronic band-pass function  $H(\omega) = h_0 * h_1 * h_2 * h_3 * h_4 * h_5$  are listed in table:readout\_electronics\_filters.

## Parameters of LFER4 model

The LFER4 model has a total of 10 parameters ( $A_1, A_2, A_3, A_4, \tau_1, \tau_2, \tau_3, \tau_4, S_{phase}, \tau_{stray}$ ) 9 of which are independent, for each bolometer. The free parameters of the LFER4 model are determined using in-flight data in the following ways:

- $S_{phase}$  is fixed at the value of the REU setting.
- $\tau_{stray}$  is measured during the QEC test during CPV.
- $A_1, \tau_1, A_2, \tau_2$  are fit forcing the compactness of the scanning beam.
- $A_3, \tau_3, A_4, \tau_4$  are fit by forcing agreement of survey 2 and survey 1 maps.
- The overall normalization of the LFER4 model is forced to be 1.0 at the signal frequency of the dipole.

The details of determining the model parameters are given in (reference P03c paper) and the best-fit parameters listed here in table:LFER4pars.

## HFI electronics filter sequence

HFI electronics filter sequence. We define  $s = i \omega$

Filter	Parameters	Function
0. Stray capacitance low pass filter	$\tau_{stray} = R_{bolo} C_{stray}$	$h_0 = \frac{1}{1.0 + \tau_{stray} * s}$
1. Low pass filter	$R_1 = 1_k \Omega$ $C_1 = 100_{nF}$	$h_1 = \frac{2.0 + R_1 * C_1 * s}{2.0 * (1.0 + R_1 * C_1 * s)}$
2. Sallen Key high pass filter	$R_2 = 51_k \Omega$ $C_2 = 1_{\mu}$	$h_2 = \frac{(R_2 * C_2 * s)^2}{(1.0 + R_2 * C_2 * s)^2}$
3. Sign reverse with gain		$h_3 = -5.1$
4. Single pole low pass filter with gain	$R_4 = 10_k \Omega$ $C_4 = 10_{nF}$	$h_4 = \frac{1.5}{1.0 + R_4 * C_4 * s}$
5. Single pole high pass filter coupled to a Sallen Key low pass filter	$R_9 = 18.7_k \Omega$ $R_{12} = 37.4_k \Omega$ $C = 10.0_{nF}$ $R_{78} = 510_k \Omega$ $C_{18} = 1.0_{\mu F}$ $K_3 = R_9^2 * R_{78} * R_{12}^2 * C^2 * C_{18}$ $K_2 = R_9 * R_{12}^2 * R_{78} * C^2 + R_9^2 * R_{12}^2 * C^2 + R_9 * R_{12}^2 * R_{78} * C_{18} * C$ $K_1 = R_9 * R_{12}^2 * C + R_{12} * R_{78} * R_9 * C_{18}$	$h_5 = \frac{2.0 * R_{12} * R_9 * R_{78} * C_{18} * s}{s^3 * K_3 + s^2 * K_2 + s * K_1 + R_{12} * R_9}$

## Parameters for LFER4 model.

Bolometer	$A_1$	$\tau_1(s)$	$A_2$	$\tau_2(s)$	$A_3$	$\tau_3(s)$	$A_4$	$\tau_4(s)$	$\tau_{stray}(s)$	$S_{phase}(s)$
100-1a	0.392	0.01	0.534	0.0209	0.0656	0.0513	0.00833	0.572	0.00159	0.00139
100-1b	0.484	0.0103	0.463	0.0192	0.0451	0.0714	0.00808	0.594	0.00149	0.00139
100-2a	0.474	0.00684	0.421	0.0136	0.0942	0.0376	0.0106	0.346	0.00132	0.00125
100-2b	0.126	0.00584	0.717	0.0151	0.142	0.0351	0.0145	0.293	0.00138	0.00125
100-3a	0.744	0.00539	0.223	0.0147	0.0262	0.0586	0.00636	0.907	0.00142	0.00125
100-3b	0.608	0.00548	0.352	0.0155	0.0321	0.0636	0.00821	0.504	0.00166	0.00125
100-4a	0.411	0.0082	0.514	0.0178	0.0581	0.0579	0.0168	0.37	0.00125	0.00125
100-4b	0.687	0.0113	0.282	0.0243	0.0218	0.062	0.00875	0.431	0.00138	0.00139
143-1a	0.817	0.00447	0.144	0.0121	0.0293	0.0387	0.0101	0.472	0.00142	0.00125
143-1b	0.49	0.00472	0.333	0.0156	0.134	0.0481	0.0435	0.27	0.00149	0.00125
143-2a	0.909	0.0047	0.0763	0.017	0.00634	0.1	0.00871	0.363	0.00148	0.00125
143-2b	0.912	0.00524	0.0509	0.0167	0.0244	0.0265	0.0123	0.295	0.00146	0.00125
143-3a	0.681	0.00419	0.273	0.00956	0.0345	0.0348	0.0115	0.317	0.00145	0.00125
143-3b	0.82	0.00448	0.131	0.0132	0.0354	0.0351	0.0133	0.283	0.00161	0.000832

143-4a	0.914	0.00569	0.072	0.0189	0.00602	0.0482	0.00756	0.225	0.00159	0.00125
143-4b	0.428	0.00606	0.508	0.00606	0.0554	0.0227	0.00882	0.084	0.00182	0.00125
143-5	0.491	0.00664	0.397	0.00664	0.0962	0.0264	0.0156	0.336	0.00202	0.00139
143-6	0.518	0.00551	0.409	0.00551	0.0614	0.0266	0.0116	0.314	0.00153	0.00111
143-7	0.414	0.00543	0.562	0.00543	0.0185	0.0449	0.00545	0.314	0.00186	0.00139
217-5a	0.905	0.00669	0.0797	0.0216	0.00585	0.0658	0.00986	0.342	0.00157	0.00111
217-5b	0.925	0.00576	0.061	0.018	0.00513	0.0656	0.0094	0.287	0.00187	0.00125
217-6a	0.844	0.00645	0.0675	0.0197	0.0737	0.0316	0.0147	0.297	0.00154	0.00125
217-6b	0.284	0.00623	0.666	0.00623	0.0384	0.024	0.0117	0.15	0.00146	0.00111
217-7a	0.343	0.00548	0.574	0.00548	0.0717	0.023	0.0107	0.32	0.00152	0.00139
217-7b	0.846	0.00507	0.127	0.0144	0.0131	0.0479	0.0133	0.311	0.00151	0.00139
217-8a	0.496	0.00722	0.439	0.00722	0.0521	0.0325	0.0128	0.382	0.00179	0.00111
217-8b	0.512	0.00703	0.41	0.00703	0.0639	0.0272	0.0139	0.232	0.00173	0.00125
217-1	0.0136	0.00346	0.956	0.00346	0.0271	0.0233	0.00359	1.98	0.00159	0.00111
217-2	0.978	0.00352	0.014	0.0261	0.00614	0.042	0.00194	0.686	0.0016	0.00125
217-3	0.932	0.00355	0.0336	0.00355	0.0292	0.0324	0.00491	0.279	0.00174	0.00125
217-4	0.658	0.00135	0.32	0.00555	0.0174	0.0268	0.00424	0.473	0.00171	0.00111
353-3a	0.554	0.00704	0.36	0.00704	0.0699	0.0305	0.0163	0.344	0.0017	0.00125
353-3b	0.219	0.00268	0.671	0.00695	0.0977	0.0238	0.0119	0.289	0.00157	0.00111
353-4a	0.768	0.00473	0.198	0.00993	0.0283	0.0505	0.00628	0.536	0.00181	0.00125
353-4b	0.684	0.00454	0.224	0.0108	0.0774	0.08	0.0149	0.267	0.00166	0.00111
353-5a	0.767	0.00596	0.159	0.0124	0.0628	0.0303	0.0109	0.357	0.00156	0.00111
353-5b	0.832	0.00619	0.126	0.0111	0.0324	0.035	0.0096	0.397	0.00166	0.00111
353-6a	0.0487	0.00176	0.855	0.006	0.0856	0.0216	0.0105	0.222	0.00199	0.00125
353-6b	0.829	0.00561	0.127	0.00561	0.0373	0.0252	0.00696	0.36	0.00228	0.00111
353-1	0.41	0.000743	0.502	0.00422	0.0811	0.0177	0.0063	0.329	0.00132	0.00097
353-2	0.747	0.00309	0.225	0.00726	0.0252	0.0447	0.00267	0.513	0.00154	0.00097
353-7	0.448	0.0009	0.537	0.0041	0.0122	0.0273	0.00346	0.433	0.00178	0.00125
353-8	0.718	0.00223	0.261	0.00608	0.0165	0.038	0.00408	0.268	0.00177	0.00111
545-1	0.991	0.00293	0.00743	0.026	0.00139	2.6	0	0	0.00216	0.00111
545-2	0.985	0.00277	0.0128	0.024	0.00246	2.8	0	0	0.00187	0.00097
545-4	0.972	0.003	0.0277	0.025	0.000777	2.5	0	0	0.00222	0.00111
857-1	0.974	0.00338	0.0229	0.025	0.00349	2.2	0	0	0.00176	0.00111
857-2	0.84	0.00148	0.158	0.00656	0.00249	3.2	0	0	0.0022	0.00125
857-3	0.36	4.22e-05	0.627	0.0024	0.0111	0.017	0.002	1.9	0.00152	0.00126
857-4	0.278	0.0004	0.719	0.00392	0.00162	0.09	0.00152	0.8	0.00149	0.000558

## System (Ken)

### List of systematics

Like all experiments, Planck/HFI had a number of "issues" which it needed to track and verify were not compromising the data. While these are discussed in appropriate sections, here we gather them together to give brief summaries of the issues and refer the reader to the appropriate section for more details.

- Cosmic Rays - Unprotected by the atmosphere and more sensitive than previous bolometric experiment, HFI was subjected to many more cosmic ray hits than previous experiments. These were detected, the worst parts of the data flagged as unusable, and "tails" were modeled and removed. This is described in XXXXX
- Elephants - Cosmic rays also hit the 100 mK stage and cause the temperature to vary, inducing small temperature and thus noise variations in the detectors. This is described in XXXXX
- 1.6 K Stage Fluctuations
- 4 K Stage Fluctuations
- Popcorn Noise - Some channels were occasionally affected by what seems to be a "split-level" noise, which has been variously called popcorn noise or random telegraphic signal. These data are usually flagged. This is described in XXXXX
- Jumps - Similar to but distinct from popcorn noise, small jumps were occasionally found in the data streams. These data are usually corrected. This is described in XXXXX.
- 4 K Cooler-Induced EM Noise - The 4 K cooler induced noise in the detectors with very specific frequency signatures, which is filtered. This is described in XXXXX.
- 4 K Cooler-Induced Microphonics - The mechanical cooler was shown in XXXXX to cause very little microphonic parasites in the detector data.
- Pointing-Change Microphonics - The changes in pointing after each pointing period were shown in XXXXX to cause very little microphonic parasitic signal in the detector data.
- Compression - Onboard compression is used to overcome our telemetry bandwidth limitations. This is explained in XXXXX.
- Noise Correlations - Correlations in noise between detectors seems to be negligible but for two polarization sensitive detectors in the same horn. This is discussed in XXXXX.
- Electrical Cross-Talk - Cross-talk is discussed in XXXXX.
- Pointing - The final pointing reconstruction for Planck is near the arcsecond level. This is discussed in XXXXX.
- Focal Plane Geometry - The relative positions of different horns in the focal plane is reconstructed using planets. This is discussed in XXXXX.
- Main Beam - The main beams for HFI are discussed in XXXXX.
- Ruze Envelope - Random imperfections or dust on the mirrors can increase the size of the beam a bit. This is discussed in XXXXX.
- Dimpling - The mirror support structure causes a pattern of small imperfections in the beams, which cause small sidelobe responses outside the main beam. This is discussed in XXXXX.
- Far Sidelobes - Small amounts of light can sometimes hit the detectors from just above the primary or secondary mirrors, or even from reflecting off the baffles. While small, when the Galactic center is in the right position, this can be detected in the highest frequency channels, so this is removed from the data. This is discussed in XXXXX.
- Planet Fluxes - Comparing the known fluxes of planets with the calibration on the CMB dipole is a useful check of calibration. This is done in XXXXX.
- Point Source Fluxes - As with planet fluxes, we also compare fluxes of known, bright point sources with the CMB dipole calibration. This is done in XXXXX.
- Time Constants - The HFI bolometers do not react instantaneously to light; there are small time constants, discussed XXXXX.

- ADC Correction - The HFI Analog-to-Digital Converters are not perfect, and are not used perfectly. Their effects on the calibration are discussed in XXXXX.
- Gain changes with Temperature Changes
- Optical Cross-Talk - This is discussed in XXXXX.
- Bandpass - The transmission curves, or "bandpass" has shown up in a number of places. This is discussed in XXXXX and YYYYY.
- Saturation - While this is mostly an issue only for Jupiter observations, it should be remembered that the HFI detectors cannot observe arbitrarily bright objects. This is discussed in XXXXX.

## Summary

(Lamarre) here remind worse sytematics and point to DPC Summary of sucess and limitations. JML. Link to early HFI in flight perf.

## References

- [1] [http://www.rssd.esa.int/livelink/fetch/-60063/3036676/3065909/3110897/3135828/3135852/PE\\_paper2.pdf#page=7](http://www.rssd.esa.int/livelink/fetch/-60063/3036676/3065909/3110897/3135828/3135852/PE_paper2.pdf#page=7)
- [2] [http://www.rssd.esa.int/livelink/fetch/-60063/3036676/3065909/3110897/3135828/3135852/PE\\_paper2.pdf#page=23](http://www.rssd.esa.int/livelink/fetch/-60063/3036676/3065909/3110897/3135828/3135852/PE_paper2.pdf#page=23)
- [3] [http://www.rssd.esa.int/livelink/fetch/-60063/3036676/3065909/3110897/3135828/3135852/PE\\_paper2.pdf#page=21](http://www.rssd.esa.int/livelink/fetch/-60063/3036676/3065909/3110897/3135828/3135852/PE_paper2.pdf#page=21)
- [4] [http://www.sciops.esa.int/wikiSI/planckpla/index.php?title=HFI\\_design,\\_qualification,\\_and\\_performance&instance=Planck\\_PLA\\_ES#Time\\_responsel](http://www.sciops.esa.int/wikiSI/planckpla/index.php?title=HFI_design,_qualification,_and_performance&instance=Planck_PLA_ES#Time_responsel)

# LFI design, qualification, and performance

---

## Overview

The Planck-LFI instrument is an array of 11 radiometric receivers in the Ka, Q and V bands, with centre frequencies close to 30, 44 and 70 GHz. The exact centre frequencies for each receiver are reported in [A. Mennella, M. Bersanelli, R. C. Butler et al. Planck early results. III. First assessment of the Low Frequency Instrument in-flight performance. A&A, 536:A3, 2011]; for simplicity, here we will refer to the three channels using their nominal centre frequency. A detailed description of the LFI instrument is given in [M. Bersanelli, N. Mandolesi, R. C. Butler et al. Planck pre-launch status: Design and description of the Low Frequency Instrument. A&A, 520:A4, 2010], and references therein.

## The LFI description

The LFI instrument (see Figure 1 below) consists of a 20 K focal plane unit hosting the corrugated feed horns, the orthomode transducers (OMTs) and the receiver front-end modules (FEMs). Fourty four composite waveguides [O. D'Arcangelo, L. Figini, A. Simonetto et al. The Planck-LFI flight model composite waveguides. Journal of Instrumentation, 4:2007, 2009] are interfaced with three conical thermal shields and connect the front-end modules to the warm (~300 K) back-end unit (BEU) containing a further radio frequency amplification stage, detector diodes and all the electronics for data acquisition and bias supply.

---

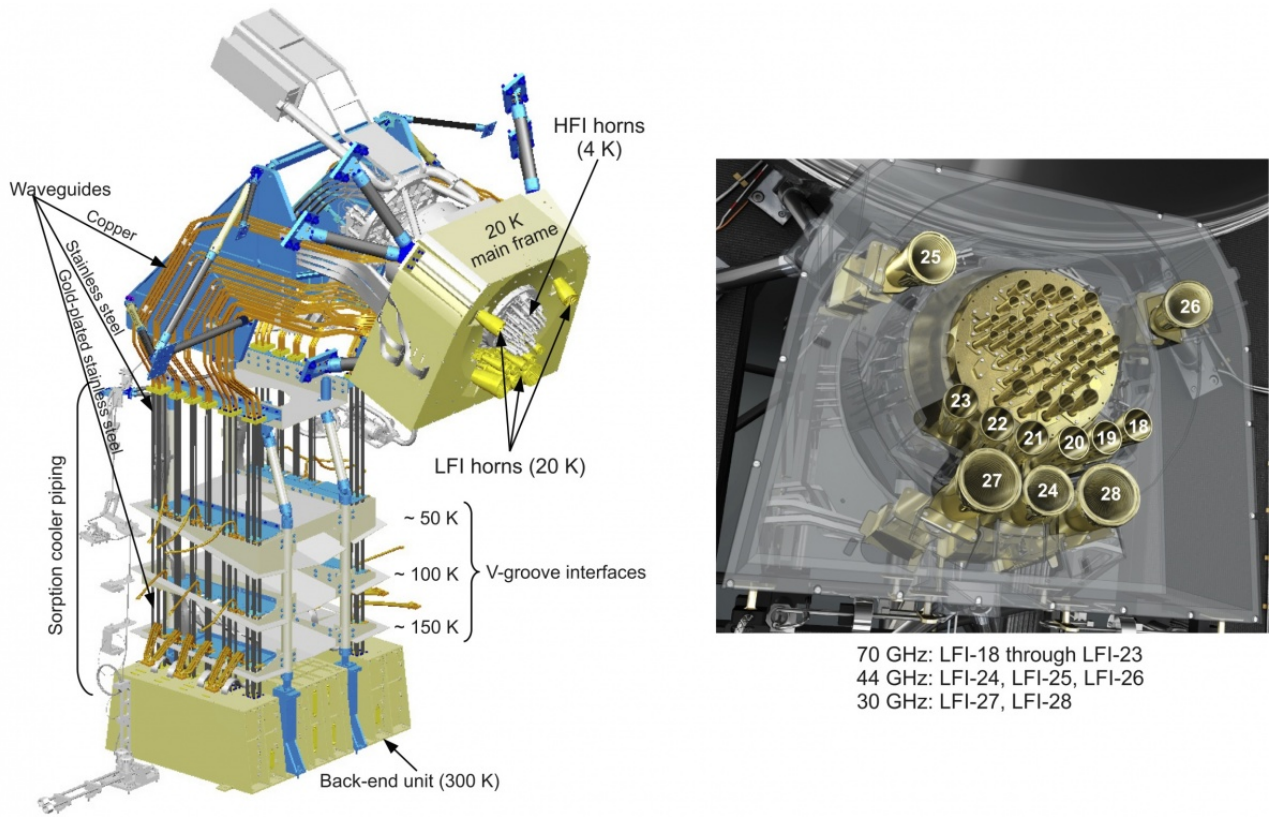


Figure 1. Left Panel: the LFI instrument with main thermal stages, focal plane, waveguides and sorption cooler piping highlighted. Right Panel: Labelling of feed horns on the LFI focal plane.

Best LFI noise performance is obtained with receivers based on InP High Electron Mobility Transistor (HEMT) low noise amplifiers (LNAs) for minimal power dissipation and best performance. To further minimise power consumption in the focal plane, the radiometers are split into two sub-assemblies connected by waveguides, one located at the telescope focal area, the other on the 300 K portion of the Planck satellite. These design features allow the entire front-end LNAs dissipation to be  $<0.55$  W, which enables the active cooling of the focal assembly. This is achieved with a vibration-less hydrogen sorption cooler, which also provides 18 K pre-cooling to the HFI helium J-T cooler. Two sorption cooler units are included in the flight hardware.

As shown schematically in Figure 2 below, the LFI consists of the following subsystems:

- Radiometer Array Assembly (RAA)
- Sorption Cooler Subsystem (SCS)
- Radiometer Electronics Box Assembly (REBA)

The RAA includes the Front End Unit (FEU) and the Back End Unit (BEU), connected via waveguides. The FEU is located at the focus of the telescope, as one component of the joint LFI/HFI focal assembly (see sections below). The BEU is mounted on the top of the Planck SVM. The Radiometer Electronics Box Assembly (REBA) and the warm parts of the Sorption Cooler System (SCS) is located on one of the lateral panels of the service module (SVM). The FEU and the Sorption Cooler Compressor (SCC) are connected by concentric stainless steel tubes. The smaller tube carries hydrogen at  $\sim 60$  atmospheres from the cooler compressors to the FEU, while the larger tube returns the hydrogen at  $\sim 0.3$  atmospheres. These units are described in detail in following sections, the SCS is described in details in the satellite section dedicated to *Cryogenics*. All LFI units are linked together by the LFI harness, which also connects to the spacecraft interface.

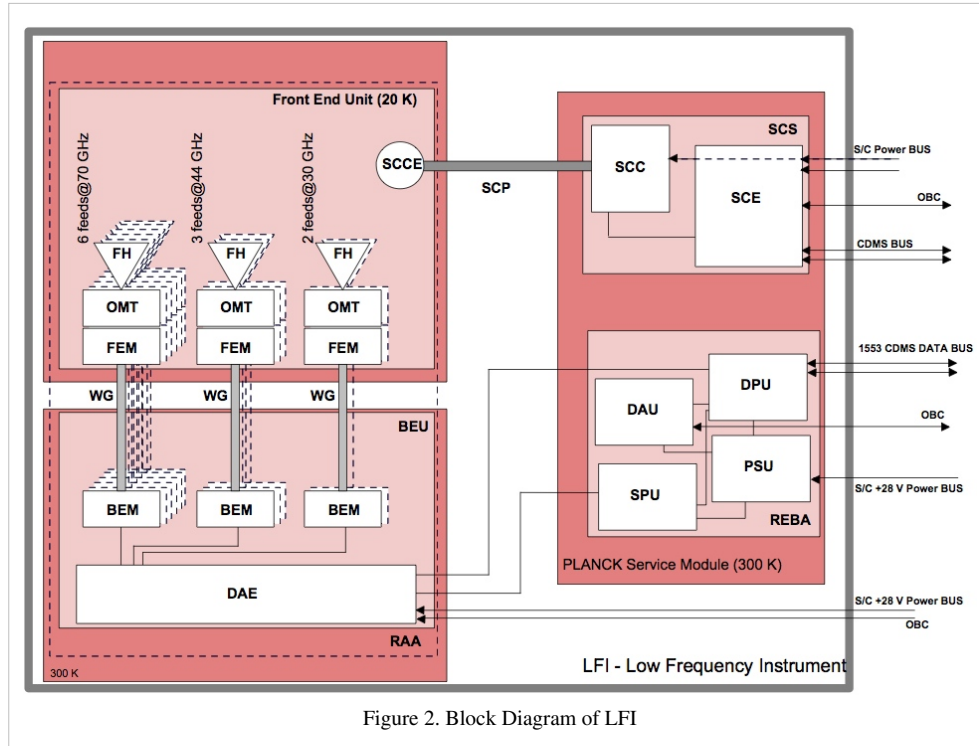


Figure 2. Block Diagram of LFI

### ***Radiometer Array Assembly (RAA)***

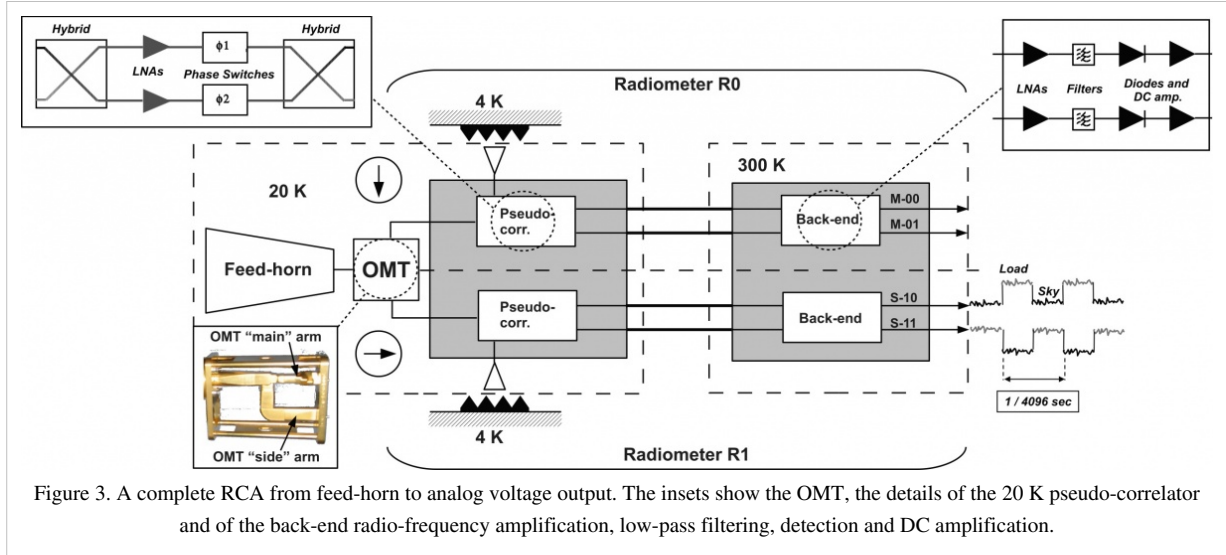
The Radiometer Array Assembly (RAA) consists of two main units (the front end unit, FPU and the Back End Unit, BEU), connected by a set of waveguides. The Focal Plane Unit (FPU) is the heart of the LFI instrument and it contains the feed array and associated orthomode transducers (OMTs) and FEMs, all cooled to 20 K by the sorption cooler. The FPU comprises a set of 11 modules, which are mounted on a mechanical support which meets the thermo-mechanical requirements of the instrument and adds thermal inertia. The BEU comprises the radiometer Back End Modules (BEM) and the Data Acquisition Electronics (DAE), which are connected by an internal harness. The HFI Unit is located inside the LFI FPU and supported by the LFI structure. The LFI structure gives the mechanical and thermal interface to the HFI unit with the proper stiffness and thermal de-coupling. The LFI structure also guarantees the proper alignment of the HFI detector with the telescope focal plane.

The time scale of the stability of the receiver is driven by the 1 rpm rotation speed of the spacecraft, which requires a very low  $1/f$ -noise or gain variation of the low noise amplifiers and other components. The LFI uses a pseudo-correlation receiver concept (Figure 3 below). This radiometer concept is chosen to maximise the stability of the instrument by reducing the effect of non-white noise generated in the radiometer itself. In this scheme, the difference between the inputs to each of the chains (the signal from the telescope and that from a reference black body respectively) is continuously being observed. To remove the effect of instability in the back-end amplifiers and detector diodes, it is necessary to switch the signal detected at the diodes at high rate. The signals from the sky and from a reference load are combined by a hybrid coupler, amplified in two independent amplifier chains, and separated out by another hybrid. The sky and the reference load power can then be measured and differenced. Since the reference signal has been subject to the same gain variations in the two amplifier chains as the sky signal, the true sky power can be recovered. The differencing receiver greatly improves the stability if the two input signals are almost equal, at a cost of a factor of  $\sqrt{2}$  in sensitivity compared to a perfectly stable total-power radiometer with the same noise temperature and bandwidth. This radiometer concept is capable of greatly reducing the knee frequency. We define as Radiometer Chain Assembly (RCA, see Figure 3) each functional unit from the feed horn to the BEM. The RAA therefore includes a set of 11 RCAs and the Data Acquisition Electronics, all mounted on a suitable mechanical structure. Although there are differences in the details of the radiometer chains at different frequencies



their overall configuration is similar, and a general description of its design is provided in this section. Planck LFI has 11 Radiometer Chain Assembly (RCA). Each RCA is constituted by feed horn and FEM in the FEU (at 20 K), BEM (at 300 K) in the BEU and four waveguides that connect each FEM-BEM couple. The frequency distribution of the RCA is the following:

- 2 RCAs at 30GHz
- 3 RCAs at 44GHz
- 6 RCAs at 70GHz



#### *Radiometer Chain Assembly (RCA);*

Every radiometer chain assembly (RCA) consists of two radiometers, each feeding two diode detectors (see Figure 3 below), for a total of 44 detectors. The 11 RCAs are labelled by a numbers from 18 to 28 as outlined in Figure 1, right panel.

Figure 3 provides a more detailed description of each radiometric receiver. In each RCA, the two perpendicular linear polarisation components split by the OMT propagate through two independent pseudo-correlation differential radiometers, labelled as *M* or *S* depending on the arm of the OMT they are connected to (*Main* or *Side*, see lower-left inset of Figure 3).

In each radiometer the sky signal coming from the OMT output is continuously compared with a stable 4 K blackbody reference load mounted on the external shield of the HFI 4 K box [L. Valenziano, F. Cuttaia, A. De Rosa et al. Planck-LFI: design and performance of the 4 Kelvin Reference Load Unit. *Journal of Instrumentation*, 4:2006, 2009.]. After being summed by a first hybrid coupler, the two signals are amplified by ~30 dB, see upper-left inset of Figure 3. The amplifiers were selected for best operation at low drain voltages and for gain and phase match between paired radiometer legs, which is crucial for good balance. Each amplifier is labelled with codes *I*, *2* so that the four outputs of the LNAs can be named with the sequence: *M1*, *M2* (radiometer *M*) and *S1*, *S2* (radiometer *S*). Tight mass and power constraints called for a simple design of the Data Acquisition Electronics (DAE) box so that power bias lines were divided into five common-grounded power groups with no bias voltage readouts; only the total drain current flowing through the front-end amplifiers is measured and is available to the house-keeping telemetry (this design has important implications for front-end bias tuning, which depends critically on the satellite electrical and thermal configuration and was repeated at all integration stages, during on-ground and in-flight satellite tests). A phase shift alternating between  $0^\circ$  and  $180^\circ$  at the frequency of 4096 Hz is applied in one of the two amplification chains and then a second hybrid coupler separates back the sky and reference load components that are further amplified and detected in the warm BEU, with a voltage output ranging from -2.5 V to +2.5 V.

Each radiometer has two output diodes which are labelled with binary codes *00*, *01* (radiometer *M*) and *10*, *11* (radiometer *S*), so that the four outputs of each radiometric chain can be named with the sequence: *M-00*, *M-01*, *S-10*, *S-11*.

After detection, an analog circuit in the DAE box removes a programmable offset in order to obtain a nearly null DC output voltage and a programmable gain is applied to increase the signal dynamics and optimally exploit the ADC input range. After the ADC, data are digitally downsampled, requantised and compressed in the radiometer electronics box assembly (REBA) according to a scheme described in [J. M. Herreros, M. F. Gómez, R. Rebolo et al. The Planck-LFI Radiometer Electronics Box Assembly. *Journal of Instrumentation*, 4:2008, 2009; M. Maris, M. Tomasi, S. Galeotta et al. Optimization of Planck-LFI on-board data handling. *Journal of Instrumentation*, 4:2018, 2009.] before preparing telemetry packets. On ground, telemetry packets are converted to sky and reference load time ordered data after calibrating the ADU samples into volt considering the applied offset and gain factors.

To first order, the mean differential power output for each of the four receiver diodes can be written as follows [M. Seiffert, A. Mennella, C. Burigana et al. *1/f* noise and other systematic effects in the Planck-LFI radiometers. *A&A*, 391:1185–1197, 2002; A. Mennella, M. Bersanelli, M. Seiffert et al. Offset balancing in pseudo-correlation radiometers for CMB measurements. *A&A*, 410:1089–1100, 2003; M. Bersanelli, N. Mandolesi, R. C. Butler et al. Planck pre-launch status: Design and description of the Low Frequency Instrument. *A&A*, 520:A4, 2010]:

$$P_{\text{out}}^{\text{diode}} = a G_{\text{tot}} k \beta [T_{\text{sky}} + T_{\text{noise}} - r (T_{\text{ref}} + T_{\text{noise}})]$$

where  $G_{\text{tot}}$  is the total gain,  $k$  is the Boltzmann constant,  $\beta$  the receiver bandwidth and  $a$  is the diode constant.  $T_{\text{sky}}$  and  $T_{\text{ref}}$  are the average sky and reference load antenna temperatures at the inputs of the first hybrid and  $T_{\text{noise}}$  is the receiver noise temperature.

The gain modulation factor [A. Mennella, M. Bersanelli, M. Seiffert et al. Offset balancing in pseudo-correlation radiometers for CMB measurements. *A&A*, 410:1089–1100, 2003; A. Zacchei, D. Maino, C. Baccigalupi et al. Planck early results. V. The Low Frequency Instrument data processing. *A&A*, 536:A5, 2011],  $r$ , is defined by:

$$r = \frac{T_{\text{sky}} + T_{\text{noise}}}{T_{\text{ref}} + T_{\text{noise}}}$$

and is used to balance (in software) the temperature offset between the sky and reference load signals and minimise the residual  $1/f$  noise in the differential datastream. This parameter is calculated from the average uncalibrated total power data using the relationship:

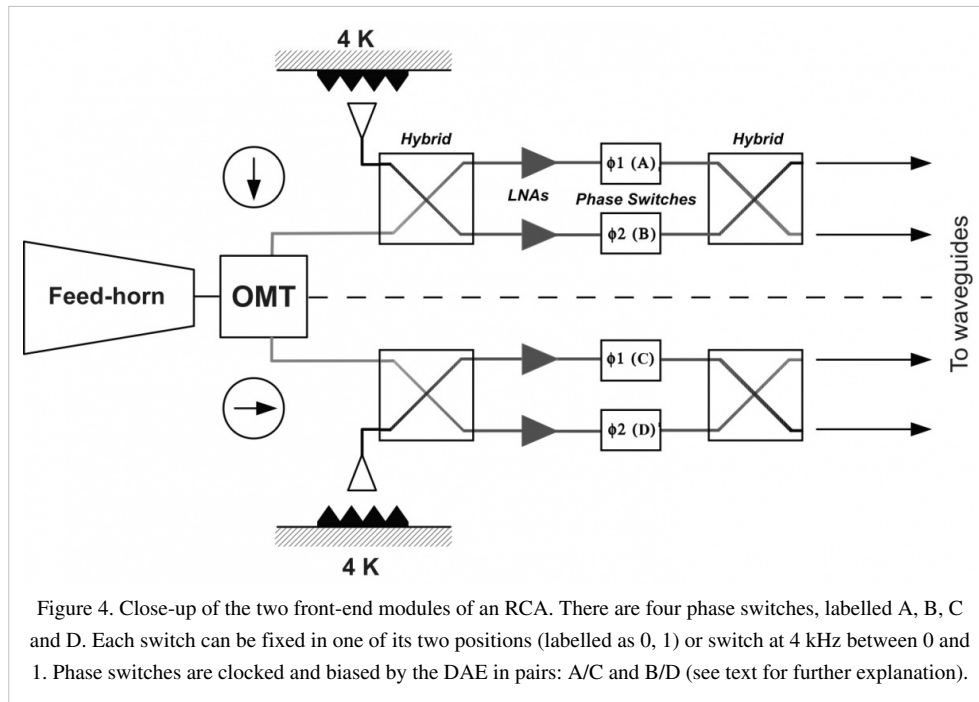
$$r = \langle V_{\text{sky}} \rangle / \langle V_{\text{ref}} \rangle,$$

where  $\langle V_{\text{sky}} \rangle$  and  $\langle V_{\text{ref}} \rangle$  are the average sky and reference voltages calculated in a defined time range. The white noise spectral density at the output of each diode is essentially independent from the reference-load absolute temperature and is given by:

$$\Delta T_0^{\text{diode}} = \frac{2(T_{\text{sky}} + T_{\text{noise}})}{\sqrt{\beta}}.$$

In Figure 4 below we show a close-up of the two front end modules of an RCA with the four phase switches which are labelled with the four letters *A* and *B* (main arm), *C* and *D* (side arm). Each phase switch is characterised by two states: state 0 (no phase shift applied to the incoming wave) and state 1 ( $180^\circ$  phase shift applied) and can either stay fixed in a state or switch at 4 kHz between the two states.

Phase switches are clocked and biased by the DAE and their configuration can be programmed via telecommand. In order to simplify the instrument electronics, phase switches are configured and operated in pairs: *A/C* and *B/D*. This means that if phase switches *A* and *C* are switching at 4 kHz then *B* and *D* are fixed both in the same state (either 0 or 1). This simplification, required during the design phase to comply with mass and power budgets, comes at the price of loosing some setup redundancy.



*Feed Horns (FH)*

*OrthoMode Transducers (OMT)*

*Front End Modules (FEM)*

*Waveguides*

*Back End Modules (BEM)*

*4K Load*

## LFI Ground Tests

During its development, the LFI flight model was calibrated and tested at various integration levels from sub-systems [R. J. Davis, A. Wilkinson, R. D. Davies et al. Design, development and verification of the 30 and 44 GHz front-end modules for the Planck Low Frequency Instrument. *Journal of Instrumentation*, 4:2002, 2009] to individual integrated receivers [F. Villa, L. Terenzi, M. Sandri et al. Planck pre-launch status: Calibration of the Low Frequency Instrument flight model radiometers. *A&A*, 520:A6, 2010] and the whole receiver array [A. Mennella, M. Bersanelli, R. C. Butler et al. Planck pre-launch status: Low Frequency Instrument calibration and expected scientific performance. *A&A*, 520:A5, 2010]. In every campaign we performed tests according to the following classification:

- *Functionality tests*, performed to verify the instrument functionality.
- *Tuning tests*, to tune radiometer parameters (biases, DC electronics gain and offset, digital quantisation and compression) for optimal performance in flight-like thermal conditions.
- *Basic calibration and noise performance tests*, to characterise instrument performance (photometric calibration, isolation, linearity, noise and stability) in tuned conditions.
- *Susceptibility tests*, to characterise instrument susceptibility to thermal and electrical variations.

Where possible, the same tests were repeated in several test campaigns, in order to ensure enough redundancy and confidence in the instrument behaviour repeatability. A critical comparison, that is central to the subject of this work, is the one between the results of on-ground and in-flight test campaigns. A matrix showing the instrument parameters measured in the various test campaigns is provided in Table 1 of [A. Mennella, M. Bersanelli, R. C. Butler et al. Planck pre-launch status: Low Frequency Instrument calibration and expected scientific performance. *A&A*, 520:A5, 2010].

The ground test campaign was developed in three main phases: cryogenic tests on the individual RCAs, cryogenic tests on the integrated receiver array (the so-called radiometer array assembly, RAA) and system-level tests after the integration of the LFI and HFI instruments onto the satellite. The first two phases were carried out at the Thales Alenia Space - Italia laboratories located in Vimodrone (Milano, Italy) (note that receiver tests on 70 GHz RCAs were carried out in Finlad, at Yilinen laboratories), system level tests (SLT) were conducted in a dedicated cryofacility at the Centre Spatiale de Liege (CSL) located in Liege (Belgium).

In Table 1 below we list the temperature of the main cold thermal stages during ground tests compared to in-flight nominal values. These values show that system-level tests were conducted in conditions that were as much as possible flight-representative, while results obtained during RCA and RAA tests needed to be extrapolated to flight conditions to allow comparison. Details about the RCA test campaign are discussed in [F. Villa, L. Terenzi, M. Sandri et al. Planck pre-launch status: Calibration of the Low Frequency Instrument flight model radiometers. A&A, 520:A6, 2010] while the RAA tests and the extrapolation methods are presented in [A. Mennella, M. Bersanelli, R. C. Butler et al. Planck pre-launch status: Low Frequency Instrument calibration and expected scientific performance. A&A, 520:A5, 2010].

Temperature	Nominal	RCA tests	RAA tests	System-level
Sky	$\sim 3$ K	$\gtrsim 8$ K	$\gtrsim 18.5$ K	$\sim 4$ K
Ref. load	$\sim 4.5$ K	$\gtrsim 8$ K	$\gtrsim 18.5$ K	$\sim 4.5$ K
Front-end unit	$\sim 20$ K	$\sim 20$ K	$\sim 26$ K	$\sim 20$ K

Table 1. Temperatures of the main cold stages during the various ground test campaigns compared to in-flight nominal values.

Cryogenic system-level tests were split into three parts:

- *Thermal balance*, to validate the overall thermal mathematical model. The ground vacuum test equipment simulated the space environment.
- *System cryogenic test*, to check and optimise the satellite and instrument performance working at nominal temperatures.
- *Thermal cycling test*, to check the reliability of all electronics equipment and instruments to temperature variations (note that to allow the thermal control of the Service Vehicle Module (SVM), the warm part of the spacecraft was surrounded by a cryogenic shroud at a temperature lower than 100 K. The temperature of the shrouds was adjustable in order to allow the thermal cycling of the SVM during the tests. The temperature ranged between the two extreme values of  $20^{\circ}\text{C}$  to  $100^{\circ}\text{C}$ ).

During the various test campaigns the instrument was switched off and moved several times in a time period of about three years. A series of functional tests were always repeated at each location and also in flight, in order to verify the instrument functionality and the response repeatability. No failures or major problems have been identified due to transport and integration procedures.

## LFI In-flight Calibration

The Planck cryo-chain [Planck Collaboration. Planck early results. II. The thermal performance of Planck. A&A, 536:A2, 2011] is composed by three coolers: a 20 K Hydrogen sorption cooler, which is passively pre-cooled by the 3<sup>rd</sup> V-groove radiator, cools the LFI focal plane and pre-cools the HFI 4K cooler; a Stirling 4K cooler that cools the HFI box and feed-horns and provides a 4K blackbody reference signal to the LFI receivers; a 0.1 K dilution cooler, which is pre-cooled by the 4K cooler and cools the HFI bolometer filters to  $\sim 1.6$  K and the HFI bolometer detectors to  $\sim 0.1$  K. The cooldown of the HFI 4K stage, in particular, was key during CPV for the LFI as it provided a variable input signal that was exploited during bias tuning.

The LFI CPV started on June, 4<sup>th</sup>2009 and lasted until August, 12<sup>th</sup> when Planck started scanning the sky in nominal mode. At the onset of CPV, the active cooling started when the radiating surfaces on the payload module reached their working temperatures ( $\sim 50$  K on the 3<sup>rd</sup>V-groove, and  $\sim 40$  K on the reflectors) by passive cooling. This was achieved during the transfer phase. Nominal temperatures were achieved on July, 3<sup>rd</sup>2009, when the dilution cooler temperature reached 0.1 K [Planck Collaboration. Planck early results. II. The thermal performance of Planck. A&A, 536:A2, 2011; P. Meinhold, R. Leonardi, B. Aja et al. Noise properties of the Planck-LFI receivers. Journal of Instrumentation, 4:2009, 2009] (see Figure 5 below).

The CPV was carried out in four phases (see Table 2 below for a summary of the overall CPV test campaign):

- LFI switch on and basic functionality verification,
- Tuning of front-end biases and back-end electronics,
- Preliminary calibration tests,
- Thermal tests.

Phase	Test	Objective
<i>LFI switch on Functionality</i>	Switch on	Verify functionality of electronics units
	CRYO-01 . . . . .	Switch on LFI front-end unit (FEU) and verify basic functionality of all front-end components
	CRYO-02 . . . . .	Verify effectiveness of pseudo-correlation in reducing $1/f$ noise
	Spike tests . . . . .	Characterise 1 Hz spurious spikes
	Drain currents . . . . .	Characterise LNAs I–V response
	Reference test . . . . .	Set a functionality reference point
<i>Tuning</i>	Stability check . . . . .	Verify instrument response stability prior to hypermatrix
	Pretuning . . . . .	Constrain LNA bias space prior to hypermatrix tuning
	Phase Switch tuning	Tune phase switch currents for optimal balance
	Hypermatrix tuning	Find the optimal LNA bias configuration by exploring the bias space $[V_{g1}^{LNA1}, V_{g2}^{LNA2}, V_{g1}^{LNA1}, V_{g2}^{LNA2}]$ . The bias space defined during pre-tuning is scanned 4 times at different temperatures of the 4 K stage. For each bias quadruplet noise temperature and isolation are calculated
	Tuning verification . . . . .	Verify optimal biases obtained from hypermatrix tuning
	DAE tuning . . . . .	Optimise DC voltage output from each detector to the ADC input
<i>Calibration</i>	REBA tuning . . . . .	Optimise digital quantisation and compression
	Noise properties . . . . .	Preliminary assessment of noise performance and photometric calibration
<i>Thermal</i>	Dyn. thermal model	Assess FPU thermal damping
	Susceptibility . . . . .	Assess radiometric thermal transfer functions

Table 2.

## LFI Performance

# The telescope

---

The telescope is an off-axis aplanatic design with two elliptical reflectors and a 1.5 m projected diameter and an overall emissivity  $\leq 1\%$ . The optical system was optimized for a set of representative detectors (eight HFI and eight LFI). The performance of the aplanatic configuration is not quite as good on the optical axis as the so-called Dragone-Mizuguchi Gregorian configuration, which eliminates astigmatism on the optical axis, but is significantly better over the large focal surface required by the many HFI and LFI feeds.

The Planck telescope consists of:

1. **The primary and secondary reflectors** (PR and SR), designed and manufactured by Astrium (Friedrichshafen, Germany);
2. **The support structure**, designed and manufactured by Oerlikon Space (Zurich, Switzerland).

For more information, see Tauber et al. 2010, A&A 520, A2.

# The standard radiation environment monitor

---

(NOTE: Adapted from IEEE TRANSACTIONS ON NUCLEAR SCIENCE, VOL. 50, NO. 6, DECEMBER 2003)

## Introduction

The standard radiation environment monitor (SREM) is a particle detector developed for satellite applications. It measures high-energy electrons and protons of the space environment with a  $\pm 20^\circ$  angular resolution, spectral information and provides the host spacecraft with radiation information. SREM was developed and manufactured by Contraves Space in cooperation with Paul Scherrer Institute under a development contract of the European Space Agency. SREM is the second generation of instruments in a programme, which was established by ESA's European Research and Technology Centre (ESTEC) to:

1. Provide minimum intrusive radiation detectors for space applications;
2. Provide radiation hazard alarm function to instruments on board spacecraft;
3. Assist in investigation activities related to possible radiation related anomalies observed on spacecraft;
4. Assist in in-flight Technology Demonstration Activities.

The design goals are low weight, small dimensions, low power consumption, combined with the ability to provide particle species and spectral information.

In the case of Planck, the use of the SREM was entirely within the scope of bullets 1 and 3 above as due to the nature of operations no real time alarms were possible

## The instrument

The SREM consists of three detectors (D1, D2, and D3) in two detector heads configurations. One system is a single silicon diode detector (D3). The main entrance window is covered with 0.7 mm aluminum, which defines the lower energy threshold for electrons to  $\sim 0.5$  MeV and for protons to  $\sim 10$  MeV. The other system uses two silicon diodes (detectors D1/D2) arranged in a telescope configuration. The main entrance of this detector is covered with 2 mm aluminum giving a proton and electron threshold of 20 and 1.5 MeV, respectively. A 1.7-mm-thick aluminum and 0.7-mm-thick tantalum layer separate the two diodes of the telescope configuration.

The telescope detector allows measurement of the high-energy proton fluxes with enhanced energy resolution. In addition, the shielding between the two diodes in the telescope prevents the passage of electrons. However, protons with energies greater than  $\sim 30$  MeV go through. Thus, using the two diodes in coincidence gives pure proton count

---

rates allowing subtraction of the proton contribution from the electron channels. A total of 15 discriminator levels are available to bin the energy of the detected events. Any two of the levels can be used to raise an alarm flag when the count rates exceed a programmable threshold. This alarm signal can then be used to control the operation of the spacecraft and its instruments. The detector electronics is capable of processing a detection rate of 100 kHz with dead-time correction below 20%. The SREM is contained in a single box of 20 × 12 × 10 and weighs 2.6 kg (see Fig. 1). The box contains the detector systems with the analog and digital front-end electronics, a power supply, and a TTC-B-01 telemetry and Telecommand interface protocol. By virtue of a modular buildup, the interface can be adapted to any spacecraft system. The power consumption is approximately 2.5 W. An essential input for the interpretation of the detection rates, in terms of particle fluxes, are the energy dependent

## The data

The SREM data are provided in the Planck Legacy Archive in the following form:

- individual FITS files per calendar day

## The fiber optic gyro unit

---

The Fiber-Optic Gyro unit (FOG) is an extra payload on-board Planck which is not used as part of the attitude control system. The FOG functioning is based on the physical phenomenon called *Sagnac effect*:

*"a solid-state optical interferometer enclosing a surface located on a rotating support will detect a phase difference of the optical signal, which is proportional to the angular rate and to the surface enclosed by the optical path".*

The FOG features the following architecture:

- An optical path enclosing a maximal surface: this is realized through the 1 km long fibre optic, winded many time round, in order to make a reasonable sized interferometer (< 120 mm in diameter).
- A source, to deliver the light to the interferometer.
- A multifunction Integrated Optical Circuit, which closes the interferometer, to share the light between the two extremities of the fiber optic coil, to filter undesirable polarization.
- A coupler to extract the optical signal coming back from the ring interferometer, which is the signal carrying the Sagnac inertial information, and to direct it towards an optical detector.
- A detection module to convert this light signal into an electrical signal.
- A closed-loop signal processing to increase the dynamic range and remove the effect of fluctuations of the optical power and of the gain of the detection chain, allowing an easy auto-calibration of the system and excellent scale factor stability and linearity.
- A biasing modulation allowing the measurement of very low rotation rates as well as the sign of those rotations.

Redundancy is offered by providing four skewed gyro channels, allowing the Attitude Control and Measurement Subsystem to use any triplet among the four axes to determine the spacecraft three axes rates. Nominally the four channels are activated, in case of failure or thermal criticalities a subset of channels could be used.

There is no dangerous FOG flight command. The FOG is designed to operate five years ON in orbit, withstanding 1000 ON/OFF cycles, and its performance is guaranteed under rotations of  $\pm 10$  deg/second, and at the temperature range of 253 K up to 333 K. Power dissipations are in the range of 5.5 up to 6.7 W/channel.

---



---

# Ground Segment and Operations

---

## Ground segment overview

---

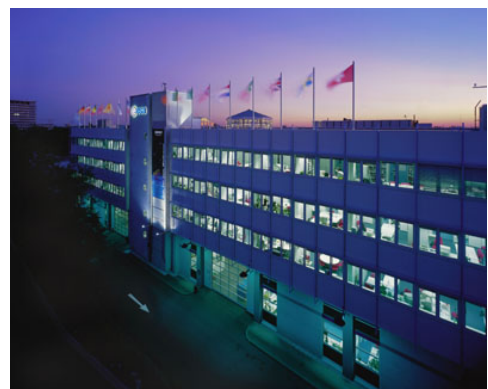
### Geographical distribution of the Planck Ground Segment

The Planck Ground Segment is made of four geographically distributed centres:

#### The Mission Operations Centre

The mission operations centre (MOC), located at ESA's operations centre in Darmstadt (Germany), is responsible for all aspects of flight control and of the health and safety of the Planck satellite, including both instruments. It plans and executes all necessary satellite activities, including instrument commanding requests by the instrument operations centres.

MOC communicates with the satellite using ESA's 35-m antenna located in New Norcia (Australia), or that in Cebreros (Spain), over a daily 3-h period, during which it uplinks a scheduled activity timeline which is autonomously executed by the satellite, and downlinks the science and housekeeping (HK) data acquired by the satellite during the past 24 h. The downlinked data are transferred from the antenna to the MOC over a period of typically 8 h; at MOC they are put onto a data server from where they are retrieved by the two Data Processing Centres.



The European Space Operations Centre in Darmstadt, Germany, home of the Planck Mission Operations Centre.

#### The Planck Science Office

The Planck Science Office (PSO) is located at ESA's European Space Astronomy Centre in Villanueva de la Cañada surroundings (Madrid, Spain).

Its main responsibilities include:

- coordinating scientific operations of the Planck instruments
- designing, planning and executing the Planck observation strategy.

It provides to MOC a detailed pointing plan with a periodicity of about one month.

- creating and updating the specifications of the Planck Legacy Archive developed by the Science Archives Team at ESAC
- testing and operating the PLA



The European Space Astronomy Centre in Villanueva de la Cañada, Madrid, Spain, see of the Planck Science Office.



## The LFI instrument operations and data-processing centre

The LFI instrument operations and data processing centre, located at the Osservatorio Astronomico di Trieste (Italy), is notably responsible for:

- the optimal operation of the LFI instrument
- the processing of the data acquired by LFI into the final scientific products of the mission.

## The HFI instrument operations and data-processing centre

The HFI instrument operations and data processing centres, located respectively at the Institut d'Astrophysique Spatiale in Orsay (France) and at the Institut d'Astrophysique de Paris (France), are similarly responsible for the optimal operation of the HFI instrument, and (with several other institutes in France and the UK) for the processing of the data acquired by HFI into the final scientific products of the mission.

## The data flow in the Planck Ground Segment

The Planck Science Office (PSO), located at ESAC, Spain, sends the pointing lists (Pre-Programmed Pointing Lists) to the Mission Operations Centre at ESOC in Darmstadt, Germany. The Flight Dynamics team at ESOC adapts them into Augmented Pre-Programmed Pointing Lists (APPL) taking into account ground station scheduling, Operational Day (OD) boundaries and other issues.

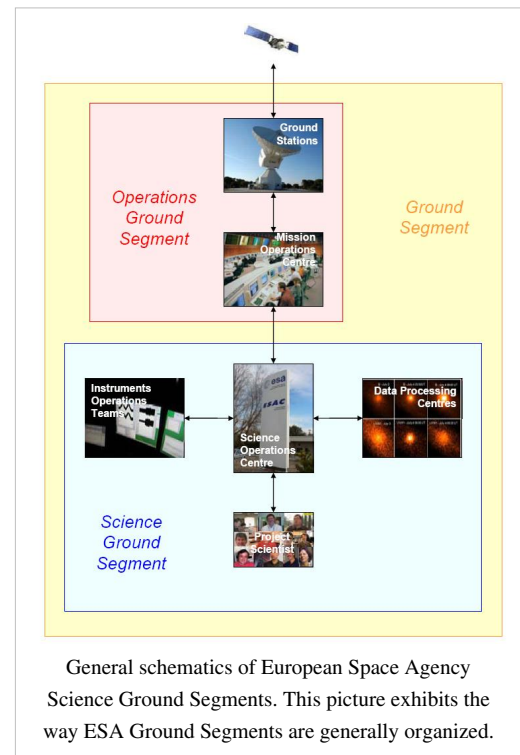
MOC sends pointing and instrument commands to the spacecraft, and receives the house-keeping telemetry and science data through the ground stations (for Planck, mostly the New Norcia and Cebreros ones).

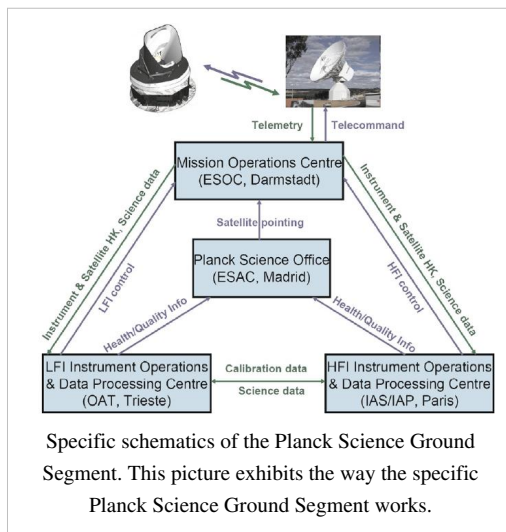
Science data is then transferred to both Data Processing Centres (DPC) which process the data and send quality reports to PSO.

Science products (timelines, maps, etc) are exchanged between DPCs in order to help calibration and other scientific issues.

## References

Tauber et al. 2010, A&A 520, A1





## Contingencies

NOTE: THE LIST IS STILL INCOMPLETE.

The main unplanned events included the following:

- Very minor deviations from the scanning law include occasional (on the average about once every two months) under-performance of the 1-N thrusters used for regular manoeuvres, which implied the corresponding pointings were not at the intended locations. These deviations had typical amplitudes of 30 arcsec, and have no significant impact on the coverage map.
- The thruster heaters were unintentionally turned off between 31 August and 16 September 2009 (the so-called “catbed” event).
- An operator error in the upload of the on-board command timeline led to an interruption of the normal sequence of manoeuvres and therefore to Planck pointing to the same location on the sky for a period of 29 h between 20 and 21 November 2009 (“the day Planck stood still”). Observations of the nominal scanning pattern resumed on 22 November, and on 23 November a recovery operation was applied to survey the previously missed area. During the recovery period the duration of pointing was decreased to allow the nominal law to be caught up with. As a side effect, the RF transmitter was left on for longer than 24 h, which had a significant thermal impact on the warm part of the satellite.
- As planned, the RF transmitter was initially turned on and off every day in synchrony with the daily visibility window, in order to reduce potential interference by the transmitter on the scientific data. The induced daily temperature variation had a measurable effect throughout the satellite. An important effect was on the temperature of the 4He-JT cooler compressors, which caused variations of the levels of the interference lines that they induce on the bolometer data (Planck HFI Core Team 2011a). Therefore the RF transmitter was left permanently on starting from 25 January 2010 (257 days after launch), which made a noticeable improvement on the daily temperature variations.
- During the coverage period, the operational star tracker switched autonomously to the redundant unit on two occasions (11 January 2010 and 26 February 2010); the nominal star tracker was restored a short period later (3.37 and 12.75 h, respectively) by manual power-cycling. Although the science data taken during this period have normal quality, they have not been used because the redundant star tracker’s performance is not fully characterised.

For more information, see Planck Collaboration 2011, A&A 536, A1.

## Operational history

---

(Note: Adapted from Planck Collaboration 2011, A&A 536, A1)

Provide a description of the product Planck Operational State History.

The major operational phases and milestones are:

### Launch and transfer to orbit: (provide date, and summary overview)

Planck was launched from the Centre Spatial Guyanais in Kourou (French Guyana) on 14 May 2009 at its nominal lift-off time of 13:12 UT, on an Ariane 5 ECA rocket of Arianespace2. ESA's Herschel observatory was launched on the same rocket. At 13:37:55 UT, Herschel was released from the rocket at an altitude of 1200 km; Planck followed suit at 13:40:25 UT. The separation attitudes of both satellites were within 0.1 deg of prediction. The Ariane rocket placed Planck with excellent accuracy (semimajor axis within 1.6% of prediction), on a trajectory towards the second Lagrangian point of the Earth-Sun system (L2). After release from the rocket, three large manoeuvres were carried out to place Planck in its intended final orbit. The first (14.35 ms<sup>-1</sup>), intended to correct for errors in the rocket injection, was executed on 15 May at 20:01:05 UT, with a slight overperformance of 0.9% and an error in direction of 1.3 deg (a touch-up manoeuvre was carried out on 16 May at 07:17:36 UT). The second and major (mid-course) manoeuvre (153.6ms<sup>-1</sup>) took place between 5 and 7 June, and a touch-up (11.8 ms<sup>-1</sup>) was executed on 17 June. The third and final manoeuvre (58.8ms<sup>-1</sup>), to inject Planck into its final orbit, was executed between 2 and 3 July. The total fuel consumption of these manoeuvres, which were carried out using Planck's coarse (20N) thrusters, was 205 kg. Once in its final orbit, very small manoeuvres are required at approximately monthly intervals (1 ms<sup>-1</sup> per year) to keep Planck from drifting away from its intended path around L2. The attitude manoeuvres required to follow the scanning strategy require about 2.6 ms<sup>-1</sup> per year. Overall, the excellent performance of launch and orbit manoeuvres will lead to a large amount (~160 kg, or ~40% of initial tank loading) of fuel remaining on board at end of mission operations.

Planck started cooling down radiatively shortly after launch. Heaters were activated to hold the focal plane at 250 K, which was reached around 5 h after launch. The valve opening the exhaust piping of the dilution cooler was activated at 03:30 UT, and the 4He-JT cooler compressors were turned on at low stroke at 05:20 UT. After these essential operations were completed, on the second day after launch, the focal plane temperature was allowed to descend to 170 K for out-gassing and decontamination of the telescope and focal plane.

### Commissioning: (provide date, and summary overview)

The first period of operations focussed on commissioning activities, i.e., functional check-out procedures of all sub-systems and instruments of the Planck spacecraft in preparation for running science operations related to calibration and performance verification of the payload. Planning for commissioning operations was driven by the telescope decontamination period of 2 weeks and the subsequent cryogenic cool-down of the payload and instruments. The overall duration of the cool-down was approximately 2 months, including the decontamination period. The sequence of commissioning activities covered the following areas:

- on-board commanding and data management;
  - attitude measurement and control;
  - manoeuvring ability and orbit control;
  - telemetry and telecommand;
  - power control;
-

- thermal control;
- payload basic functionality, including:
- the LFI;
- the HFI;
- the cryogenic chain;
- the Standard Radiation Environment Monitor;
- the Fibre-Optic Gyro unit (FOG), a piggy-back experiment which is not used as part of the attitude control system.

The commissioning activities were executed very smoothly and all sub-systems were found to be in good health. The most significant unexpected issues that had to be addressed during these early operational phases were the following.

- The X-band transponder showed an initialisation anomaly during switch-on which was fixed by a software patch.
- Large reorientations of the spin axis were imperfectly completed and required optimisation of the on-board parameters of the attitude control system.
- The data rate required to transmit all science data to the ground was larger than planned, due to the unexpectedly high level of Galactic cosmic rays, which led to a high glitch rate on the data stream of the HFI bolometers (Planck HFI Core Team 2011a); glitches increase the dynamic range and consequently the data rate. The total data rate was controlled by increasing the compression level of a few less critical thermometers.
- The level of thermal fluctuations in the 20-K stage was higher than originally expected. Optimisation of the sorption cooler operation led to an improvement, though they still remained  $\sim 25\%$  higher than expected (Planck Collaboration 2011b).
- The 20-K sorption cooler turned itself off on 10 June 2009, an event which was traced to an incorrectly set safety threshold.
- A small number of sudden pressure changes were observed in the 4He-JT cooler during its first weeks of operation, and were most likely due to impurities present in the cooler gas (Planck Collaboration 2011b). The events disappeared after some weeks, as the impurities became trapped in the cooler system.
- The 4He-JT cooler suffered an anomalous switch to standby mode on 6 August 2009, following a current spike in the charge regulator unit which controls the current levels between the cooler electronics and the satellite power supply (Planck Collaboration 2011b). The cooler was restarted 20 h after the event, and the thermal stability of the 100-mK stage was recovered about 47 h later. The physical cause of this anomaly was not found, but the problem has not recurred.
- Instabilities were observed in the temperature of the 4He-JT stage, which were traced to interactions with lower temperature stages, similar in nature to instabilities observed during ground testing (Planck Collaboration 2011b). They were fixed by exploring and tuning the operating points of the multiple stages of the cryo-system.
- The length of the daily telecommunications period was increased from 180 to 195 min to improve the margin available and ensure completion of all daily activities.

The commissioning activities were formally completed at the time when the HFI bolometer stage reached its target temperature of 100 mK, on 3 July 2009 at 01:00 UT. At this time all the critical resource budgets (power, fuel, lifetime, etc.) were found to contain very significant margins with respect to the original specification

## Calibration and Performance Verification: (provide date, and summary overview)

Calibration and performance verification (CPV) activities started during the cool-down period and continued until the end of August 2009. Their objectives were to:

- verify that the instruments were optimally tuned and their performance characterised and verified;
- perform all tests and characterisation activities which could not be performed during the routine phase;
- characterise the spacecraft and telescope characteristics of relevance for science;
- estimate the lifetime of the cryogenic chain.

CPV activities addressed the following areas:

- tuning and characterisation of the behaviour of the cryogenic chain;
- characterisation of the thermal behaviour of the spacecraft

and payload;

- for each of the two instruments: tuning; characterisation and/or verification of performance, calibration (including thermal, RF, noise and stability, optical response); and data compression properties;
- determination of the focal plane footprint on the sky;
- verification of scanning strategy parameters;
- characterisation of systematic effects induced by the spacecraft and the telescope, including:
  - dependence on solar aspect angle;
  - dependence on spin;
  - interference from the RF transmitter;
  - straylight rejection;
  - pointing performance.

The schedule of CPV activities consumed about two weeks longer than initially planned, mainly due to:

- the anomalous switch to standby mode of the 4He-JT cooler on 6 August (costing 6 days until recovery);
- instabilities in the cryo-chain, which required the exploration of a larger parameter phase space to find an optimal setting point;
- additional measurements of the voltage bias space of the LFI radiometers, which were introduced to optimise its noise performance, and led to the requirement of artificially slowing the natural cool-down of the 4He-JT stage.

A more detailed description of the relevant parts of these tests can be found in Mennella et al. (2011) and Planck HFI Core Team (2011a). On completion of all the planned activities, it was concluded that:

- the two instruments were fully tuned and ready for routine operations. No further parameter tuning was expected to be needed, except for the sorption cooler, which requires a weekly change in operational parameters (Planck Collaboration 2011b);
- the scientific performance parameters of both instruments was in most respects as had been measured on the ground before launch. The only significant exception was that, due to the high level of Galactic cosmic rays, the bolometers of HFI were detecting a higher number of glitches than expected, causing a modest ( $\sim 10\%$ ) level of systematic effects on their noise properties (see details in Planck HFI Core Team 2011a);
- the telescope survived launch and cool-down in orbit without any major distortions or changes in its alignment;
- the lifetime of the cryogenic chain was adequate to carry the mission to its foreseen end of operations in November 2010, with a margin of order one year;
- the pointing performance was better than expected, and no changes to the planned scanning strategy were required;
- the satellite did not introduce any major systematic effects into the science data. In particular, the telemetry transponder did not result in radio-frequency interference, which implies that the data acquired during visibility periods is useable for science.

## Nominal Mission: (provide date, and summary overview)

The routine operations phase of Planck is characterised by continuous and stable scanning of the sky and data acquisition by LFI and HFI. It started with the First Light Survey (FLS) on 13 August of 2009, at 14:15 UT.

The FLS was the last major activity planned before the start of routine surveying of the sky. It was conceived as a two-week period during which Planck would be fully tuned up and operated as if it was in its routine phase. This stable period could have resulted in the identification of further tuning activities required to optimise the performance of Planck in the long-duration surveys to come. The FLS was conducted between 13 and 27 August, and in fact led to the conclusion that the Planck payload was operating stably and optimally, and required no further tuning of its instruments. Therefore the period of the FLS was accepted as a valid part of the first Planck survey.

## Survey scanning and performance

### The observation strategy

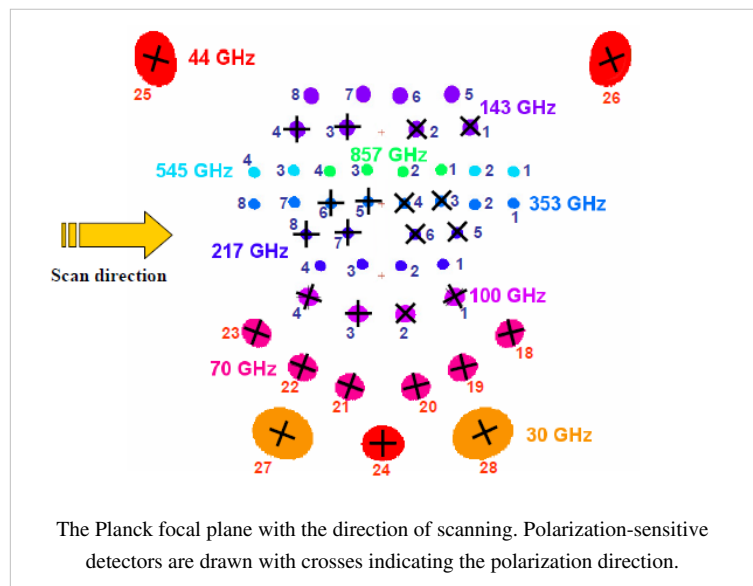
The Planck *observation strategy*, or *scanning strategy*, makes use of the characteristics of the Planck spacecraft and orbit in order to achieve the survey goals in terms of sky coverage and scanning directions.

The Planck focal plane scans the sky in the way explained in the figure below.

The 353 GHz row scans the sky in small circles with a 85 deg. bore-sight angle from the spin axis. 545 GHz, 857 GHz, 143 GHz bolometers as well as LFI 25-26 radiometers have a slightly smaller bore-sight angle, while the other part of the Planck focal plane have larger ones (up to  $\sim 89$  deg.). The Planck spacecraft spins at a rate of 1 rpm.

Planck, being at L2, moves along the Ecliptic at  $\sim$  one degree per day, and needs to keep the Solar aspect angle below  $\sim 9$  degrees at all times. In practice, during the surveys, the limit considered is 8 deg. Another celestial constraint is that the angle

between the Planck spin axis and the anti-Earth direction cannot exceed 15 deg. (relaxed to 17 deg. from Survey 5 onward). These constraints have a very direct influence on the chosen scanning strategy.



The path followed by the Planck spin axis is defined with respect to the Ecliptic plane. It corresponds to a motion in longitude which maintains an anti-Sun pointing (about one degree per day), to which is added a cycloidal motion (precession) of the spin axis around the anti-Sun position (fiducial point). The cycloidal path is defined by the following functions:

$$\lambda = \theta \sin((-1)^n \omega (t - t_0) + \varphi) \quad (\text{eq. 1})$$

$$\beta = -\theta \cos((-1)^n \omega (t - t_0) + \varphi) \quad (\text{eq. 2})$$

where  $\lambda$  is the angular distance from the fiducial point in Ecliptic longitude,  $\beta$  the angular distance from the fiducial point in Ecliptic latitude,  $\theta$  the spin axis precession amplitude,  $\omega$  the pulsation of the precession,  $\varphi$  its phase,  $n$  the parameter which controls the motion direction of the precession,  $t$  is the time, and  $t_0$  is the first time during the Planck survey at which the fiducial point crosses the 0 Ecliptic longitude line.

The reasons to decide to use such a precession of the spin axis are the following :

- An excursion of the spin axis from the anti-Sun direction is required to fully observe the whole sky (no excursion would leave a large area unobserved around the Ecliptic poles)
- The precession motion allows to keep the Sun aspect angle constant during the whole survey, therefore minimizing the thermal constraint variations on the spacecraft

The following precession parameters have been chosen for the BSS:

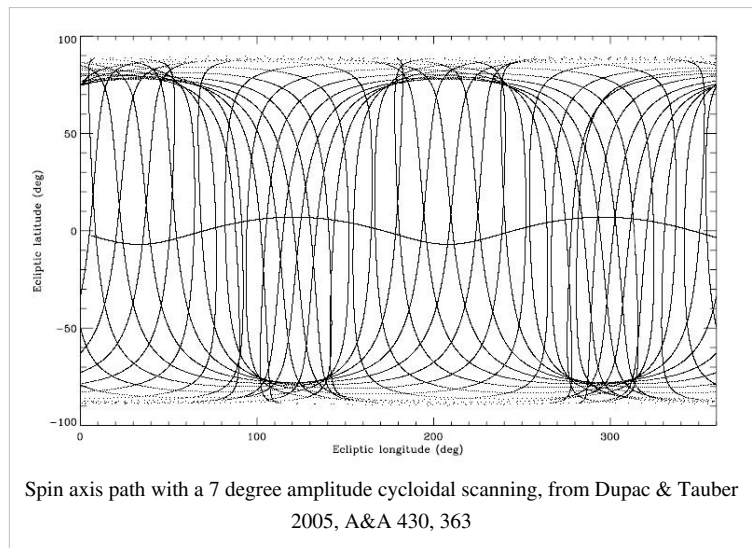
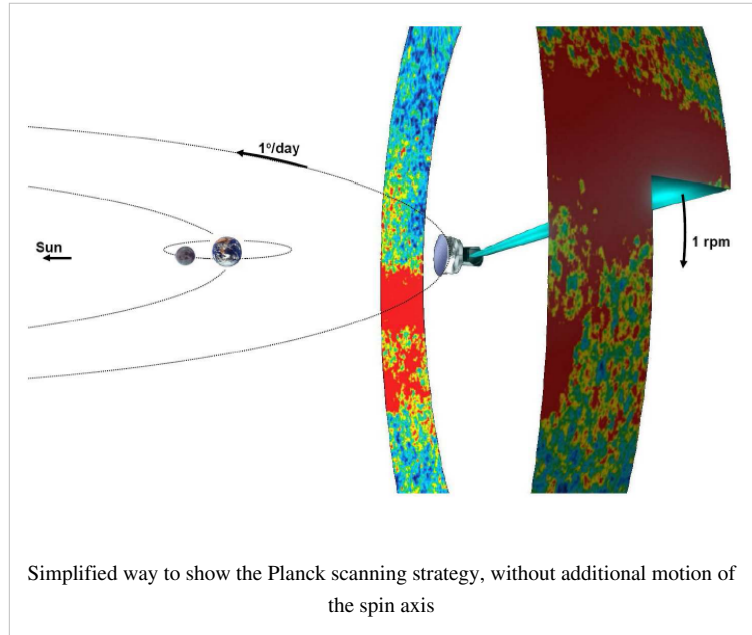
- amplitude  $\theta = 7.5^\circ$  (this value is the lowest possible which allows to cover the whole sky with all detectors)
- $n = 1$  (anti-clockwise motion as seen from the Sun)
- pulsation  $\omega = 2\pi / (\text{half a year})$ . Faster precession was considered, and has interesting advantages, but is not possible given the constraints if one wants to keep a  $7.5^\circ$  amplitude (which is necessary to cover the whole sky).
- The phase of the precession was decided according to this set of criteria (in order of importance):

a) respecting the operational constraints,

b) allowing the largest possible angle between two scans on the Crab,

c) avoiding null dipole amplitude for the whole mission,

d) optimizing the position of the planets in the beginning of the survey and with respect to the feasibility of their recovery,



- e) placing the two “deep fields” where Galactic foregrounds are minimum,
- f) allowing a reasonable survey margin (i.e. the time allowed to recover lost pointings if a problem occurs)

The phase is 340 deg. for Surveys 1 to 4, and 250 deg. for Surveys 5 to 8.

The scanning strategy for the second year of Routine Operations (i.e. Surveys 3 and 4) is exactly the same as for the first year, except that all pointings are shifted by 1 arcmin along the cross-scanning direction, in order to provide finer sky sampling for the highest frequency detectors when combining two years of observations.

The change of phase between Survey 4 and Survey 5 occurred because it was found essential especially on the HFI side that scanning direction crossings are increased in the Planck survey. By choosing a phase 90 deg. away from the original one, one optimizes the scanning strategy in this respect.

The details of the justifications for these parameters can be found in PL-WG9-TN-001.

The scanning strategy parameters are input to the PSO Survey Planning and Performance Tool, which is the software which generates the series of pointing records to be sent out to MOC for implementation.

An approximate visualisation of the Planck scanning strategy can be found here [1] and there [2].

## Spin axis manoeuvres and exact pointings

The motion of the spin axis is not continuous. Every change in the spin axis position is initiated by a manoeuvre which requires less than 5 minutes time to complete.

The duration between spin-axis manoeuvres is hereafter referred to as “dwelling times”; and the angular distance between manoeuvres along the spin axis path is hereafter referred to as “spacing”.

The dwelling times and spacings are defined as follows:

- The spacings are fixed to 2' which roughly corresponds to Nyquist criterion for sampling the highest-frequency HFI detectors.
- The dwell times vary from 2360 s to 3904 s.

The exact series of coordinates and dwell times are set by equations 1 and 2 when one has fixed the spacings.

## Data gap recoveries

Gaps in the data flow can occur because of various reasons:

- Anomalies may occur at spacecraft or instrument level, but also due to failures in the ground-to-spacecraft link or the ground segment itself. The adverse effects of such anomalies may be the loss of scientific data corresponding to one or several planned pointings, which have either not been acquired and/or stored in memory.
- Failure to acquire proper scientific data may occur to one or both instruments

In case a gap occurs, scientific criteria are applied to decide whether to recover the data through the Small-Gap Recovery procedure.

The Small-Gap Recovery (SGR) procedure can be applied by MOC or PSO:

- **MOC-triggered SGR:** Within its nominal scheduling procedure for an OD, the MOC searches the PPL for PREF corresponding to the OD being processed and any pointings which are subject of a Small Gap Recovery. As the PREF are sorted in chronological order according to their nominal start time, those corresponding to a small gap will naturally be the earliest. After checking attitude constraints, all observable pointings are listed and their dwell times reduced (initially) to the Minimum Dwell Time (MDT) as given in the PPL.

Having included all valid PREF the required slew times are calculated. With the required slew times and minimum dwell times for all pointings, the OD schedule may be under-populated; in this case the dwell times of all scheduled pointings will be increased equally to make use of all available time in the OD. If the resulting schedule is over-populated, even with MDT for all pointings, the recovery cannot be constrained to a single OD. The sequence



of pointings for the ODs involved will be optimized in PREF scheduling and dwell times in order to effect the recovery and revert to the nominal timeline as quickly as possible.

- **PSO-triggered SGR:**

PSO declares a small gap when pointings that have been executed result in data of insufficient quality or inadequate frequency coverage. This assessment is based on data quality and instrument health information provided by the DPCs. The algorithm that is used by the PSO to check the scientific validity of a pointing is implemented within the SPPT software tool. The SPPT ingests on a weekly basis a Weekly Health Report (WHR) for the HFI and LFI containing information on the current working status of each detector and their expected condition over the next four weeks. On a daily basis, a Daily Quality Report (DQR) provided by the DPCs for both instruments, includes a set of parameters that describe the quality of the detection achieved by each individual detector for every pointing executed.

The scheme for declaring a Small-Gap Recovery from PSO is the following:

- If a pointing fails to meet the chosen requirement, it becomes an SGR candidate
- If there are at least 12 consecutive pointings which are declared SGR candidates, and the problem has been identified and solved, then an SGR is triggered Recoveries are only carried out if the recovery slewing out is guaranteed to be in OCM. MOC carries out this analysis and decides whether they perform the SGR accordingly.
- The start and end times of the gap and the list of the pointing numbers (or just the numbers of the first and last pointings to be recovered) are then sent to MOC by E-mail, with the notification to start a Small-Gap Recovery
- MOC implements the Small-Gap Recovery, provided the pointings can still be scheduled with respect to their latest start time, using the same scheme as described in the MOC-triggered SGR section

Throughout the Planck mission, data losses have been very rare. Small-Gap Recovery has been applied only a couple of times.

## Special observations

The special observations are:

- normal scanning on Solar System objects for calibration purposes

This concerns the following objects (planets): Mars, Jupiter, Saturn, Uranus and Neptune whose thermal emission in the far-infrared and their point-source-like quality make them essential calibrators for spider-web bolometers and radiometers.

Mars is a particularly interesting calibrator for Planck because of its proper motion. However this proper motion makes it difficult to observe it many times during the mission.

Jupiter is the brightest source for (non-polarized) calibration. Saturn is also used a lot, and Uranus and Neptune are secondary calibrators.

- normal scanning on other (non-moving) sources for calibration purposes

This concerns mostly the Crab Nebula for polarizer calibration purposes. This supernova remnant is highly polarized and as such represents the main polarization calibrator for Planck.

- special pointings during the calibration phase, not relative to celestial sources



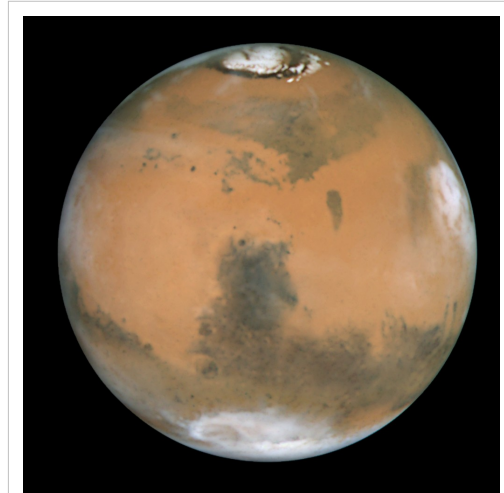
The Crab Nebula (Messier 1, NGC 1952, Taurus A), here seen by the Hubble Space Telescope

- "deep rings" : these special observations are performed on each passage of Jupiter and the Crab Nebula, from January 2012 onward.

They consist of very deeply sampled observations (0.5') with the spin axis along the Ecliptic plane, during typically two to three weeks.

These observations benefit from special relaxing of the celestial constraints with Solar Aspect Angles  $< 9$  deg. rather than  $< 8$  deg. during cycloidal surveying.

- "drift scans" : these special observations are performed on Mars, making use of its proper motion



Mars as seen by the Hubble Space Telescope in 1999

## Start and end of surveys

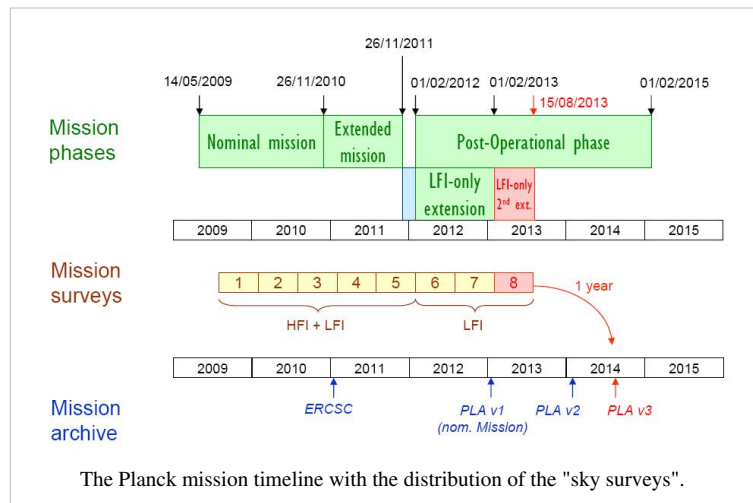
The completion of a given "survey" is declared when the logical AND of all frequency-coverage maps is greater than 95 %, OR the sky has been surveyed over a consecutive period of 7.5 months. Note that this definition is that of the Project Scientist and Planck Science Office. Data Processing Centres do not use the same concept of surveys to create "survey" maps.

In practice, since the gaps during the surveys have always been very small, it results in  $\sim$  six months per survey.

- **Survey 1:** starts August 13, 2009, ends Feb. 13, 2010
- **Survey 2:** starts Feb. 14, 2010, ends Aug. 13, 2010
- **Survey 3:** starts Aug. 14, 2010, ends Feb. 13, 2011
- **Survey 4:** starts Feb. 14, 2011, ends July 29th, 2011

This survey was shortened in ordered to start earlier with the new scanning strategy (see above).

- **Survey 5:** starts July 29th, 2011, ends January 30th, 2012
- **Survey 6 (LFI only):** starts January 30th, 2012, ends July 31st, 2012
- **Survey 7 (LFI only):** starts July 31st, 2012, ends January 31st, 2013
- **Survey 8 (LFI only):** starts February 1st, 2013, ends August 1st, 2013



## Completion of full sky coverage during Surveys 1-2

The picture gallery below exhibits the progress of sky coverage during the first months of survey (black color = unobserved areas).

The HFI 353 GHz integration time after N months of survey. Unit is seconds per square degree, normalized to one detector.

## Main planet and Crab observations during Surveys 1-7

Solar System objects and the Crab Nebula have been observed many times during the Planck surveys. Here is a complete list of these observations. Note that the *deep rings* and *drift scans* (Mars only) are in **boldface**.

- Crab: Sept. 16-22, 2009
- Mars: Oct. 17-29, 2009
- Jupiter: Oct. 25 – Nov. 1, 2009
- Neptune: Nov. 1-8, 2009
- Uranus: Dec. 6-16, 2009
- Saturn: Jan. 2-8, 2010
- Crab: March 6-12, 2010
- Mars: April 9-18, 2010
- Neptune: May 15-23, 2010
- Saturn: June 13-22, 2010
- Uranus: June 27 – July 5, 2010
- Jupiter: July 1-9, 2010
- Crab: Sept. 15-21, 2010
- Neptune: Nov. 3-11, 2010
- Jupiter: Dec. 9-18, 2010
- Uranus: Dec. 12-21, 2010
- Saturn: Jan. 15-22, 2011
- Crab: March 7-12, 2011
- Neptune: May 18-26, 2011
- Saturn: June 30 - July 9, 2011
- Uranus: July 3-11, 2011
- Jupiter: Aug. 9-15, 2011
- Crab: Sept. 10-18, 2011

This Crab scan was performed with the 250 deg. phase cycloidal strategy.

- Crab: Sept. 20-23, 2011

This Crab scan was performed with the 340 deg. phase cycloidal strategy.

- **Mars**: Dec. 8-16, 2011 ("drift scan": Mars is let move through the Planck focal plane via its proper motion)
- Mars: Dec. 17-26, 2011 (normal scanning)
- **Jupiter**: Jan. 8-30, 2012 (deep ring)

- **Crab:** Feb. 26 - March 16, 2012 (deep ring)
- **Jupiter:** Sept. 1-14, 2012 (deep ring)
- **Crab:** Sept. 14 - Oct. 1, 2012 (deep ring)
- Neptune: Nov. 19-27, 2012
- Uranus: Dec. 24-30, 2012
- Saturn: Jan. 30 - Feb. 5, 2013
- **Jupiter:** Feb. 2013 (deep ring)

## Resulting integration time distribution

The integration time after the end of HFI operations (January 2012) is shown in the following picture gallery.

Units are seconds per square degree, normalized to one detector, for all maps. The projection is full-sky Mollweide centered on the Galactic Centre.

Integration time after the end of HFI operations (January 2012). Units are seconds per square degree, normalized to one detector.

## References

[1] <http://www.youtube.com/watch?v=WwFXuZ0B3B8>

[2] <http://www.youtube.com/watch?v=7Zu-aiEiDtY>

# Thermal environment

---

(Note: Adapted from Planck Collaboration 2011, A&A 536, A1)

The satellite design and its location at L2 provide an extremely stable thermal environment. The main temperature variation on long timescales is driven by the total radiative power absorbed by the solar panels, which varies depending on distance from the Sun and the solar aspect angle (i.e. the angle between the solar direction and the spin axis). On shorter timescales, temperature variations are driven by active thermal regulation cycles. Both seasonal and shorter-timescale variations are observed across the satellite's service module (SVM), but are heavily damped and almost unobservable within the payload module (PLM).

Specific operations and deviations from the scanning strategy have a thermal influence on the satellite and payload. Some significant effects are listed below.

- The thruster heaters were unintentionally turned off between 31 August and 16 September 2009 (the so-called “catbed” event).
  - As planned, the RF transmitter was initially turned on and off every day in synchrony with the daily visibility window, in order to reduce potential interference by the transmitter on the scientific data. The induced daily temperature variation had a measurable effect throughout the satellite. An important effect was on the temperature of the 4He-JT cooler compressors, which caused variations of the levels of the interference lines that they induce on the bolometer data (Planck HFI Core Team 2011a). Therefore the RF transmitter was left permanently on starting from 25 January 2010 (257 days after launch), which made a noticeable improvement on the daily temperature variations.
  - A significant thermal effect arises from the (approximately) weekly adjustments to the operation of the Sorption Cooler.
-

The thermal environment of the payload module is – by design – extremely well decoupled from that of the service module. As a consequence, in spite of the significant thermal perturbations originating in the SVM, the thermal variability affecting the detectors is essentially completely due to the operation of the cryogenic cooling chain (described in detail in Planck Collaboration 2011b), which ensures their cold environment.

## Radiation environment

(Note: Adapted from Planck Collaboration 2011, A&A 536, A1)

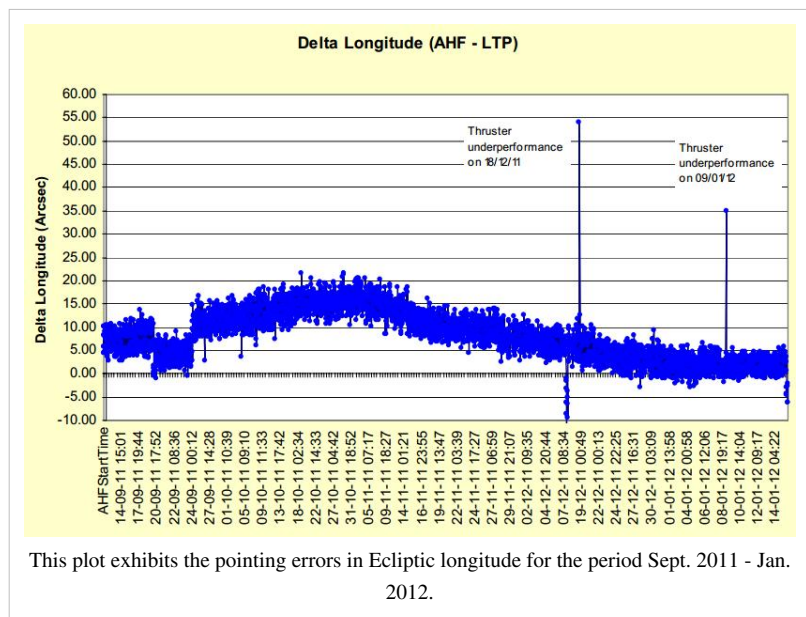
The Standard Radiation Environment Monitor on board Planck (SREM, Buehler et al. 1996) is a particle detector which is being flown on several ESA satellites. The SREM consists of several detectors sensitive to different energy ranges, which can also be used in coincidence mode. In particular, the SREM measures count rates of high energy protons with  $E > 20$  MeV, electrons with  $E > 0.5$  MeV and Ions with  $150 \text{ MeV} < E < 185 \text{ MeV}$ .

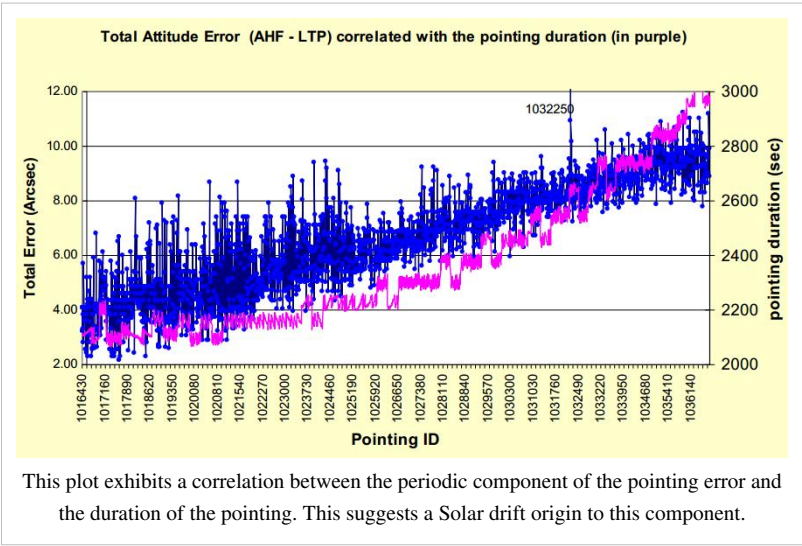
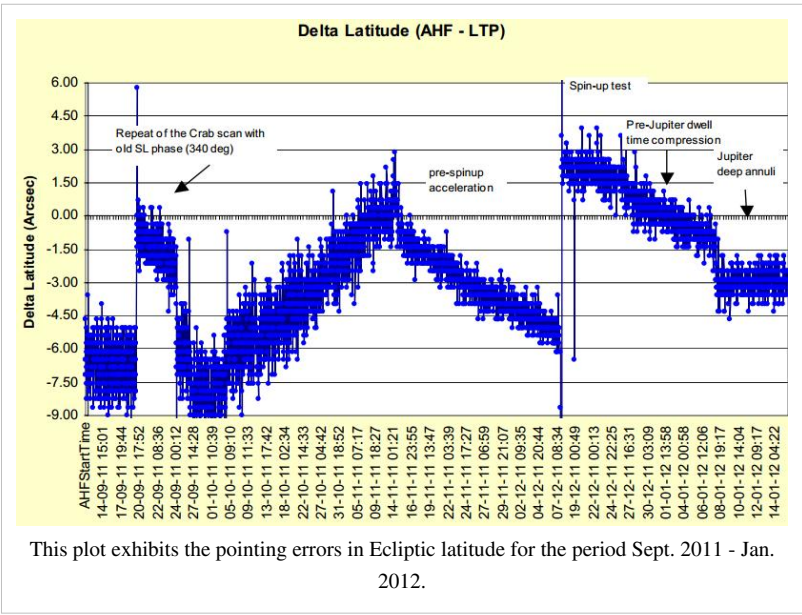
Particle fluxes measured by the SREM on board Planck are shown in Fig. 8. The radiation environment of Planck is characterised by the current epoch near the minimum in the solar cycle. As a consequence, the particle flux is dominated by Galactic cosmic rays, rather than by the solar wind. The time evolution of the SREM measurements is well correlated with that of identical units flying simultaneously on other satellites (e.g., Herschel, Rosetta) and with indicators of Galactic cosmic rays, and is anti-correlated with solar flare events and with the solar cycle (Fig. 8). More importantly for Planck, the SREM measurements are very well correlated with the heat deposition on the coldest stages of the HFI, and with glitch rates measured by the detectors of HFI. A more detailed interpretation of these data is provided in Planck HFI Core Team (2011a).

## Pointing performance

The pointing performance of Planck can be measured by the difference between the executed pointings as described in the Attitude History Files (using the Star Trackers and the Fiber Optics Gyroscope), and the planned pointings by PSO in the Pre-Programmed Pointing Lists.

The pointing performance of Planck has been very good throughout operations, as the plots in the right panel show.





---

# Data Processing

---

## Data flow overview

---

(Note: Adapted from Planck Collaboration 2011, A&A 536, A1 & Tauber et al. 2012, A&A 520, A1)

The Planck satellite generates (and stores on-board) data continuously at the following typical rates: 21 kilobit s<sup>-1</sup> (kbps) of house-keeping (HK) data from all on-board sources, 44 kbps of LFI science data and 72 kbps of HFI science data. The data are brought to ground in a daily pass of approximately 3 h duration. Besides the data downloads, the passes also acquire realtime HK and a 20 min period of real-time science (used to monitor instrument performance during the pass). Planck utilises the two ESA deep-space ground stations in New Norcia (Australia) and Cebreros (Spain), usually the former. Scheduling of the daily telecommunication period is quite stable, with small perturbations due to the need to coordinate the use of the antenna with other ESA satellites (in particular Herschel).

At the ground station the telemetry is received by redundant chains of front-end/back-end equipment. The data flows to the mission operations control centre (MOC) located at ESOC in Darmstadt (Germany), where it is processed by redundant mission control software (MCS) installations and made available to the science ground segment. To reduce bandwidth requirements between the station and ESOC only one set of science telemetry is usually transferred. Software is run post-pass to check the completeness of the data. This software check is also used to build a catalogue of data completeness, which is used by the science ground segment to control its own data transfer process. Where gaps are detected, attempts to fill them are made as an offline activity (normally next working day), the first step being to attempt to reflow the relevant data from station. Early in the mission these gaps were more frequent, with some hundreds of packets affected per week (impact on data return of order 50 ppm) due principally to a combination of software problems with the data ingestion and distribution in the MCS, and imperfect behaviour of the software gap check. Software updates implemented during the mission have improved the situation such that gaps are much rarer, with a total impact on data return well below 1 ppm.

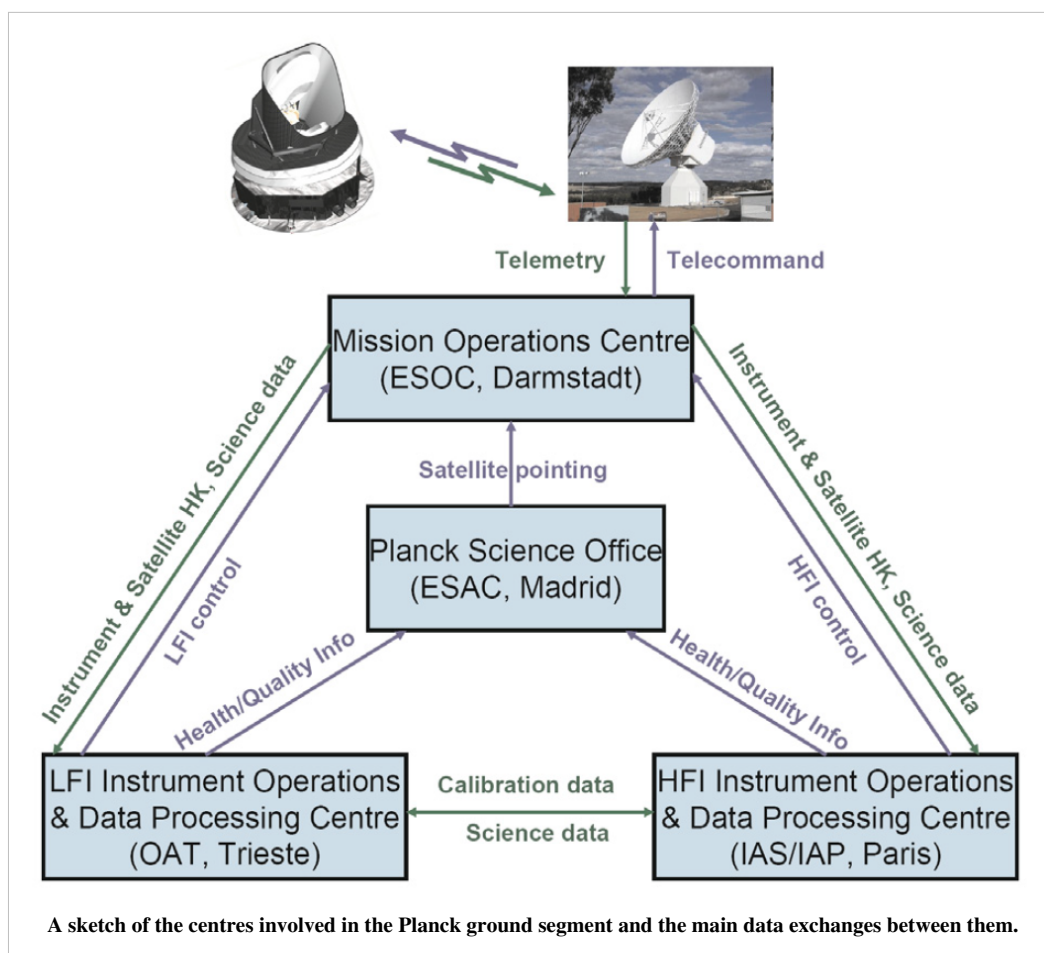
Redump of data from the spacecraft is attempted when there have been losses in the space link. This has only been necessary on three occasions. In each case the spacecraft redump has successfully recovered all the data.

An operational principle of the mission is to avoid impact on the nominal science of a completely missed ground station pass. Commanding continuity is managed by keeping more than 24 h of commanding-timeline queued on-board. The telemetry resides on board the satellite in a ~60 h circular buffer in solidstate memory, and can be recovered subsequently using the margin in each pass, or more rapidly by seeking additional station coverage after an event. The lost-pass scenario has in fact occurred only once (on 21 December 2009), when snow on the dish at Cebreros led to the loss of the entire pass. A rapid recovery was made by using spare time available on the New Norcia station. Smaller impacts on the pass occur more often (e.g., the first ~10 min of a pass may be lost due to a station acquisition problem) and these can normally be recovered simply by restarting a software task or rebooting station equipment. Such delays are normally accommodated within the margin of the pass itself, or during the subsequent pass.

All the data downloaded from the satellite, and processed products such as filtered attitude information, are made available each day for retrieval from the MOC by the LFI and HFI Data Processing Centres (DPCs). Typically, the data arrive at the LFI (resp. HFI) DPC 2 (resp. 4) hours after the start of the daily acquisition window. Automated processing of the incoming telemetry is carried out each day by the LFI (resp. HFI) DPCs and yields a daily data quality report which is made available to the rest of the ground segment typically 22 (resp. 14) hours later. More sophisticated processing of the data in each of the two DPCs is described in Zacchei et al. (2011) and Planck HFI Core Team (2011b).

---







# On-board processing

---

## MOC processing

---

(Note: Adapted from Tauber et al. 2010, A&A 520, A1 & private communication from S. Foley)

The mission operations centre (MOC), located at ESA's operations centre in Darmstadt (Germany), is responsible for all aspects of flight control and of the health and safety of the Planck satellite, including both instruments. It plans and executes all necessary satellite activities, including instrument commanding requests by the instrument operations centres. MOC communicates with the satellite using two ESA deep-space ground stations in New Norcia (Australia) and Cebreros (Spain), usually the former, over a daily 3-h period, during which it uplinks a scheduled activity timeline which is autonomously executed by the satellite, and downlinks the science and housekeeping (HK) data acquired by the satellite during the past 24 h. The downlinked data are transferred from the ground station to the MOC over a period of typically 8 h; at MOC they are put onto a data server from where they are retrieved by the two Data Processing Centres.

There is no data processing done at MOC. Only transfer and storage of data is performed at this stage. MOC verifies the reception of all telemetry packets, which are transferred from the spacecraft via the ground station, as given by the Source Sequence Count related to each Virtual Channel (VC) and Application ID (APID). All data are stored in the Long Term Archive (LTA) as telemetry packets (duplicated in A and B archives). The LTAs present an archive of all data, both science and house-keeping, acquired through the whole mission.

## The HFI DPC

---

The HFI DPC has been organized into different "Levels": 1, 2, 3, 4 and "S". In brief, during operations, L1 feeds the database resulting in time-ordered information (TOI) objects. L2 is the core of the processing, which turns TOIs into clean calibrated sky maps. L3 transforms these maps at specific frequencies into more scientific products, like catalogues, maps and spectra of astrophysical components. L3 can rely on simulation provided by the LS, while L4 refers to delivering the DPC products to ESA. This processing relies on dedicated software and hardware infrastructures developed pre-launch.

The data processing applied for the *"Early Planck results"* series of publications was described in early paper VI <sup>[1]</sup>. The and its co-papers provide the reference for the processing done for the 2013 Data release. An Annex of P03 specifies what had been done (and resulting characteristics) for the *"Intermediate Planck results"* series of publications.

## Level 1: building the reference database during flight operations

(L1): consists in receiving the telemetry and ancillary data files and ingesting them into the DPC database. This involves decompressing, in some cases changing data formats, computing the time of individual data samples from the time of the compression slices, but otherwise no processing proper. Other steps are:

- data ingestion (science, HK, ancillary, other?)
- construction of ToS in science data group
- pointing interpolation
- construction of other TOI and ROI objects from AHF, ...

This is further described in the Pre-processing section.

## Level 2: converting temporal information into clean calibrated maps

(L2): this is where the data are processed from timelines into maps. The main processing steps are

- Timeline (or Time-Ordered Information = TOI) processing, which includes conversion from ADUs to engineering units (Volts), demodulation, deglitching, conversion from engineering to physical units (Watts), removal of known systematic effects (non-linearities, 4K lines, Jumps, ring flagging), removal of the instrumental signature (time transfer function), temporal noise Estimation. Details here.
- Pointing and beam of each detector. See section Pointing&Beams.
- map-making & photometric calibration: projecting the TOIs onto all-sky maps, etc. See section Map-making.
- Characterisation/validation through angular power spectra. See section PowerSpectra.
- Overall HFI data validation, through difference tests, comparison to detailed simulations, etc., See section HFI-Validation
- The resulting data characteristics are given in section Summary.

## Level 3: Basic analyses of (Level 2) Frequency maps

(L3): This is where the data in the form of frequency maps are converted to catalogues and full sky astrophysical component maps. Much of this is done in common with the LFI DPC, and is further described in the HFI/LFI common sections .

## Level 4 : Delivering results

Level 4 is the "Archive Level". No processing done, but rather exporting, reformatting, documenting.

## Level S : A common HFI/LFI simulation software

Level S is the so-called "Simulation Level" software suite common to both consortia, which, given a sky model (generated by the Planck sky model, PSM), detectors pointing and beams, generates the infalling power on each detector. It can also provide a simplified description of eg. the noise. It is further described in the HFI/LFI common section. HFI specific developments (configuration control & MC bench, specific effects like 4K lines, glitches, ADC non-linearity, etc.) are described in the HFI data validation section.

## HFI DPC Infrastructures

The HFI Data Processing Centre can be thought of as a centralized backbone providing hardware and software infrastructures to a relatively large number of geographically distributed groups of developers and other R&D groups in the HFI and LFI core teams.

An overview was given in the HFI data processing paper of the *"Planck Early Results"* series. In particular:

- Code and configuration management can be found at early paper VI <sup>[2]</sup>.
- Data management at early paper VI <sup>[2]</sup>.
- Instrument model (IMO) database at early paper VI <sup>[3]</sup>.
- Data flow management at early paper VI <sup>[3]</sup>.
- Hardware at early paper VI <sup>[4]</sup>.

## References

- [1] [http://www.rssd.esa.int/livelink/fetch/-60063/3036676/3065909/3110897/3135828/3135852/PE\\_paper6.pdf#page=1](http://www.rssd.esa.int/livelink/fetch/-60063/3036676/3065909/3110897/3135828/3135852/PE_paper6.pdf#page=1)
- [2] [http://www.rssd.esa.int/livelink/fetch/-60063/3036676/3065909/3110897/3135828/3135852/PE\\_paper6.pdf#page=34](http://www.rssd.esa.int/livelink/fetch/-60063/3036676/3065909/3110897/3135828/3135852/PE_paper6.pdf#page=34)
- [3] [http://www.rssd.esa.int/livelink/fetch/-60063/3036676/3065909/3110897/3135828/3135852/PE\\_paper6.pdf#page=35](http://www.rssd.esa.int/livelink/fetch/-60063/3036676/3065909/3110897/3135828/3135852/PE_paper6.pdf#page=35)
- [4] [http://www.rssd.esa.int/livelink/fetch/-60063/3036676/3065909/3110897/3135828/3135852/PE\\_paper6.pdf#page=36](http://www.rssd.esa.int/livelink/fetch/-60063/3036676/3065909/3110897/3135828/3135852/PE_paper6.pdf#page=36)

# Pre-processing

---

## Overview

In terms of data processing, the HFI ground segment handles two types of data, both made available via the MOC:

- telemetry data transmitted from the satellite. These come from the different subsystems of the satellite service module, from the sorption cooler and from the two instruments.
- auxiliary data. These are data produced by MOC. The only 3 products used by the HFI DPC are the pointing data, the orbit data, and the time correlation data.

All data are retrieved by the HFI level 1 software and stored in the HFI database.

## Telemetry data

The digitized data from the satellite are assembled on board in packets according to the ESA Packet Telemetry Standard and Packet Telecommand Standard, the CCSDS Packet Telemetry recommendations and the ESA Packet Utilization Standard. The packets are dumped to the ground during the Daily Transmission Control Period, consolidated by and stored at MOC. Telemetry data contain the housekeeping data and the bolometer (ie science) data.

## Housekeeping data

For several reasons (systems monitoring, potential impact of the environment, understanding of the bolometer data), the HFI level 1 software gathers and stores in its database the satellite subsystems housekeeping parameters:

- Command and Data Management System
  - Attitude Control & Measurement Subsystem
  - Thermal Control System
  - Sorption Cooler System
  - HFI housekeeping parameters
-

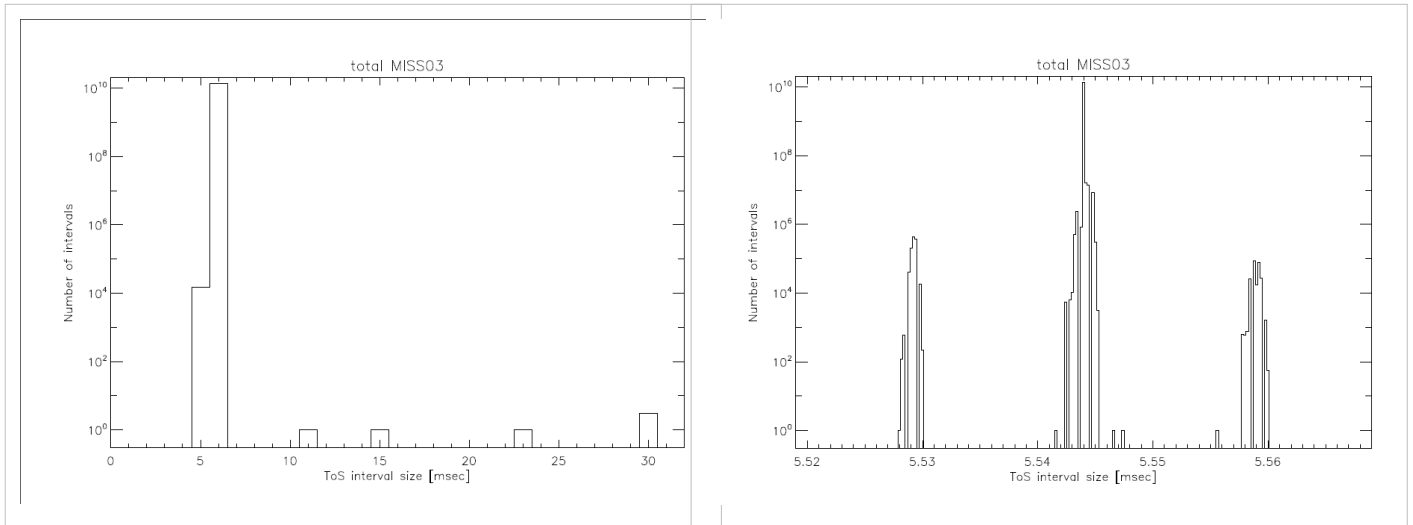
The structure and the frequency of the packets built by these subsystems and the format of the house keeping parameters are described in the Mission Information Bases [refer to an hypothetical MIB section under MOC responsibility]. The HFI L1 software uses these MIBs to extract the house keeping parameters from the packets. Given the status of each subsystem, the parameters are gathered in the HFI database in groups. The HFI L1 software builds in each group a vector of time (usually named TIMESEC) and a single vector per housekeeping parameter.

## Bolometer data

The HFI science data is retrieved and reconstructed as described in section 3.1 of early paper VI<sup>[1]</sup>.

On board, the signal from the 72 HFI channels is sampled at 180.4Hz by the Read-out Electronic Unit. 254 samples per channel are grouped into a compression slice. The Data Processing Unit then builds a set of several telemetry packets containing the compression slice data and adds to the first packet the start time of the compression slice. When receiving this set of telemetry packets, the L1 software extracts the samples and computes the time of each sample based on the compression slice start time (digitized with  $2^{-16}s = 15.26\mu s$  quantization steps) and a mean sample time between samples. For the nominal instrument configuration, the sample integration time is measured to be  $T_{\text{samp}} = 5.54404 \text{ ms}$

The two plots show the histogram of time differences between two successive samples for the full mission. 6 samples intervals ( $> 6 \text{ ms}$ ) correspond to 3 occurrences of packets lost on board when the on board software of the Command and Data Management Unit has been patched (18, 19 and 20th of August 2009). The right plot is a blow up of the left one. It shows the distribution around the mean value of 5,54 ms and the 15  $\mu s$  quantization step.



## Transfer functions

In order to ease the reading data in the HFI database, so called transfer functions are created. They allow software items to read data on which functions are applied on the fly. A simple example of a transfer function is the conversion of a thermometer data in Analogic to Digital Units (ADU) to Kelvins. Here we show the 2 transfer functions applied on the bolometer samples in the data processing pipelines:

**From raw signal to non demodulated signal in Volts** (transf1\_nodemod)

$$Signal\_ND\_V_{bc} = \frac{\frac{C_{bc}}{N_{sample} - N_{blank}_{bc}} - offset_{bc}}{F1_{bc}} \times \frac{G_{amp_{ETAL}}}{G_{amp_{bc}}}$$

where:

- $bc$  refers to a bolometer usually labelled by its electronic belt and channel. Eg.  $bc=00$  refers to the  $a$  part of the first 100 GHz Polarized Sensitive Bolometer.
- $C_{bc}$  is the bolometer sample in Analogic Digital Units (ADU)
- $N_{sample}$  is the number of samples in half a modulation period. This parameter is common to all bolometer channels and - although kept fixed during the whole mission - is read from the housekeeping parameter.  
 $N_{sample} = 40$
- $N_{blank}_{bc}$  is the number of samples suppressed at the beginning of each half modulation period. Although kept fixed during the whole mission, it is read from the housekeeping parameter. For  $bc=00$ ,  $Gamp_{ETAL} = 1$
- $F1_{bc}$  is a calibration factor. For  $bc=00$ ,  $F1_{00} \simeq 1.8 \times 10^7$ .
- $offset_{bc}$  is close to 32768
- $Gamp_{ETAL}$  is the gain amplifier measured during the calibration phase. For  $bc=00$ ,  $Gamp_{ETAL} = 1$
- $Gamp_{bc}$  is the current gain amplifier. Although kept fixed during the whole mission, it is read from the housekeeping parameter. For  $bc=00$ ,  $Gamp_{00} = 1$

#### From raw signal to demodulated signal in Volts (transf1)

The same formula as above is used but with the demodulation and a 3-point filter computed as:

$$Signal\_V_{bc}[n] = -\frac{1}{4}(-1)^{parity_{n-1}} Signal\_ND\_V_{bc}[n-1] + \frac{1}{2}(-1)^{parity_n} Signal\_ND\_V_{bc}[n] - \frac{1}{4}(-1)^{parity_{n+1}} Signal\_ND\_V_{bc}[n+1]$$

where:

- $n - 1$ , and  $n + 1$  refer to the samples before and after the given  $n_{sample}$  to demodulate
- $parity$  is computed by the HFI L1 software

#### Statistics on the telemetry data

The table gives some statistics about the data handled at the pre-processing level:

-	Nominal mission <sup>(1)</sup>	Full mission <sup>(1)</sup>	From launch to the end of full mission <sup>(1)</sup>
Duration	473days	884days	974days
Number of HFI packets generated onboard (HSK/science) <sup>(2)</sup>	19 668 436/ 376 294 615	37 762 493/ 704 852 262	41 689 4090/765 043 713
Number of HFI packets lost <sup>(3)</sup> (HSK/science)	2/20	2/20	2/20
ratio of HFI lost packets vs generated on board (HSK/science)	$1 \times 10^{-7}/5 \times 10^{-8}$	$5 \times 10^{-8}/3 \times 10^{-8}$	$5 \times 10^{-8}/3 \times 10^{-8}$
Number of different housekeeping parameters stored in the database (HFI/SCS/sat)	3174/708/12390		
Number of science samples stored in the database	530 632 594 653	991 929 524 565	1 090 125 748 960
Number of missing science samples	2 537 499	6 634 491 <sup>(4)</sup>	7 521 758
Ratio of missing science samples vs samples stored	$5 \times 10^{-6}$	$7 \times 10^{-6}$	$7 \times 10^{-6}$

- <sup>(1)</sup>: mission periods are defined in this page.
- <sup>(2)</sup>: science packets refer to the number of telemetry packets containing science data (ie: bolometer data and *fine thermometer* data) when the instrument is in observation mode (Application Program Identifier = 1412). HSK packets refer to the number of HFI *non essential* housekeeping telemetry packets (Application Program Identifier = 1410).
- <sup>(3)</sup>: all lost packets have been lost on board ; no HFI packet has been lost at ground segment level.
- <sup>(4)</sup>: this amount of lost science samples is distributed as

- 0.3% are due to Single Event Unit
- 18.5% have been lost during the 3 CDMU patch days and the consecutive clock resynchronisation
- 29.1% have been lost because of compression errors
- 52.1% have been lost due to the EndOfSlew buffer overflow being triggered by solar flare events

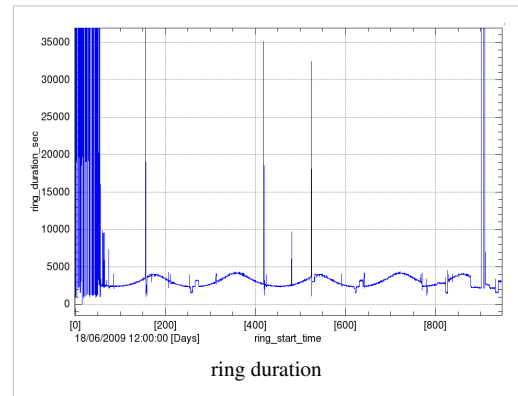
## Pointing data

The pointing data are built by the MOC Flight Dynamics team. The pointing data are made available to the DPC via AHF files. See AHF description document <sup>[2]</sup> and AHF files repository <sup>[3]</sup>. All data contained in the AHF files are ingested in the HFI database. The present section describes the steps to produce the HFI pointing solution.

- During the stable pointing period (ie during the dwell), data sampling rate is given at 8 Hz while it is at 4 Hz during the satellite slews. Those data are thus interpolated to the bolometer sampling rate using a spherically linear interpolation as described in section 3.4 of early paper VI <sup>[4]</sup>.
- The pointing solution is then amended from the wobble effect as delivered by MOC Flight Dynamics in the AHF files.
- A final correction is then applied based on the study of main planets and point sources seen by the bolometers.

**Note HFI ring** : a ring corresponds to a duration during each stable pointing period, when the spin axis is pointing towards an essentially fixed direction in the sky and the detectors repeatedly scan the same circle on the sky. More precisely the **HFI ring** start time is defined as the *time of the first thruster firing*. The end time of the HFI ring is the start time of the following ring.

The plot shows the evolution of the ring duration along the whole mission. It mainly reflects the scanning strategy and few *long* rings due to operational constraints or tests.



## Orbit data

Satellite orbit velocity is built by the MOC Flight Dynamics team and made available to the HFI DPC via orbit files. See Orbit description document <sup>[5]</sup> and orbit files repository <sup>[6]</sup>. As those orbit files contain both effective and predictive data, they are regularly ingested updated in the HFI database.

*Note: these same data are also ingested in parallel into the NASA JPL Horizons system (<http://ssd.jpl.nasa.gov/>) under ESA's responsibility.*

The satellite orbit data preprocessing is the following.

- The sampling of the MOC provided orbit velocity data is approximately 1 every 5 mn. These data are interpolated to the time of the middle of the HFI rings.
- The reference frame of the orbit data is translated from the MOC given Earth Mean Equator and Equinox J2000 (EME2000) reference frame to the ecliptic reference frame in cartesian coordinates.
- The earth velocity provided by the NASA JPL Horizons system (<http://ssd.jpl.nasa.gov/>) is interpolated to the time of the middle of the HFI rings. It is then added to the satellite velocity data.

The use of the satellite orbit velocity is three-fold:

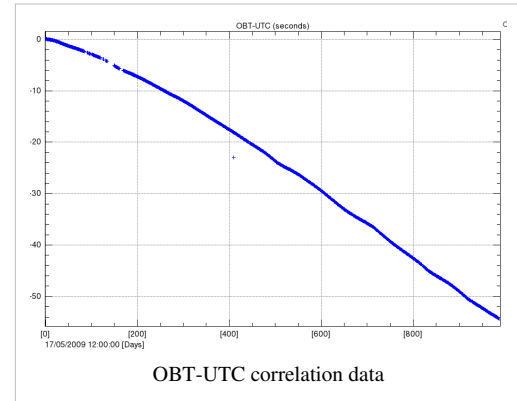
1. computation of the CMB orbital dipole (see calibration section)
2. computation of the positions of solar system objects (see data masking section)
3. computation of the aberration correction.

## Time correlation data

The MOC is responsible for providing information about the relationship between the satellite On Board Time (OBT) and Universal Coded Time (UTC). This information comes via several measurements of OBT and UTC pairs each day, measured during the satellite ranging. See Time Correlation document <sup>[7]</sup> and [\[refer to the PLA TCO folders\]](#) Time Correlation files repository.

The plot shows the (OBT, UTC) data couples provided by MOC since Planck launch. The x axis is in number of days since the 17th of May 2009 while the y axis is the difference of OBT and UTC in seconds. The very slow drift is approximately 0.05 seconds per day. The small wiggles are due to the satellite global temperature trends due to its orbit and distance to the sun. *Note: The extra couple on the 1st of June 2010 is not significant and due to a misconfiguration of the ground station parameters.*

An order 3 polynomial is then fitted to the data. As the whole HFI data management and processing uses OBT, the OBT-UTC information is only used when importing orbit data from Horizons.



## References

- [1] [http://www.rssd.esa.int/livelink/fetch/-60063/3036676/3065909/3110897/3135828/3135852/PE\\_paper6.pdf#page=5](http://www.rssd.esa.int/livelink/fetch/-60063/3036676/3065909/3110897/3135828/3135852/PE_paper6.pdf#page=5)
- [2] [http://www.rssd.esa.int/livelink/fetch/-60063/3036676/3065909/3110897/3139172/ICD\\_AHF.pdf#page=1](http://www.rssd.esa.int/livelink/fetch/-60063/3036676/3065909/3110897/3139172/ICD_AHF.pdf#page=1)
- [3] [http://pla.esac.esa.int/pla/aio/metadata-action?PAGE\\_SIZE=1500&PAGE=1&RESOURCE\\_CLASS=OPERATIONAL\\_FILE&SELECTED\\_FIELDS=OPERATIONAL\\_FILE&OPERATIONAL\\_FILE\\_TYPE.NAME=AHF&RETURN\\_TYPE=HTML](http://pla.esac.esa.int/pla/aio/metadata-action?PAGE_SIZE=1500&PAGE=1&RESOURCE_CLASS=OPERATIONAL_FILE&SELECTED_FIELDS=OPERATIONAL_FILE&OPERATIONAL_FILE_TYPE.NAME=AHF&RETURN_TYPE=HTML)
- [4] [http://www.rssd.esa.int/livelink/fetch/-60063/3036676/3065909/3110897/3135828/3135852/PE\\_paper6.pdf#page=6](http://www.rssd.esa.int/livelink/fetch/-60063/3036676/3065909/3110897/3135828/3135852/PE_paper6.pdf#page=6)
- [5] [http://www.rssd.esa.int/livelink/fetch/-60063/3036676/3065909/3110897/3139172/ICD\\_ODAT.pdf#page=1](http://www.rssd.esa.int/livelink/fetch/-60063/3036676/3065909/3110897/3139172/ICD_ODAT.pdf#page=1)
- [6] [http://pla.esac.esa.int/pla/aio/metadata-action?PAGE\\_SIZE=1500&PAGE=1&RESOURCE\\_CLASS=OPERATIONAL\\_FILE&SELECTED\\_FIELDS=OPERATIONAL\\_FILE&OPERATIONAL\\_FILE\\_TYPE.NAME=ORB&RETURN\\_TYPE=HTML](http://pla.esac.esa.int/pla/aio/metadata-action?PAGE_SIZE=1500&PAGE=1&RESOURCE_CLASS=OPERATIONAL_FILE&SELECTED_FIELDS=OPERATIONAL_FILE&OPERATIONAL_FILE_TYPE.NAME=ORB&RETURN_TYPE=HTML)
- [7] [http://www.rssd.esa.int/livelink/fetch/-60063/3036676/3065909/3110897/3139172/ICD\\_TCO.pdf#page=1](http://www.rssd.esa.int/livelink/fetch/-60063/3036676/3065909/3110897/3139172/ICD_TCO.pdf#page=1)

# TOI processing

---

This Section is kept short as this Planck release does not contain TOIs. The main information in the HFI processing paper is not duplicated here.

## Overview

We describe here the how the TOIs are processed in order to be used for map production. We do not repeat the general features of the pipeline which are given in the HFI Data Processing article (REF). Here we give complementary explanations on some details. The TOI of each bolometer is processed independently of the other bolometers, so as to keep the noise properties as uncorrelated as possible. The processing involves modifying the TOI itself for what concerns the conversion to absorbed power and the correction of glitch tails. It also adds a flag TOI that masks the TOI samples that are not to be projected on maps for various reasons.

## Input TOI

The input TOI consists in the AC modulated voltage output of the readout of each bolometer. The input has previously been decompressed, and converted from internal digital units to voltage via a constant factor. The TOI has a regular sampling at the acquisition frequency of  $f_{acq}=180.373700\pm0.000050$  Hz. There are almost no missing data in the TOIs, except for few hundred samples of 545 and 857GHz TOIs which are lost in the on-board compression due to saturation on the Galactic Center crossings.

## General Pipeline Structure

The figure on the right shows how the initial ccTOI is transformed and how flags are produced:

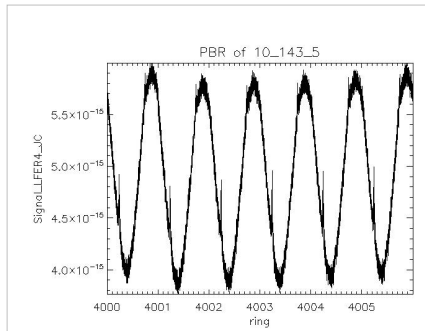
## Output TOIs and products

A TOI of clean calibrated samples (ccTOI) and a combined flag TOI (fTOI) are the outputs of the processing. The ccTOI is calibrated so as to represent the instantaneous power absorbed by the detector up to a constant (which will be determined by the map-making destriper). It is worth mentioning how the ccTOI is changed with respect to the input TOI, beyond the harmless constant conversion factor from voltage to absorbed power. The demodulation stage allows to get the demodulated bolometer voltage. The non-linearity correction is a second-order polynomial correction based on the physical but static bolometer model. In order to avoid too much masking after glitches, a glitch tail is subtracted after an occurrence of a glitch in the TOI. The 4K cooler lines noise is substituted at a series of 9 single temporal frequencies. Finally, the temporal response of the bolometer is deconvolved. This affects mostly the high-temporal frequency part of the TOI, although a small but significant low frequency (the long time response) tail is corrected too. Although flagged samples are not projected, their value influences the valid samples somehow. Hence interpolation procedures introduce some indirect modifications of the TOI. The flag TOI is a combination a dozen flags with an OR logic. Only unflagged data are projected. The exhaustive list of flags is given here: CompressionError, NoData, SSO, UnstablePointing, Glitch, BoloPlateFluctuation, RTS, Jump, PSBab. A complete qualification of the data is obtained at the ring level. If the TOI shows an anomalous behaviour on a given ring, this ring is discarded from projection. A special production of TOIs is also made as an input to the beam analysis with Mars, Jupiter and Saturn.

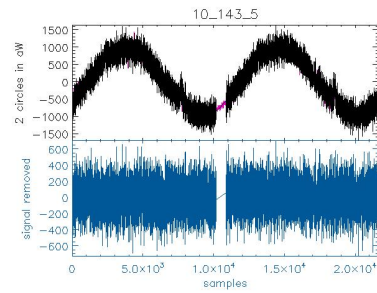
---



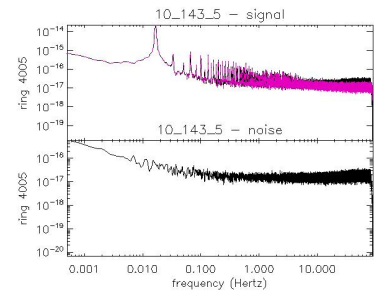
## Examples of clean TOIs



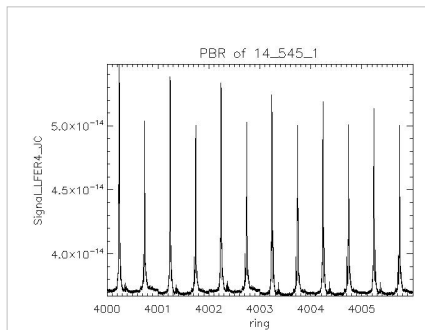
Phase-binned signal (PBR) for 6 consecutive rings from 4000 to 4005



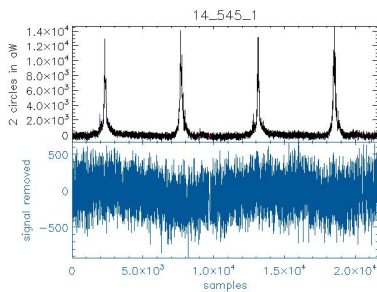
Valid signal (up) and noise (bottom) for 2 consecutive circles of the ring 4000



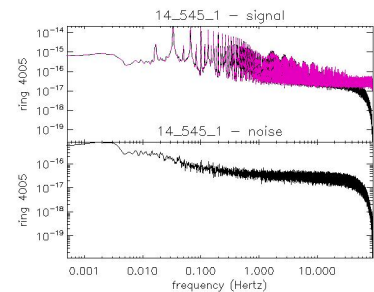
Fourier power spectral density of the first 30 minutes of the ring 4005 with signal before (pink) and after (black) deconvolution (top) and noise (bottom)



Phase-binned signal (PBR) for 6 consecutive rings from 4000 to 4005



Valid signal (up) and noise (bottom) for 2 consecutive circles of the ring 4000



Fourier power spectral density of the first 30 minutes of the ring 4005 with signal before (pink) and after (black) deconvolution (top) and noise (bottom)

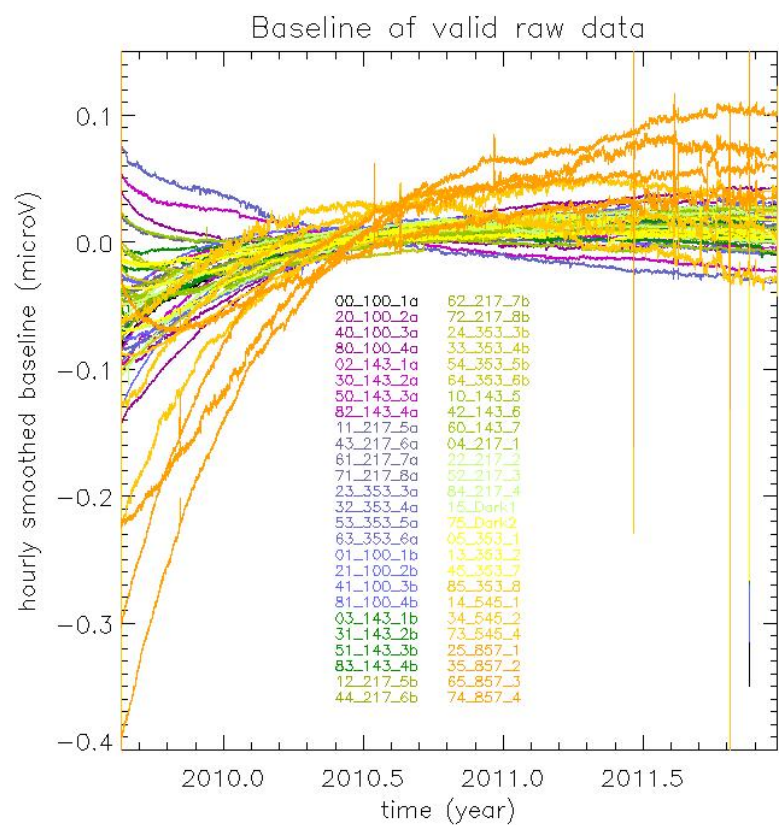
Samples of PBR, TOIs, and PSDs of all detectors are shown in this file

## Trends in the output processing variables

Here we intend to show the trend of the systematic effects that are dealt with in the TOI processing. The full impact of each of them is analyzed in HFI-Validation.

### ADC baseline

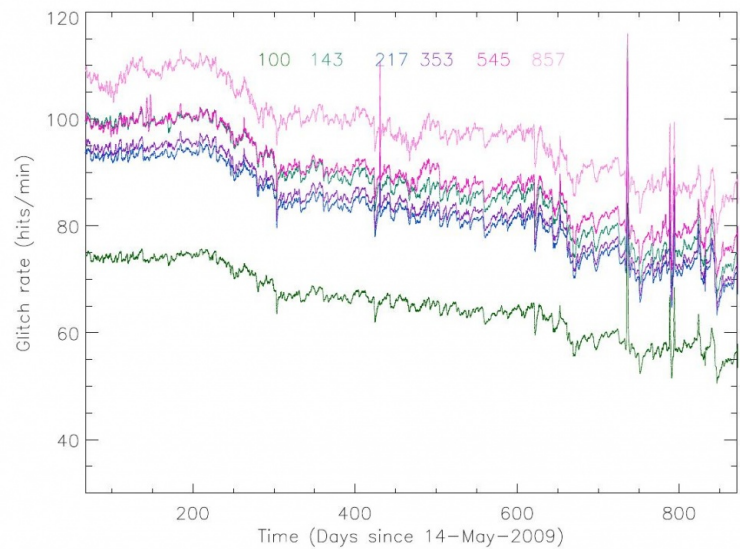
The following figure shows the ADC baseline which is used prior to demodulation (a constant offset is removed for clarity). This baseline is obtained by smoothing on an hour block average the undemodulated TOI on unflagged



samples.

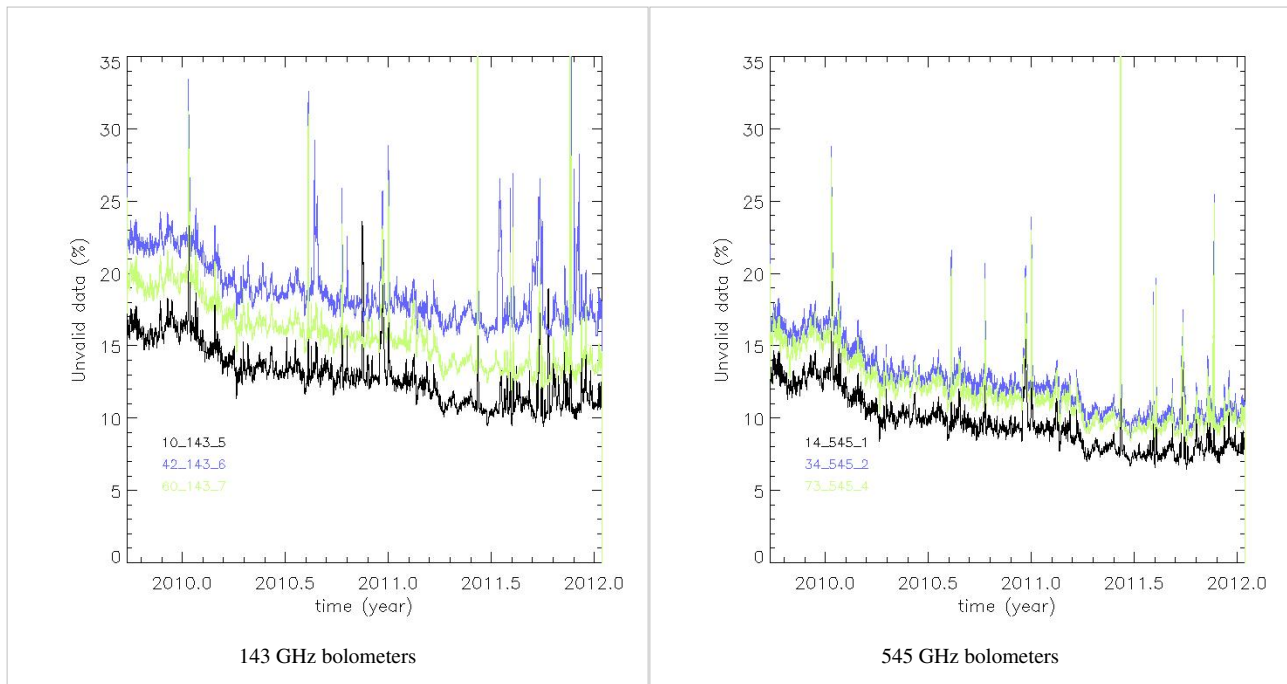
Glitch statistics

The glitch rate per channel is shown in this figure. For details, see copap.



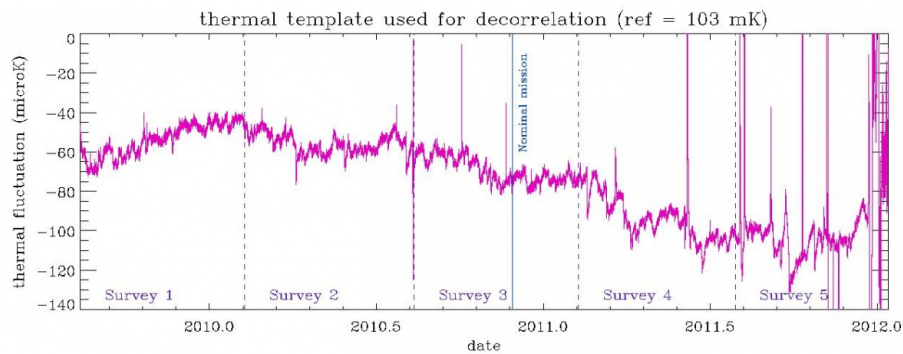
The percentage of flagged data (mostly due to Cosmic Rays) at the ring level is shown in these examples. No smoothing was applied. Only valid rings are shown.

### Percentage of flagged data



The complete set of plots is [here](#)

### Thermal template for decorrelation

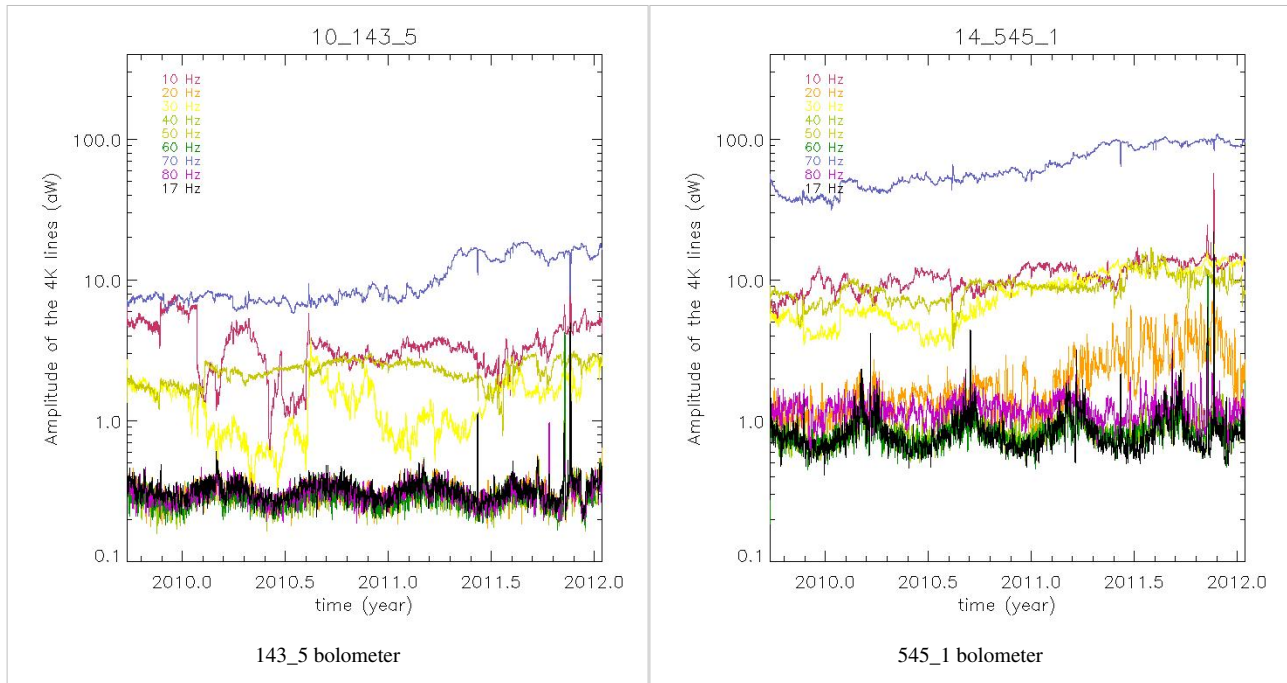


A simple linear decorrelation is performed using the 2 dark bolometers as a proxy of the bolometer plate temperature. Coupling coefficients were measured during the CPV phase.

### 4K cooler lines variability

The amplitude of the nine 4K cooler lines in aW at 10, 20, 30, 40, 50, 60, 70, 80 and 17 Hz is shown for 2 bolometers in the following figures. The trend is smoothed over 31 ring values after having discarded measurements done at a ring which is discarded for all bolometers.

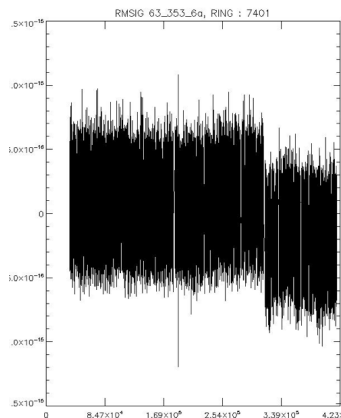
Amplitude of the nine 4K cooler lines



The 4K cooler line coefficients of all bolometers are shown in this file

### jump correction

A piecewise constant value is removed to the TOI if a jump is detected. See a jump example in this figure:

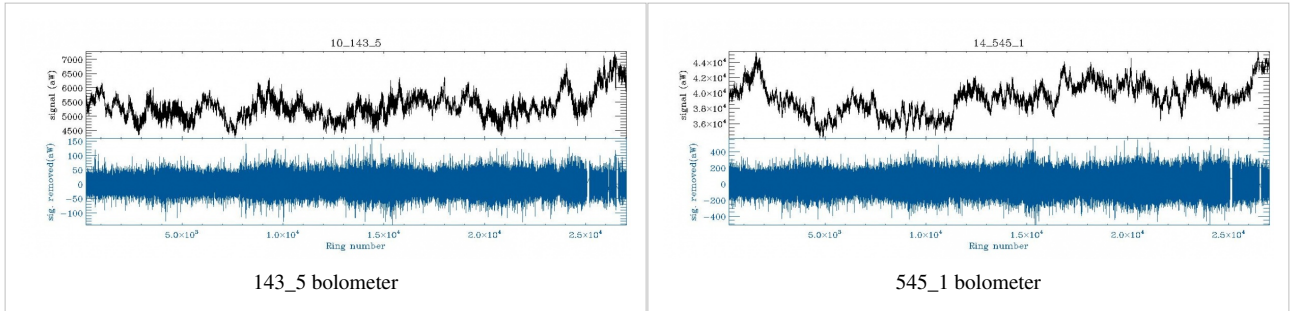


The number of jumps per day (all bolometers included) is shown in this figure:

The jumps are uncorrelated from bolometer to bolometer. The total number of jumps detected in the nominal and full mission is shown here:

## Trends in noise and signal

Signal (top) and noise (bottom) smoothed at 1 minute. All values falling in a discarded ring are not plotted.



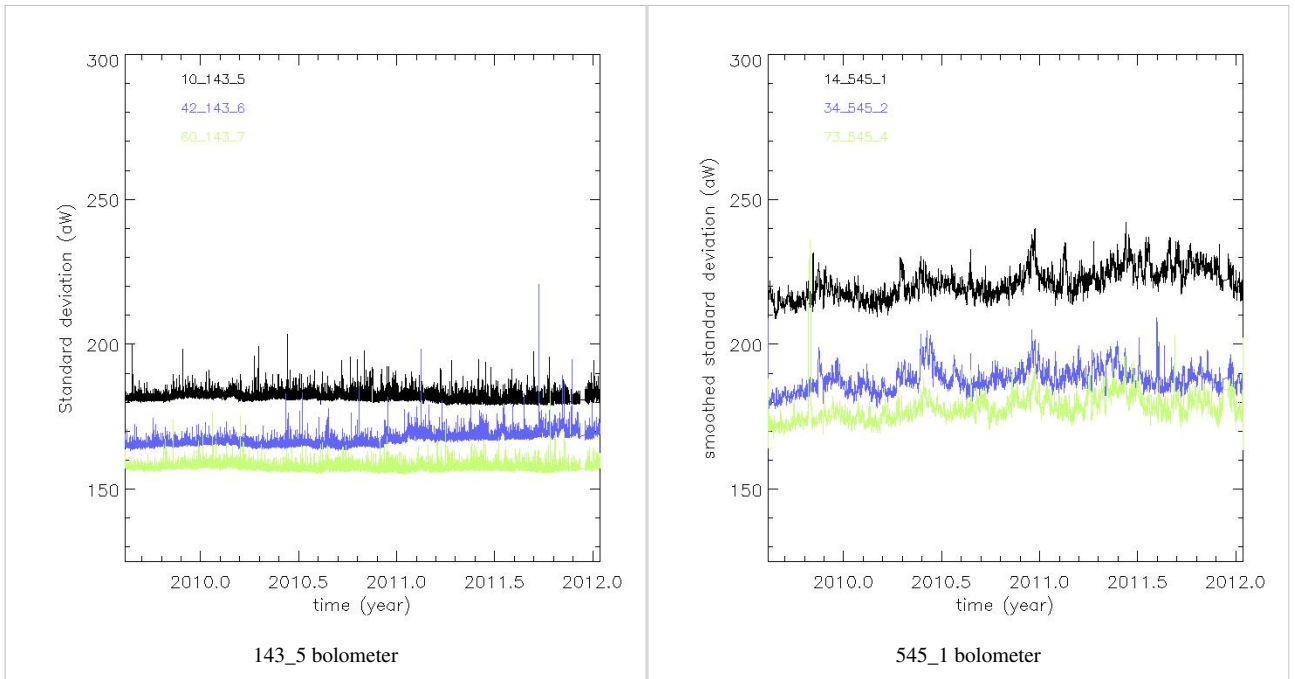
The smooth TOIs of all detectors are shown in this file

## Noise stationarity

This is not the final version but gives a good idea of power spectra at the detector level of rmsigTOIs. All PSDs can be seen in this file

The standard deviation per ring corrected by ring duration bias is given here, one per bolometer using only valid rings. No smoothing is applied (except a 31-point smoothing for the 545 and 857 GHz channels) but values for rings discarded for all bolometers are not used. The standard deviation is computed on samples valid for map-making which are also not affected by the Galaxy or the point-sources using the usual flags. Two examples are given here.

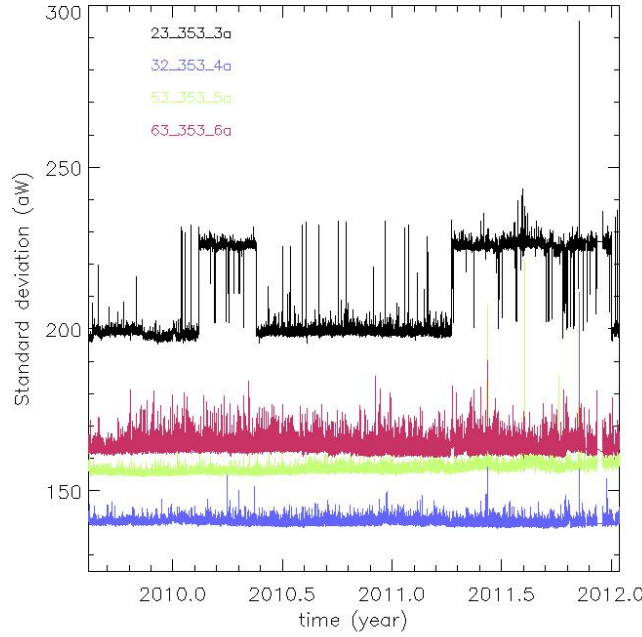
## Standard deviation per ring



The full series of plots is here: Standard deviation of rmsig TOIs at the ring level

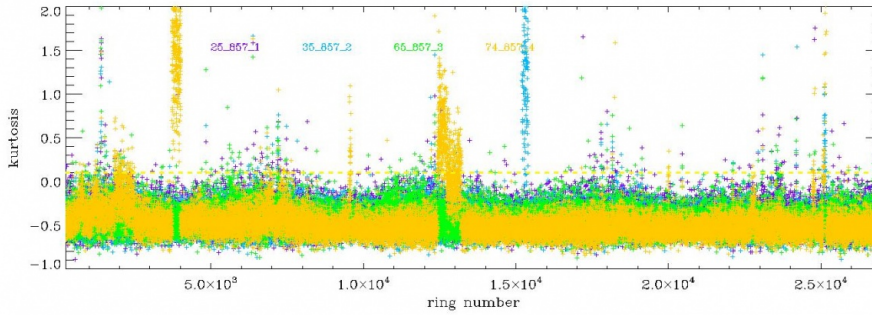


Note the presence for 3 bolometers of a two-level noise system. No correction can be done for that effect. See one



example here:

An example of the higher order statistics which are used to unveil rings affected by RTS problems.



## Flag description

### Input flags

These flags are used as inputs to the TOI processing

- The point-source flag (PSflag):

An earlier version of HFI point-source catalog is read back into a flag TOIs, at a given frequency. In practice, 5 sigma sources are masked within a radius of 1.3 FWHM (9, 7, 5, 5, 5, 5 arcmin at 100,143,217,353,545,857 GHz) TBC.

- the galactic flag (Galflag):

An earlier version of HFI maps is thresholded and apodized. The produced masks are read into flag TOIs. The retained threshold corresponds to a sky coverage of respectively 70, 70, 80, 90, 90, 90% at 100,143,217,353,545,857 GHz.

- Solar System Object flag

For the TOI flag, Mars, Jupiter, Saturn are flagged up to a radius of NbBeam= 2,3,3,4,4,4 times the fiducial SSO\_FWHM with SSO\_FWHM= 9, 7, 5, 5, 5, 5 arcmin at 100,143,217,353,545,857 GHz.

As an input to planet mask for maps, Mars, Jupiter, Saturn are flagged with a radius computed as a coefficient depending on the planet (Factor\_per\_source) times NbBeam times SSO\_FWHM, with Factor\_per\_source = 1.1,

2.25, 1.25 for Mars, Jupiter, Saturn respectively and NbBeam = 2.25, 4.25, 4.0, 5.0, 6.0, 8.0 at 100, 143, 217, 353, 545, 857 GHz. This flag is called SSOflag4map.

A small trailing tail is added to the mask to take into account the non-deconvolution of the planet signal which has been replaced by background values. The width of that tail is 10 % of the main flag diameter. The number of samples which are additionally flagged are the Factor\_per\_Source times AddSNafter with 10, 30, 20, 20, 30, 40 samples at 100, 143, 217, 353, 545, 857 GHz.

Uranus and Neptune together with detected asteroids are masked by HFI. They are masked at the TOI level using an exclusion radius of 1.5 SSO\_FWHM. At 857 GHz, 24 asteroids have been detected with HFI : 1Ceres, 2Pallas, 3Juno, 4Vesta, 7Iris, 8Flora, 9Metis, 10Hygiea, 11Parthenope, 12Victoria, 13Egeria, 14Irene, 15Eunomia, 16Psyche, 18Melpomene, 19Fortuna, 20Massalia, 29Amphitrite, 41Daphne, 45Eugenia, 52Europa, 88Thisbe, 704Interamnia, 324Bamberg.

## Output flags

A FlagTOIproc is produced by the TOIprocessing. It marks measurements which are not reliable for any of the following reasons :

- gap (no valid input data), enlarged by one sample on each side. It flags less than 0.00044% (resp. 0.00062%) of the nominal (resp. complete) mission. It is equivalent to less than 3 (resp. 8) minutes of data.
- glitch : samples where the signal from a cosmic ray hit dominates the sky signal at more than 3  $\sigma$  are discarded.
- jump as 100 samples are flagged around the computed position of the jump to take into account the error on this position.

With and without point-sources, identical to a and b PSBs.

Flags produced for the map making :

- UnstablePointing Flag OR FlagTOIproc OR SSOflag4map OR SSOflag seen
- FlagTOIproc = glitch OR jump OR flag thermal template
- PSB flag glitch = flag glitch A OR flag glitch B

Flag used in the destripping: same + point-source flag

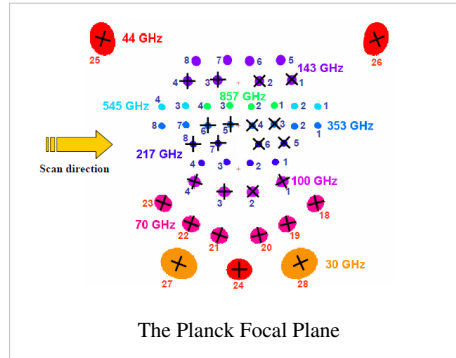
# Pointing&Beams

## Detector Pointing and Beams (and Errors)

### Detector Pointing

#### Introduction and Summary

The overall geometry of the Planck focal plane is shown here:



In order to take full advantage of the HFI beams, we must know the individual detector positions to a precision of better than several arcseconds, over the course of the entire mission. Spacecraft pointing comes from the on-board star tracker at 4 Hz. This is translated via a series of three-dimensional rotations to a pointing for the centre of the focal plane and resampled to the HFI TOI data rate for convenience. We must then further translate this focal-plane boresight pointing to the individual detector locations. Because neither the rotations from the star tracker to the boresight nor those from the boresight to the individual detectors are known exactly a priori, we must calibrate using flight data. Specifically, measurements of HFI Detector pointing are based largely on observations of individual planets, with information from the much more frequent observation of lower-flux galactic and extragalactic high-frequency sources used to monitor and build a model of overall pointing drift. This long-term drift of the spacecraft attitude is due to changes in the moment of inertia and includes specific events which may induce sudden changes, essentially random as far as our ability to predict the effects thereof. Note that the resulting pointing model cannot easily be directly compared to a physical/optical model: in particular, it includes an unmeasured phase shift in the scan direction from the convolution and deconvolution of the detector transfer function, which is complex in the Fourier domain ref. Comparison with the initial optical model indicates that the in-scan change due to this phase shift is of the order of 1 arcminute. Note also that aberration is corrected in all observations. The final pointing model is measured to be better than 2 arcsecond rms in the co-scan and cross-scan directions averaged over ten-day periods.

#### Initial measurements: Mars 1 and other planets

The first observation of Mars, which occurred around OD 80, is the baseline against which other objects are compared. Here, we show the relative pointing of Mars 1 to the pre-launch RFFM.

#### Focal plane drift: map-based measurement of detector positions

Prior to modeling of systematic changes in the Planck pointing, we find secular drifts of order one arcminute over the course of the nominal mission. We monitor this by making point-source catalogs based on single Planck surveys, only counting those objects which are observed over the course of less than seven days (this limits us to observations away from the ecliptic poles where Planck's observing strategy is highly cross-linked). We cross-match these catalog positions to the known IRAS point-source catalog [MRR REF] and average the deviations in ten-day blocks (the



individual measurements are shown as lighter points; error bars assume equal weighting for all points, but the results are not sensitive to any imposed S/N cutoff):

A similar analysis performed directly in the timestream gives similar results:

### **A model for Planck Pointing**

These analyses allow us to build a model for the pointing drift.

The correction is based on the measurement of pointing offset directly from the timeline, on a small sample of known and bright radio sources and planets. First the beam shape of each detector is measured by stacking individual timeline observation of bright planets. This process is of course amperes by pointing error, but those are reduced by allowing each pass on the planet to be slightly displaced in order to correct for the observed location of the planet. This process yield a very clean estimate of the beam of each detector.

Then those beam are used to determine the offset of observed location of planets (Mars, Saturn & Jupiter) as well as a few (~10) bright radio sources.

This offset are estimated for all detectors for the planet, and only for 100Ghz to 217Ghz one for the radio sources.

From the planet observations, one can recover the alignment of each detector in the focal plane, as well as a first pointing correction at the time of planet observations. This pointing correction is obtained by fitting splines on the planet observation from each detector. We further allow this correction to have a sharp jump between the first and second survey (SCS switchover).

This first pointing correction is further refined using the point sources observations in order to fill the period between planet observations. The radio sources offsets require further treatment than the planet based offsets. First, the brightness of the sources being much smaller than planets, the offset on individual detector observation are very noisy, and we filter out the noise by building median offsets for each point source observation. Second, since the sources can be slightly extended we still observe systematic offset above and below the planet based pointing correction in a regular alternating pattern. This is due to the fact that we are observing those extended objects scanning in alternating directions, and our fit of those extended sources to our beam translate into this systematic alternating pattern. We thus allow for a small, arcsec correction of those offsets : i.e. each object is allowed a single offset displacement of order arc seconds in order to minimize the offset between different observations of the same object at different time.

The resulting list of point source offsets is then merged with the planet offsets. Again a spline based correction is built fitting all of this data, and allowing rupture of continuity at the time of the SCS switchover and other major onboard event (typically between each surveys).

Once we assume the full Planck pointing model and re-measure the position of Mars for this observation, we see sub-arcsecond deviations (as expected); this gives an indication of the purely numerical limitations of the method. Further planet observations show the small remaining uncorrected drift present in the pointing model: Redoing the single-survey map- and catalog-based computation with the corrected pointing shows that Planck has achieved the arcsecond-scale goal of pointing rms:

## Scanning Beams

The scanning beams describe the instrument's instantaneous beam profile. Due to the near constant spin rate of the spacecraft, time domain effects (including residual time response and lowpass filtering) are degenerate with the spatial response due to the optical system. The scanning beam reconstruction recovers both of these effects, aside from residual time domain effects on a longer time scale than can be captured with the extent of the scanning beam model.

In the paper [cite P03c](#) we consider two models of the beam in order to better understand systematics in the reconstruction. Here we describe only the BSpline beams which are used to compute the delivered effective beam (see next section).

## BSpline Beam construction

We use seasons 1 and 2 of the Mars observation to reconstruct the beam. The data are processed with the bigPlanets TOI processing. We use JPL Horizons ephemerides to determine the pointing of each detector relative to the planet. We subtract the astrophysical background in the time domain using a bicubic interpolation of the Planck maps.

The time ordered data are used to fit a two dimensional BSpline surface using a least square minimization and a smoothing criterion to minimize the effects of high spatial frequency variations. We therefore assume the scanning beam to be smooth. The smoothing criterion as well as the locations of the nodes used to compute the B-Spline basis functions are set using GRASP physical optics simulations as inputs which are the best assumptions on the spatial frequency content of the in-flight beams.

The smoothing criterion is defined as follows:

And the global inversion criterion :

$$\zeta = \eta + p \times \delta$$

with  $\delta$  usual least square estimator and  $p$  coefficient giving the relative weight to  $\delta$  with respect to the smoothing criterion.

The BSpline nodes are located on a regular spaced grid in the detector coordinate framset. At the edge of the reconstructed beam map area, 4 coincident nodes are added to avoid vanishing basis functions.

Let  $B_{i,k+1}$ ,  $k$  degree B-Spline build using nodes  $\{\lambda_i, \dots, \lambda_{i+k+1}\}$  (De Boor & Cox, 1972) :

$$B_{i,l+1}(x) = \frac{x - \lambda_i}{\lambda_{i+l} - \lambda_i} B_{i,l}(x) + \frac{\lambda_{i+l+1} - x}{\lambda_{i+l+1} - \lambda_{i+1}} B_{i+1,l}(x)$$

$$l = 1, \dots, k$$

## Simulations and errors

We estimate the reconstruction bias and noise in the measurements using an ensemble of simulated planet observations for each channel. Kept fixed in each simulation are:

- the input beam assumed: we use a supersampled version of the reconstructed BSpline beam (or whatever comes out of the current ongoing tests!)
- Astrophysical background is the same as that subtracted from the real data.
- StarTracker pointing (using the ptc6 pointing model).

The following are varied in each simulation:

- detector noise realizations obtained by filtering randomly generated white noise with the measured noise PSDs
- random pointing errors with 2 arcsecond rms, and a spectrum that replicates the real errors.
- simulated glitches and the deglitching procedure
- Mars brightness temperature variability

400 simulated timelines are generated for each bolometer and for each of the two seasons of Mars observations used in the beam reconstruction. The simulated timelines are made into beam maps, projecting onto the BSpline basis in the same way as the real data.

The beam maps are propagated to effective beam window functions using the quickbeam approach (see effective beams below) and used to evaluate the reconstruction bias and to construct error eigenmodes in the effective beam window function.

Figure: random pointing error PSD Figures: error envelope plots (or should those go under effective beams?)

## Residuals

There are two known beam effects that are not included in the main beam model and are estimated as a separate bias in flux and angular power spectrum measurement: 1. long tails due to errors in low frequency time response deconvolution, and 2. near sidelobes.

We stack all five observations of Jupiter to estimate the long time scale residuals due to incomplete deconvolution of the long time scale response.

Add some kind of mean tail plot

Near sidelobes are also evaluated using stacked Jupiter (hopefully they will just be part of the v53bis BSpline beams). The main features in the near sidelobes include a wide beam skirt, and dimpling lobes Add sidelobe plots and tables

## Effective Beams

Several methods of effective beams determination have been developped and cross-validated. Need satisfactory comparison plot

## FEBecoP

To be coordinated with GracaSee Mitra et al (2011

## FICSBell

Since the HFI beams are not azimuthally symmetric, the scanning strategy has to be taken into account in the effective beam response modelling. This is done using the FICSBell method (Hivon et al, in preparation), which generalizes to polarization and to include other sources of systematics the approach used for TT  $C(l)$  estimation in WMAP-3yr Hinshaw et al (2007) and by Smith et al (2007) in the detection of CMB lensing in WMAP maps. The different steps of the method used for this study can be summarized as follows:

1. The scanning related information (i.e., statistics of the orientation of each detector within each pixel) is computed first, and only once for a given observation campaign. Those orientation hit moments are only computed up to degree 4, for reasons described in point 2 below. At the same time, the first two moments of the distribution of samples within each pixel (ie, their center of mass and moments of inertia) are computed and stored on disc.
2. The scanning beam map or beam model of each detector  $d$  is analyzed into its Spherical Harmonics coefficients where is the beam map centered on the North pole, and is the Spherical Harmonics basis function. Higher  $s$  indexes describes higher degrees of departure from azimuthal symmetry and, for HFI beams, the coefficients  $b_{ls}^d$  are decreasing functions of  $s$  at most  $l$  considered. It also appears that, for  $l < 3000$ , the coefficients with  $|s| > 4$  account for 1% or less of the beam throughput. For this reason, only modes with  $|s| \leq 4$  are considered in the present analysis. Armitage-Caplan and Wandelt (2009) reached a similar conclusion in their deconvolution of Planck-LFI beams.
3. The  $b_{ls}^d$  coefficients computed above are used to generate  $s$ -spin weighted maps, as well as the first and second order derivatives, for a given CMB sky realization.

4. The spin weighted maps and orientation hit moments of the same order  $s$  are combined for all detectors involved, to provide an “observed” map. Similarly the local spatial derivatives are combined with the location hit moments to describe the effect of the non-ideal sampling of each pixel (see [sec:pixelization]). In this combination, the respective number of hits of each detector in each pixel is considered, as well as the weighting (generally proportional to the inverse noise variance) applied to each detector in order to minimize the final noise.
5. The power spectrum of this map can then be computed, and compared to the input CMB power spectrum to estimate the effective beam window function over the whole sky, or over a given region of the sky.

Monte-Carlo (MC) simulations in which the sky realisations are changed can be performed by repeating steps 3, 4 and 5. The impact of beam model uncertainties can be studied by including step 2 into the MC simulations.

## QuickBeam

Planck observes the sky after convolution with a “scanning beam”, which captures its effective response to the sky as a function of displacement from the nominal pointing direction. Decomposing the scanning beam into harmonic coefficients  $B_{lm}$ , each time-ordered data (TOD) sample can be modelled as (neglecting the contribution from instrumental noise, which is independent of beam asymmetry) where the TOD samples are indexed by  $i$ , and  $\tilde{T}_{lm}$  is the underlying sky signal. The spin spherical harmonic  ${}_sY_{lm}$  rotates the scanning beam to the pointing location  $(\theta, \phi)$ , while the  $e^{-is\alpha_i}$  factor gives it the correct orientation. Eq. may be evaluated with the “TotalConvolver” algorithm of [Wandelt and Gorski \(2001\)](#), accelerated using the “convirt” recursion relations [Prezeau and Reinecke \(2010\)](#). This approach is implemented in LevelS, although because it involves working with a TOD-sized object it is necessarily slow.

On the small angular scales comparable to the size of the beam, it is a good approximation to assume that the procedure of mapmaking from TOD samples is essentially a process of binning: where  $H(p)$  is the total number of hits in pixel  $\hat{n}$ .

Start with a normalized, rescaled harmonic transform of the beam  $B_{lm}$ , sky multipoles  $\tilde{T}_{lm}$  and a scan history object  $w(\hat{n}, s)$  given by  $w(\hat{n}, s) = \sum_{j \in p} e^{is\alpha_j} / H(\hat{n})$  where the sum is over all hits  $j$  of pixel  $p$  at location  $\hat{n}_p$ , and  $\alpha_j$  is the scan angle for observation  $j$ . The harmonic transform of this scan-strategy object is given by  ${}_s w_{LM} = \int d^2\hat{n} {}_s Y_{LM}^*(\hat{n}) w(\hat{n}, s)$ . The beam-convolved observation is then given by  $\tilde{T}(\hat{n}) = \sum_{slm} w(\hat{n}, -s) B_{ls} T_{lms} Y_{lm}(\hat{n})$ . Taking the ensemble average of the pseudo-Cl power spectrum of these  $T_{lm}$  we find

where is a cross-power spectrum of scan history objects. Note that the  $w(n,s)$  which we have used here can also incorporate a position dependent weighting to optimize the pseudo-Cl estimate, such as inverse-noise or a mask—the equations are unchanged. Writing the pseudo-Cl in position space (a la [Dvorkin and Smith \(2009\)](#)) with Wigner-d matrices we have

This integral can be implemented exactly using Gauss-Legendre quadrature, with a cost of . For simplicity, we’ve written all the equations here for the auto-spectrum of a single detector, but the generalization to a map made by adding several detectors with different weighting is straightforward. The cost to compute all of the necessary terms exactly in that case becomes .

Are beams really so difficult? On the flat-sky beam convolution is easy: just multiplication in Fourier space by a beam rotated onto the scan direction. Multiple hits with different scan directions are incorporated by averaging (as the “scan history” objects above encapsulate). Does the sphere really require everything to be so complicated? For a scan strategy which is fairly smooth across the sky, we can pretend that we are observing many independent flat-sky patches at high- $L$  with fairly good accuracy. There is in fact a fairly good approximation to the beam convolved pseudo-Cl power spectrum which is essentially a flat-sky approximation. In the limit that  $L \gg l_1$ , with  $C_{l_2}$  and  $B_{l_2}$  being slowly-varying function in  $l_2$  the pseudo-Cl sum above can be approximated as where the average  $\langle \rangle_p$  is

taken over the full sky. It's illustrative to consider three limits of this equation: for a "raster" scan strategy in which each pixel is observed with the same direction, we have and the predicted pseudo-Cl is just the power spectrum of the beam. For a "best-case" scan strategy, in which each pixel is observed many times with many different orientation angles, we have  $\langle |w(\mathbf{M})|^2 \rangle_p = M_0$ , and the transfer function is just the azimuthally symmetric part of the beam. Note that this is for a full-sky observation— in the presence of a mask, the average above produces an fsky factor, as expected. It just neglects the coupling between L multipoles (which can be calculated with the more complete equations above).

## Pixelization Artifacts

- Several codes available to simulate effects of pixelization.
- Mixes the CMB gradient into a pixelization ``noise with a level comparable to that of  $2\mu\text{K arcmin}$  instrumental noise.
- Quantitative estimate of effect should be included with each released map, but expect not to matter significantly for CMB analysis, as small compared to instrumental noise.

[sec:pixelization]

Planck maps are produced at resolution 11 ( $N_{\text{side}} = 2048$ ), corresponding to pixels with a typical dimension of  $1.7'$ , comparable to the spacing between scanning rings. This results in an uneven distribution of hits within pixels, which introduces some complications in the analysis and interpretation of the maps. A sample of the hit distribution is illustrated in Fig. [fig:pixcoverage]. Below we discuss the simulation and modeling of this pixelization effect in more detail.

[!ht]

[fig:pixcoverage]

The collaboration has produced 3 codes which may be used to simulate the effect of pixelization on the observed sky, LevelS/TotalConvolver/Conviqt, FeBeCoP, and FICSBell [references and further discussion of the three methods and how they each simulate the pixelization effect.](#)

For the measurement of CMB fluctuations, it is also possible to gain intuition for the effects of pixelization analytically. On the small scales relevant to pixelization, the observed CMB is smooth, both due to physical damping as well as the convolution of the instrumental beam. Taylor expanding the CMB temperature about a pixel center to second order, the typical gradient amplitude is given by

$$\langle |\nabla T|^2 \rangle = \frac{1}{4\pi} \sum_l l(l+1)(2l+1) C_l^T W_l \approx 1 \times 10^9 \mu K^2 / \text{rad}^2$$

where the approximate value is calculated

for a  $\Lambda\text{CDM}$  cosmology with a  $7'$  fwhm Gaussian beam. The typical curvature of the observed temperature, on the other hand is given by  $\langle |\nabla^2 T|^2 \rangle = \frac{1}{4\pi} \sum_l [l(l+1)]^2 (2l+1) C_l^T W_l \approx 7 \times 10^{14} \mu K^2 / \text{rad}^4$ . On the scales

relevant to the maximum displacement from the center of a  $1.7'$  pixel, the maximum displacement is , and so the gradient term tends to dominate, although the curvature term is still non-negligible. For each observation of a pixel, we can denote the displacement from the pixel center as  $\mathbf{d} = d_\theta + i d_\phi$ . The average over all hits within a pixel gives an overall deflection vector which we will denote for a pixel center located at  $\hat{n}$  as  $\mathbf{d}(\hat{n})$ . This represents the center of mass of the hit distribution; in Fig. [fig:pixcoverage] we have plotted these average deflections using black arrows. The deflection field  $\mathbf{d}(\hat{n})$  may be decomposed into spin-1 spherical harmonics as  $d_{lm} = \int_{4\pi} Y_{lm}^* d(\hat{n})$ .

With a second order Taylor expansion of the CMB temperature about each pixel center, it is then possible to calculate the average pseudo-Cl power spectrum of the pixelized sky. This is given by

where  $R^d = \langle |\mathbf{d}|^2 \rangle / 2$  is half the mean-squared deflection magnitude (averaged over hits within a pixel, as well as over pixels).  $C_l^{d+}$  is the sum of the gradient and curl power spectra of  $d_{lm}$ , and  $C_l^{d-}$  is the gradient spectrum minus the curl spectrum. The  $R^d$  term describes a smearing of the observed sky due to pixelization. For uniform pixel

coverage of  $N_{\text{side}} = 2048_{\text{pixels}}$   $\sqrt{\langle |d|^2 \rangle} = 0.725'$ . For the hit distribution of Planck frequency maps,  $R^d$  is typically within maps, looks like will be better than 10% percent of this value, and so this term is accurately described by the pixel window function, which is derived under the assumption of uniform pixel coverage.

The effect of pixelization is essentially degenerate with that of gravitational lensing of the CMB, with the difference that it (1) acts on the beam-convolved sky, rather than the actual sky and (2) produces a curl-mode deflection field as well as a gradient mode. This is discussed further in [cite lensing paper](#), where the subpixel deflection field constitutes a potential source of bias for the measured lensing potential. Indeed, Eq. [eqn:clt ixelized] is just a slightly modified version of the usual first order CMB lensing power spectrum ([Hu \(2000\)](#), [Lewis and Challinor \(2006\)](#)) to accommodate curl modes.

A useful approximation to Eq. which is derived in the unrealistic limit that the deflection vectors are uncorrelated between pixels, but in practice gives a good description of the power induced by the pixelization, is that the  $d(\hat{n})$  couples the CMB gradient into a source of noise with an effective level given by

where the average is taken over all pixels and  $R^T$  is half the mean-squared power in the CMB gradient:

$$R^T = \frac{1}{8\pi} \sum_l l(l+1)(2l+1) \tilde{C}_l^T$$

For frequency-combined maps,  $\sqrt{\langle |d(\hat{n})|^2 \rangle}$  is typically on the order of  $0.1'$

, and so the induced noise is at the level of  $\sigma^N \sim 2\mu K \text{ arcmin}$ . This is small compared to the instrumental contribution, although it does not disappear when taking cross-spectra, depending on how coherent the hit distributions of the two maps in the cross-spectrum are.

## Map-making

---

### Map-Making and photometric calibration

#### Introduction

This page will give an overview of the map-making and photometric calibration procedures used by the HFI DPC to build detector and frequency maps. This processing and its performances are described in the [the HFI DPC Paper](#) and the [the HFI DPC Calibration co-Paper](#) [which will be completed prior to this page].

To build HFI maps, we work under destripping approximation, where the noise is assumed to decompose into two components : white noise plus low frequency drifts. Using the sky redundancy, the low frequency component is modelled as one constant, or offset, per pointing period. To speed up the ulterior processing we first build intermediate products, by taking advantage of redundancies : we average signal and detector orientation on healpix pixels visited during each fixed pointing period, which we call hereafter 'ring'. This intermediate product is called HPR for healpix pixel ring. This new dataset is used as input in the following steps.

#### Photometric calibration

##### dipole calibration (100 to 353 GHz)

For the 2013 data release, the calibrator for the CMB frequency was the Solar dipole, as measured by the WMAP team. We use a two component template fitting procedure, performed for each detector independently, to determine ring by ring a estimation of the dipole gain. We average these estimation for a subset of rings in the first survey (2000 to 6000) in which the dipole's amplitude is high enough with respect to that of the sky template, to get a single dipole gain per detector. The two fitted component are the Solar dipole and a sky template. We used the PSM for thermal dust emission at the detector's frequency as a first approximation of the sky template. Using the HFI channel map as a template brings negligible change in the averaged gain, but reduces the systematic ring-to-ring dispersion

---

of our estimation.

Several pieces of evidence led to the conclusion that our bolometers presented apparent gain variation in time, after comparing the 3rd scan of the sky with the first one. This was later (mid-2012) explained by inequalities in the steps of the ADC used in the bolometer's electronic chain. These devices had to be characterized using warm data after the end of the HFI observations. This process is still on-going (01/2012).

In the mean time we used an empiric correction, looking for a gain estimation and an offset per ring. This amounts at solving the non-linear equation :

where  $d$  is the detector measurement,  $S$  the sky signal,  $g$  the detector gain,  $O$  the offset (for ring no  $i$ ) are the unknowns to be determined, and  $n$  the noise. We linearized this equation starting from the constant gain approximation, to get a measurement of the apparent time-varying gains for each bolometer independently. The limitations of this process are intrinsic signal variability from one observation to the other, like polarization or intra-pixel gradient. This procedure was thus only used for the 100 to 217 GHz detectors, for which the dipole signal is brighter and galactic signal (and polarization). A mask was used to removed the inner part of the Galactic plane.

[TBC : give precision]

### Higher frequency calibration (545 and 857 GHz)

For the two highest frequencies, we calibrate the response using dust spectra measured by FIRAS. We use analytic fits to these spectra to extrapolate the dust signal within each detector's bandpass. These extrapolation are used to build  $n_{\text{side}}=8$  maps. We build on the other hand uncalibrated maps that we convolve with the beam of the FIRAS instrument. Finally we may derive one gain  $K$  and zero point  $Z$  per detector.

While the gains are used only for the two highest frequencies, the zero point  $Z$  are used for all frequencies.

[TBC : give precision]

## Building of Maps

Using the photometric calibration parameters, we build maps in two steps :

- we determine the destripping offsets using the full mission data
- we build the maps, using these offsets, by inverting the photometric equation :

where  $d$  is the destripped and calibrated signal at the HPR level. Detector's data are combined with an inverse noise weights derived from each detector's NEP. Q and U maps are build whenever possible. We propagate the white noise by building the 3x3 (or 1x1 if only I is reconstructed) covariance matrices in each pixel. At each frequency we build maps combining all detectors and independent detector sets. We use the offsets build for the full mission for building maps for each scan survey. We also build maps from the two independent halves of each rings. Altogether, more than 6000 maps are built at each release.

## Noise properties

Map noise properties can be evaluated using several methods, thanks to the high level of observation redundancies. We can use the maps built from the difference between the first and second half of each rings, or compare individual sky scans, of detector sets with each other.

Low resolution ( $n_{\text{side}} = 8$  to 32 ?) pixel-to-pixel noise covariance matrices are build using an analytic approach from the measured noise power spectra.

## Zodi correction

At the highest Planck frequencies (353-857 GHz -- it is not important for the CMB), Zodiacal emission is visible:

This map is a difference between the 857 GHz Survey 2 map and the 857 GHz Survey 1 map. As the Solar elongation is different for measurements of the same point on the sky for the two surveys, we see Zodiacal emission, while all emission from further sources is removed. The zodiacal emission follows the Ecliptic plane, which starts at the lower left of the image, then crosses the center of the plot towards the upper right. Note that the "arcs" at the top and bottom of the image are images of the Galactic center in the Far Sidelobes, which are discussed in the section below. Note also that the image above is from an early processing and will be updated.

Zodiacal Emission is removed from the 353, 545 and 857 GHz channels. It is described in [the HFI DPC Paper](#), but a synopsis of the procedure is as follows:

- During each survey, a large fraction of the sky has observations which all fall within a week of each other. That is, during a single survey, most pixels are observed during a short, well-defined period. The contribution from Zodiacal Emission to the total brightness seen, then, is well defined.
- We use the COBE model of the Zodiacal Light to make predictions for this Zodiacal emission for those pixels observed over a span of one week or less, and use GRASP models of the beams to predict the emission from the Galaxy given our sidelobes.
- We fit the survey difference maps with these model templates to estimate the emissivity of each Zodi component and sidelobe at the Planck wavelengths. The results of these fits at each frequency are shown here.
- We reconstruct each ring of the full mission using the combination of the COBE geometric model with the emissivities determined above and the sidelobe models.
- We remove the reconstruction above from each ring of data.
- We then make maps as described previously in this section.

## Far Sidelobe Correction

The far sidelobe correction is described in the section above. Note that this correction is done only for the 857 and 545 GHz channels, as it is not seen at longer wavelengths. As for the Zodiacal emission correction, it is not important for the CMB.

We note in particular that neither the Zodiacal light, nor the far sidelobes are seen in the "cosmology" channels. To illustrate this, here is a similar difference map to the one above, this time at 100 GHz:

Note that this image is not from the most recent processing, and will be updated.

## CO Correction

This is described in the [the CO Paper](#)



# PowerSpectra

---

This is the page regarding the HFI-based power spectra

We call intra-frequency checks those performed between detectors (or sets of) in the same frequency bands, which thus respond similarly to the sky emission. Interfrequency-checks on the other hand correspond to checks between detector in different frequency bands, imposing further reliance on a sky model to perform the test.

## Intra-frequency checks

These compare the power spectra between various detector sets operating within the same frequency channel. They see the same sky, and should therefore give consistent results, up to the noise level, and up to color corrections due to their somewhat different spectral band passes. These corrections are rather small if one restricts the comparison to specific portions of the sky, for instance dominated by extra-Galactic components, like it is done for extracting the CMB power spectrum in the likelihood analysis where  $f_{\text{sky}} \sim 0.4$ .

### Consistency checks

The pictures shows in grey the prior deduced from the beam parameters uncertainty analysis. At 217 GHz, the distance between PSB and SWB suggests an accounted for effect (fortunately small enough for the likelihood analysis). The relative calibration appear to be at the 0.1% level.

This shows that whatever systematic effect might remain, it has to be common to all detectors within a frequency band to a very high level of accuracy.

## HFI-Validation

---

The HFI validation is mostly modular. That is, each part of the pipeline, be it timeline processing, map-making, or any other, validates the results of its work at each step of the processing, looking specifically for known issues. In addition, we do additional validation with an eye towards overall system integrity by looking at generic differences between sets of maps, in which most problems will become apparent, whether known or not. Both these are described below.

### Expected systematics and tests (bottom-up approach)

Like all experiments, Planck/HFI had a number of "issues" which it needed to track and verify were not compromising the data. While these are discussed in appropriate sections, here we gather them together to give brief summaries of the issues and refer the reader to the appropriate section for more details.

- Cosmic Rays - Unprotected by the atmosphere and more sensitive than previous bolometric experiment, HFI was subjected to many more cosmic ray hits than previous experiments. These were detected, the worst parts of the data flagged as unusable, and "tails" were modeled and removed. This is described in XXXXX
  - Elephants - Cosmic rays also hit the 100 mK stage and cause the temperature to vary, inducing small temperature and thus noise variations in the detectors. This is described in XXXXX
  - 1.6 K Stage Fluctuations
  - 4 K Stage Fluctuations
  - Popcorn Noise - Some channels were occasionally affected by what seems to be a "split-level" noise, which has been variously called popcorn noise or random telegraphic signal. These data are usually flagged. This is described in XXXXX
-

- Jumps - Similar to but distinct from popcorn noise, small jumps were occasionally found in the data streams. These data are usually corrected. This is described in XXXXX.
- 4 K Cooler-Induced EM Noise - The 4 K cooler induced noise in the detectors with very specific frequency signatures, which is filtered. This is described in XXXXX.
- 4 K Cooler-Induced Microphonics - The mechanical cooler was shown in XXXXX to cause very little microphonic parasites in the detector data.
- Pointing-Change Microphonics - The changes in pointing after each pointing period were shown in XXXXX to cause very little microphonic parasitic signal in the detector data.
- Compression - Onboard compression is used to overcome our telemetry bandwidth limitations. This is explained in XXXXX.
- Noise Correlations - Correlations in noise between detectors seems to be negligible but for two polarization sensitive detectors in the same horn. This is discussed in XXXXX.
- Electrical Cross-Talk - Cross-talk is discussed in XXXXX.
- Pointing - The final pointing reconstruction for Planck is near the arcsecond level. This is discussed in XXXXX.
- Focal Plane Geometry - The relative positions of different horns in the focal plane is reconstructed using planets. This is discussed in XXXXX.
- Main Beam - The main beams for HFI are discussed in XXXXX.
- Ruze Envelope - Random imperfections or dust on the mirrors can increase the size of the beam a bit. This is discussed in XXXXX.
- Dimpling - The mirror support structure causes a pattern of small imperfections in the beams, which cause small sidelobe responses outside the main beam. This is discussed in XXXXX.
- Far Sidelobes - Small amounts of light can sometimes hit the detectors from just above the primary or secondary mirrors, or even from reflecting off the baffles. While small, when the Galactic center is in the right position, this can be detected in the highest frequency channels, so this is removed from the data. This is discussed in XXXXX.
- Planet Fluxes - Comparing the known fluxes of planets with the calibration on the CMB dipole is a useful check of calibration. This is done in XXXXX.
- Point Source Fluxes - As with planet fluxes, we also compare fluxes of known, bright point sources with the CMB dipole calibration. This is done in XXXXX.
- Time Constants - The HFI bolometers do not react instantaneously to light; there are small time constants, discussed XXXXX.
- ADC Correction - The HFI Analog-to-Digital Converters are not perfect, and are not used perfectly. Their effects on the calibration are discussed in XXXXX.
- Gain changes with Temperature Changes
- Optical Cross-Talk - This is discussed in XXXXX.
- Bandpass - The transmission curves, or "bandpass" has shown up in a number of places. This is discussed in XXXXX and YYYYY.
- Saturation - While this is mostly an issue only for Jupiter observations, it should be remembered that the HFI detectors cannot observe arbitrarily bright objects. This is discussed in XXXXX.

## Generic approach to systematics

While we track and try to limit the individual effects listed above, and we do not believe there are other large effects which might compromise the data, we test this using a suite of general difference tests. As an example, the first and second years of Planck observations used almost exactly the same scanning pattern (they differed by one arc-minute at the Ecliptic plane). By differencing them, the fixed sky signal is almost completely removed, and we are left with only time variable signals, such as any gain variations and, of course, the statistical noise.

In addition, while Planck scans the sky twice a year, during the first six months (or survey) and the second six months (the second survey), the orientations of the scans and optics are actually different. Thus, by forming a difference between these two surveys, in addition to similar sensitivity to the time-variable signals seen in the yearly test, the survey difference also tests our understanding and sensitivity to scan-dependent noise such as time constant and beam asymmetries.

These tests use the `Yardstick` simulations below and culminate in the "Probabilities to Exceed" tests just after.

## HFI simulations

The 'Yardstick' simulations allows gauging various effects to see whether they need be included in monte-carlo to describe data. It also allows gauging the significance of validation tests on data (e.g. can null test can be described by the model?). They are completed by dedicated 'Desire' simulations (`Desire` stands for DETector SIMulated REsponse), as well as Monte-Carlo simulations of the Beams determination to determine their uncertainty.

### Yardstick simulations

The `Yardstick V3.0` characterizes the DX9 data which is the basis of the data release. It goes through the following steps:

1. The input maps are computed using the Planck Sky Model, taking the RIMO bandpasses as input.
2. The `LevelS` is used to project input maps on timeline using the RIMO(B-Spline) scanning beam and the DX9 pointing (called `ptcor6`). The real pointing is affected by the aberration that is corrected by map-making. The `Yardstick` does not simulate aberration. Finally, the difference between the projected pointing from simulation and from DX9 is equal to the aberration.
3. The simulated noise timelines, that are added to the projected signal, have the same spectrum (low and high frequency) than the DX9 noise. For the `yardstick V3.0` Although detectable, no correlation in time or between detectors have been simulated.
4. The simulation map making step use the DX9 sample flags.
5. For the low frequencies (100, 143, 217, 353), the `yardstick` output are calibrated using the same mechanism (e.g. dipole fitting) than DX9. This calibration step is not performed for higher frequency (545, 857) which use a different principle
6. The Official map making is run on those timelines using the same parameters than for real data.

A `yardstick` production is composed of

- all survey map (1,2 and nominal),
- all detector Detsets (from individual detectors to full channel maps).

The `Yardstick V3.0` is based on 5 noise iterations for each map realization.

NB1: the `Yardstick` product is also the validating set for other implementations which are not using the HFI DPC production codes, an exemple of which are the so-called `FFP` simulations, where `FFP` stands for Full Focal Plane and are done in common by HFI & LFI. This is further described in HL-sims

NB2: A dedicated version has been used for Monte-Carlo simulations of the beams determination, or `MCB`. See [Pointing&Beams#Simulations\\_and\\_errors](#)

### Desire simulations

Complementary to the `Yardstick` simulations, the `Desire` simulations are used in conjunction with the actual TOI processing, in order to investigate the impact of some systematics. The `Desire` pipeline allows to simulate the response of the HFI-instrument, including the non-linearity of the bolometers, the time transfer-function of the readout electronic chain, the conversion from power of the sky to ADU signal and the compression of the science data. It also includes various components of the noise like the glitches, the white and colored noise, the one-over-f

noise and the RTS noise. Associated to the Planck Sky Model and LevelS tools, the Desire pipeline allows to perform extremely realistic simulations, compatible with the format of the output Planck HFI-data, including Science and House Keeping data. It goes through the following steps (see Fig. *Desire* End-to-End Simulations) :

1. The input maps are computed using the Planck Sky Model, taking the RIMO bandpasses as input;
2. The LevelS is used to project input maps into Time ordered Inputs TOIs, as described for the Yardstick simulations;
3. The TOIs of the simulated sky are injected into the Desire pipeline to produce TOIs in ADU, after adding instrument systematics and noise components;
4. The official TOI processing is applied on simulated data as done on real Planck-HFI TOIs;
5. The official map-making is run on those processed timelines using the same parameters as for real data;

This Desire simulation pipeline allows to explore systematics such as 4K lines or Glitches residual after correction by the official TOI processing, as described below.

## Simulations versus data

The significance of various difference tests performed on data can be assessed in particular by comparing them with *Yardstick* realisations.

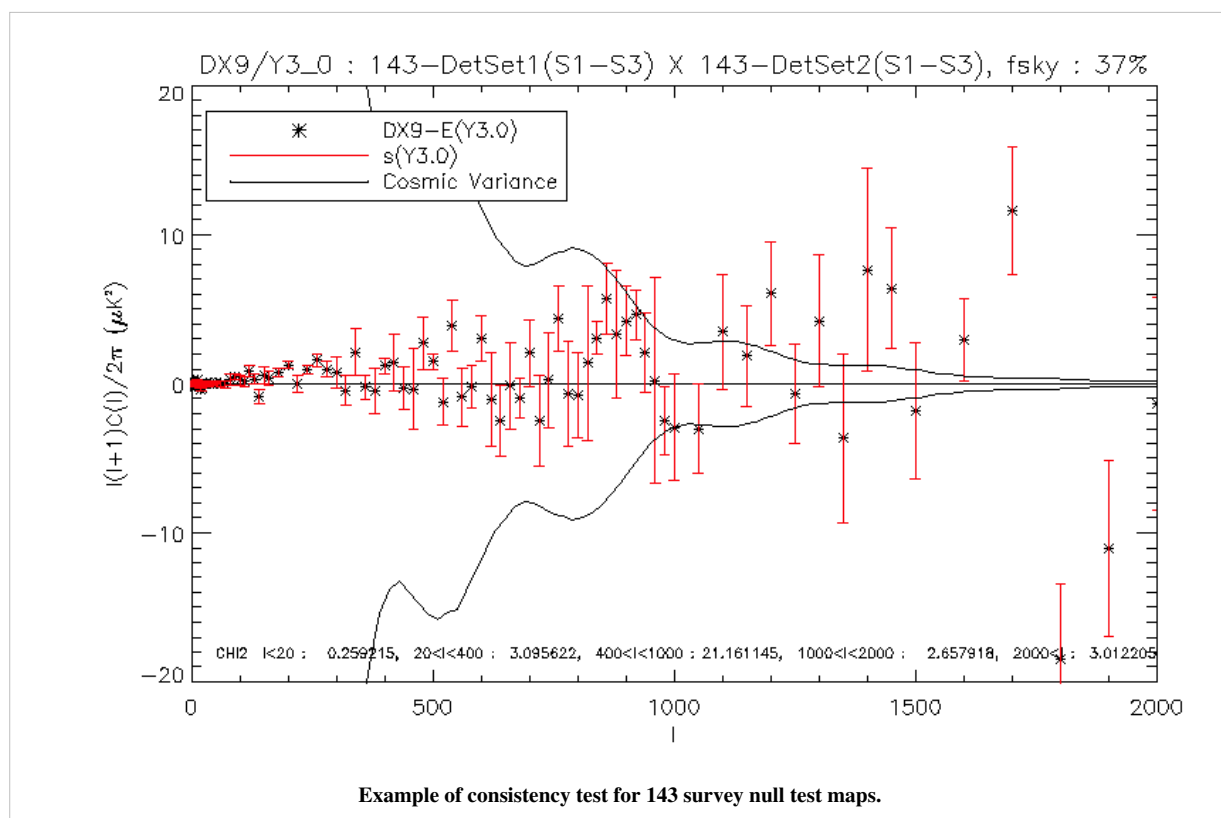
*Yardstick* production contains sky (generated with *LevelS* starting from *PSM* V1.77) and noise timeline realisations proceeded with the official map making. *DX9* production was regenerated with the same code in order to get rid of possible differences that might appear for not running the official pipeline in the same conditions.

We compare statistical properties of the cross spectra of null test maps for the 100, 143, 217, 353 GHz channels. Null test maps can either be survey null test or half focal plane null test, each of which having a specific goal :

- survey1-survey2 (S1-S2) aim at isolating transfer function or pointing issues, while
- half focal plane null tests enable to focus on beam issues.

Comparing cross spectra we isolate systematic effects from the noise, and we can check whether they are properly simulated or need to. Spectra are computed with *spice* masking either *DX9* point sources or simulated point sources, and masking the galactic plane with several mask width, the sky fraction from which spectra are computed are around 30%, 60% and 80%.

*DX9* and the *Y3.0* realisations are binned. For each bin we compute the statistical parameters (mean and variance) of the *Yardstick* distribution. The following figure is a typical example of a consistency test, it shows the differences between *Y3.0* mean and *DX9* considering the standard deviation of the yardstick. We also indicate chi square values, which are computed within larger bin : [0,20], [20,400], [400,1000][1000,2000], [2000, 3000], using the ratio between  $(\text{DX9-Y3.0 mean})^2$  and *Y3.0* variance within each bin. This binned chi-square is only indicative: it may not be always significant, since *DX9* variations sometimes disappear as we average them in a bin, the mean is then at the same scale as the yardstick one.



Here will be a link to a (big) pdf file with all those plots, and/or a visualisation page.

## Systematics Impact Estimates

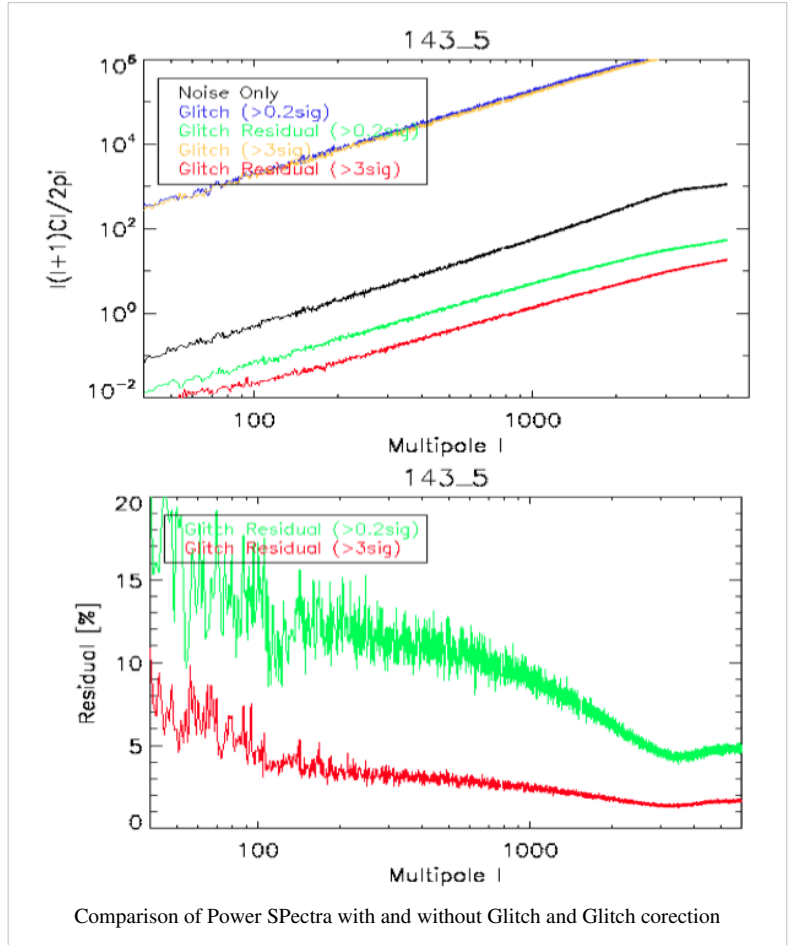
### Cosmic Rays

We have used `Desire` simulations to investigate the impact of glitch residuals at 143GHz. We remind that TOIs are highly affected by the impact of cosmic rays inducing glitches on the timelines. While the peak of the glitch signal is flagged and removed from the data, the glitch tail is removed from the signal during the TOI processing. We have quantified the efficiency and the impact of the official TOI processing when removing glitch tails on the scientific signal.

The Glitch model used in this set of simulations has been built using the real data extraction, in order to reproduce the 3 families observed (i.e. long, short and snail) and their relative distribution. This modelling has been validated on 143GHz channels, by comparing the glitch statistics of simulated timelines with real ones. Two types of models have been introduced for these simulations: the first only includes detectable glitches, with a glitch amplitude at the level of at least 3 times the noise level ; the second model also includes undetectable glitches until a level of 0.3 times the noise level.

The input sky used for these end-to-end simulations includes the CMB signal, our Galaxy, the compact sources and the planets. Not any other kind of systematics has been introduced, except the glitches associated with a white and colored noise to reproduce realistic data. For each bolometer three sets of simulated TOIs have been produced: (i) white plus colored noise only, (ii) noise plus "detectable glitches model" and (iii) noise plus "undetectable glitches model". On the simulated TOIs with glitches, two options of the TOI-processing have been used: with or without correction of the glitches (Despike Module), leading to a set of 5 processed TOIs. Maps and power spectra can be built on these sets of data.

It appears that in the case of the "detectable glitch model", the glitch tail residual represents less than 10% of the noise for  $\ell < 100$  and less than 5% for  $\ell > 100$ . In the case of the "undetectable glitch model", these numbers goes to 20% for  $\ell < 100$  and 15% for  $\ell > 100$ . Nevertheless the number of undetectable glitches remains largely unknown, and can only be extrapolated from power laws. Hence the results obtained for model 2 including undetectable glitches have to be taken as upper limits of the impact of glitch residuals on the power spectrum. These simulations also show that the glitch tail residuals do not produce any kind of  $1/f$  supplementary noise.



## 1.6K and 4K stages Fluctuations

The 4K and 1.6K stages are thermally regulated. The level of (controlled) fluctuations is less than  $20\mu\text{K}/\sqrt{\text{Hz}}$  above the spin frequency (and below 0.2 Hz) for the 4K stage and  $10\mu\text{K}/\sqrt{\text{Hz}}$  for the the 1.6K stage. Using a typical coupling coefficient of  $150\text{ fW/K}_4\text{K}$ , this translates into a noise of  $3\text{ aW}/\sqrt{\text{Hz}}$ . This is 4% of the bolometer noise variance (with a NEP of typically  $15\text{ aW}/\sqrt{\text{Hz}}$ ), and is thus negligible.

## RTS Noise

The Random Telegraphic Signal (RTS) noise, also called Popcorn Noise, appears as 2-levels jumps added on the baseline signal. Three bolometers are known to be affected by a high-RTS noise: 143-8, 545-3 and 857-4. While the 143-8 and 545-3 detectors are currently excluded from use in any products, other bolometers may show small amounts of small RTS.

We have investigated the probable impact of RTS noise present below the detection limit, i.e. 0.2 times the standard deviation noise of the signal. The *Desire* simulations with and without RTS noise have been produce on 143GHz bolometers. The analysis performed on the TOIS has shown that the impact measured is in perfect agreement with the expectation derived from the pre-launch RTS report. Residual RTS appears to be strongly limited, with a negligible impact on TOI noise – does not dominate over the  $1/f$  noise at low frequencies (0.01Hz or below), and it would disappear rapidly above 1 Hz, very probably irrelevant at map level.

## Baseline Jumps

Similar to but distinct from popcorn noise, small baseline jumps were occasionally found in the data streams. They differ from the RTS noise by a much longer duration of the plateau. These data are usually corrected by subtracting a constant baseline before and after the jumps. About 320 jumps are found per bolometers, this represents 16 jumps per day for hFI, i.e. 12800 over the mission lifetime. While the detection efficiency of the biggest jumps is extremely high, the question of the impact of the jumps with amplitudes lower than 0.5% of the standard deviation of signal is still open. *Desire* simulations are about to be produced to answer this.

## Split-Level Noise

The Split-Level noise is the major component of the non-stationnary noise. It appears as a strong increase of the noise level during one or a few rings, and is characterized by the addition of anoher  $1/f$  noise component. The impact of such a systematics effect is under investigation using dedicated *Desire* simulations at 143GHz.

## Pointing-Change Microphonics

The "Thruster signal" is not present for all bolometer for 100, 143, 217 GHz. After the peak "Thruster signal", the relaxing time "normal noise" is about the same for all bolometers over channels, i.e. 12 seconds, but amplitude is different. Thus the effect of the manouver has decayed away long before the end of the "unstable" period, which would be minutes after the first thrust.

This effect can be neglected, and does not need to be included in the simulation runs.

## Electrical Cross-Talk

The Electrical Cross-Talk consists in the electrical contamination received by a given channel and coming from the other channels of the focal plane. This is mainly driven by the locations of the channels inside the electronic devices of the readout chain, and not by their locations in the focal plane.

This effect has been first measured during the ground calibration phase, and then during the inflight 'Calibration, Performance and Validation' phase (CPV Phase) after launch. These two sets of measurements agree to show that the level of electrical cross-talk is smaller than 0.01% for SWBs and 0.1% for PSBs. These estimates have been confirmed by the analysis of the glitches. While the thousands of detected glitches have been flagged for a given channel, the signal of the neighbor channels have been stacked at the same dates of the glitch flags to reveal the amount of electrical contamination coming from the glitched signal. Strong glitches have also been used in the same scope in a second study. These two analysis based on glitches give the same estimates of electrical cross-talk as measured during calibration phases.

Hence the electrical cross-talk has a negligible impact on science data, except probably for PSBs on which further *Desire* simulations will be carried out.

## Optical Cross-Talk

It has been shown using planets crossing that the optical cross-talk is negligible, with an upper limit of 0.01%. This effect can be neglected in the total budget error, without any end-to-end simulation.

## Time Constant

The impact of the uncertainty of the time response has been studied using a set of 50 *Yardstick* simulations with CMB only on 8 143GHz bolometers. The set of 50 Time Transfer Function (TF) realizations have been chosen with a Low Frequency Excess Response (LFER) varying within 1.5% around its nominal value. While the same CMB sky map has been convolved through the optical beam, projected into TOIs and convolved with each of the 50 TF realizations, it has then been deconvolved by the nominal TF, leading to the deconvolved TOIs. Maps and power spectra have then been produced using these TOIs and compared to each others.

These simulations have shown that an uncertainty of 1.5% of the LFER yields 1% of error on the power spectrum at all scales, and even less at large scales.

## 4K lines Residuals

The 4K lines are the 4 K cooler induced noise in the detectors with very specific frequency signatures. They are filtered and corrected during the TOI-processing. The efficiency of this correction has been studied using two types of simulations at 143GHz: *Yardstick* and *Desire* simulations.

The *Yardstick* simulations have explored the impact of 4K lines residuals on CMB signal only, by adding a 4K lines pattern on the CMB TOIs, and by applying the same module of correction as used in the TOI-processing. The impact on the CMB power spectrum has been estimated by comparing the spectra obtained on data without 4K lines and data with corrected 4K lines.

The end-to-end *Desire* simulations include a complete sky (i.e. CMB, Galaxy and point sources) and the complete TOI-processing on the simulated data. The analysis and comparison is then performed on the maps directly and on the power spectra. It has been checked that the 4K lines modeling inputs used in the two sets of simulation are in agreement between them and with in-flight data. Those simulations have been performed on the full 143GHz channel, i.e. 12 detectors, and the full nominal mission range.

Both analysis converge to show that the 4K lines residual represent 2% to 2.5% maximum of the noise level at particular  $\ell$  values affected by the 4K lines (such as  $\ell=1800$ ). These residuals are well below the one-sigma discrepancy of the noise itself at the same particular  $\ell$  values.



Hence the 4K lines residuals are negligible. Nevertheless, the correlation between the 4K lines and the ADC correction discussed in XXXX may have an impact on the gain variation estimates at the end of the processing. This has still to be quantified.

## Saturation

The Planck-HFI signal is converted into digital signal (Raw-Signal) by a 16 bit ADC. This signal is expressed in ADU, from 1 to 65535, and centered around 32768. A full saturation of the ADC corresponds to the value of 1310680 ADU, corresponding to the number of samples per half period times,  $N_{\text{sample}}$ , times  $2^{15}$ . Nevertheless, the saturation of the ADC starts to appear when a fraction of the raw signal hits the 32767 ( $2^{15}$ ) value.

We have used the SEB tool (standing for Simulation of Electronics and Bolometer) to simulate the response of the Readout Electronics Chain at a very high sampling, to mimic the high frequency behavior of the chain and investigate sub-period effects. It has been shown by this kind of simulations that the saturation of the ADC starts to appear if the signal is more than  $7 \cdot 10^5 - 8 \cdot 10^5$  ADU. Hence the variation of the gain, due to the saturation of the ADC, has an impact only when crossing Jupiter for SWB353GHz and SWB857GHz bolometers. This effect can be neglected.

## Summary

This page will contain mostly the same information as what will be in the summary section of the HFI DPC paper. It will center on a table similar to that in the Early DPC paper (shown below) which describes the most important characteristics and figures of the HFI instrument and data.

**Table 4.** Summary of the main characteristics of HFI early maps. The first column refers to following notes pertaining to the content of the line, while the units are between brackets [] at the right of column 2.

HFI Early Maps - Main Characteristics								
$a1$	$\nu$	[GHz]	100	143	217	353	545	857
$a2$	$N_{Bolo}$		8	11	12	12	3	3
$a3$	$c_{WN}$	[ $\mu$ K degree]	1.6	0.9	1.4	5.0	70	1180
$b1$	$\theta_S$	[arcmin]	9.53	7.08	4.71	4.50	4.72	4.42
$b2$	$\Delta\theta_S$	[arcmin]	0.10	0.12	0.17	0.14	0.21	0.28
$b3$	$e_S$		1.20	1.03	1.13	1.10	1.17	1.35
$b4$	$\Delta\alpha_S$	[degree]	0.80	2.08	0.28	0.28	0.13	0.07
$c1$	$\bar{\theta}_M$	[arcmin]	9.88	7.18	4.87	4.65	4.72	4.39
$c2$	$\sigma_{\theta_M}$	[arcmin]	0.04	0.02	0.03	0.04	0.06	0.05
$c3$	$\bar{e}_M$		1.15	1.01	1.06	1.05	1.14	1.19
$c4$	$\sigma_{e_M}$		0.02	0.01	0.02	0.02	0.03	0.05
$d1$	CMB relative calibration accuracy		$\lesssim 1\%$	$\lesssim 1\%$	$\lesssim 1\%$	$\lesssim 2\%$		
$d2$	CMB absolute calibration accuracy		$\lesssim 2\%$	$\lesssim 2\%$	$\lesssim 2\%$	$\lesssim 2\%$		
$d3$	FIRAS gain calibration accuracy						$\sim 7\%$	$\sim 7\%$
$d4$	FIRAS zero point uncertainty [MJy sr <sup>-1</sup> ]		0.8			1.4	2.2	1.7
$e1$	$F_U$	[MJy sr <sup>-1</sup> /mK <sub>CMB</sub> ]	$2.42 \cdot 10^{-1}$	$3.69 \cdot 10^{-1}$	$4.81 \cdot 10^{-1}$	$2.88 \cdot 10^{-1}$	$5.83 \cdot 10^{-2}$	$2.24 \cdot 10^{-3}$
$e2$	$\Delta F_U$		$\lesssim 1\%$	$\lesssim 1\%$	$\lesssim 1\%$	$\lesssim 1\%$	$\lesssim 1\%$	$\sim 3\%$
$e3$	$C(\alpha), \alpha = -2$		1.011	1.025	0.999	0.997	0.998	1.011
	$C(\alpha), \alpha = 0$		0.999	0.985	1.009	1.011	1.012	0.999
	$C(\alpha), \alpha = 1$		1.008	0.980	1.027	1.031	1.035	1.007
	$C(\alpha), \alpha = 2$		1.027	0.985	1.053	1.060	1.068	1.024
$e4$	$F_{CO}$	[ $\mu$ K <sub>CMB</sub> /K <sub>RJ</sub> km s <sup>-1</sup> ]	$14.2 \pm 1.0$		$44.2 \pm 1.0$	$171.0 \pm 6.0$		

This table is from the Early DPC paper, and will be updated when all figures are ready

# The LFI DPC

---

## Overview

The LFI DPC processing is organized into different "Levels": 1,2,3,4 and S. In brief the Level-1 has the scope to analyze the data in a daily base, transform the telemetry packets in to timelines containing engineering values and feed it in the DPC database. Level-2 use the output of the Level-1 transforming raw TOI in to calibrated timelines with all the know systematic sources removed, those timelines are then used in the mapmaking process to create all the possible maps combinations. Level-3 use the Level-2 output of both DPC to derive astrophysical results like Catalogue, CMB map, foreground etc.... Level-S is the common simulation pipeline used to validate the results and any algorithm before its introduction into the official pipeline. Finally the Level-4 just act as a collector pointing used to reformat, document and deliver the products to the final archive.

## Level 1: From packets to TOI

Level 1 takes input from the MOC's Data Distribution System (DDS), decompresses the raw data, and outputs Time Ordered Information for Level 2. This will be done by using software. The input to Level 1 are the telemetry (TM) and auxiliary data as they are released by the MOC (Mission Operation Centre). Level 1 will use TM data for performing a routine analysis (RTA) of the S/C and P/L with the aim of monitoring the overall health of the payload and detecting possible anomalies, and performing a quick-look data analysis of the science TM to monitor the operation of the observation plan and to verify the behavior of the instrument. Additional tasks of Level 1 relate to its role of instrument control and as the DPC interface with the MOC. Level-1 processing is described in detail in the Pre-processing section

## Level 2: From TOI to Maps

The DPC Level 2 has many tasks. The first one is the creation of differenced data. Level 1 stores data from both Sky and Load. These two have to be properly combined to produce differenced data therefore reducing the impact of 1/f noise. This is done via the computation of the so-called gain modulation factor "R" which is derived taking the ratio of the mean signals from both Sky and Load. After differenced data are produced, the next step are the removal of know systematic effects and then the photometric calibration where calibrated means essentially that TOD are in physical units instead of engineering units; the following major task is the production of frequency maps calibrated and free from systematic effects (which is a complex task and involves several sub-pipelines). Level-2 processing is described in detail in the TOI processing section

## Level 3: From Maps to Component

The aim of Level 3 is to transform the frequency maps produced by both instruments into preliminary maps of the underlying astrophysical components by means of pipeline processing and to provide other data sets including description of astrophysical sources (final catalogue of point sources, extended source maps and catalogues, description of global or statistical properties etc ...). Data from both HFI and LFI are analyzed jointly to reach the final expected result. Level-3 processing is described in detail in the L3\_LFI and HFI/LFI joint data processing section

## Level S : A common HFI/LFI simulation software

Level S is the so-called "Simulation Level" software suite common to both consortia, which, given a sky model (generated by the Planck sky model, PSM), detectors pointing and beams, generates the infalling power on each detector. It can also provide a simplified description of eg. the noise. It is further described in the HFI/LFI common section.

## LFI DPC Infrastructures

The LFI DPC provide a centralized hardware and software infrastructure to a large number of geographically distributed institution participating to the Planck mission. In few word the data are interfaced to a database where only meta-information are stored. This allow very high flexibility to eventually modify the product to be delivered.

## Published Paper

The description of the pipeline applied to the *"Early Planck results"* can be found at the following link Planck early results. V. The Low Frequency Instrument data processing <sup>[1]</sup> and instrument performances are reported Planck early results. III. First assessment of the Low Frequency Instrument in-flight performance <sup>[2]</sup>

## References

- [1] [http://www.aanda.org/index.php?option=com\\_article&access=standard&Itemid=129&url=/articles/aa/abs/2011/12/aa16484-11/aa16484-11.html](http://www.aanda.org/index.php?option=com_article&access=standard&Itemid=129&url=/articles/aa/abs/2011/12/aa16484-11/aa16484-11.html)
- [2] [http://www.aanda.org/index.php?option=com\\_article&access=standard&Itemid=129&url=/articles/aa/abs/2011/12/aa16480-11/aa16480-11.html](http://www.aanda.org/index.php?option=com_article&access=standard&Itemid=129&url=/articles/aa/abs/2011/12/aa16480-11/aa16480-11.html)

# Pre-processing LFI

---

## Overview

The first processing level of the LFI DPC is the so called Level 1. The source data of the Level 1 software includes:

- raw housekeeping telemetry packets retrieved from different satellite subsystems: the LFI instrument, the Sorption cooler, the HFI instrument and the Central Data Management Unit (CDMU).
- the LFI raw scientific telemetry
- Additional auxiliary data provided by the MOC and the Flight dynamics:
  - The Attitude History File (AHF)
  - Time correlation data (time correlation coefficients and time couples)
  - Command History data
  - The Sorption cooler out of limit data

Only a subset of the raw housekeeping telemetry packets is daily processed and converted into TOIs, i.e. those relevant to the LFI Daily Quality Report production and the estimation of the LFI instrument systematic effects.

---

## The LFI scientific telemetry

Each LFI radiometer provides two analog outputs, one for each amplifier chain. In a nominal configuration, each output yields a sequence of alternating  $V_{sky}$ ,  $V_{load}$  signals at the frequency of the phase switch. By changing the phase switches configuration, the output can be a sequence of either  $V_{sky}$  or  $V_{load}$  signals.

The conversion from analog to digital form of each radiometer output is performed by a 14 bits Analog-to-Digital Converter (ADC) in the Data Acquisition Electronics unit (DAE). The DAE transforms the signal in the range  $[-2.5 \text{ V}, +2.5 \text{ V}]$ : first it applies a tunable *offset*,  $O_{DAE}$ , then it amplifies the signal with a tunable *gain*,  $G_{DAE}$ , in order to make full use of the resolution of the ADC, and finally the signal is integrated. To eliminate phase switch raise transients, the integration takes into account a *blanking time*, i.e. a blind time in the integrator where data are not considered. The default value of the blanking time is  $7.5 \mu\text{s}$ . Both the  $O_{DAE}$ , the  $G_{DAE}$  and the blanking time are parameters set through the LFI on-board software. The equation applied to transform a given input signal  $V_{in}$  into an output  $V_{out}$  is:

$$V_{out} = G_{DAE}(V_{in} + O_{DAE}) + Z_{DAE}$$

with  $G_{DAE} = 1, 2, 3, 4, 6, 8, 12, 16, 24, 48$ ,  $O_{DAE}$  is one of 255 possible offset steps from  $+0$  up to  $+2.5 \text{ V}$  and where  $Z_{DAE}$  is a small offset introduced by the DAE when applying a selected gain. The values of  $G_{DAE}$  and  $O_{DAE}$  are set by sending, through specific telecommands, the DAE Gain Index (DGI) and the DAE Offset Index (DOI) associated to the desired values.

The ADC quantizes the  $V_{out}$  uniformly in the range  $-2.5 \text{ V} \leq V_{adc} \leq +2.5 \text{ V}$ , so that the quantization step is  $q_{ADC} = 5.0/2^{14} = 0.30518 \text{ mV}$ . The quantization formula is

$$S = \text{round} \left( \frac{V_{out} + 2.5}{q_{ADC}} \right),$$

and the output is stored as an unsigned integer of 16 bits.

The digitized scientific data is then processed by the Radiometer Electronics Box Assembly (REBA) which runs the LFI on-board software. For each LFI detector, the REBA processes the data in the form of time series which are split into telemetry packets. To satisfy the LFI assigned telemetry budget limit of 53.5 Kbps, the REBA implements 7 acquisition modes (processing types) which reduce the scientific data rate by applying a number of processing steps. The following figure illustrates the main steps of the on-board processing and the corresponding processing types (PTypes).

### PType 0

in this mode the REBA just packs the raw data of the selected channel without any processing.

### PType 1

consecutive  $S_{sky}$  or  $S_{load}$  samples are coadded and stored as unsigned integers of 32 bits. The number of consecutive samples to be coadded is specified by the  $N_{aver}$  parameter.

### PType 2

in this mode, two main processing steps are applied. First, pairs of averaged  $S_{sky}$  and  $S_{load}$  samples, respectively  $\bar{S}_{sky}$  and  $\bar{S}_{load}$ , are mixed by applying two different gain modulation factors, GMF1 and GMF2: The operations are performed as floating point operations. Then the two values obtained are requantized, converting them into two 16-bit signed integers:

### PType 3

with respect to PType 2, in this mode only a single gain modulation factor is used, GMF1, obtaining:

$$P = \bar{S}_{sky} - \text{GMF1} \cdot \bar{S}_{load}$$

and analogously to PType 2, the value is requantized obtaining a 16-bit signed integer.

### PTypes 4, 5, 6

with the processing types PType 4, PType 5 and PType 6, the REBA performs a loss-less adaptive arithmetic compression of the data obtained respectively with the processing types PType 0, PType 2 and PType 3. The compressor takes couples of 16 bit numbers and stores them in the output stream up to the complete filling of the data segment for the packet in process.

A set of REBA processing parameters —  $N_{aver}$ , GMF1, GMF2,  $q$  and Offset — is selected for each of the 44 LFI channels. They are also included in a tertiary header of each scientific telemetry packet sent to ground. The REBA can acquire data from a channel in two modes at the same time. This capability is used to verify the effect of a certain processing type on the data quality. So, in nominal conditions, the LFI instrument uses PType 5 for all its 44 detectors and every 15 minutes a single detector, in turn, is also processed with PType 1, in order to periodically check the gain modulation factors and the second quantization parameters. The other processing types are mainly used for diagnostic, testing or contingency purposes.

Packets generated by the REBA follow the ESA Packet Telemetry Standard and Packet Telecommand Standard, the CCSDS Packet Telemetry recommendations and the ESA Packet Utilization Standard (PUS). The packet structure for an LFI scientific telemetry packet is shown in the following figure.

## From packets to raw TOIs

On a daily basis, the LFI Level 1 software pipeline retrieves the housekeeping and scientific telemetry packets dumped from the satellite on-board memory through the MOC Data Disposition System (DDS). The Level 1 software has to recover most accurately the values of the original (averaged) sky and load samples acquired on-board. Data acquired with PTypes 4, 5 and 6 is first uncompressed. The loss-less compression applied on-board is simply inverted and the number of samples obtained is checked with the value stored in the tertiary header.

The digitized data, processed by the REBA, are not in physical units but in ADU (Analog to Digital Unit). Conversion of  $S_{sky}$  and  $S_{load}$  in Volt requires the Data Source Address (DSA), i.e. the radiometer and detector from which the data are generated, the blanking time (indicated by the Blanking Time Index, BTI), the DGI and the DOI. The DSA and BTI values are recovered from the packet tertiary header, while the DGI and DOI values are recovered from the LFI HK telemetry. Hence, the value in Volt is obtained as:

$$V_i = \frac{S_i \cdot q_{ADC} - Z_{DAE} - 2.5}{G_{DAE}} - O_{DAE} \approx \frac{S_i - \tilde{Z}_{DAE}(DSA, BTI, DGI)}{\tilde{G}_{DAE}(DSA, BTI, DGI)} - \tilde{O}_{DAE}(DSA, BTI, DOI)$$

where  $\tilde{G}_{DAE}(DSA, BTI, DGI)$ ,  $\tilde{O}_{DAE}(DSA, BTI, DOI)$  and  $\tilde{Z}_{DAE}(DSA, BTI, DGI)$  are look-up tables estimated during the LFI ground calibration campaign with:

- $\tilde{G}_{DAE}(DSA, BTI, DGI) \approx \frac{G_{DAE}}{q_{ADC}}$ ,
- $\tilde{O}_{DAE}(DSA, BTI, DOI) \approx O_{DAE}$ ,
- $\tilde{Z}_{DAE}(DSA, BTI, DGI) \approx \frac{Z_{DAE} + 2.5}{q_{ADC}}$ .

This conversion is the only processing required by PTypes 0 and 3 and it is the last step in the processing of all the other processing types. Since PType 1 data is just coadded on-board, the division by  $N_{aver}$  is performed by the Level 1 software. PType 2 and 5 data have to be dequantized by:

$$P_i = \frac{Q_i}{q} - \text{Offset}$$

and then demixed to obtain  $\bar{S}_{sky}$  and  $\bar{S}_{load}$ :

## On-board time reconstruction

The On-Board Time (OBT) reconstruction for scientific data has to take into account the phase switch status and the processing type applied on-board. If the phase switch is off, it means that the packet contains consecutive values of either sky or load samples, and the sampling frequency,  $f_{sampling}$ , is 8192 Hz. Denoting with  $i \geq 0$  the sample index within the packet, for PType 0 and 4 we have that:

$$t_i^{obt} = t_0^{obt} + i \frac{1}{f_{sampling}},$$

where  $t_0^{obt}$  is the on-board time of the packet ( $t_{pkt}^{obt}$ ) and  $i = 0$  denotes the first sample in the packet. If the switching status is on, either consecutive pairs of (sky, load) samples or (load, sky) samples are stored in the packets. Hence, consecutive couples of samples have the same time stamp and  $f_{sampling} = 4096$  Hz.

For averaged data (PTypes 1, 2, 3, 5, 6), the first sample of a scientific packet is the sum (mean) of  $N_{aver}$  samples, and the packet time,  $t_{pkt}^{obt}$ , is the time of the first of the  $N_{aver}$  samples. In this case,  $t_0^{obt}$  is computed as:

$$t_0^{obt} = t_{pkt}^{obt} + \frac{N_{aver} - 1}{2} \frac{1}{f_{sampling}}$$

and

$$t_i^{obt} = t_0^{obt} + i \frac{N_{aver}}{f_{sampling}}, \text{ for } i \geq 1$$

## Housekeeping telemetry handling

Some information should be added for the handling of the housekeeping telemetry, using the Mission Information Base (MIB)

## Auxiliary data handling

Some information concerning the handling of the Attitude History Files, Time Correlation data and Time Couples, OBT/UTC conversion, Out Of Limit data

# TOI processing LFI

---

## Overview

The LFI Level2 Pipeline analyzes each horn of the instrument separately, one pointing period at time, and store results in object the length of an OD. Each diode of the horn is corrected from systematic, differentiated and then combined with its complementary diode in the same radiometer. The horn is then calibrated and the photometric calibration is applied.

## Pre-processing

Before the run of the Level2 pipeline and to improve the analysis the Mission information and data sampling divisions are stored in the database.

The Mission information is a set of objects, one for each Operational Day (OD, as defined in REFERENCE??), in which are stored Pointing Period data: DPC pointing ID (where 1 is the first pointing of the nominal mission), PSO pointing ID, start OBT of the pointing maneuver, start OBT of the stable pointing, end OBT of the pointing, spin axis ecliptic longitude and latitude.

The sampling information is a set of objects, one for each LFI frequency, in which are stored for each pointing ID: start OBT of the pointing maneuver, start OBT of the stable pointing, end OBT of the pointing, number of samples of the pointing, number of stable samples of the pointing, start sample of the stable pointing and sample number from the start of the nominal mission. Valid samples and OBTs are defined where any of the radiometers from that frequency cohort contain valid data.

## ADC Correction

During analysis it appeared that white noise and calibration seemed affected by something in common. It turn out to be a non linearity in the Analogic/Digital Converter on board. More on P02 and P02a.

## Evaluation

The mathematical model represents the digital ADC output as:

$$X = (V - \Delta)\gamma + x_0$$

where  $V$  is the voltage input,  $\gamma$  is the DAE gain,  $\Delta$  is the DAE offset and  $x_0$  is the DAE  $T_{zero}$ .

We can model the non-linearity as a function of the input voltage  $R(V)$ . So we have the apparent inferred voltage  $V'$  and we can link it to the actual input voltage with:

$$((V - \Delta)\gamma + x_0)R(V) = X = ((V' - \Delta)\gamma + x_0)$$

so that:

$$R(V) = \frac{(V' - \Delta)\gamma + x_0}{(V - \Delta)\gamma + x_0}$$

Since  $V \gg \Delta$  and  $V\gamma \gg x_0$  we can use the much simpler relation:

$$R(V) = \frac{V'}{V}$$

and we expect it to be very near to unity for all  $V$ .

To find the response curve we have only the apparent voltage to work with, so we had to use the inverse response function  $R'(V')$  and replace the real input voltage with  $T_{sys}$  times the time varying gain factor  $G(t)$ .

$$V = V' R'(V') = G(t) T_{sys}$$


---

If we introduce a small signal on top of  $T_{sys}$  which leads to increased detected voltage and corresponding apparent voltage increment:

$$V + \delta V = (V' + \delta V') = (V' + \delta V')R'(V' + \delta V') = G(t)(T_{sys} + \delta T)$$

so carrying out the differentiation respect to  $V'$  to the relation between true and apparent signal voltage leads to:

$$\delta V = \left( V' \frac{dR'(V')}{dV' + R'(V')} \right) \delta V' = G(t) \delta T$$

We now assume  $T_{sys}$  and  $\delta T$  are fixed and that the variations are due to slow drifts in the gain. So we can isolate the terms:

$$V' = \frac{G(t)T_{sys}}{R'(V')}$$

$$\delta V' = \frac{G(t)\delta T}{V' \frac{dR'(V')}{dV'} + R'(V')}$$

Combining the equations through the gain factor to remove it:

$$\frac{V' R'(V')}{T_{sys}} = \frac{\delta V' \frac{dR'(V')}{dV'} + R'(V')}{\delta T}$$

Rearranging and putting  $a = \frac{\delta T}{T_{sys}}$

$$\frac{dR'(V')}{dV'} = \left( \frac{a}{dV'} - \frac{1}{V'} \right) R'(V')$$

So there is the expected direct proportionality of  $\delta V'$  to  $V'$  due to the assumption that the variations in voltage are due to overall gain drift, so the amplitude of voltage and signal will vary together. Then there is the additional differential term which will pull signal amplitude away from the linear relationship. So if we plot measured white noise or dipole gain factor against recovered voltage we should see this linear curve with variations due to local slope changes at particular voltages. The linear part can be taken out and the differential part fitted. This was numerically integrated up to get the inverse response curve, what we need to convert the measured voltages to corrected voltages.

## Application

For each of the 44 LFI diodes there is the corresponding object in the Database. Each object contains 4 columns: the input voltages coming from the sky channel and the corresponding linearized output, the input voltages coming from the reference channel and the corresponding linearized output.

Data loaded by the module are used to initialize two different interpolators using CSPLINE and the functions from gsl (GNU Scientific Libraries<sup>[1]</sup>) libraries. The interpolators are then used to correct each sample.

## Spikes Removal

Some of the LFI receivers exhibit a small artifact with exactly 1 second repetition, which visible in the power spectra. The effect is a set of spikes at 1 Hz and harmonics. The spurious signal is very well modeled and is removed from the timelines. More information can be found in P02 and P02a.

## Modeling

The cause of the spikes at 1 Hz and harmonics is a tiny 1 second square wave embedded in affected channels. The method to estimate the 1 Hz signal is to build a template in time domain synchronized with the spurious signal. The first step is dividing each second of data into time bins using OBT. The number of bins is computed using:



$$n_{bins} = fsamp * template\_resolution$$

where  $fsamp$  is the sampling frequency and is 136 at 70 GHz, 80 at 44 GHz and 56 at 30 GHz. Then the bins vector is initialized with time intervals. To avoid aliasing effects template resolution is  $\sqrt{3}$ . We can write the process adding an index to the time sample: lower index denotes the particular time sample, while the upper index labels the bin into which the sample falls. The linear filter can be written as:

$$s(t_i^j) = a_j (1 - \Delta x(t_i^j)) + a_{j+1} \Delta x(t_i^j)$$

Here  $\Delta x(t_i^j)$  is the filter weight which is determined by where within the bin sample lies. If we use  $t^j$  with only an upper index to denote the start of each bin, then we can write the filter weight as follows:

$$\Delta x(t_i^j) = \frac{t_i^j - t^j}{t^{j+1} - t^j}$$

In other words, the filter weight is the time sample value minus the start of the bin divided by the width of the bin.

We must estimate the parameters  $a_j$  from the data. With the assumption that the instrument has stable noise properties, we can use a least square algorithm to estimate the bin values:

This can be represented in matrix equation:

$$M_{jk} a_k = b_j$$

with the following definitions:

$$\begin{aligned} M_{k,k-1} &= \sum_i (1 - \Delta x(t_i^{k-1})) \Delta x(t_i^{k-1}) \\ M_{k,k} &= \sum_i (1 - \Delta x(t_i^k))^2 \Delta x(t_i^{k-1})^2 \\ M_{k,k+1} &= \sum_i (1 - \Delta x(t_i^k)) \Delta x(t_i^k) \\ M_{k,k+n} (|n| > 1) &= 0 \\ b_j &= \sum_i d_i^k (1 - \Delta x(t_i^k)) + d_i^{k-1} \Delta x(t_i^{k-1}) \end{aligned}$$

With these definitions we have to make use of periodic boundary conditions to obtain the correct results, such that if  $k = 0, k - 1 = n - 1$  and  $k = n - 1, k + 1 = 0$ . Once this is done, we have a symmetric tridiagonal matrix with additional values at the upper right and lower left corners of the matrix. The matrix is solved with LU decomposition. In order to be certain of the numerical accuracy of the result, we can perform a simple iteration. The solving of the linear system and the iterative improvement of the solution are implemented as suggested in Numerical Recipes.

## Application

For each of the 44 LFI diodes there is the corresponding object in the Database. Because of the amplitude of the spikes we choose to apply the correction only on the 44 GHz radiometers. Each object contains 3 columns: the bins start time vector, the sky amplitudes and the reference amplitudes.

For each sample the value to be subtracted is computed using:

$$V = skyAmp_k (1 - \Delta x(t_k)) + skyAmp_{k+1} \Delta x(t_k)$$

where  $k$  is the index of the bins at a given time.

## Gaps Filling

During the mission some of the data packets were lost (see P02). Moreover in two different and very peculiar situations LFI was shutdown and restarted, giving inconsistencies in data sampling. All of those data aren't used for scientific purpose but to avoid discrepancies in data analysis all of the radiometers at the same frequency must have the same samples.

To accomplish this the length of the data stream to be reduced in a specific pointing period is compared with the data stored in the sample information object. If the length is not the same the OBT vector is filled with missing sample times, the data vector is filled with zeros and in the flag column the bit for gap is raised.

## Gain Modulation Factor

The pseudo-correlation design of the LFI radiometers dramatically reduces the  $1/f$  when the  $V_{sky}$  and  $V_{load}$  outputs. The two streams are slightly unbalanced, as one looks at the 2.7 K sky and the other looks at the ~4.5 K reference load. To force the mean of the difference to zero, the load signal is multiplied by the Gain Modulation Factor (R). For each pointing period the factor is computed using:

$$R = \frac{\langle V_{sky} \rangle}{\langle V_{load} \rangle}$$

Then the data are differenced using:

This value for R minimizes the  $1/f$  and the white noise in the difference timestream. The  $i$  index represents the diode and can be 0 or 1.

At this point the maneuver flag bit is set to identify which samples have missing data, using the information stored in the sampling information object. This identifies which data to ignore in the next step of the Pipeline.

The R values are stored in the database. At the same time the mean values of  $V_{sky}$  and  $V_{load}$  are stored in order to be used in other steps of the analysis.

## Diode Combination

The two complementary diodes of each radiometer are combined. The relative weights of the diodes in the combination are chosen for optimal noise. We assign relative weights to the uncalibrated diode streams based on their first order calibrated noise.

## Evaluation

From first order calibration we compute an absolute gain  $G_0$  and  $G_1$ , subtract an estimated sky and calculate the calibrated white noise  $\sigma_0$  and  $\sigma_1$ , for the pair of diodes. The weights for the two diodes ( $i=0$  or  $1$ ) are:

$$W_i = \frac{\sigma_i^2}{G_{01}} \frac{1}{\sigma_0^2 + \sigma_1^2}$$

where the weighted calibration constant is given by:

$$G_{01} = \frac{1}{\sigma_0^2 + \sigma_1^2} [G_0 \sigma_1^2 + G_1 \sigma_0^2]$$

The weights are fixed to a single value per diode for the entire dataset. Small variations in the relative noise of the diodes would in principle suggest recalculating the weights on shorter timescales, however, we decided a time varying weight could possibly induce more significant subtle systematics, so chose a single best estimate for the weights for each diode pair.

Horn	Weight M-00	Weight M-01	Weight S-10	Weight S-11
18	0.567304963	0.432695037	0.387168785	0.612831215
19	0.502457723	0.497542277	0.55143474	0.44856526
20	0.523020094	0.476979906	0.476730576	0.523269424
21	0.500324722	0.499675278	0.563712153	0.436287847
22	0.536283158	0.463716842	0.553913461	0.446086539
23	0.508036034	0.491963966	0.36160661	0.63839339
24	0.602269189	0.397730811	0.456037835	0.543962165
25	0.482050606	0.517949394	0.369618239	0.630381761
26	0.593126369	0.406873631	0.424268188	0.575731812
27	0.519877701	0.480122299	0.484831449	0.515168551
28	0.553227696	0.446772304	0.467677355	0.532322645

## Application

The weight in the table above are used in the formula:

$$TOI_{diff} = w_0 TOI_{diff0} + w_1 TOI_{diff1}$$

## Planet Flagging

Why we flag planets.

## Extraction Method

The planets Temperature have been estimated from chunk of samples affected, plus a surrounding region, projected onto a grid (microstripes), by assuming an elliptical Gaussian beam using parameters from instrument database.

Microstripes are a way to extract and store relevant samples for planets detection. Relevant samples are samples affected by the planet plus samples in the neighbor. The search radius to select samples as relevant is 5 deg around the planet position, computed at the pointing period mid time. For each sample we store SCET (Spacecraft Event Time), pointing directions and calibrated temperature. Destriping is applied during application.

Random errors are estimated by taking the variance of samples entering each micromap pixel. This is fast and the major problems (near a bright source the noise gives a larger value and it is difficult to extract the correlation matrix) causes the noise to be overestimated by a factor of two that in this situation is not a major drawback.

The apparent position of Planets as seen from Planck at a given time is derived from JPL Horizon <sup>[2]</sup>. Position are sampled in tables at steps of 15 minutes and then linearly interpolated at the sampling frequency of each detector. JPL Horizons tables allow also to derive other quantities such as the Planet-Planck distance and the Planet-Sun distance nad the planet angular diameter affecting the apparent brightness of the planet.

The antenna temperature is a function of the dilution factor, according to:

$$T_{ant,obs} = 4 \log 2 T_{ant,1} \left( \frac{\theta}{b_{fwhm}} \right)^2$$

where  $T_{ant,obs}$  and  $T_{ant,1}$  are the observed and reduced  $T_{ant}$ ,  $\theta$  the instantaneous planets angular diameter and  $b_{fwhm}$  the beam full width half maximum.

With the above definition  $T_{ant,1}$  could be considered as the  $T_{ant}$  for a planet with  $b_{fwhm} = \theta$ , but a more convenient view is to take a Reference Dilution factor  $D_0$ , as the dilution factor for a standardized planet angular

diameter and beam fwhm  $b_{fwhm}, \theta_0$ , to have:

$$D_0 = \left( \frac{\theta_0}{b_0} \right)^2$$

leading to the following definition of a standardized  $T_{ant}$ :

$$T_{ant,obs} = 4 \log 2 T_{ant,0} \left( \frac{b_{fwhm,0}}{b_{fwhm}} \frac{\theta}{\theta_0} \right)^2$$

with the advantage of removing variations among different detectors and transits while keeping the value of  $T_{ant}$  similar to that seen by the instrument and then allowing a prompt comparison of signals and sensitivities.

## Application

The OBT vector found by the search are saved in a set of object, one for each horn. In Level2 Pipeline those OBTs are compared with the OBT vector of the data to raise planet bit flag where needed.

## Photometric Calibration

Photometric calibration is the procedure used to convert data from volts to kelvin. The source of the calibration is the well known CMB dipole, caused by the motion of the Solar System with respect to the CMB reference frame. To this signal we add the modulation induced by the orbital motion of Planck around the Sun. The resulting signal is then convoluted with the horn beam to get the observed Dipole.

## Beam Convoluted Dipole

In computing the beam convoluted dipole we used an elegant algorithm to save time and computing power. In computing the cosmological dipole signal it is usually assumed a pencil-like beam acting as a delta of Dirac. In this case a dipole timeline is defined as:

$$\Delta T_{D,\delta}(t) = \mathbf{P}_E(t) \cdot \mathbf{D}_E$$

where  $\mathbf{P}_E(t)$  is the pointing direction, in the observer reference frame and  $\mathbf{D}_E$  is the dipole axis scaled by the dipole amplitude again in the same reference frame.

In general the true signal would have to be convoluted with the beam pattern of the given radiometer, usually described as a fixed map in the Beam reference frame or as a time dependent map in the observer reference frame. In this case it is easiest to describe the convolution in the beam reference frame, since the function to be convoluted is described by a single vector.

Denoting with  $\mathcal{U}(t)$  the matrix converting pointings from the observer to the beam reference frame, so that:

$$\mathcal{U}(t) \mathbf{P}_E(t) = \mathbf{e}_z$$

the instantaneous dipole direction in the beam reference frame is:

$$\mathbf{D}(t) = \mathcal{U}(t) \mathbf{D}_E$$

By denoting with  $\mathbf{P}$  a pointing direction in the beam reference frame then:

$$\Delta T_D(t) = N \int_{4\pi} B(\mathbf{P}) \mathbf{P} \cdot \mathbf{D}(t) d^3 \mathbf{P}$$

where  $N$  is a normalization constant.

$$N^{-1} = \int_{4\pi} B(\mathbf{P}) d^3 \mathbf{P}$$

Denoting with  $\mathbf{P}_x, \mathbf{P}_y, \mathbf{P}_z$  the three cartesian components of the  $\mathbf{P}$  the integral of the dot product can be decomposed in three independent integrals:

$$S_x = N \int_{4\pi} B(\mathbf{P}) P_x d^3\mathbf{P}$$

$$S_y = N \int_{4\pi} B(\mathbf{P}) P_y d^3\mathbf{P}$$

$$S_z = N \int_{4\pi} B(\mathbf{P}) P_z d^3\mathbf{P}$$

those integrals define a time independent vector characteristic of each radiometer and constant over the mission.

Detector ID	$S_x$	$S_y$	$S_z$
LFI18S	1.4105692317321994e-03	-3.7689062388084022e-04	9.9999893412338192e-01
LFI18M	1.1200251268914613e-03	-3.2838598619563524e-04	9.9999931885294768e-01
LFI19S	1.7861136968831050e-03	-4.4036975450455066e-04	9.9999830793473898e-01
LFI19M	1.4292780457919835e-03	-4.7454175238335579e-04	9.9999886598655352e-01
LFI20S	1.7008692096818349e-03	-6.1036624911600191e-04	9.9999836724715374e-01
LFI20M	1.5548897911626446e-03	-5.9289001736737262e-04	9.9999861539862389e-01
LFI21S	1.6975720932854463e-03	6.0961185087824777e-04	9.9999837330986663e-01
LFI21M	1.5486274949897787e-03	5.9228926426513112e-04	9.9999862547220986e-01
LFI22S	1.7861136968831245e-03	4.4036975450366470e-04	9.9999830793473898e-01
LFI22M	1.4292780457920242e-03	4.7454175238250377e-04	9.9999886598655352e-01
LFI23S	1.4105692317321714e-03	3.7689062387997129e-04	9.9999893412338203e-01
LFI23M	1.1200251268914476e-03	3.2838598619481239e-04	9.9999931885294757e-01
LFI24S	3.4636411743209074e-04	-2.8530917087092225e-07	9.9999994001590664e-01
LFI24M	4.3939553230170735e-04	-2.9414231975370517e-07	9.9999990346573508e-01
LFI25S	-1.0428719495964051e-04	1.9328051933678115e-04	9.9999997588341061e-01
LFI25M	-1.1004766833423990e-04	2.7656488668259429e-04	9.9999995570068612e-01
LFI26S	-1.0428719495970346e-04	-1.9328051933760877e-04	9.9999997588341061e-01
LFI26M	-1.1004766833430009e-04	-2.7656488668343130e-04	9.9999995570068612e-01
LFI27S	1.6613273546973915e-03	6.6518363019636186e-04	9.9999839875979735e-01
LFI27M	1.5583345016298123e-03	6.4183510236962536e-04	9.9999857981963269e-01
LFI28S	1.6633788116048607e-03	-6.6629002345089925e-04	9.9999839461297824e-01
LFI28M	1.5571200481047094e-03	-6.4144198187461837e-04	9.9999858196366442e-01

By using this characteristic vector the calculation of the convoluted dipole is simply defined by a dot product of the vector  $\mathbf{S}$  by the dipole axis rotated in the beam reference frame.

$$\Delta T(t) = \mathbf{S}^T \mathbf{U}(t) \mathbf{D}_E$$

## Binning

In order to simplify the computation and to reduce the amount of data used in the calibration procedure the data are phase binned in map with Nside 256. The low resolution is sufficient for the purpose because the Dipole signal lives over large angular scale. During phase binning all the data with flagged for maneuvers, planets, gaps and the ones flagged in Level1 analysis as not recoverable are discharged.

## Fit

The first order calibration values are given by a Least Square Fit between the signal and the dipole. For each pointing a gain ( $g_k$ ) and an offset ( $b_k$ ) values are computed minimizing:

$$\chi^2 = \sum_{i \in k} \frac{[\Delta V(t_i) - \Delta V_m(t_i | g_k, b_k)]^2}{rms_i^2}$$

The sum includes samples outside a Galactic mask.

## Mademoiselle

The largest source of error in the fit arises from unmodeled sky signal  $\Delta T_a$  from CMB anisotropy. To correct this we iteratively project the calibrated data (without the dipole) onto a map, scan this map to produce a new TOD with astrophysical signal removed, and finally run a simple destriping algorithm to find the corrections to the gain and offset factors.

To reduce the impact of the noise during the iterative procedure the sky estimation is built using data from both radiometers of the same horn.

## Smoothing

To improve accuracy given by the iterative algorithm and remove noise from the solution a smoothing algorithm must be performed. We used two different algorithms: OSG for the 44 and 70 GHz radiometers, and DV/V Fix for the 30 GHz. The reasons behind this choice can be found in P02b.

### OSG

OSG is a python code that performs smoothing with a 3 step algorithm.

The first step is a Moving Average Window: the gain and offset factors are streams containing one value for each pointing period, that we call dipole fit raw streams. The optimized window has a length of 600 pointing period.

The second step is a wavelet algorithm, using pywt (Discrete Wavelet Transform in Python <sup>[3]</sup>) libraries. Both dipole fit raw streams and averaged streams are denoised using wavelets of the Daubechies family extending the signals using symmetric-padding.

The third step is the combination of dipole fit raw and averaged denoised signal using knowledge about the instrument performance during the mission.

### 4 K total-power and Fix

For the 30 GHz channels we used 4K total-power to track gain changes. The theory and explanation of the choice can be found in P02b.

The algorithm uses  $V_{loadmean}$  values computed during differentiation and raw gains as they are after iterative calibration, performing a linear weighted fit between the two streams using as weight the dipole variance in single pointing periods. The fit is a single parameter fit, so the offsets are put to zero in this smoothing method. It uses the gsl libraries.

In addition to the smoothing, to better follow sudden gain changes due to instrument configuration changes, a fix algorithm is implemented. The first step is the application of the 4k total-power smoothed gains to the data and the production of single radiometer maps in the periods between events. The resulting maps are then fit with dipole maps covering the same period of time producing two factor for each radiometer:  $corrM$  is the result of the fit using the main radiometer and  $corrS$  the one coming from the side radiometer. The correction to be applied to the gain values is then computed as:

$$corr = \frac{1}{1 + \frac{corrM + corrS}{2}}$$

## Gain Application

The last step in TOI processing is the creation of the calibrated stream. For each sample we have:

where  $t$  is the time and  $k$  is the pointing period.  $convDip$  is the CMB Dipole convoluted with the beam.

## References

- [1] <http://www.gnu.org/software/gsl/>
- [2] <http://ssd.jpl.nasa.gov/?horizons>
- [3] <http://www.pybytes.com/pywavelets/>

# TOI-Noise LFI

---

## Overview

This pipeline step aims at the reconstruction of the noise parameters from calibrated flight TOI. The goal is two-folds: one the one side we need to know the actual noise properties of our instrument in order to properly take them into account especially during the following processing and analysis steps like map-making and power spectrum estimation. On the other side evaluation of noise properties along the instrument life-time is a way to track down possible variations, anomalies and general deviations from the expected behaviour.

## Operations

Noise estimation is performed on calibrated data and since we would like to track possible noise variations along mission life-time, we select data in chunks of 5 ODs (Operational Days). These data are processed by the ROMA Iterative Generalized Least Square (IGLS) map-making algorithm which includes a noise estimation tool. In general an IGLS map-making is a quite consuming in terms of time and resources required. However the length of the data is such that running on the DPC cluster in very short time (~1-2 minutes).

The method implemented can be summerized as follows. We model the calibrated TOI as

$$\mathbf{\Delta T} = \mathbf{P} \mathbf{m} + \mathbf{n}$$

where  $\mathbf{n}$  is the noise vector and  $\mathbf{P}$  is the pointing matrix that links a pixel in the map  $\mathbf{m}$  with a sample in the TOI  $\mathbf{d}$ . The zero-th order estimation of the signal is obtained simply rebinning TOI into a map. Then an iterative approach follows in which both signal and noise are estimated according to

$$\hat{\mathbf{n}}_i = \mathbf{\Delta T} - \mathbf{P} \hat{\mathbf{m}}_i$$

$$\hat{\mathbf{m}}_{i+1} = (\mathbf{P}^T \hat{\mathbf{N}}_i^{-1} \mathbf{P})^{-1} \mathbf{P}^T \hat{\mathbf{N}}_i^{-1} \mathbf{\Delta T}$$

where  $\hat{\mathbf{N}}_i$  is the noise covariance matrix in time domain out from iteration  $i$ . After three iterations convergence is achieved.

---

We then perform an FFT (Fast Fourier Transform) on the noise time stream out from the iterative approach and then fit the resulting spectrum.

## Fitting Pipeline

In the very first release of Planck data, once noise spectra were extracted a simply log-periodogram fitting approach was applied to derive the most important noise parameters (white noise level, knee-frequency and slope of the low-frequency noise component). However during mission life-time there were some specific events (e.g. the switch over of the sorption coolers) that we expect were able to cause variation in instrument behaviour and hence in its noise properties. In this respect we have improved our fitting pipeline adding a Monte Carlo Markov Chain approach to estimate noise parameters.

## MCMC approach

This new approach allows us to improve our noise model. Indeed this can be parametrized by the usual combination of white plus  $1/f$  noise

$$P(f) = \sigma^2 \left[ 1 + \left( \frac{f}{f_k} \right)^\beta \right]$$

with three basic noise parameters. However it is also possible to work with a functional form with two more parameters as

$$P(f) = \sigma^2 \left[ 1 + \left( \frac{f}{f_{k1}} \right)^{\beta_1} + \left( \frac{f}{f_{k2}} \right)^{\beta_2} \right]$$

This latter could be useful when there are clearly two different behaviour in the low-frequency part of the spectrum where, beside usual radiometric  $1/f$  noise, appears signature of thermal fluctuations induced noise.

As for the white noise part, this is, as before, computed making a simple average of noise spectrum on the last 10% of frequency bins. This percentage works well for almost all radiometers at 44 and 70 GHz but it is indeed quite delicate for the 30 GHz radiometers which show typical values of knee-frequency around 100 mHz and, therefore, require a smaller number to get an un-biased white noise estimation. Once white noise is computed, the code creates Markov Chains for the other parameters. Discarding the burn-in period of the chains we can directly get from the chain samples distribution, the expected value and variance of each noise parameters sampled.

The left panel of the following Figure shows a typical spectrum at 70 GHz with superimposed the simple log-periodogram fit (purple line) and the new MCMC derived spectrum (blue line). The right panel instead shows distribution for knee-frequency and slope derived from the example spectrum.

## The final noise parameters

As already reported we know that during the nominal operations there was a quite dramatic change in LFI induced by the switch over of the two sorption coolers and particularly we expect to see the effect of degradation of the performance of the first sorption cooler and the onset of the redundant one.

In the following figure we report a set of noise frequency spectra for three LFI radiometers (LFI28M, LFI24S and LFI18M) from the beginning of the operation till the time of the current data release. Some comments are in order. First of all the white noise level is extremely stable in all the three cases (but this is also true for all the LFI radiometer). Also knee-frequency and low-frequency slope are quite stable till OD 326. After that period spectra show a noise increase and two slopes for the low-frequency part which become more evident for spectra around OD 366 and OD 466 where the first cooler starts to be less effective and produces low-frequency thermal noise. After the switch-over to the redundant cooler data still present (the very last spectrum) thermal noise at very low-frequency. This behaviour is almost present in all radiometers with different trends ranging from the small effect shown by



LFI24S to more prominent effect as shown by LFI28M and LFI18M.

## Pointing LFI

### Detector Pointing

Detector pointing reconstruction requires knowledge of the spacecraft attitude and the location of the horns in the focal plane. The AHF (Attitude History File REFERENCE??) gives the orientation of the spacecraft spin axis in quaternions sampled at 8 Hz, as well as the beginning and the end times for each pointing period.

The computation needs to initialize the horn and beam information: it reads the  $\theta$ ,  $\phi$  and  $\psi$  position and rotation angles from the instrument database and builds the rotation matrix from the spin axis to the focal plane (*ax2det*). At the same time the major corrections are initialized.

### Wobble Angle

Wobble angles are the angles which defines the relationship between the Principal Axis Reference Frame of Planck and the Body Reference Frame of Planck, both of which have their origin in the Planck Baricenter (ACMS, AHF-ICD).

Pointings are determined by a set of rotations converting coordinates in the STR reference frame to ecliptical reference frame, i.e. defining the rotation matrix  $R_{ecl, str}$ . The matrix can be decomposed in a sequence of matrix multiplications:

$$R_{ecl, str} = R_{ecl, A} R_{A, B} R_{B, str}$$

here we used  $R_{rfb, rfa}$  to denote transformation from Reference Frame RFA to Reference Frame RFB, and  $R_{rfa, rfb} = R_{rfb, rfa}^{-1}$ .

The  $R_{B, str}$  converts from STR coordinates to Body Reference Frame coordinates, it is a constant matrix.

$$\begin{bmatrix} \cos \beta & 0 & -\sin \beta \\ 0 & 1 & 0 \\ \sin \beta & 0 & \cos \beta \end{bmatrix}$$

where  $\beta = 85deg$  is the STR boresight angle assumed to be constant and aligned with the telescope LOS, but this is not the case. The STR is located on the SVM, at about 1.5 m from the origin of the Body reference frame, a change in its position of 0.15 mm will result in a change of its orientation of about  $10^{-4}$  radians about 20 arcsec.

There is no way to measure directly those changes. So the effect is that to have an apparent change in the  $\psi_1$ ,  $\psi_2$  (tilt angles as defined in the AHF) and  $\psi_3$  (azimuth angle as defined in the AHF) angles: the reason is apparent immediately when looking at the way a perturbation in STR reference frame orientation propagates.

AHF provides wobble angle measures at 1 minute ( $\psi_1$ ,  $\psi_2$ ) and one OD ( $\psi_3$ ) rate. Indeed  $\psi_3$  is provided at each pointing period but measures within each given OD are constant.

Assuming to have quaternions represented by rotation matrix  $R_{ecl, B}(t)$  at a time  $t$ , and assuming to have representative values of true wobble angles  $\psi_{1,0}$ ,  $\psi_{2,0}$ ,  $\psi_{3,0}$  and a way to estimate the apparent  $\delta\psi_1(t)$ ,  $\delta\psi_2(t)$ ,  $\delta\psi_3(t)$  it is possible to remove the apparent effect.

With the available information it can be done for  $\psi_1$  and  $\psi_2$ .

The correction algorithm initializes two rotation matrices as references using  $\psi_1$  and  $\psi_2$  from the first pointing period of the nominal mission:

$$R_{psi1} = \begin{bmatrix} \cos \psi_{1,ref} & \sin \psi_{1,ref} & 0 \\ -\sin \psi_{1,ref} & \cos \psi_{1,ref} & 0 \\ 0 & 0 & 1 \end{bmatrix}$$

$$R_{psi2} = \begin{bmatrix} \cos \psi_{2,ref} & 0 & -\sin \psi_{2,ref} \\ 0 & 1 & 0 \\ \sin \psi_{2,ref} & 0 & \cos \psi_{2,ref} \end{bmatrix}$$

Then, for each pointing period, builds two correction matrices using  $\psi_1$  and  $\psi_2$  as provided by the AHF in the Observation section:

$$R_{psi1}^T = \begin{bmatrix} \cos \psi_1 & -\sin \psi_1 & 0 \\ \sin \psi_1 & \cos \psi_1 & 0 \\ 0 & 0 & 1 \end{bmatrix}$$

$$R_{psi2}^T = \begin{bmatrix} \cos \psi_2 & 0 & \sin \psi_2 \\ 0 & 1 & 0 \\ -\sin \psi_2 & 0 & \cos \psi_2 \end{bmatrix}$$

From these matrices the correction matrix is build:

$$R = R_{psi1}^T R_{psi2}^T R_{psi2} R_{psi1}$$

Each quaternion of the AHF is finally corrected using  $R$ .

### Stellar Aberration

The corrected quaternions are interpolated using Spherical Linear Interpolation algorithm and transformed in cartesian vector, which we call  $DPT$ . For each sample the stellar aberration correction is applied:

$$DPT = DPT - \frac{v_{sat}}{c}$$

where  $v_{sat}$  is the satellite velocity and  $c$  is the speed of light. After this operation the vector is normalized.

Finally the cartesian vector is converted in Ecliptic Coordinates, the detector pointing.

### Beam Rotation

The rotation of the beam with respect the north direction is the  $\psi$  angle and is computed rotating the corrected quaternions  $Q$  using:

$$R = R_\theta R_\phi Qax2det$$

The resulting rotation matrix represents the rotation of the beam, the  $\psi$  angle is then:

$$\psi = -\arctan(R[0][1], R[0][0])$$

# Map-making LFI

---

## Map-making

EK: This section is supposed to be a practical manual to the data products the way in which we create the maps. This section should thus include:

Description of the map products:

- what data range does each map cover
- what combination of radiometers
- baseline length
- flags applied
- mask applied
- radiometer weights used
- resolution
- exact recipe for construction of the noise prior
- handling of bad pixels
- how are uncovered pixels marked
- relation to toi and pointing objects
- auxiliary data: white noise covariance

Basically, necessary information for someone to reconstruct the maps from the same inputs

Many of the information listed above can be filled only after we know exactly which data products are released and in which file format.

Insert a table of maps delivered: -file name -radiometers included -PID/OD range -resolution -polarization included or not -sky coverage -baseline length

Explain the format of the files, what is in what column, in what units.

Information common for all maps: LFI maps were constructed with the Madam map-making code (version 3.7.4). Maps are in Healpix format, in nested pixeling scheme. Each of the LFI maps has three columns, which represent the three Stokes parameters I,Q,U. The maps are in K\_cmb units and galactic coordinate system.

Maps are constructed in galactic coordinates, i.e. we rotate the detector pointings from ecliptic to galactic coordinate system before running the map-making pipeline. The conversion from ecliptic to galactic coordinate system is described by rotation matrix

```
( -0.054882486,  0.494116468, -0.867661702,
  -0.993821033, -0.110993846, -0.000346354,
  -0.096476249,  0.86228144,   0.497154957 )
```

Insert a table of horn weights.

Noise prior is constructed based on a four-parameter noise model (sigma, knee frequency, slope, and minimum frequency).. List the noise parameters here or refer elsewhere.

Handling of bad pixels: To solve the three Stokes maps I,Q,U in a given pixel, we need sufficient coverage in the psi angle, which defines the direction of polarization sensitivity of a sample. In general, two horns, each having two radiometers with orthogonal polarization angles provide sufficient sensitivity. As the criterion for sufficient sensitivity we have used the rcond (reverse conditioning number) value of the 3x3 pixel matrix. Pixels with rcond below 0.01, or with no detections at all, were rejected from the maps. Rejected pixels are marked by the special

---

value Healpix\_undef=-1.6375e30,

## Low resolution maps and Noise Covariance Matrices

### Overview

Low resolution ( $l \leq 32$ ) maps are needed in the analysis of the largest scales. Number of different schemes to obtain the low resolution maps are discussed in \cite{keskitalo2009}. Each of the methods have their pros and cons. We chose to downgrade the maps using the inverse noise weighting. For our purposes the inverse noise weighted maps gives us more accurate signal at the cost of higher noise, when compared to maps directly produced at the target resolution, whereas naïve averaging of the pixels in the high resolution maps lead to higher noise, but less altered signal. Later the temperature component was smoothed to alleviate aliasing due to high frequency power in the maps.

We need not only low resolution maps, but also corresponding noise covariance matrices describing the residual noise present in the low resolution to fully exploit the information contained in the largest scales. The statistical description of the residuals is given in the form of a pixel-to-pixel noise covariance matrix (NCVM), as described in \cite{keskitalo2009}. We calculated the NCVMs using a NCVM module integrated into the Madam map-maker. Therefore the code interface and the inputs are essentially the same as in the standard map-making runs. However some approximations had to be made to the map-making procedure used for the high resolution flight maps:

- The full statistical noise description can only be utilized at low resolution, i.e. at large angular scales, due to resource limitations. Therefore we first calculated the NCVMs at resolution  $N_{\mathrm{side}} = 32$ , and subsequently downgraded the results to resolution  $N_{\mathrm{side}} = 16$  of the final products.

-

### Low Resolution Maps

#### Inputs

We took the high resolution maps described in LFI-Map-making and the corresponding  $3 \times 3$  matrices as an input for this analysis step.

#### Production

The high resolution maps were downgraded to  $N_{\mathrm{side}} = 16$  using inverse noise weights (given by the  $3 \times 3$  matrices), and subsequently the temperature part was smoothed with a symmetric Gaussian beam with  $\mathrm{FWHM} = 440 \mathrm{arcmin}$ .

### Noise Covariance Matrices

#### Inputs

The noise model was given in the form of the three noise parameters: white noise level  $\sigma$ , slope, and knee frequency  $f_{\mathrm{knee}}$ . We actually used three sets of noise parameters one for the entire mission (nominal mission), and one per each sky survey (SS1 and SS2).

We used the same pointing as in the noise Monte Carlo simulations. See the description in Noise Monte Carlo simulations.

We used the gap files produced during the making of the flight maps to leave out samples that were flagged bad for various reasons.

## Production

The output of the NCVM module of Madam map-maker are inverse NCVMs. Since the inverse matrices are additive, we divided the computations into a number of small chunks to save computational resources. Therefore we firstly calculated one inverse NCVM per radiometer per survey at resolution  $N_{\mathrm{side}}=32$ , and secondly combined the individual inverse matrices to form the actual inverse matrices. The map-making parameters were almost identical to the standard map-making runs. The differing parameter values are listed below:

- Baseline lengths were 0.25 s/ 8 samples, 0.50 s/ 24 samples, and 0.50 s/39 samples for 30 GHz, 44 GHz, and 70GHz, respectively.

- The calculations were performed at resolution  $N_{\mathrm{side}} = 32$ .
- No destriping mask was applied.
- The horns were weighted optimally.

To get the noise covariance from its inverse, the matrices are inverted using the eigen decomposition of a matrix. The monopole of the temperature map cannot be resolved by the map-maker, and thus the matrix becomes singular. The ill-determined mode is left out of the analysis.

Having calculated the eigen decomposition in the previous step, we can apply the same linear operators to modify the eigenvectors as was applied to the high resolution maps while downgrading them. The eigenvectors are downgraded to  $N_{\mathrm{side}} = 16$  using inverse noise weights, and subsequently the temperature part is smoothed with a symmetric Gaussian beam with  $\mathrm{FWHM} = 440 \mathrm{arcmin}$ .

The final matrices are then recomposed from the original eigenvalues and modified eigenvectors.

The low resolution noise covariance matrices

- are in C binary format files.
- are organized in block form,

```

$$
\left( \begin{matrix}
II & IQ & IU \\
QI & QQ & QU \\
UI & UQ & UU
\end{matrix} \right) .
$$

```

- are in HEALPix nested pixelisation scheme. Resolution is  $N_{\mathrm{side}} = 16$ , and thus there are  $N_{\mathrm{pix}} = 3072$  pixels.
- are in Galactic coordinates.
- have units  $\mathrm{K}_{\mathrm{CMB}}$ .
- uncovered pixels are marked with
- T-only?
- number of files

## Half-ring jackknife Noise Maps

### Overview

In order to estimate the noise directly at the map level and in the angular power spectra, we divided the time-ordered data into two halves and produced half-ring jackknife maps as described in Planck First Results: II. The Low Frequency Instrument performance and data processing.

Briefly: Instead of using the full time ordered data as described above, we produced two sets of maps using either only the first half of each pointing period (map named  $\mathbf{j}_1$  below) or only the second half of each pointing period (map named  $\mathbf{j}_2$ ). At each pixel  $p$ , these half-ring jackknife maps  $\mathbf{j}_1$  and  $\mathbf{j}_2$  contain the same sky signal, since they result from the same scanning pattern on the sky. However, because of instrumental noise, the maps  $\mathbf{j}_1$  and  $\mathbf{j}_2$  are not identical.

We estimated the noise level in each map  $\mathbf{m}$  made using the full(ring) data, by constructing a half-ring difference map

$$\mathbf{n}_m(p) = [\mathbf{j}_1(p) - \mathbf{j}_2(p)] / \sqrt{\mathbf{w}_{\text{hit}}(p)},$$

with weights

$$\mathbf{w}_{\text{hit}}(p) = \sqrt{\mathbf{hit}_{\text{full}}(p) \left[ \frac{1}{\mathbf{hit}_1(p)} + \frac{1}{\mathbf{hit}_2(p)} \right]},$$

Here  $\mathbf{hit}_{\text{full}}(p) = \mathbf{hit}_1(p) + \mathbf{hit}_2(p)$  is the hit count at pixel  $p$  in the full map  $\mathbf{m}$ , while  $\mathbf{hit}_1$  and  $\mathbf{hit}_2$  are the hit counts of  $\mathbf{j}_1$  and  $\mathbf{j}_2$ , respectively. The weight factor  $\mathbf{w}_{\text{hit}}(p)$  is equal to 2 only in those pixels where  $\mathbf{hit}_1(p) = \mathbf{hit}_2(p)$ . In a typical pixel,  $\mathbf{hit}_1(p)$  will differ slightly from  $\mathbf{hit}_2(p)$  and hence the weight factor is  $\mathbf{w}_{\text{hit}}(p) > 2$ .

The half-ring difference maps  $\mathbf{n}_m$  are the most direct measure of the noise in the actual maps. The other noise estimates (NCVM and noise Monte Carlo) rely on specific modelling of the noise and this modelling can be validated by comparing to the half-ring difference maps. However, the half-ring difference maps can only capture the noise that varies faster than half of the duration of the pointing period, i.e., the noise whose frequency is  $\gtrsim 2/20 \text{ min} = 1.7 \text{ mHz}$ .

We calculated the noise maps  $\mathbf{n}_m$ , from half-ring jackknife maps for temperature (I) and polarization (Q and U) and as a first quality check of the maps (and as one of the tests of the whole data processing pipeline up to the maps) tested both numerically and visually that these noise maps divided pixel-by-pixel by square root of the white noise covariance maps were approximately Gaussian with variance near to unity. Temperature noise maps for the nominal survey and for the first and second sky surveys are shown in the next subsection. Further we calculated from the noise maps the temperature and polarization (E and B mode) auto-correlation and cross-correlation noise angular power spectra by anafast and compared to these the results from the white noise covariance matrices and from the noise Monte Carlo simulations. A similar comparison was made between downgraded half-ring noise maps, downgraded noise Monte Carlo maps and the low resolution noise covariance maps. Detailed results are presented in the Systematic Effects paper.

## Examples of Half-ring Difference Maps and Noise Angular Power Spectra

### Hit Count Weighted Half-ring Difference Maps

Here we show some hitcount weighted half-ring difference maps, i.e., noise maps for temperature. The columns are for different LFI frequencies: 30, 44, and 70 GHz. The rows are the nominal survey (a bit more than 1 year of observations), survey 1 (the first sky survey, approx first half a year of observations) and survey 2 (the second sky survey, approx the second half a year of observations). Some features are visible in particular in the galactic plane. These are due to "gradient leakage". (In regions where the gradient in the sky signal is very large even a tiny difference in the pointing of the first and second half of each pointing period causes the signal to "leak" to the half-ring difference map. In practice this is not a problem for noise estimation, since these regions - the galaxy, orion, crab nebula, etc - will be masked in the cosmology analysis.

**Half-ring difference maps** calculated at the native nsidc 1024 resolution. Columns: frequency (30, 44, 70 GHz), rows: sky survey (nominal, survey\_1, survey\_2).

Half-ring difference maps (the same as above, but) **smoothed** with 60 arcmin fwhm Gaussian. Columns: frequency (30, 44, 70 GHz), rows: sky survey (nominal, survey\_1, survey\_2).

### Hit Count Weighted Half-ring Difference Maps Normalized by sqrt of white noise variance at each pixel

Now we show the same as above, but divided by the square root of the estimate of white noise variance in each pixel. These normalized noise maps should be approximately Gaussian with a unit variance (at the native resolution), apart from some stripes that are due to correlated (non-Gaussian) 1/f noise. The large-scale 1/f noise is more apparent in the smoothed version of the figure that follows after the native resolution version.

**Normalized Half-ring difference maps** calculated at the native nsidc 1024 resolution. Columns: frequency (30, 44, 70 GHz), rows: sky survey (nominal, survey\_1, survey\_2).

Normalized Half-ring difference maps (the same as above, but) **smoothed** with 60 arcmin fwhm Gaussian. Columns: frequency (30, 44, 70 GHz), rows: sky survey (nominal, survey\_1, survey\_2).

### Noise Angular Power Spectra from Half-ring Difference Maps

The noise angular power spectra calculated by anafast from half-ring difference temperature maps and normalized by the sky coverage to estimate the noise level if there was a full sky coverage in order to make a comparison of different surveys easier. Columns: frequency (30, 44, 70 GHz). Colors: black = nominal, red = survey\_1, blue = survey\_2.

## Noise Monte Carlo Simulation

### Overview

Calculating and handling full pixel-to-pixel noise covariance matrices for Planck maps is feasible only at low resolution. To support the analysis of high-resolution maps, a Monte Carlo set of noise maps were produced. These maps were produced from noise timelines using the same map-making procedure as for the flight data. In the noise Monte Carlo it was possible to follow exactly the map-making procedure used for the flight maps, whereas for the calculation of noise covariance matrices some approximations had to be made. Such noise Monte Carlos were produced at two levels of the analysis: 1) LFI Monte Carlo (MC) as part of the LFI data processing, and 2) Full Focal Plane (FFP) Monte Carlo as part of the joint HFI/LFI data processing. This page describes the LFI noise MC. For the FFP MC, see HL-sims.

## Inputs

The noise MC uses a three-parameter (white noise level ( $\sigma$ ), slope, and knee frequency ( $f_{\text{knee}}$ )) noise model, where the noise consists of white noise and correlated ( $1/f$ ) noise and the latter has a power spectrum

$$P(f) = \frac{2\sigma^2}{f_{\text{knee}}} \left( \frac{f}{f_{\text{knee}}} \right)^{\text{slope}}.$$

Here  $f_{\text{sample}}$  is the sampling frequency of the instrument. The noise parameters were determined separately for each radiometer as described in TOI-Noise LFI, assuming they stayed constant over the mission.

The detector pointing was reconstructed from satellite pointing, focal-plane geometry, pointing correction (tilt angle), and sample timing, using Level-S simulation software. The same pointing solution (two focal planes) was used as for the LFI flight maps. Due to numerical accuracy, the detector pointing in the noise MC was not exactly the same as for the flight maps, but some data samples (of the order of one in a thousand) whose pointing was near the pixel boundary ended up assigned to the neighboring pixel. During the map-making from the flight data, a gap file was produced to represent the samples that were omitted from map-making due to various flags. This gap file was used in the noise MC instead of the full set of flags. The flight map-making used a destriping mask to exclude regions of strong signal gradients from contributing to the noise baseline solution. These same destriping masks (one for each frequency channel) were used for the noise MC.

## Production

The noise was generated internally in the Madam map-making code using a Stochastic Differential Equation (SDE) method, to avoid time-consuming writing and reading noise timelines to/from disk. Noise for each pointing period was generated separately, using a double-precision random number seed constructed from the realization number, radiometer number, and the pointing period number; to allow regeneration of the same noise realization when needed. White noise and  $1/f$  noise were generated separately.

The same map-making code (Madam) with the same parameter settings was used for the noise MC as for the flight maps. In addition to the destriped maps from the full noise (output maps), also binned maps from just the white noise (binned white noise maps) were produced; they represent the white noise part of the output maps. The difference between these two maps represent the residual correlated noise in the output map. The maps were made at Healpix resolution  $N_{\text{side}} = 1024$ . For low-resolution analysis, these maps were downgraded (and the temperature part was smoothed) to  $N_{\text{side}} = 32$  and  $N_{\text{side}} = 16$ .

When the noise MC for the first Planck data release was performed, calibrated data for five sky surveys were available. In addition to frequency maps for the nominal survey and the full survey (all five sky surveys), single-survey and 70 GHz horn-pair maps were produced in the noise MC, resulting in 27 different cases of LFI maps, a subset of the map cases produced from the flight data. For each case 102--1026 realizations were produced.

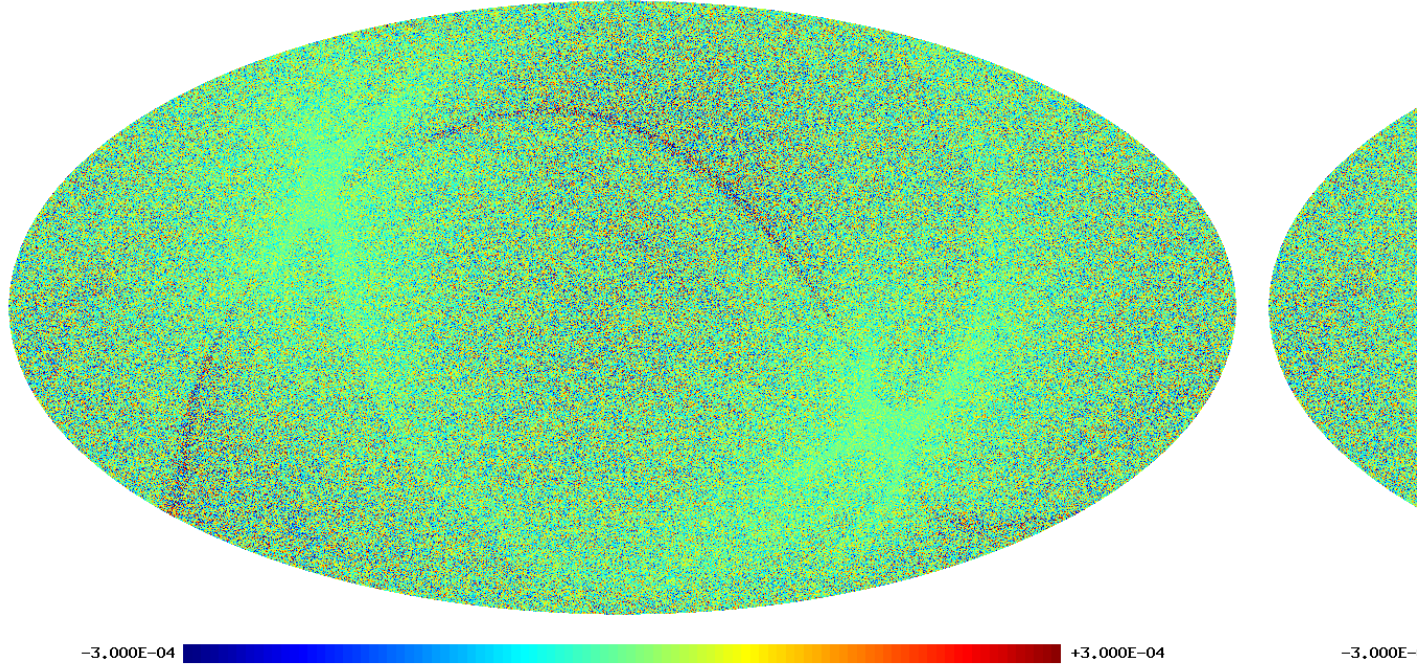
## Usage

These noise Monte Carlo maps were used for a number of things in LFI data analysis. They were compared to the low-resolution noise covariance matrices, generated for the same noise model to see the impact of the approximations in the noise covariance matrix calculation. They were compared to the half-ring noise maps to see how well the noise model matches the noise in the flight maps (noting, however, that the half-ring noise maps misrepresent the lowest noise frequencies in the flight maps, and contain some effects from the sky signal). They were also used in power spectrum estimation and non-Gaussianity estimation.



## Examples

As an example, we show below images of the first realization of the 70 GHz frequency map noise for the nominal survey. The images are in order: destriped full noise, binned white noise, residual correlated noise. Note that it is difficult to see any difference between the first two images, since the residual correlated noise is more than an order of magnitude below the white noise level. The units are CMB K.



The following two images show the statistics of the angular power spectra of 101 realizations of the 70 GHz frequency map noise for the nominal survey. The thick black line shows the median  $\ell$ , and the green line the mean  $\ell$ . Thin black lines show the minimum, 16% quantile, 84% quantile, and the maximum  $\ell$ . The red line is the 102nd realization. The first plot is for the full noise in the output map, the second plot is for the residual correlated noise.

# LFI-Validation

---

## Overview

Data validation is a step of paramount importance in the complex process of data analysis and the extraction of the final scientific goals of an experiment. The LFI approach to data validation is based upon null-tests approach and here we present the rationale behind envisaged/performed null-tests and the actual results for the present data release. Also we will provide results of the same kind of tests performed on previous release to show the overall improvements in the data quality.

## Null-tests approach

In general null-tests are performed in order to highlight possible issues in the data related to instrumental systematic effect not properly accounted for within the processing pipeline and related to known events of the operational conditions (e.g. switch-over of the sorption coolers) or to intrinsic instrument properties coupled with sky signal like stray-light contamination.

Such null-tests are expected to be performed considering data on different time scales ranging from 1-minute to one year of observations, at different unit level (radiometer, horn, horn-pair, within frequency and cross-frequency both in total intensity and, when applicable, to polarisation).

This is quite demanding in terms of all possible combinations. In addition some tools are already available and can be properly used for this kind of analysis. However it may be possible that on some specific time-scale, detailed tools have to be developed in order to produce the desired null-test results. In this respect the actual half-ring jack-knives are suitable to track any effects on pointing period times scales. On time-scales between half-ring and survey there are lot of possibilities. It has to be verified if the actual code producing half-ring jack-knives (madam) can handle data producing jack-knives of larger (e.g. 1 hour) times scales.

It is fundamental that such test have to be performed on DPC data product with clear and identified properties (e.g. single \$R\$, \$DV/V\$ single fit, etc.) in order to avoid any possible mis-understanding due to usage of non homogeneous data sets.

Many of the null-tests proposed are done at map level with sometime compression of their statistical information into an angular power spectrum. However together with full-sky maps it is interesting to have a closer look on some specific sources. It would be important to compare fluxes from both polarized and un-polarized point sources with different radiometers in order to assess possible calibration mis-match and/or polarization leakage issues. Such comparison will also possibly indicate problems related to channel central frequencies. The proposed set of sources would be: M42, Tau A, Cas A and Cyg A. However other H<sub>II</sub> regions like Perseus are valuable. One can compare directly their fluxes from different sky surveys and/or the flux of the difference map and how this is consistent with instrumental noise.

Which kind of effect is probed with a null-test on a specific time scale? Here it is a simple list. At survey time scale it is possible to underlying any side-lobes effects, while on time scales of full-mission, it is possible to have an indication of calibration problems when observing the sky with the same S/C orientation. Differences at this time scale between horns at the same frequency may also reveal central frequency and beam issues.

---

## Total Intensity Null Tests

In order to highlight different issues, several time scales and data combinations are considered. The following table is a sort of null-test matrix to be filled with test results. It should be important to try to set a sort of pass/fail criteria for each of the tests and to be prepared to detailed actions in order to avoid and correct any failure of the tests. To assess the results an idea could be to proceed as in the nominal pipeline i.e. to compare the angular power spectra of null test maps with a fiducial angular power spectrum of a white noise map. This could be made automatic and, in case the test does not pass then a more thorough investigation could be performed. This will provide an overall indication of the residuals. However structures in the residual are important as well as the overall average level and visual inspection of the data is therefore fundamental.

Concerning null-tests on various time scales a comment is in order. At large time scales (i.e. of the order of a survey or more) it is clear that the basic data set will be made of the single survey maps at radiometer/horn/frequency level that will be properly combined to obtain the null-test under consideration. For example at 6 months time scale we will analysis maps of the difference between different surveys for the radiometer/horn/frequency under test. On the other hand at 12 months time scale we will combine surveys 1 and 2 together to be compared with the same combination for surveys 3 and 4. At full-mission time scale, the analysis it is not always possible e.g. at radiometer level we have only one full-mission data set. However it would be interesting to combine odd surveys together and compare them with even surveys again combined together. On shorter time scales (i.e. less than a survey) the data products to be considered are different and will be the output of the jack-knives code when different time scales are considered: the usual half-ring JK on pointing period time scale and the new, if possible, jack-knives on 1 minute time scale. Therefore null-tests will use both surveys/full-mission maps as well as tailored jack-knives maps.

The following table reports our total intensity null-tests matrix with a  $\checkmark$  where tests are possible.

Data Set	1minute	1 hour	Survey	Full Mission
Radiometer (M/S)	$\checkmark$	$\checkmark$	$\checkmark$	$\checkmark$
Horn (M+S)	$\checkmark$	$\checkmark$	$\checkmark$	$\checkmark$
Horn Pair <sup>1</sup>			$\checkmark$	$\checkmark$
Frequency	$\checkmark$	$\checkmark$	$\checkmark$	$\checkmark$
Cross-Frequency			$\checkmark$	$\checkmark$

<sup>1</sup> this is  $(M+S)/2$  and differences are between couple of horns (e.g.  $(28M+28S)/2 - (27M+27S)/2$ )

## Polarisation Null Tests

The same arguments applies also for polarization analysis with only some differences regarding the possible combination producing polarized data. Radiometer will not be available, instead of sum between M and S radiometer we will consider their difference.

Data Set	1minute	1 hour	Survey	Full Mission
Horn (M-S)	\$\checkmark\$	\$\checkmark\$	\$\checkmark\$	\$\checkmark\$
Horn Pair <sup>1</sup>			\$\checkmark\$	\$\checkmark\$
Frequency	\$\checkmark\$	\$\checkmark\$	\$\checkmark\$	\$\checkmark\$
Cross-Frequency			\$\checkmark\$	\$\checkmark\$

<sup>1</sup> this is difference between couple of horns (e.g. (28M-28S)/2- (27M-27S)/2)

## Practical Considerations

For practical purposed and visual inspection of the null-tests results it would be useful to produce results smoothed at  $3^\circ$  (and at  $10^\circ$  for highlight larger angular scales) for all the total intensity maps. For polarization, as we already did several times when comparing to WMAP data, a downgrade of the product at  $N_{\rm side}=128$  would be useful to highlight large scale residuals. These considerations are free to evolve according to our needs.

Due to large possibilities and number of data sets to be considered, it would be desirable to have sort of automatic tools that ingest two, or more, inputs maps and produce difference map(s) and corresponding angular power spectrum(spectra). This has been implemented using Python language and interacting directly with FITS files of a specific data release. The code is parallel and can run both at NERSC and at DPC producing consistent results. In addition for each null-tests performed a JSON DB file is produced in which main test informations are stored together with interesting computed quantities like mean, standard deviation of the residual maps. Beside JSON files also GIF images of the null-test are produced. Such JSON and GIF files are used to create (both with Python again and with Scheme) a report in form of an HTML page from the LFI Wiki.

Together with images, power spectra of the residual are also produced and compared with the expected level of white noise derived from the half-ring jack-knives. With these quantities are combined to produce a sort of  $\chi^2$ . This gives an indication of the deviation of the residuals with respect to the white noise level. Of course underlying signal does not posses a Gaussian statistic and therefore with non-Gaussian data, the  $\chi^2$  tests is less meaningful. However this gives a hint on the presence of residuals which in some cases are indeed expected: in fact making difference between odd and even survey at horn and frequency level, is a way to show the signature of the external stray-light which, although properly accounted for during the calibration procedure, has not been removed from the data.

## Data Release Results

# HL

---

HFI/LFI common processing uses as basic input the maps at the 9 frequencies covered by the two instruments.

The goal is to obtain various catalogues, identify the different astrophysical components whose superposition leads to the observed sky, and provides a statistical characterisation of the CMB, in particular through a likelihood code (of a particular theoretical  $C(l)$  given Planck data).

## Catalogues

Are described here

## Component maps

Are described here

## Power spectra and likelihood code

Are described here

## Simulations

Are described here

## Scientific analysis products

Are described here

---

# Catalogues

## Planck Catalogue of Compact Sources

The PCCS source list in each frequency is structured as a FITS binary table having one row for each detected source.

The FITS primary header will have the following structure:

### FITS primary header

FITS Keyword	Data Type	Units	Description
INSTRUME	String		LFI or HFI
VERSION	String		Version of PCCS
DATE	String		Date file created:yyyy-mm-dd
ORIGIN	String		Name of organization responsible for the data (LFI-DPC – HFI-DPC)
TELESCOP	String		PLANCK
CREATOR	String		Pipeline Version
DATE-OBS	String	days	Start-up time of the survey: yyyy-mm-dd
DATE-END	String	days	Ending time of the survey: yyyy-mm-dd

The Fits extension is composed by several columns described below:

### FITS header

Column Name	Data Type	Units	Description
<b>Identification</b>			
NAME	String		Source name – see Note 1
<b>Source Position</b>			
GLON	Real*8	degrees	Galactic longitude based on extraction algorithm
GLAT	Real*8	degrees	Galactic latitude based on extraction algorithm
RA	Real*8	degrees	Right ascension (J2000) transformed from (GLON,GLAT)
DEC	Real*8	degrees	Declination (J2000) transformed from (GLON,GLAT)
<b>Photometry</b>			
DETFLUX	Real*4	mJy	Flux density of source as determined by detection method
DETFLUX_ERR	Real*4	mJy	Uncertainty (1 sigma) in derived flux density from detection method
APERFLUX	Real*4	mJy	Flux density of source as determined from the aperture photometry
APERFLUX_ERR	Real*4	mJy	Uncertainty (1 sigma) in derived flux density from the aperture photometry
PSFFLUX	Real*4	mJy	Flux density of source as determined from PSF fitting
PSFFLUX_ERR	Real*4	mJy	Uncertainty (1 sigma) in derived flux density from PSF fitting
GAUFLUX	Real*4	mJy	Flux density of source as determined from 2-D Gaussian fitting
GAUFLUX_ERR	Real*4	mJy	Uncertainty (1 sigma) in derived flux density from 2-D Gaussian fitting
GAU_SEMI1	Real*4	arcmin	Gaussian fit along axis 1
GAU_SEMI1_ERR	Real*4	arcmin	Uncertainty (1 sigma) in derived Gaussian fit along axis 1

GAU_SEMI2	Real*4	arcmin	Gaussian fit along axis 2
GAU_SEMI2_ERR	Real*4	arcmin	Uncertainty (1 sigma) in derived Gaussian fit along axis 2
GAU_THETA	Real*4	deg	Gaussian fit orientation angle counting anti-clockwise from the x -axis
GAU_THETA_ERR	Real*4	deg	Uncertainty (1 sigma) in derived gaussian fit orientation angle
GAU_FWHM_EFF	Real*4	arcmin	Gaussian fit effective FWHM
<b>Flags and validation</b>			
EXTENDED	Integer*2		Flag indicated that source is extended
CIRRUS_N	Integer*4		Number of sources detected at 857 GHz within HFI TBC degrees
EXT_VAL	Integer*2		Flag indicated external validation - see Note 2
ERCSC	String		Name of the ERCSC counterpart if any
<b>ONLY 857 GHz Catalogue</b>			
APERFLUX_217	Real*4	mJy	Source flux density at 217 GHz (best estimation) of the object detected at 857
APERFLUX_ERR_217	Real*4	mJy	Uncertainty in source flux density
APERFLUX_353	Real*4	mJy	Source flux density at 353 GHz (best estimation) of the object detected at 857
APERFLUX_ERR_353	Real*4	mJy	Uncertainty in source flux density
APERFLUX_545	Real*4	mJy	Source flux density at 545 GHz (best estimation) of the object detected at 857
APERFLUX_ERR_545	Real*4	mJy	Uncertainty in source flux density

**Note 1.-** Source name designations consist of a prefix and a positional qualifier, the latter is in Galactic coordinates and specified as "Glll.ll±bb.bb" where the (l,b) values are truncated. The prefix used in the single band portion of the PCCS is PLCKddd PCCS catalogue at ddd GHz.

For example, a source detected at (l,b) = (120.237, 4.231) in the 545 GHz Planck map would be labelled PLCK545 G120.23±04.23.

**Note 2.-** The EXTENDED flag has the value of 0 if the source is compact and the value of 1 is it extended. The source size is determined by the geometric mean of the Gaussian fit FWHMs, with the criteria for extension being  $\sqrt{\text{GAU\_FWHMMAJ} * \text{GAU\_FWHMIN}} > 1.5$  times the beam FWHM.

**Note 3.-** The EXT\_VAL flag has the value of 0, 1, or 2, based on the following conditions:

- 2 – The source has a clear counterpart in one of the catalogues considered as ancillary data.
- 1 – The source has NOT a clear counterpart in one of the catalogues considered as ancillary data but it has been detected by the internal multi-frequency method.
- 0 – The source has NOT a clear counterpart in one of the catalogues considered as ancillary data and it has NOT been detected by the internal multi-frequency method.

# HLcomp

---

## CMB Cleaning

## C2

---

The main product to express cosmological constraints posed by Planck data is a Likelihood code. One of its by-product is the derived Maximum-likelihood CMB spectrum.

**NB: This is very much a scientific product, whose development status will be described in a dedicated talk at the review.**

## Principles used to build the Planck Likelihood

We have used an hybrid approach for the likelihood which is:

- Pixel-based at low-ell
- based on fine-grained pseudo-CL at high-ell. I.e. it uses all independent groupings of detectors at 100, 143 and 217GHz.

This allows easy “Planck-Ext” (stitching of high(er)-ell likelihoods, in particular ACT & SPT).

The Planck code, CLIK, provides a unique interface (and it allows internally to keep cross-checking with various approaches), at V4.1 now (V1 was mid-2011).

We derived from CLIK our “best” CTT, together with a basic (diagonal) error estimate, which will allow making plots & quick model checks, comparison with various sources of uncertainties comparison with the CTT derived from the CMB map(s) issued from Component Separation activities...

## CLIK - The Planck **C(I) LIK**elihood code

*This section is a copy/extract of the private wiki pages of the collaboration, from which the updates will be made for major Exp.Sup. releases*

*[-Last modified 2012-10-10 -]*

`clik` is a package with both a code and data files to distribute the current planck likelihood. It is available from ESA through the [PLA <sup>[1]</sup>] under *operational files*, then clicking the *supplementary data* icon on the toolbar

---

## Overview

Here follows a description of the last release of `clik`

### !! Version 4.0

Main improvements for this release are the addition of

- CAMspec\_v5.2dust hi-ell likelihood,
- plik\_dx9\_v2 hi-ell likelihood and
- an early october version of the actspt likelihood.

Partial compatibility between those likelihood has been implemented : all three share the same cib modeling and either CAMspec or plik can be this way used with actspt. CAMspec further use the same sz and szXcib modeling. plik neglect the sz and szXcib foregrounds for now (as they approximatively cancel in planck range of ells).

---



No update has been made on the low-ell likelihood. To recover the files (still compatible with the last version of the code) one has to retrieve klik v3.5 and use the file contained therein.

**Beware that the previous CAMspec files will not work with the current release.**

## Code

klik code is at version *4.0b2*

Known issues

- none for now.

Changes:

- from 3.5

```
** inclusion of actspt
** removal of dependency on gel
** removal/cleanup of lot's of legacy code
** better discovery of the hdf5 version (in particular version 1.8.X compiled in pure 1.6.X compatibility mode)
** better detection of some weird python install
** plik likelihood code has been improved and is now 20times faster
** correction for the C++ boilerplate
** correction of the klik_config scripts with the addition of laking libs
```

## Data

- hi-ell

```
** plik_dx9_v2.klik
** CAMspec_5.2dust.klik
```

- hi-ell non planck

```
** actspt_2012_10_08.klik
```

Changes:

- CAMspec has changed a lot and now include beam parameters
- actspt is new
- new easily modifiable foreground modeling module for plik.

### An important note for actspt

As for the low-ell likelihood, actspt code relies on data being installed in a specific place. The file is usable as is, but will dump some data in /tmp at each initialization. If this is not a desirable behaviour, data can be dumped once and for all by following the procedure described here.

## Exemple of output

We'll give here an actual exemple of use and result of an exploration

Also Link to where we shall make available all the explorations of the (model/data) combinations we shall release in the scientific product section

## Current Best-fit CMB spectrum

This is still evolving

## References

[1] [http://www.sciops.esa.int/index.php?project=planck&page=Planck\\_Legacy\\_Archive](http://www.sciops.esa.int/index.php?project=planck&page=Planck_Legacy_Archive)

# HL-sims

---

The `PSM` or "*Planck Sky Model*" is an updated version (using knowledge derived from Planck observations) of the software tool described in Ref to the PSM paper of 2012. This can take in actual band-passes (in a RIMO) and create sky maps and catalogues at the specified frequencies. It can be supplemented by ad-hoc simulation software for particular (theoretical) CMB maps

The Level S (`LS` in short) is a generic simulation tool common to HFI and LFI. One version was described in ref to the old LS paper. It can take in input the output of the PSM, a pointing and beam description in order to generate the infalling power on detectors as a function of time. It can additionally create some noise realisation as a very simplified version of the actual instruments. Alternatively, the output can be used as input to a detailed simulation of the instrumental behaviour.

The `PSM` together with the `LS` therefore provide two basic bricks of a more extensive instrument specific simulation environment. For HFI, see HFI-Validation#sims.

Joint simulations provides an environment for checking algorithms in a realistic context. The latest series is the "FFP6", which provides a Full Focal Plane simulation of the DPC maps in the 2013 data release. They were initially provided (partially) "blind", ie without knowledge of the actual sky components used, but with an exact description of the Bandpasses, beams, and calibration.

## CMB maps simulations

The basic maps are simple Gaussian realisation determined by their power spectrum generated by, eg., CAMB external Ref to CAMB site and papers Here.

Several non-Gaussian signatures can also be generated by dedicated software, like the lensing-induced deformations, a version of which is included in the standard `PSM` package. But other cases have been developped within Planck as part of its scientific preperation, in particular the  $f_{NL}$  and  $g_{NL}$  maps of Ref to Elzner and Wandelt paper and the string maps of ref to Ringeval and Bouchet paper }. Maybe also, the Bianchi model or other non sts=atistically anisotropic cases. For convenience, they are available through the PLA Link here to PLA once ESA has finsihed developing the interface.

## Planck Sky Model PSM

this is the abstract of the pre-launch PSM paper, arXiv:1207.3675

The Planck Sky Model (PSM) is a parametric model for the generation of all-sky, few arcminute resolution maps of sky emission at submillimetre to centimetre wavelengths, in both intensity and polarisation. Several options are implemented to model the cosmic microwave background, Galactic diffuse emission (synchrotron, free-free, thermal and spinning dust, CO lines), Galactic H-II regions, extragalactic radio sources, dusty galaxies, and thermal and kinetic Sunyaev-Zeldovich signals from clusters of galaxies. Each component is simulated by means of educated interpolations/extrapolations of data sets available at the time of the launch of the Planck mission, complemented by state-of-the-art models of the emission.

Distinctive features of the simulations are: spatially varying spectral properties of synchrotron and dust; different spectral parameters for each point source; modeling of the clustering properties of extragalactic sources and of the power spectrum of fluctuations in the cosmic infrared background.

The PSM enables the production of random realizations of the sky emission, constrained to match observational data within their uncertainties, and is implemented in a software package that is regularly updated with incoming information from observations. The model is expected to serve as a useful tool for optimizing planned microwave and sub-millimetre surveys and to test data processing and analysis pipelines. It is, in particular, used for the development and validation of data analysis pipelines within the Planck collaboration. A version of the software that can be used for simulating the observations for a variety of experiments is made available on a dedicated website.

## Level S LS

The LS software package simulates the incoming sky radiation on detectors as a function of time. ref to LS docs , paps

## FFP6 data set

The sixth round of simulations of the "Full Focal Plane" of Planck encompasses the basic characteristics of Planck (Temperature) maps in support of scientific analyses, from component separation and power spectrum estimation to measures of non-gaussianity. They are simplified/idealized in the sense that TOI processing is considered perfect. (For HFI for instance, there are no transfer function nor pointing error, no 4K nor glitch residuals, no noise correlation, etc). But the actual pointing, spectral bandpasses, beams, noise determinations were used.

The basis sky maps are available here - link to PLA, including for convenience the individual components (which were initially hidden to the Planck collaboration, but for the generators :-)).

# Science

---

In addition to formal deliverables, The Planck scientific collaboration will make available useful additional information. In particular, some scientific publications will obtain informations best given in numerical form, and this section will cover all those, i.e. provide an overview of the product, a reference to the publication for in-depth description, and links to the numerical information in the PLA.

**NB: The following content is only indicative (20/10/2012), and will evolve according to what the Planck Science Team deems fit to publication at the time when the supplement will be frozen for the 2013 data release.**

## Cosmological parameters

While papers concerned with parameters will describe the salient results obtained by the collaboration, we plan to make available constraints posed by PLANCK on a rather large number of (model/data set) combinations.

In addition, here are specific parametrisation/models considered for the inflation paper:

1. Harrison-Zeldovich (HZ), HZ + free number of relativistic degrees of freedom, HZ + free Helium abundance
2.  $\Lambda$ CDM (LCDM)
3. LCDM + tensors (r)
4. LCDM + running, LCDM + running + r
5. LCDM by PCA on reionization, LCDM + r by PCA on reionization
6. LCDM + r + curvature
7. Inflaton potential reconstruction in the observable range (standard cosmological parameters plus inflationary potential parameters)
8. LCDM + super-imposed oscillations (currently LCDM model plus 3 parameters, others to be considered)
9. LCDM + r for generalized scalar field (without tensor-to-scalar consistency condition)
10. LCDM + isocurvature (including uncorrelated or anti-correlated mixture, broken law power spectrum).

## MCMC Chains for the Planck likelihood

In addition to the parameter constraints, we will probably (TBC) make available MCMC chains.

## PICO training sets

PICO interpolates the CMB powerspectrum as a function of cosmological parameters for very fast and very accurate parameter estimation. (See <http://arxiv.org/abs/astro-ph/0606709> and <http://arxiv.org/abs/0712.0194>)

Because PICO is trained using CAMB calls on the highest accuracy settings, PICO can in some cases be more accurate than CAMB on default accuracy.

PICO comes with easy interfaces into CAMB and CosmoMC

The latest PICO version will be available here as well as the PICO website <http://cosmos.astro.illinois.edu/pico/>.

Therefore delivery through PLA is TBC (but we shall at least refer to the specific version used)

---

## Science Maps

Here will be the specific product which are not obtained by the general component separation approach. These scientific products may be available only in some fraction of the sky and/or using dedicated ancillary data, etc.

# PSO processing

---

## Introduction

PSO processing during the mission was mostly related with mission planning and instrument health checks. The mission planning part consisted in the elaboration of the so called long term plan (LTP) and the pre-programmed pointing list (PPL). The PPL was required by MOC to prepare the lists of pointings that were uploaded to the satellite.

The health check consisted in the ingestion of

## Long term plan production

The long term plan was updated regularly and as the name indicates it covers long periods of time. In general it was updated to cover

## AHF ingestion

The AHF delivered by Flight Dynamics on a daily basis was ingested by the PSO. During the ingestion process, for each PID the planned pointing (PPL) was compared with the actual pointing and any discrepancies larger than a pre defined threshold where flagged and a warning issued. In general this resulted in a clarification request to MOC. Most pointing discrepancies where caused by thruster under or overperformance.

During the ingestion the duration of the PID was also compared against the planned duration as defined in the PPL and the start and end times where also checked. This allowed to the PSO to closely follow any deviation from the pointing law.

## Quality Reports ingestion

The data quality reports produced by both DPCs (Daily Quality Report and Weekly Health Report) where ingested daily by the PSO. The reports contained among other things estimates of the noise per pointing period, calibration constants per pointing period, representative temperatures for the subsystems of the two instruments and, in the case of the HFI, glitch rates. The purpose of these reports was three fold:

1. Evaluate status of the mission in terms of sky coverage using pointing information and noise provided in the DQR;
2. Evaluate the general health of the instrument;
3. Provide information that allowed the PSO in the declaration of a small gap

## SREM calibrated data analysis

SREM calibrated data is produced by Paul Buehler at the PSI in Zurich and delivered to the PSO on a daily basis. Once the data is delivered, plots showing the calibrated SREM data are then automatically generated. There was a delay of around 48 hours between the data acquisition and the delivery of the data files to the PSO. This prevented this data from being used to raise an alarm during periods of unusually large solar activity (although such warnings where not necessary as both instruments where never at risk of serious damage from space weather). This data was

---

however used to correlate with HFI glitches and temperature fluctuations in the 100mK stage.

---

# Planck Legacy Archive

---

---

## Planck Legacy Archive

---

### Introduction

The Planck Legacy Archive (PLA) contains all public products originating from the Planck mission. A graphical user interface accessible from this page allows to list, display, inspect, select, and download these products.

The first public product present in the Planck Legacy Archive was the Early-Release Compact Source Catalogue (ERCSC) released in January 2011.

As of January 2013, the PLA contains all temperature maps per Planck frequency, as well as ancillary maps like Survey maps, detector maps, etc. It also contains the first public version of the Planck Catalogue of Compact Sources and information about the spacecraft, instrument and survey history, notably through all the operational files and the Planck Operations State History (POSH).

### Purpose

The PLA will mainly serve the needs of professional astrophysicists wishing to carry out astronomical research, related to various astronomy fields as the Cosmic Microwave Background, extragalactic astronomy, Galactic interstellar medium, and Solar System studies, among others. In addition to these professional users, a number of others will be browsing the PLA, including members of the general public and members of the press. In both cases, they will be looking for general information on the Planck satellite and its scientific results, news about Planck, pictures and other public-relations material, among other things.

### Contents

The Planck Legacy Archive contains the following classes of products as of January 2013:

- frequency maps at all nine frequencies of Planck (in temperature only)
- sky component maps per frequency per component
- various ancillary maps like survey maps, detector maps, detector set maps, etc
- the first version of the Planck Legacy Catalogue of Compact Sources
- the Early-Release Compact Source Catalogue (since January 11th, 2011)
- operational files for the first six surveys (approximately first three years of Planck routine operations): pointing lists (programmed and achieved), orbit information, data-quality reports, instrument health reports, etc)
- the Planck Operational State History (POSH) - the "state vector" of the Planck mission
- documents associated to the above products

In addition to these public products, the same archive has an internal part (Planck Internal Archive or PIA) containing products restricted to the Planck collaboration.

---

## Software

The data browsing and retrieval from the PLA interface involves the following actions:

- there are several search panels or tabs (Maps, Catalogues, Time-Ordered Information, Documents...) which offer a set of filters to set the search criteria for the data queries
- after executing a query, a new result panel is automatically created with the result contents
- each result tab contains a list of the data which match the specified query. From this page several operations can be performed, depending on the type of data to be retrieved (e.g. display a set of sources, save result tables as XML or CSV, send them to another application, download the products, etc).

Some products require authentication (only those pertaining to the Planck Internal Archive, restricted to some people in the Planck Collaboration). The user must enter their username and password (Planck LDAP credentials) in the login window. If authorisation is granted, the status bar in the left bottom corner of the application window will be updated to the current user's ID and login time.

A general set of help pages is present on the Java interface. Please refer to these pages for further explanations on the software.

## Access

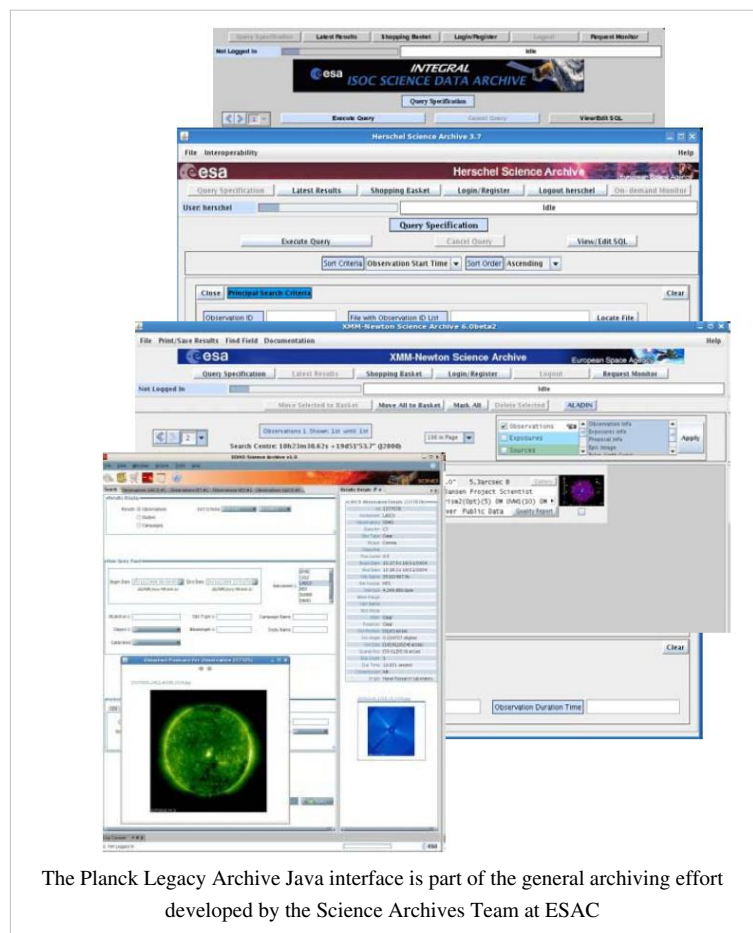
The PLA main page can be accessed here [1].

The Java interface can also be directly launched from here [2].

## Trouble shooting for the PLA Java client

To run the PLA your web browser must be Java compliant (Java version 1.5.x or higher is required for running the PLA), if not please install the latest Java following the instructions provided here [3].

In case of problem, and to make sure that you are using the latest version of our software, please clean your Java Web Start cache (see below) and run the application again. If the problem persists, please open a web browser (Internet Explorer, Mozilla Firefox, Safari, ...) and send us the output from this page [4] (which lists your configuration) along with the description of your problem. If the problem is related to data searching, it will be very helpful if you include the contents of your Log Console, which you'll find at the bottom of the ERCSC window, when you contact us (see Helpdesk section).



The Planck Legacy Archive Java interface is part of the general archiving effort developed by the Science Archives Team at ESA



How to clean your Java Web Start cache on Windows systems:

- Click on the "Start" icon in the lower left hand corner of your screen, followed by clicking on the "Run" menu choice.
- In the run box, type "javaws -viewer" (w/o the quotes) and hit "Enter".
- Select all the entries and then click on the "Remove Selected Applications/Items/Entries" button/icon.

On Linux systems:

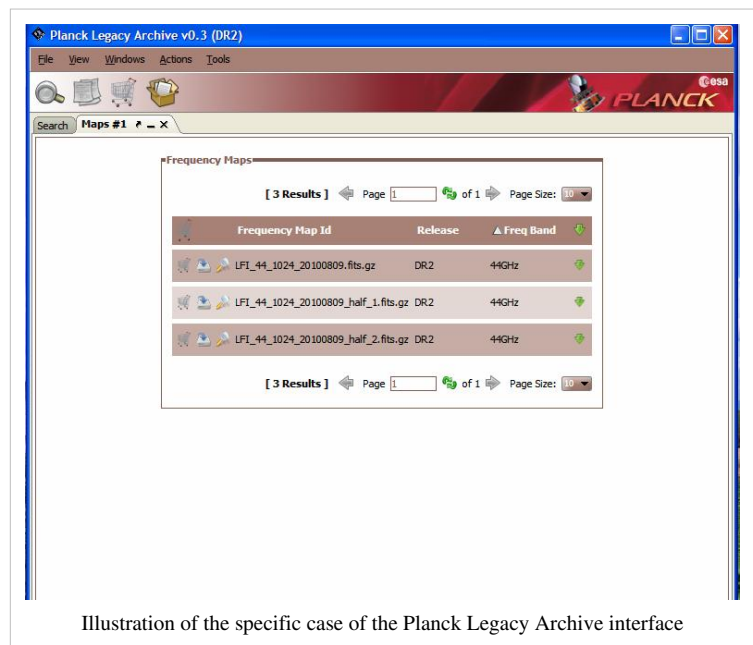
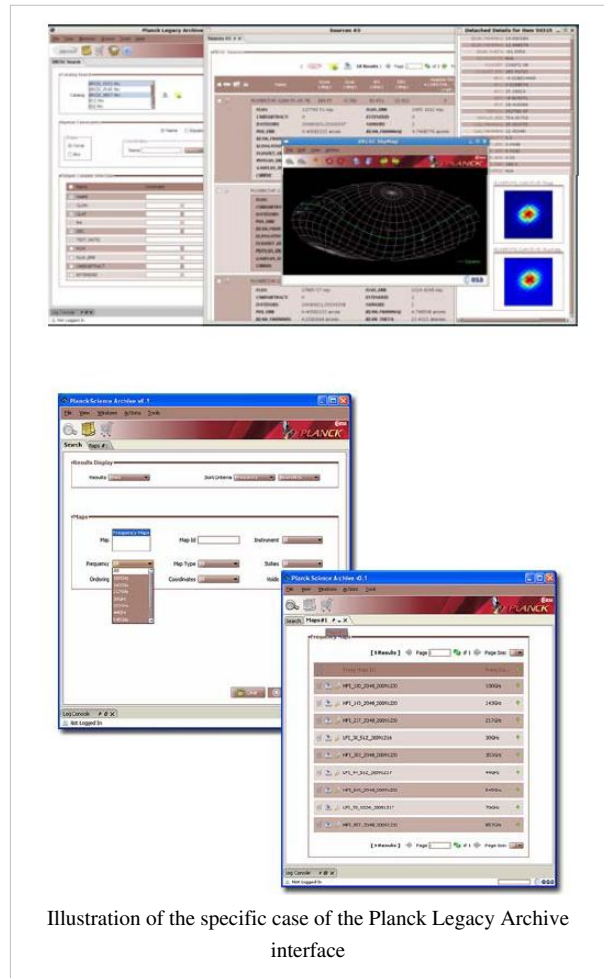
- Find out what version of Java you are running by and typing in "java -version" at the command line (w/o the quotes).
- Type in the command "\$JAVA\_HOME/jre/javaws/javaws" or "\$JAVA\_HOME/jre/javaws/javaws -viewer" on the command line if your Java version is 1.5 or 1.6 respectively.
- Select all the entries and then click on the "Remove Selected Applications/Items/Entries" button/icon.

On Mac OS X systems:

- Find out what version of Java you are using by running "Applications/Utilities/Terminal" and typing in "java -version" at the command line (w/o the quotes).
- Type in the command "javaws" or "javaws -viewer" on the command line if your Java version is 1.5 or 1.6 respectively.
- Select all the entries and then click on the "Remove Selected Applications/Items/Entries" button/icon.

On Windows systems, in case of trouble with Java WebStart and Comodo Firewall:

- When trying to launch the archive interface, Java WebStart may return the error "splash recv failed".
- Possible solution: Add Java WebStart to the list of authorized applications in the Comodo Firewall.



## Planck Legacy Archive Helpdesk

The PLA Helpdesk consists of the three scientists of Planck Science Office. For some questions related to data products and instruments, the questions may be re-directed to data-processing or instrument specialists in science institutes of the Planck Ground Segment.

In order to send a request to the Helpdesk, please simply send an E-mail to "piahelp at sciops.esa.int".

## References

- [1] [http://www.sciops.esa.int/index.php?page=Planck\\_Legacy\\_Archive&project=planck](http://www.sciops.esa.int/index.php?page=Planck_Legacy_Archive&project=planck)
- [2] <http://pla.esac.esa.int/pla/pla.jnlp>
- [3] <http://www.java.com/en/download/manual.jsp>
- [4] <http://www.java.com/en/download/testjava.jsp>

# Mission Science products overview

---

DPC products include different flavors of timelines, of maps, and of power spectra, and also instrumental parameters such as detector positions, noise levels, bandpasses and beam descriptions. They are packaged into FITS files that contain a main product (e.g., a map) and one or more other products to characterize it (e.g., an error map and a hit-count map). The details of the FITS file structures can be found in the "Exchange Format Design Document" (EFDD, ref), and the other parameters are described in the "Timelines Exchange ICD" (ICD-030, ref) and in the "Maps and Power Spectra Exchange ICD" (ICD-031, ref). This section gives a general description of the FITS files, with the salient points and examples for each type of data products given in the subsections on the different product types.

The FITS files begin with a minimal primary header containing no data, and some generic keywords like the creation date, the version of the EFDD and of the ICD with which the structure complies. The data are written into a one or more 'BINTABLE' extensions, with keywords giving the necessary descriptions.

Timelines of science data are split by OD (operation day) in order to keep their size manageable, and in the case of HFI they are further split into 5 files, each containing the data of ~ 10 bolometers. These files also contain the OBT associated with each sample, a global flag on the OBT which will include information valid for all samples obtained at that time (such as stable pointing), and a "local" flag on each bolometer timeline. The OBT and each data timeline, with its flag, are written into different extensions.

Maps are always full sky HEALPIX maps in Galactic coordinates, with "NESTED" ordering, and Nside of 1024 or 2048. The maps can be produced for a single detector or for an ensemble of detectors, can be Temperature only, or Polarized, and can cover all or part of the mission. The map data are written as columns of a BINTABLE, and in addition to the signal columns (I, and optionally Q and U), there will be associated variance columns (the diagonal elements of the II and optionally IQ, IU, QQ, QU, and UU covariance matrices) and a hit-count column.

Astrophysical component maps are written as a single map, in the case of the CMB which does not vary with frequency, or as 9 maps, one for each Planck frequency, together with errors (variance?) and a mask. In the case of Polarized data, the number of maps is multiplied by 3.

Power spectra ... TBW

Instrument data are given in two "RIMOs" (Reduced Instrument Models", one for each DPC, which have similar, but not identical structures. They contain scalar and vector information on the detectors (beam position and size, noise parameters, spectral bandpasses, noise spectra, etc.) and for maps, or combinations of detectors.

---

# Timelines

---

**There will be no timelines in the 1st data release.**

## Semi-raw signal timelines

### HFI timelines

Originally defined to be the raw (ADU) data demodulated and converted to engineering units (V) via the HFI transfer functions (includes 3-pt filtering?). But (1) this is not the same demodulation method as used in the TOI prod pipeline, and (2) the ADC correction (or at least one method thereof) implies a modification of the raw data before demodulation. Thus what the HFI will deliver is not yet decided

### LFI timelines

TBW

## Cleaned and calibrated signal timelines

### HFI processing

The calibrated timelines are produced by the *TOIprod* pipeline ([link to wiki](#); [link to paper](#)) which in brief performs the following operations:

demodulation

this is performed around a variable level which is determined from the valid input data (a validity flat from a previous version of the processing is determined for this purpose), and the data are converted to engineering units (V) using known conversion coefficients.

despiking

using the demodulated data converted to V (by the transfer function) the glitches are identified and fitted with templates. A glitch flag is produced that identifies the strongest part of the glitches, and a timeline of glitch tails is produced from the template fits, and subtracted from the demodulated timeline from step 1. Finally, the flagged ranges are replaced with data from TBC (*is this done here, if not where?*)

dark template removal

*TBW*

conversion to absorbed power

the timeline is converted to watts of absorbed power using the bolometer function. This includes a non-linearity correction

removal of the 4K cooler lines

*TBW*

at this point a timeline in W and a glitch flag are written to disk

deconvolution by the time transfer function

*TBW*

jump correction

removes some (relatively rare) jumps in the signal baseline

---

at this point a *tau-deconvolved* and *jump-corrected* timeline and its associated glitch flag are written to disk. These timelines are later used in the flux calibration and mapmaking stages

Note that these timelines contain the full sky signal, i.e. including the solar and orbital dipoles and the Zodiacal light. The dipoles are necessary for the flux calibration and are removed by the pipeline at the mapmaking stage.

**Need to discuss dipoles removal and conversion to astrophysical units at the export stage**

## LFI processing

TBW

## Pointing timelines

The pointing is determined starting from the AHF produced by MOC, which gives the direction and orientation of the LOS of a fiducial position in the focal plane at frequencies of 8Hz during stable pointing and 4 Hz during maneuvers (TBC for details, reference). This is interpolated to the times of data observation (ref to method), corrected for the wobble and other time-dependent offsets determined from the observed positions of a large number of sources around the sky, and finally converted to the LOS of each detector using the quaternions in the IMO (which are determined from observations of bright planets - see the Focal plane reconstruction pipeline).

*Details of delivery are TBD*

## FITS file structure

The FITS files will begin with a minimal primary header that will be followed by several BINTABLE extensions: the first one for the OBT and its (global) flag, the following ones for each detector signal data and its (local) flag.

Filenames will be of the form *{H\L\FI\_HscN-DDDD-R-yyymmdd.fits*, where *DDDD* is the OD number, *sc* indicates science data, and *N=1-5* for the 5 HFI files, and *R* indicates it is reduced (i.e., cleaned and calibrated) data.

*NB. this is the current name used in DPC exchanges, perhaps it should be changed ... eg. replace the date with the release number. Will also indicate that they are calibrated in astrophysical units and will have the dipoles removed, thus they are for delivery to the external community.*

## Header keywords

An example is given below.

### EXTENSION 0:

```
SIMPLE = T / file does conform to FITS standard
BITPIX = 32 / number of bits per data pixel
NAXIS = 0 / number of data axes
EXTEND = T / FITS dataset may contain extensions
COMMENT FITS (Flexible Image Transport System) format is defined in 'Astronomy
COMMENT and Astrophysics', volume 376, page 359; bibcode: 2001A&A...376..359H
EFDD_VER= '99.9 '
ICD_VER = '99.9 '
IMO = 'IMO_2_62'
DATE = '2012-09-04T13:45:59' / file creation date (YYYY-MM-DDThh:mm:ss UT)
END
```

where EFDD\_VER and ICD\_VER are the versions of the respective documents in which the structure is defined (dummy values in the example).

**EXTENSION 1: OBT**

```

XTENSION= 'BINTABLE'          / binary table extension
BITPIX   =                    8 / 8-bit bytes
NAXIS    =                    2 / 2-dimensional binary table
NAXIS1   =                    9 / width of table in bytes
NAXIS2   =                   15573106 / number of rows in table
PCOUNT   =                    0 / size of special data area
GCOUNT   =                    1 / one data group (required keyword)
TFIELDS  =                    2 / number of fields in each row
TTYPE1   = 'OBT              ' / label for field   1
TFORM1   = '1K              ' / data format of field: 8-byte INTEGER
TUNIT1   = '2**(-16)sec'      / physical unit of field
TTYPE2   = 'Flag           ' / label for field   2
TFORM2   = '1B             ' / data format of field: BYTE
TUNIT2   = 'N/A           ' / physical unit of field
EXTNAME  = 'OBT            ' / name of this binary table extension
TIMEZERO= '1660237181'
END

```

where TIMEZERO is the value of the first timesample in the units of TUNIT1

**EXTENSION 2: 14\_545\_1\_LFER4\_JC\_v51**

This is the first of the extensions containing the detector data, and is followed by more like it for the other detectors.

```

XTENSION= 'BINTABLE'          / binary table extension
BITPIX   =                    8 / 8-bit bytes
NAXIS    =                    2 / 2-dimensional binary table
NAXIS1   =                    5 / width of table in bytes
NAXIS2   =                   15573106 / number of rows in table
PCOUNT   =                    0 / size of special data area
GCOUNT   =                    1 / one data group (required keyword)
TFIELDS  =                    2 / number of fields in each row
TTYPE1   = 'Signal        ' / label for field   1
TFORM1   = '1E            ' / data format of field: 4-byte REAL
TUNIT1   = 'KCMB          ' / physical unit of field
TTYPE2   = 'Flag          ' / label for field   2
TFORM2   = '1B            ' / data format of field: BYTE
TUNIT2   = 'N/A           ' / physical unit of field
EXTNAME  = '14_545_1_LFER4_JC_v51' / name of this binary table extension
TIMEZERO= '1660237181'
CHANNEL  = '545-1         '
END

```

Note that NAXIS must be the same for all extensions.

*NB. may want to change EXTNAME to be just the detector name; the rest was for internal purposes only*

# Single detector maps

---

## Introduction

**There are no single detector maps in the first release.  
This section will serve for later releases.**

Maps for single detectors are built for full or part of the mission and are used primarily for characterization purposes: while the ones built with an unpolarized detector have a scientific value, the ones built using a polarization sensitive one have little, since, among other things, the polarization angle varies around the sky. Each signal map will be accompanied by a hit map and a variance map. All maps are in Healpix format, with Nside of 2048 for HFI and of 1024 for LFI, in Galactic coordinates, and Nested ordering. The three maps will be packaged into a FITS files with a single *BINTABLE* extension containing a table of three columns; the structure of the FITS file is given in the FITS file structure section below.

The FITS filenames are of the form  $\{H\backslash L\}FI_{\{detname\}}_{nnnn\_yyyymmdd\_}\{type\}_{mission}.fits$ , where *detname* is a detector identifier, and *nnnn* is the Healpix Nside of the map, the optional *type* indicates the subset of input data used, and *mission* indicates the coverage period, i.e., *full*, *nominal*, or *survey\_n* (TBC; an alternative of the type  $\{H\backslash L\}FI_{detname\_}\{type\}_{mission\_}Rn.mm.fits$  is being considered, where *Rn.mm* is the release number). A full list of products, by their names, is given in the List of products below. These

## HFI Processing

See Frequency Maps section

## LFI PRocessing

TBW

## List of products

### First release

None

### Second Release

TBW

## FITS file structure

The FITS file structure is like that of Intensity-only frequency maps as described in the next section

---

## Header keywords

A typical header for the extension is

```
XTENSION= 'BINTABLE'           / binary table extension
BITPIX   =                      8 / 8-bit bytes
NAXIS    =                      2 / 2-dimensional binary table
NAXIS1   =                     12 / width of table in bytes
NAXIS2   =                   50331648 / number of rows in table
PCOUNT   =                      0 / size of special data area
GCOUNT   =                      1 / one data group (required keyword)
TFIELDS  =                      3 / number of fields in each row
TTYPE1   = 'I_Stokes'          / label for field  1
TFORM1   = '1E8'               / data format of field: 4-byte REAL
TUNIT1   = 'K_CMB'             / physical unit of field
TTYPE2   = 'Hits'              / label for field  2
TFORM2   = '1J'               / data format of field: 4-byte INTEGER
TUNIT2   = 'none'              / physical unit of field
TTYPE3   = 'II_cov'            / label for field  3
TFORM3   = '1E8'               / data format of field: 4-byte REAL
TUNIT3   = '(K_CMB)^2'         / physical unit of field
EXTNAME  = 'CH-MAP'            / name of this binary table extension
FREQ     = '857'               '
PIXTYPE  = 'HEALPIX'           '
COORDSYS= 'GALACTIC'           '
ORDERING= 'NESTED'             '
FILENAME= 'HFI_857-2_2048_20120210_nominal.fits'
NSIDE    =                     2048
CHANNEL  = '857-2'             '
FIRSTPIX=                      0
LASTPIX  =                   50331647
EXTVER   = '1'                 '
PROCV   = 'v50'                '
BAD_DATA= '-1.63750E+30'
COMMENT  = 'Rel DR4'           '
```

END

# Frequency Maps

---

## Introduction

Frequency maps are produced by combining appropriately the data of several detectors over some period of the mission. They may be intensity only or polarized, meaning that they will consist of a set of three maps of I, Q, and U. These will be accompanied by a hit-count map and by a set of variance maps. All maps are in Healpix format, with Nside of 2048 for HFI and of 1024 for LFI, in Galactic coordinates, and Nested ordering. The maps are packaged into a single *BINTABLE* extension; the structure of the FITS file is given in the FITS file structure section below.

The FITS filenames are of the form  $\{H\backslash L\}FI\_fff\_nnnn\_yyyymmdd\_ \{type\}\_ \{mission\}.fits$ , where *fff* are three digits to indicate the Planck frequency band, and *nnnn* is the Healpix Nside of the map, the optional *type* indicates the subset of input data used, and *mission* indicates the coverage period, i.e., *full*, *nominal*, or *survey\_n* (TBC; an alternative of the type  $\{H\backslash L\}FI\_fff\_ \{type\}\_ \{mission\}\_Rn.mm.fits$  is being considered, where *Rn.mm* is the release number). A full list of products, by their names, is given in the List of products below.

## HFI processing

The cleaned TOIs of each detector (calibrated in Watts) with their associated flags (flagged samples and anomalous rings) are first used to build Healpix rings, each ring containing the combined data of one pointing period. These are then calibrated in brightness, cleaned of the dipole signals, and projected onto Healpix maps as explained in the following sections.

Gains are initially determined for each pointing period. These estimates are systematically biased by Galactic foregrounds. These gains are averaged over a time interval in the first survey where the Solar dipole amplitude is large enough to reduce these bias. For 100 to 217 GHz, evidence of apparent gain variations of order 1 to 2% over a few tens to thousands of pointing periods led us to adopt a more sophisticated approach, where we determined relative gains for each pointing period, smoothed with a 50 pointing period width.

At the higher frequencies, 545 and 857 GHz, calibration was initially determined by fitting HFI data onto FIRAS data, but these are then corrected on the basis of results from planet observations, the CMB itself, and more. These zero point are applied for all frequencies to set them at the same scale.

A destriping approach is used, where noise is modelled as the sum of a white noise component and a constant, aka offset, per pointing period which represent the low frequency 1/f noise. After subtracting these offsets, calibrated data are projected onto Healpix maps, with the data of each bolometer weighted by a factor of 1/NET of that bolometer. Maps are build after a simple classical dipole removal based on WMAP measurements.

The Zodiacal light and the Far-side-lobes are modeled separately at HPR-level, and subtracted from the signal HPR before projecting them onto the maps. A product showing the difference between the uncorrected and the corrected maps is provided.

Together with signal maps, hit count and variance maps are also produced. The hit maps give the (integer) number of valid TOI-level samples that contribute to the signal of each pixel. All valid samples are counted in the same way, i.e., there is no weighting factor applied. The variance maps project the white noise estimate, provided by the NETs, in the sky domain. They give the covariance between the Stokes parameters I,Q and U inside each pixels, whenever polarization is reconstructed.

---



## LFI processing

TBW

## Types of maps

### Full channel maps

Full channel maps are built using all the valid detectors of a frequency channel and cover the full mission (or the nominal mission for the 1st release). For HFI, the 143-8 and 545-3 bolometers are rejected entirely as they are seriously affected by RTS noise.

### Single survey maps

Single survey maps are built using all valid detectors of a frequency channel, but cover separately the different sky surveys. The single sky surveys are defined in terms of the direction of the satellite's spin axis: the first survey covers from the beginning of the science observations (the First Light Survey) to the time when the spin axis has rotated by 180 degrees (to the nearest pointing period), the following ones covers from 180 to 360, and so on. In the case of the nominal mission, the process stops at the third survey, which is incomplete. In the case of the full mission the 4th survey was interrupted shortly before completing the 180 degree rotation (see [LINK](#)), in order to begin observing with a different scanning law. The HFI mission ended slightly before the natural end of the 5th survey, the LFI mission continued to the XXX survey. The coverage of each of these periods in terms of ring number, pointingID, and OD, is given in the table below. Note that the OD numbers are only to indicate during which OD the period boundary occurs.

**Missions and sky survey coverage periods**

Name	Ini_OD	Ini_Ring	Ini_ptgID	End_OD	End_ring	End_ptgID
Nominal	91	240	00004200	807	14724	04243900
HFI-Full	91	240	00004200	563	27008	06344800
LFI-Full	91	240	00004200	TBD	TBD	TBD
SCAN1	91	240	00004200	270	5720	01059820
SCAN2	270	5721	01059830	456	11194	02114520
SCAN3	456	11195	02114530	636	16691	03193660
SCAN4	636	16692	03193670	807	21720	04243990
SCAN5	807	21721	95000020	974	27008	06344800

### Detector-set maps

**There are no detset maps in the first release.  
This section will serve for later releases.**

Detector-set (detset) maps are built for the full (or nominal) mission using a minimal set of detectors. This concept is applicable to polarization maps, which are built using two PSB pairs at the proper orientations. The HFI polarized channels are designed to provide two detsets (or quads) each, namely:

### HFI detector sets or quads

<b>100–ds1:</b> 100-1a,100-1b,100-4a,100-4b	<b>100–ds2:</b> 100-2a,100-2b,100-3a,100-3b
<b>143–ds1:</b> 143-1a,143-1b,143-3a,143-3b	<b>143–ds2:</b> 143-2a,143-2b,143-4a,143-4b
<b>217–ds1:</b> 217-5a,217-5b,217-7a,217-7b	<b>217–ds2:</b> 217-6a,217-6b,217-8a,217-8b
<b>353–ds1:</b> 353-5a,353-5b,353-3a,353-3b	<b>353–ds2:</b> 353-6a,353-6b,353-4a,353-4b

Some maps built using a set of a single detector are also provided, and are described in Single detector maps

The LFI Detector-set maps are built using pairs of horns in the same scanning row, namely:

### LFI Couple Horn sets

<b>18_23:</b> 18M,18S,23M,23S
<b>19_22:</b> 19M,19S,22M,22S
<b>20_21:</b> 20M,20S,21M,21S
<b>24:</b> 24M,24S
<b>25_26:</b> 25M,25S,26M,26S

### Half-ring maps

Half-ring maps are built using only the first or the second half of the stable pointing period data. There are thus two half-ring maps per frequency channel named *ringhalf\_1* and *ringhalf\_2* respectively. These maps are built for characterization purposes in order to perform null tests.

## List of products

### First release

For the first release, all maps will be Intensity-only

Full channel maps

```
LFI_030_2048_yyyymmdd_nominal.fits
LFI_044_2048_yyyymmdd_nominal.fits
LFI_070_2048_yyyymmdd_nominal.fits
HFI_SkyMap_100_2048_R1.00_nominal.fits
HFI_SkyMap_143_2048_R1.00_nominal.fits
HFI_SkyMap_217_2048_R1.00_nominal.fits
HFI_SkyMap_353_2048_R1.00_nominal.fits
HFI_SkyMap_545_2048_R1.00_nominal.fits
HFI_SkyMap_857_2048_R1.00_nominal.fits
```

Single survey maps

```
LFI_030_2048_yyyymmdd_survey_1.fits
LFI_030_2048_yyyymmdd_survey_2.fits
LFI_030_2048_yyyymmdd_survey_3.fits
LFI_044_2048_yyyymmdd_survey_1.fits
LFI_044_2048_yyyymmdd_survey_2.fits
LFI_044_2048_yyyymmdd_survey_3.fits
```

```
LFI_070_2048_yyyymmdd_survey_1.fits
LFI_070_2048_yyyymmdd_survey_2.fits
LFI_070_2048_yyyymmdd_survey_3.fits
HFI_SkyMap_100_2048_R1.00_survey_1.fits
HFI_SkyMap_100_2048_R1.00_survey_2.fits
HFI_SkyMap_143_2048_R1.00_survey_1.fits
HFI_SkyMap_143_2048_R1.00_survey_2.fits
HFI_SkyMap_217_2048_R1.00_survey_1.fits
HFI_SkyMap_217_2048_R1.00_survey_2.fits
HFI_SkyMap_353_2048_R1.00_survey_1.fits
HFI_SkyMap_353_2048_R1.00_survey_2.fits
HFI_SkyMap_545_2048_R1.00_survey_1.fits
HFI_SkyMap_545_2048_R1.00_survey_2.fits
HFI_SkyMap_857_2048_R1.00_survey_1.fits
HFI_SkyMap_857_2048_R1.00_survey_2.fits
```

### Half-ring maps

```
LFI_030_2048_yyyymmdd_ringhalf_1_nominal.fits
LFI_030_2048_yyyymmdd_ringhalf_2_nominal.fits
LFI_044_2048_yyyymmdd_ringhalf_1_nominal.fits
LFI_044_2048_yyyymmdd_ringhalf_2_nominal.fits
LFI_070_2048_yyyymmdd_ringhalf_1_nominal.fits
LFI_070_2048_yyyymmdd_ringhalf_2_nominal.fits
HFI_SkyMap_100_2048_R1.00_nominal_ringhalf_1.fits
HFI_SkyMap_100_2048_R1.00_nominal_ringhalf_2.fits
HFI_SkyMap_143_2048_R1.00_nominal_ringhalf_1.fits
HFI_SkyMap_143_2048_R1.00_nominal_ringhalf_2.fits
HFI_SkyMap_217_2048_R1.00_nominal_ringhalf_1.fits
HFI_SkyMap_217_2048_R1.00_nominal_ringhalf_2.fits
HFI_SkyMap_353_2048_R1.00_nominal_ringhalf_1.fits
HFI_SkyMap_353_2048_R1.00_nominal_ringhalf_2.fits
HFI_SkyMap_545_2048_R1.00_nominal_ringhalf_1.fits
HFI_SkyMap_545_2048_R1.00_nominal_ringhalf_2.fits
HFI_SkyMap_857_2048_R1.00_nominal_ringhalf_1.fits
HFI_SkyMap_857_2048_R1.00_nominal_ringhalf_2.fits
```

### Zodi and Far-side-lobes correction maps

```
HFI_SkyMap_ZodiCorr_2048_R1.00.fits
```

## Second release

All the above + TBD, including polarization for the polarized frequency channels.

## FITS file structure

The FITS file will have one of the following structures:

The exact order of the columns is indicative only, and the details will be given in the keywords. Keywords will also indicate the coordinate system (GALACTIC), the Healpix ordering scheme (NESTED), the units (K\_cmb), and of course the detector. Details of the FITS file general structure can be found in the EFDD (ref), and the specifics of certain parameters in ICD-031 (ref)

## Header keywords

A typical header for the data extension of an intensity only map is:

```
;-----
; EXTENSION 1: FREQ-MAP
; - Header
;-----
XTENSION= 'BINTABLE'           /Written by IDL:  Fri Nov 30 15:13:55 2012
BITPIX   =                      8 /
NAXIS    =                      2 /Binary table
NAXIS1   =          603979776 /Number of bytes per row
NAXIS2   =                      1 /Number of rows
PCOUNT   =                      0 /Random parameter count
GCOUNT   =                      1 /Group count
TFIELDS  =                      3 /Number of columns
COMMENT
COMMENT  *** End of mandatory fields ***
COMMENT
COMMENT  *** Column names ***
COMMENT
TTYPE1   = 'I_STOKES'           /
TTYPE2   = 'HITS'               /
TTYPE3   = 'II_COV'            /
COMMENT
COMMENT  *** Column formats ***
COMMENT
TFORM1   = '50331648E'          /
TFORM2   = '50331648E'          /
TFORM3   = '50331648E'          /
COMMENT
COMMENT  *** Column units ***
COMMENT
TUNIT1   = 'K_CMB'              /
TUNIT2   = ' '                  /
TUNIT3   = 'K_CMB'              /
COMMENT
```

```

COMMENT *** Planck params ***
COMMENT
UNITCONV=          0.00000 / (MJy/sr)/K_cmb unit conv. factor
EXTNAME = 'FREQ-MAP'      /
COORSYS = 'GALACTIC'      / Coordinate system
ORDERING= 'NESTED'        / Healpix ordering
NSIDE   =          2048 / Healpix Nside
FIRSTPIX=          0 /
LASTPIX =          50331647 /
FILENAME= 'HFI_SkyMap_100_2048_R1.00_nominal.fits' / FITS filename
FILEDATE= '2012-11-30 15:13' / File creation date
BAD_DATA=          -1.63750E+30 / bad pixel value
PROCVER = 'DX9-delta'      / Product version
COMMENT
COMMENT -----
COMMENT Full channel frequency map for nominal mission
COMMENT -----
COMMENT HFI-DMC objects:
COMMENT in-group: MAP_DX9_2048_GALACTIC_0240_27008/
COMMENT Creation date - object name
COMMENT 12-05-29 13:38 - 100GHz_W_TauDeconv_nominal_I
COMMENT 12-05-29 13:38 - 100GHz_W_TauDeconv_nominal_H
COMMENT 12-05-29 13:38 - 100GHz_W_TauDeconv_nominal_II
COMMENT -----
END

```

The header of the Zodiacal light (and FSL) correction maps is:

```

; -----
; EXTENSION 1: COMP-MAP
; - Header
; -----
XTENSION= 'BINTABLE'      /Written by IDL:  Fri Nov 30 15:29:58 2012
BITPIX   =          8 /
NAXIS    =          2 /Binary table
NAXIS1   =        603979776 /Number of bytes per row
NAXIS2   =          1 /Number of rows
PCOUNT   =          0 /Random parameter count
GCOUNT   =          1 /Group count
TFIELDS  =          3 /Number of columns
COMMENT
COMMENT *** End of mandatory fields ***
COMMENT
COMMENT *** Column names ***
COMMENT
TTYPE1   = 'CORR_353'      / Correction 353 GHz
TTYPE2   = 'CORR_545'      / Correction 545 GHz

```

```

TTYPE3 = 'CORR_857' / Correction 857 GHz
COMMENT
COMMENT *** Column formats ***
COMMENT
TFORM1 = '50331648E' /
TFORM2 = '50331648E' /
TFORM3 = '50331648E' /
COMMENT
COMMENT *** Column units ***
COMMENT
TUNIT1 = 'K_CMB' /
TUNIT2 = 'MJy/sr[nuI(nu)=cst]' /
TUNIT3 = 'MJy/sr[nuI(nu)=cst]' /
COMMENT
COMMENT *** Planck params ***
COMMENT
EXTNAME = 'COMP-MAP' /
AST-COMP= 'ZODI-FSL' / Component
COORSYS = 'GALACTIC' / Coordinate system
ORDERING= 'NESTED' / Healpix ordering
NSIDE = 2048 / Healpix Nside
FIRSTPIX= 0 /
LASTPIX = 50331647 /
FILENAME= 'HFI_SkyMap_ZodiCorr_2048_R1.00.fits' / FITS filename
FILEDATE= '2012-11-30 15:29' / File creation date
BAD_DATA= -1.63750E+30 / bad pixel value
PROCVER = 'DX9-delta' / Product version
COMMENT
COMMENT -----
COMMENT This is a map representation of the modelled Zodiacal light and Far Side
COMMENT Lobe contributions that have been removed from nominal mission frequency
COMMENT maps. See the Explanatory Supplement for details.
COMMENT -----
COMMENT HFI-DMC objects:
COMMENT group uncorr 353: /data/dmc/MISS03/DATA/MAP_v53_noZodi_2048_GALACTIC_024
COMMENT group nozodi 353: /data/dmc/MISS03/DATA/MAP_DX9_2048_GALACTIC_0240_27008
COMMENT group uncorr GAL: /data/dmc/MISS03/DATA/MAP_v53_MJyResca_noZodi_2048_GAL
COMMENT group nozodi GAL: /data/dmc/MISS03/DATA/MAP_v53_MJyResca_2048_GALACTIC_0
COMMENT Creation date - object name
COMMENT 12-11-26 22:19 - 353GHz_W_TauDeconv_nominal_I
COMMENT 12-06-07 21:20 - 353GHz_W_TauDeconv_nominal_I
COMMENT 12-11-26 17:54 - 545GHz_W_TauDeconv_nominal_I
COMMENT 12-11-24 19:31 - 545GHz_W_TauDeconv_nominal_I
COMMENT 12-11-26 17:24 - 857GHz_W_TauDeconv_nominal_I
COMMENT 12-11-24 21:09 - 857GHz_W_TauDeconv_nominal_I
COMMENT -----
END

```

# Astrophysical component maps

---

## Overview

This section is very preliminary. Its purpose is to give examples of what these products could look like.

Different structures are used for these products:

structure independent of frequency

in this case a single map to give the structure suffices. It will (optionally) be accompanied by an uncertainty map a mask and possibly a beam window function, and a method will be given to convert the structure map to the map at a given frequency. This applies to the CMB and to the dust opacity.

structure variable with frequency

in this case the file will contain up to 10 signal maps, for the 10 Planck frequencies, accompanied (optionally) by uncertainties a mask.

## CMB maps

The details will depend on which methods methods. In all cases the FITS file will contain

- a CMB signal map in K
- an uncertainty or a variance map
- a mask
- residuals at each Planck frequency: in practice these are the foregrounds (Galaxy, point sources, etc.)

Optionally there will be another extension with

- Beam transfer function

## SIMCA

In this case:

- the uncertainty is given by the noise derived from the half-ring maps, and thus it is a reasonable estimate of the uncertainties at hi  $l$ , but not at low  $l$ , where residuals from the foregrounds become important.

```

; -----
; EXTENSION 1: COMP-MAP
; -----
XTENSION= 'BINTABLE'           /Written by IDL:  Thu Aug  2 10:15:09 2012
BITPIX   =                      8 /
NAXIS    =                      2 /Binary table
NAXIS1   =                   9216 /Number of bytes per row
NAXIS2   =                      1 /Number of rows
PCOUNT   =                      0 /Random parameter count
GCOUNT   =                      1 /Group count
TFIELDS  =                      3 /Number of columns
COMMENT
COMMENT  *** End of mandatory fields ***
COMMENT
AST-COMP= 'CMB'                 / Component
COMMENT
COMMENT  *** Column names ***

```

```

COMMENT
TTYPE1  = 'I          '          / Intensity map
TTYPE2  = 'I_ERR     '          / Error
TTYPE3  = 'MASK      '          / Mask
COMMENT
COMMENT  *** Column formats ***
COMMENT
TFORM1  = '768E      '          /
TFORM2  = '768E      '          /
TFORM3  = '768E      '          /
COMMENT
COMMENT  *** Column units ***
COMMENT
TUNIT1  = 'K_cmb     '          /
TUNIT2  = 'K_cmb     '          /
TUNIT3  = 'none      '          /
COMMENT
COMMENT  *** Planck params ***
COMMENT
EXTNAME  = 'COMP-MAP '          /
COORSYS  = 'GALACTIC '          / Coordinate system
ORDERING = 'NESTED   '          / Healpix ordering
NSIDE    =              8 / Healpix Nside
FIRSTPIX =              0 /
LASTPIX  =              767 /
FILENAME = 'COM_cmb_20120802_smica.fits' / FITS file name
BAD_DATA = -1.63750E+30 / bad pixel value
PROCVAR  = 'v53/DX9 '          / Product version
METHOD   = 'SEVEM    '          / Separation method
END

;-----
; EXTENSION 2: BEAM B_L
;-----
XTENSION= 'BINTABLE'          /Written by IDL:  Thu Aug  2 10:15:09 2012
BITPIX  =              8 /
NAXIS   =              2 /Binary table
NAXIS1  =             8000 /Number of bytes per row
NAXIS2  =              1 /Number of rows
PCOUNT  =              0 /Random parameter count
GCOUNT  =              1 /Group count
TFIELDS =              1 /Number of columns
COMMENT
COMMENT  *** End of mandatory fields ***
COMMENT
EXTNAME  = 'BEAM B_L'          /Extension name
COMMENT

```



```

COMMENT *** Column names ***
COMMENT
TTYPE1  = 'BEAM      '          / Beam transfer function
TUNIT1  = 'NONE      '          /
COMMENT
COMMENT *** Column formats ***
COMMENT
TFORM1  = '2000E     '          /
PROCVER = 'v53/DX9   '          / Product version
END

```

## Synchrotron and free-free maps

These (or a single one if they are combined) will be given as a set of maps. The form could be like:

```

;-----
; EXTENSION 1: COMP-MAP
;-----
XTENSION= 'BINTABLE'          /Written by IDL:  Thu Aug  2 10:15:10 2012
BITPIX   =                      8 /
NAXIS    =                      2 /Binary table
NAXIS1   =                   30720 /Number of bytes per row
NAXIS2   =                      1 /Number of rows
PCOUNT   =                      0 /Random parameter count
GCOUNT   =                      1 /Group count
TFIELDS  =                   10 /Number of columns
COMMENT
COMMENT *** End of mandatory fields ***
COMMENT
COMMENT *** Column names ***
COMMENT
TTYPE1   = 'I_030     '          / 030 GHz Intensity map
TTYPE2   = 'I_044     '          / 044 GHz Intensity map
TTYPE3   = 'I_070     '          / 070 GHz Intensity map
TTYPE4   = 'I_100     '          / 100 GHz Intensity map
TTYPE5   = 'I_143     '          / 143 GHz Intensity map
TTYPE6   = 'I_217     '          / 271 GHz Intensity map
TTYPE7   = 'I_353     '          / 353 GHz Intensity map
TTYPE8   = 'I_545     '          / 545 GHz Intensity map
TTYPE9   = 'I_857     '          / 857 GHz Intensity map
TTYPE10  = 'MASK      '          / Mask
COMMENT
COMMENT *** Column formats ***
COMMENT
TFORM1   = '768E      '          /
TFORM2   = '768E      '          /
TFORM3   = '768E      '          /

```

```

TFORM4  = '768E      ' /
TFORM5  = '768E      ' /
TFORM6  = '768E      ' /
TFORM7  = '768E      ' /
TFORM8  = '768E      ' /
TFORM9  = '768E      ' /
TFORM10 = '768E      ' /
COMMENT
COMMENT  *** Column units ***
COMMENT
TUNIT1  = 'K_cmb      ' /
TUNIT2  = 'K_cmb      ' /
TUNIT3  = 'K_cmb      ' /
TUNIT4  = 'K_cmb      ' /
TUNIT5  = 'K_cmb      ' /
TUNIT6  = 'K_cmb      ' /
TUNIT7  = 'K_cmb      ' /
TUNIT8  = 'K_cmb      ' /
TUNIT9  = 'K_cmb      ' /
TUNIT10 = 'none       ' /
COMMENT
COMMENT  *** Planck params ***
COMMENT
EXTNAME  = 'COMP-MAP ' /
AST-COMP= 'SYNCHRO  ' / Component
COORSYS  = 'GALACTIC' / Coordinate system
ORDERING= 'NESTED  ' / Healpix ordering
NSIDE    =              8 / Healpix Nside
FIRSTPIX=              0 /
LASTPIX  =             767 /
FILENAME= 'SYNCHRO_20120802_commrul.fits' / FITS file name
BAD_DATA=      -1.63750E+30 / bad pixel value
PROCVAR  = 'v53/DX9  ' / Product version
METHOD   = 'Comm-Rul ' / Separation method
END

```

## Dust opacity map and model

The first BINTABLE extension will give the opacity structure at Nside=???; the second extension will give the scaling table (two columns: frequency, scaling factor) to scale the opacity structure map to other frequencies.

## CO emission maps

There are three products included here:

- a set of *CO correction* maps for the 100, 217, and 353 GHz channels, in K\_cmb, giving the broadband CO signal level in the 1-0, 2-1, and 3-2 lines expected in each channel
- a single *CO discovery* map giving ... TBW
- two *CO line emission* maps, giving ...TBW

## Other maps

This section will be for the various CO maps, CIB maps, and others. The overall structure of the FITS files will be similar to the cases above, though the details will be tailored to the individual products.

# Spectra

---

## CMB angular power spectra

Angular power spectra are provided in the Planck Legacy Archive with the following file structure:

# Likelihood Code

---

**see for now the Data processing pages C2.**

# The RIMO

---

## Overview

The RIMO, or *Reduced Instrument Model* is a FITS file containing selected instrument characteristics that are needed by users who work with the released data products. It is described in detail in *The HFI and LFI RIMO ICD* (ref). There will be two RIMOs, one for each instrument, which will follow the same overall structure, but will differ in the details. The type of data in the RIMO can be:

Parameter

namely scalars to give properties such as a noise level or a representative beam FWHM

Table

to give, e.g., filter transmission profiles or noise power spectra

Map

namely 2-D "flat" maps, to give, e.g., the main beam shape

The different types of data are written into different BINTABLE extensions of the FITS file, and these are described below.

---

## Detector-level parameter data

**There are no detector-level products in the first release, so there will be no detector-level parameters in the accompanying RIMO.**

The detector parameter data are given in the form of a table giving the parameter values for each detector. The table columns are (with the column names in parentheses):

*DETECTOR*

---

These are the detector names. For HFI these will be of the form *217-3* for SWBs or *100-3b* for PSBs, and for LFI they will have the form *27M* or *18S*. There are 52 HFI detectors and 22 LFI detectors.

Focal plane geometry parameters - *PHI\_UV*, *THETA\_UV*, and *PSI\_UV*

These parameters give the geometry of the focal plane, or the positions of the detectors in the focal plane. The angles that give the rotation of the beam pattern from a fiducial orientation (forward beam direction (z-axis) pointing along the telescope line of sight, with y-axis aligned with the nominal scan direction) to their positions in the focal plane. The fiducial position is that given by the Star Tracker. All angles are in radians.

Polarization parameters - *PSI\_POL*, *EPSILON*

These are the direction of maximum polarization, defined with the beam in the fiducial orientation described above, that is, before rotation onto the detector position, and the cross-polarization contamination (or leakage).

Beam parameters - *FWHM*, *ELLIPTICITY*, *POSANG*

These are the mean FWHM of the scanning beam (arcmin TBC), the beam ellipticity (no units), and the position angle of the beam major axis. The scanning beam is that recovered from the observation of bright planets.

Noise parameters - *NET\_TOT*, *NET\_WHT*, *F\_KNEE*, *ALPHA*

Two NETs are given: one determined from the total noise (rms of the noise timeline) and one determined from the white noise level of the noise spectrum. The *F\_KNEE* and *ALPHA* parameters are the frequency where the *1/f* noise component meets the white noise level, and the slope of the former. The NETs are in units of Kcmb or MJy/sr \* sqrt(s).

The basic structure of the BINTABLE extension is as follows:

```
;-----
; Detector parameters
;-----
XTENSION= 'BINTABLE'           / binary table extension
BITPIX   =                      8 / array data type
NAXIS     =                      2 / number of array dimensions
NAXIS1    =                   120 / length of dimension 1
NAXIS2    =                   52 / length of dimension 2
PCOUNT    =                      0 / number of group parameters
GCOUNT    =                      1 / number of groups
TFIELDS   =                   15 / number of table fields
EXTNAME    = 'CHANNEL PARAMETERS' / extension name
TTYPE1     = 'DETECTOR'
TFORM1     = '8A'
TUNIT1     = 'n/a'
TTYPE2     = 'PHI_UV'
TFORM2     = 'D'
TUNIT2     = 'deg'
TTYPE3     = 'THETA_UV'
TFORM3     = 'D'
TUNIT3     = 'deg'
TTYPE4     = 'PSI_UV'
TFORM4     = 'D'
TUNIT4     = 'deg'
TTYPE5     = 'PSI_POL'
```

```

TFORM5  = 'D      '
TUNIT5  = 'deg    '
TTYPER6 = 'EPSILON '
TFORM6  = 'D      '
TUNIT6  = 'n/a    '
TTYPER7 = 'FWHM   '
TFORM7  = 'D      '
TUNIT7  = 'arcmin '
TTYPER8 = 'ELLIPTICITY'
TFORM8  = 'D      '
TUNIT8  = 'n/a    '
TTYPER9 = 'POSANG  '
TFORM9  = 'D      '
TUNIT9  = 'deg    '
TTYPER10 = 'NET    '
TFORM10 = 'D      '
TUNIT10 = 'K*s^1/2 '
TTYPER11 = 'F_KNEE '
TFORM11 = 'D      '
TUNIT11 = 'Hz     '
TTYPER12 = 'ALPHA  '
TFORM12 = 'D      '
TUNIT12 = 'n/a    '
TTYPER13 = 'F_MIN  '
TFORM13 = 'D      '
TUNIT13 = 'Hz     '
TTYPER14 = 'F_MAX  '
TFORM14 = 'D      '
TUNIT14 = 'Hz     '
TTYPER15 = 'F_SAMP '
TFORM15 = 'D      '
TUNIT15 = 'Hz     '

```

## Map-level parameter data

The map-level data table contains the beam solid angle (total and out to different FWHM) and noise information as follows:

### *FREQUENCY*

a 3-digit string giving the reference frequency in GHz, i.e., of the form *044* or *217*

### *Omega\_total*

total beam solid angle in  $\text{armin}^2$

### *Omota\_1fwhm*

beam solid angle out to 1FWHM in  $\text{armin}^2$

### *Omega\_2fwhm*

beam solid angle out to 2FWHM in  $\text{armin}^2$

### *FWHM\_eff*

FWHM of a Gaussian beam having the same (total) solid angle, in sr. This is the best value for source flux determination

*FWHM\_gauss*

FWHM derived from best Gaussian fit to beam maps, in sr. This is the best value for source identification

*NOISE*

This is TBD: noise/observation sample or ...

For the Omega columns, the 'DISP' column gives an estimate of the spatial variation as a function of position on the sky.

The BINTABLE extension has the following structure

TABLE TO BE ADDED

## Single detector and combined bandpasses

**There are no detector-level products in the first release, so there will be no detector-level bandpasses in the accompanying RIMO, but only the combined bandpasses**

The effective filter bandpasses are given in different BINTABLE extensions. The extension is named *BANDPASS\_{name}*, where *name* specified the detector or the map. In the case of the maps, the bandpasses are a weighted average of the bandpasses of the detectors that are used to built the map. For details see ref to 03d HFI\_Spectral Band. The bandpasses are given as 4-column tables containing

*WAVENUMBER*

the wavenumber in cm-1

*TRANSMISSION*

the transmission (normalized to 1 at the max for HFI and to have an integral of 1 for LFI)

*ERROR*

the uncertainty

*FLAG*

a flag

The BINTABLE extension has the following structure

```

;-----
; Bandpasses (detector or combined)
;-----
XTENSION= 'BINTABLE'           / binary table extension
BITPIX   =                      8 / array data type
NAXIS    =                      2 / number of array dimensions
NAXIS1   =                     25 / length of dimension 1
NAXIS2   =                   12315 / length of dimension 2
PCOUNT   =                      0 / number of group parameters
GCOUNT   =                      1 / number of groups
TFIELDS  =                      4 / number of table fields
EXTNAME  = 'BANDPASS_100-2A'    / extension name
TTYPE1   = 'WAVENUMBER'
```

```

TFORM1  = 'D      '
TUNIT1  = '1/cm    '
TTYPER2 = 'TRANSMISSION'
TFORM2  = 'D      '
TUNIT2  = 'n/a     '
TTYPER3 = 'UNCERTAINTY'
TFORM3  = 'D      '
TUNIT3  = 'n/a     '
TTYPER4 = 'FLAG     '
TFORM4  = 'L      '
TUNIT4  = 'n/a     '
COMMENT Spencer v2.02 injection
END

```

## Detector noise spectra

**There are no detector-level products in the first release,  
so there will be no detector noise spectra in the accompanying RIMO.**

The noise power spectra are the result of the *detnoise* pipeline.

### HFI

these are the ring noise spectra averaged for rings NN to MM in order to give a representative spectrum. The spectra of all 50 valid bolometers are given in a single table.

### LFI

#### TBW

The keyword *F\_NYQ* gives the Nyquist frequency, and can be used together with the number of points in the spectrum to reconstruct the frequency scale. The BINTABLE has the following structure:

```

XTENSION= 'BINTABLE'           /Written by IDL:  Wed Aug  8 13:36:33 2012
BITPIX   =                      8 /
NAXIS    =                      2 /Binary table
NAXIS1   =          13631488 /Number of bytes per row
NAXIS2   =                      1 /Number of rows
PCOUNT   =                      0 /Random parameter count
GCOUNT   =                      1 /Group count
TFIELDS  =          52 /Number of columns
COMMENT
COMMENT  *** End of mandatory fields ***
COMMENT
EXTNAME  = 'NOISE_SPECTRA'      /Extension name
DBPATH   = '/data/dmc/MISS03/DATA/detnoise/' /
TAG      = '_MeanSpectrum_deconv_byRing_p17_survey_3_v53' /
N_PTS    =          65536 /
F_NYQ    =          90.0000 /
UNITS    = 'W/rt (Hz) '        /
PROCVAR  = 'v53/DX9 '          / HFI Product version

```

```

COMMENT
COMMENT   *** Column names ***
COMMENT
TTYPE1   = 'SPECTRUM_100_1A'      /
TTYPE2   = 'SPECTRUM_100_1B'      /
. . . .

TTYPE52  = 'SPECTRUM_857_4'       /
COMMENT
COMMENT   *** Column formats ***
COMMENT
TFORM1   = '65536E'               /
TFORM2   = '65536E'               /
. . . .

TFORM52  = '65536E'               /
END

```

## Beam Window Functions

Beam window functions and associated error descriptions are given into a BINTABLE for each *detection unit*, where *detection unit* consists of an auto or a cross product of one or two frequency maps or detset maps used in the likelihood. Here they are:

- the 6 HFI frequency channels, producing 21 extensions
- 26 detsets, producing 351 extensions; the detsets used are, by frequency channel:
  - 100\_ds1, 100\_ds2,
  - 143\_ds1, 143\_ds2, 143\_5, 143\_6, 143\_7,
  - 217\_ds1, 217\_ds2, 217\_1, 217\_2, 217\_3, 217\_4,
  - 353\_ds1, 353\_ds2, 353\_1, 353\_2, 353\_7, 353\_8,
  - 545\_1, 545\_2, 545\_4,
  - 857\_1, 857\_2, 857\_3, 857\_4

Each extension contains:

- a *NOMINAL* column (mandatory) with the window function proper,
- a *BIAS* column (optional),
- a number of *EIGEN<sub>n</sub>* vectors, 5 for Release 1) of error modes.
- a keyword *NUMVECT* (Integer) specified the number of eigenmode vectors, and
- the keyword *NAXIS2* gives the length of each vector

An example of the FITS header is:

```

;-----
; EXTENSION 11: BEAM_143_DS1X143_5
;-----
XTENSION= 'BINTABLE'           / binary table extension
BITPIX   =                      8 / array data type
NAXIS    =                      2 / number of array dimensions
NAXIS1   =                   24 / length of dimension 1
NAXIS2   =                  4001 / length of dimension 2

```



```

PCOUNT      =                0 / number of group parameters
GCOUNT      =                1 / number of groups
TFIELDS     =                6 / number of table fields
TTYPE1      = 'NOMINAL '
TFORM1      = 'E           '
TTYPE2      = 'EIGEN_0 '
TFORM2      = 'E           '
TTYPE3      = 'EIGEN_1 '
TFORM3      = 'E           '
TTYPE4      = 'EIGEN_2 '
TFORM4      = 'E           '
TTYPE5      = 'EIGEN_3 '
TFORM5      = 'E           '
TTYPE6      = 'EIGEN_4 '
TFORM6      = 'E           '
EXTNAME     = 'BEAM_143_DS1X143_5' / extension name
NUMVECT     =                5 / Number of eigenvectors
END

```

### Beam Window Function Uncertainty Correlation Matrix

Two of these matrices are given, one for the frequency channels (21x21) and one for the detsets (351x351). Each is a symmetric matrix with 1-valued diagonal, made of NBEAMS\*NBEAMS blocks, each block being NMODES\*NMODES in size. Each row- (and column-) block entry relates to the B(l) model whose name is indicated in ROW\* keywords below, and the corresponding eigenmodes are stored in a HDU of the same name. The header is of the form:

```

; -----
; EXTENSION 381: CORRBEAM_DET
; -----
XTENSION= 'IMAGE ' /
EXTNAME = 'CORRBEAM_DET' /
BITPIX = -32 / IEEE single precision floating point
NAXIS = 2 /
NAXIS1 = 1755 /
NAXIS2 = 1755 /
DATE = '2012-11-23' / Creation date (CCYY-MM-DD) of FITS header
...
NDETS = 26 / number of detector assemblies
NBEAMS = 351 / number of beams = NDETS*(NDETS+1)/2
NMODES = 5 / number of eigen modes for each beam B(l)
DATAMIN = -0.979880 / minimum value (should be >=-1)
DATAMAX = 1.00000 / maximum value (should be 1)
ROW1 = 'BEAM_100-DS1x100-DS1' / block #1 on row (or column)
ROW2 = 'BEAM_100-DS1x100-DS2' / block #2 on row (or column)
ROW3 = 'BEAM_100-DS1x143-DS1' / block #3 on row (or column)
...
ROW350 = 'BEAM_857-3x857-4' / block #350 on row (or column)
ROW351 = 'BEAM_857-4x857-4' / block #351 on row (or column)

```

END

## **Additional Science products**

---

## **Data products**

---

## **Specially processed maps**

---

## **Additional catalogues**

---

## **Additional angular power spectra**

---

## **The Planck Sky Model**

---

# Ancillary data

---

## Scientific data used to generate Planck products

---

## Simulation data

---

## Mission history

---

## Survey history

---

### Pre-Programmed Pointing Lists

The Pre-Programmed Pointing Lists (PPL) are made by Planck Science Office from the Baseline Scanning Strategy with the help of the Software Planning and Performance Tool. They are sent to MOC/FD for use in making the Augmented Pre-Programmed Pointing Lists (APPL) used for commanding the spacecraft attitude.

The PPL file name is the following: YYYYMMDD\_yyyymmdd\_NNNN\_X.PPL

with YYYYMMDD = start date of the valid span of the PPL file

yyymmdd = end date of the valid span of the PPL file

NNNN = unique sequence number, in the range  $0000 \leq \text{NNNN} \leq 9999$ , incrementing sequentially throughout the mission and uniquely identifying each new PPL file that is generated (i.e. no repeated numbers and no gaps in the sequence of PPLs) o 0000-8999 reserved for PSO o 9000-9999 reserved for attitude manoeuvres generated by MOC

X = type of PPL, as follows: o R = Routine (standard 4-week PPL) o C = Contingency (3-day replanning) o L = Long-Term PPL (LTPPL) o S = Special

PPLs contain the following information in ASCII columns:

- pointing reference number
- Ecliptic longitude
- Ecliptic latitude
- nominal start time for pointing
- earliest allowed start time
- latest allowed start time
- nominal dwell time
- observation type
- comments

PPLs can be found in the Planck Legacy Archive.

---

## **Augmented Pre-Programmed Pointing Lists**

APPLs are made by MOC / Flight Dynamics using pointing information (PPLs) from the Planck Science Office.

The APPLs incorporate information about the Operational Days boundaries in order to fit pointings into each OD.

## **Attitude History Files**

The pointing history of Planck is described in the Attitude History Files (AHF) sequence. All the AHF can be found in the Planck Legacy Archive, for three different methods of computation (AHF, DHF, GHF).

The GHF are made using refined pointing information from the Fiber Optics Gyroscope.

The AHF contain the following information ordered in columns:

## **Focal plane geometry**

The Spacecraft-Instrument Alignment Matrix contains the information.....

## **Orbit file**

The orbit file is produced by the Flight Dynamics team at ESOC and contains the information of the Planck orbital history throughout the whole mission (since launch).

## **Planck operational state history**

The POSH consists of two parts:

- mission events
- state vector

# **Satellite history**

---

For PLA 2.0

## **Design and performance documentation**

The design and performance documentation can be downloaded from the "documents" tab of the Planck Legacy Archive interface.

---

# Payload design

---

## Instrument performance

---

Documentation

Spectral response per detector

Polarisation responses

Photometric responses

Main beam

$4\pi$  beams

Systematics effects

## Telescope

---

# Thermal

---

## FOG

---

## SREM

---

### Design, performance and calibration documentation

#### SREM counters

Name	Logic	Particle	Energy ( <i>MeV</i> )
TC1	D1	protons	>20
S12	D1	protons	20 - 550
S13	D1	protons	20 - 120
S14	D1	protons	20 - 27
S15	D1	protons	20 - 34
TC2	D2	protons	>39
S25	D2	ions	150 - 185
C1	D1 *D2	coinc. protons	40 - 50
C2	D1 *D2	coinc. protons	50 - 70
C3	D1 *D2	coinc. protons	70 - 120
C4	D1 *D2	coinc. protons	>130
TC3	D3	electrons	>0.5
S32	D3	electrons	0.55 - 2.3
S33	D3	protons	11 - 90
S34	D3	protons	11 - 30
PL1	D1	Dead Time	NA
PL2	D2	Dead Time	NA
PL3	D3	Dead Time	NA

## Processed data

### Description of the product

The SREM data files contain calibrated data for the different energy and particle species channels available in the SREM. Each data file contains 24 hours of data - from midnight to midnight (note this is **not** an OD) - with the date covered by the file easily identifiable through the file name.

### Pipeline

TBW

### Input Data

SREM calibrated data was produced from the SREM raw data acquired during the entire mission.

### Related Products

Data for the SREM on board Herschel can be retrieved from the Herschel Science Archive <sup>[1]</sup>.

SREM data from previous missions can be retrieved from the SREM archive <sup>[2]</sup> at the Paul Scherrer Institut (PSI).

### Data format

- **Naming convention**

The files containing the SREM calibrated data will have a name of the form SREMPlanck\_PACC\_YYYYMMDD.fits where PACC stands for Processed ACCumulated data and YYYYMMDD is the date the data in the file was acquired.

- Units
- Format

Each file contains three binary table extensions named CDFITS1, CDFITS2 and CDFITS3. The first extension contains the accumulated counts data, the second extension the labels to identify the data in the first extension and the third extension the total radiation dosis. The contents of each extension are as follows.

#### CDFITS1

Column Name	Contents	Format	Unit
<b>EPOCH</b>	vector containing 1 string with UTC for center of accumulation interval in ISO format (YYYY-MM-DDTHH:MM:SS.MMMZ)	A24	NA
<b>COUNTRATE</b>	vector containing 15 elements (1 for each channel) with counts for accumulation period identified in the EPOCH column	E15.4	$s^{-1}$
<b>ORBIT</b>	position of the SREM in the XXX frame	E15.4	$Km$
<b>ATTITUDE</b>	TBW	E15.4	NA
<b>PROT FITQUAL</b>	this is a another keyword	I1	NA
<b>ODPF</b>	this is a another keyword	E15.4	$Hz$
<b>ODPFERR</b>	this is a another keyword	E15.4	$Hz$
<b>ELEC FITQUAL</b>	this is a another keyword	I1	$Hz$
<b>ODEF</b>	this is a another keyword	E15.4	$Hz$
<b>ODEFERR</b>	this is a another keyword	E15.4	$Hz$

<b>ANISOTROPY</b>	this is a another keyword	E15.4	<i>NA</i>
<b>TEMPERATURE</b>	2 element vector containing temperature of the two detector heads at each EPOCH	E15.4	$^{\circ}\text{C}$

### CDFFITS2

Column Name	Contents	Format	Unit
<b>EPOCH</b>	this is a keyword	$Km^2$	

### CDFFITS3

Column Name	Contents	Format	Unit
<b>RADEPOCH</b>	this is a keyword	A24	$Km^2$
<b>RADFET</b>	this is a another keyword	E15.4	$Hz$

- N. Of Files

1500 (TBC)

**Note:** SREM calibrated data files where initially provided in the Common Data Format (cdf) format <sup>[3]</sup>. This has traditionally been the preferred data format for SREM on board previous ESA missions. However, as cdf is not widely used in the astrophysics community it was later agreed with the provider that fits files should also be provided. This meant taking the original cdf format and converting it to fits. The original cdf files can be retrieved from the SREM site <sup>[2]</sup> at the PSI.

### Header keywords

For data provided in the form of fits files a table containing a description of all the header keywords should be included here. The table should follow this format

Keyword Name	Description	Unit
<b>Keyword1</b>	this is a keyword	$Km^2$
<b>Keyword2</b>	this is a another keyword	$Hz$

### References

- [1] [http://herschel.esac.esa.int/Science\\_Archive.shtml](http://herschel.esac.esa.int/Science_Archive.shtml)
- [2] [http://srem.web.psi.ch/html/srem\\_home.shtml](http://srem.web.psi.ch/html/srem_home.shtml)
- [3] <http://cdf.gsfc.nasa.gov/>



# Software utilities

---

## Unit Conversion and color correction

The Unit conversion and Color correction software (UC\_CC) consists of a set of IDL procedures and functions that read the band transmission from the DPC RIMOs and perform the requested conversions. The package is delivered as a tarfile and contains a detailed instruction manual. The full list of its contents is:

```
UC_CC_v100/get_hfibolo_list.pro
UC_CC_v100/hfi_co_correction.pro
UC_CC_v100/hfi_colour_correction.pro
UC_CC_v100/hfi_lfi_test_script.pro
UC_CC_v100/hfi_read_avg_bandpass.pro
UC_CC_v100/hfi_read_bandpass.pro
UC_CC_v100/hfi_unit_conversion.pro
UC_CC_v100/lfi_read_avg_bandpass.pro
UC_CC_v100/lfi_read_bandpass.pro
UC_CC_v100/README.txt
UC_CC_v100/Instructions.pdf
```

The package is currently available on [[1]]

## References

[1] <http://externaltools.planck.fr>

---

# Appendix

---

## Appendix

---

## Acronym list

---

---

---

# References

---

## References

---

<biblio>

1. planck2012-I bibtex=@ARTICLE{planck2012-I,  
author = {Planck Collaboration I,}, title = {Planck intermediate results. I. Further validation of new Planck clusters with XMM-Newton}, journal = {A&A}, year = {2012}, volume = {543}, pages = {A102} }
  1. planck2012-II bibtex=@BOOK{planck2012-II,  
author = {Planck and AMI Collaborations,}, title = {Planck intermediate results. II. Comparison of Sunyaev-Zeldovich measurements from Planck and from the Arcminute Microkelvin Imager for 11 galaxy clusters}, journal = {Submitted to A&A}, keywords = {Astrophysics}, year = {2012}, publisher = {Submitted to A&A, [arXiv:astro-ph/1204.1318]} }
  1. planck2012-III bibtex=@BOOK{planck2012-III,  
author = {Planck Collaboration III,}, title = {Planck intermediate results. III. The relation between galaxy cluster mass and Sunyaev-Zeldovich signal}, journal = {Submitted to A&A}, keywords = {Astrophysics}, year = {2012}, publisher = {Submitted to A&A, [arXiv:astro-ph/1204.2743]} }
  1. planck2012-IV bibtex=@BOOK{planck2012-IV,  
author = {Planck Collaboration IV,}, title = {Planck intermediate results. IV. The XMM-Newton validation programme for new Planck clusters}, journal = {Submitted to A&A}, keywords = {Astrophysics}, year = {2012}, publisher = {Submitted to A&A, [arXiv:astro-ph/1205.3376]} }
  1. planck2012-V bibtex=@BOOK{planck2012-V,  
author = {Planck Collaboration V,}, title = {Planck intermediate results. V. Pressure profiles of galaxy clusters from the Sunyaev-Zeldovich effect}, journal = {Submitted to A&A}, keywords = {Astrophysics}, year = {2012}, publisher = {Submitted to A&A, [arXiv:astro-ph/1207.4061]} }
  1. planck2012-VI bibtex=@BOOK{planck2012-VI,  
author = {Planck Collaboration VI,}, title = {Planck intermediate results. VI. The dynamical structure of PLCKG214.6+37.0, a Planck discovered triple system of galaxy clusters}, journal = {Submitted to A&A}, keywords = {Astrophysics}, year = {2012}, publisher = {Submitted to A&A, [arXiv:astro-ph/1207.4009]} }
  1. planck2012-VII bibtex=@BOOK{planck2012-VII,  
author = {Planck Collaboration VII,}, title = {Planck intermediate results. VII. Statistical properties of infrared and radio extragalactic sources from the Planck Early Release Compact Source Catalogue at frequencies between 100 and 857 GHz}, journal = {Submitted to A&A}, keywords = {Astrophysics}, year = {2012}, publisher = {Submitted to A&A, [arXiv:astro-ph/1207.4706]} }
  1. planck2011-1-1 bibtex=@ARTICLE{planck2011-1.1,  
author = {Planck Collaboration I,}, title = {Planck early results. I. The Planck mission}, journal = {A&A}, year = {2011}, volume = {536}, pages = {A1} }
  1. planck2011-1-3 bibtex=@ARTICLE{planck2011-1.3,  
author = {Planck Collaboration II,}, title = {Planck early results. II. The thermal performance of Planck}, journal = {A&A}, year = {2011}, volume = {536}, pages = {A2} }
-

1. planck2011-1-4 bibtex=@ARTICLE{planck2011-1.4,  
author = {Mennella et al.}, title = {Planck early results. III. First assessment of the Low Frequency Instrument in-flight performance}, journal = {A&A}, year = {2011}, volume = {536}, pages = {A3} }
1. planck2011-1-5 bibtex=@ARTICLE{planck2011-1.5,  
author = {Planck HFI Core Team.}, title = {Planck early results. IV. First assessment of the High Frequency Instrument in-flight performance}, journal = {A&A}, year = {2011}, volume = {536}, pages = {A4} }
1. planck2011-1-6 bibtex=@ARTICLE{planck2011-1.6,  
author = {Zacchei et al.}, title = {Planck early results. V. The Low Frequency Instrument data processing}, journal = {A&A}, year = {2011}, volume = {536}, pages = {A5} }
1. planck2011-1-7 bibtex=@ARTICLE{planck2011-1.7,  
author = {Planck HFI Core Team.}, title = {Planck early results. VI. The High Frequency Instrument data processing}, journal = {A&A}, year = {2011}, volume = {536}, pages = {A6} }
1. planck2011-1-10 bibtex=@ARTICLE{planck2011-1.10,  
author = {Planck Collaboration VII.}, title = {Planck early results. VII. The Early Release Compact Source Catalogue}, journal = {A&A}, year = {2011}, volume = {536}, pages = {A7} }
1. planck2011-1-10sup bibtex=@BOOK{planck2011-1.10sup,  
author = {Planck Collaboration.}, title = {The Explanatory Supplement to the Planck Early Release Compact Source Catalogue}, keywords = {Astrophysics}, year = {2011}, publisher = {ESA} }
1. planck2011-5-1a bibtex=@ARTICLE{planck2011-5.1a,  
author = {Planck Collaboration VIII.}, title = {Planck early results. VIII. The all-sky early Sunyaev-Zeldovich cluster sample}, journal = {A&A}, year = {2011}, volume = {536}, pages = {A8} }
1. planck2011-5-1b bibtex=@ARTICLE{planck2011-5.1b,  
author = {Planck Collaboration IX.}, title = {Planck early results. IX. XMM-Newton follow-up for validation of Planck cluster candidates}, journal = {A&A}, year = {2011}, volume = {536}, pages = {A9} }
1. planck2011-5-2a bibtex=@ARTICLE{planck2011-5.2a,  
author = {Planck Collaboration X.}, title = {Planck early results. X. Statistical analysis of Sunyaev-Zeldovich scaling relations for X-ray galaxy clusters}, journal = {A&A}, year = {2011}, volume = {536}, pages = {A10} }
1. planck2011-5-2b bibtex=@ARTICLE{planck2011-5.2b,  
author = {Planck Collaboration XI.}, title = {Planck early results. XI. Calibration of the local galaxy cluster Sunyaev-Zeldovich scaling relations}, journal = {A&A}, year = {2011}, volume = {536}, pages = {A11} }
1. planck2011-5-2c bibtex=@ARTICLE{planck2011-5.2c,  
author = {Planck Collaboration XII.}, title = {Planck early results. XII. Cluster Sunyaev-Zeldovich optical Scaling relations}, journal = {A&A}, year = {2011}, volume = {536}, pages = {A12} }
1. planck2011-6-1 bibtex=@ARTICLE{planck2011-6.1,  
author = {Planck Collaboration XIII.}, title = {Planck early results. XIII. Statistical properties of extragalactic radio sources in the Planck Early Release Compact Source Catalogue}, journal = {A&A}, year = {2011}, volume = {536}, pages = {A13} }
1. planck2011-6-2 bibtex=@ARTICLE{planck2011-6.2,  
author = {Planck Collaboration XIV.}, title = {Planck early results. XIV. Early Release Compact Source Catalogue validation and extreme radio sources}, journal = {A&A}, year = {2011}, volume = {536}, pages = {A14} }
1. planck2011-6-3a bibtex=@ARTICLE{planck2011-6.3a,

author = {Planck Collaboration XV,}, title = {Planck early results. XV. Spectral energy distributions and radio continuum spectra of northern extragalactic radio sources}, journal = {A&A}, year = {2011}, volume = {536}, pages = {A15} }

1. planck2011-6-4a bibtex=@ARTICLE{planck2011-6.4a,

author = {Planck Collaboration XVI,}, title = {Planck early results. XVI. The Planck view of nearby galaxies}, journal = {A&A}, year = {2011}, volume = {536}, pages = {A16} }

1. planck2011-6-4b bibtex=@ARTICLE{planck2011-6.4b,

author = {Planck Collaboration XVII,}, title = {Planck early results. XVII. Origin of the submillimetre excess dust emission in the Magellanic Clouds}, journal = {A&A}, year = {2011}, volume = {536}, pages = {A17} }

1. planck2011-6-6 bibtex=@ARTICLE{planck2011-6.6,

author = {Planck Collaboration XVIII,}, title = {Planck early results. XVIII. The power spectrum of cosmic infrared background anisotropies}, journal = {A&A}, year = {2011}, volume = {536}, pages = {A18} }

1. planck2011-7-0 bibtex=@ARTICLE{planck2011-7.0,

author = {Planck Collaboration XIX,}, title = {Planck early results. XIX. All-sky temperature and dust optical depth from Planck and IRAS --- constraints on the dark gas in our Galaxy}, journal = {A&A}, year = {2011}, volume = {536}, pages = {A19} }

1. planck2011-7-2 bibtex=@ARTICLE{planck2011-7.2,

author = {Planck Collaboration XX,}, title = {Planck early results. XX. New light on anomalous microwave emission from spinning dust grains}, journal = {A&A}, year = {2011}, volume = {536}, pages = {A20} }

1. planck2011-7-3 bibtex=@ARTICLE{planck2011-7.3,

author = {Planck Collaboration XXI,}, title = {Planck early results. XXI. Properties of the interstellar medium in the Galactic plane}, journal = {A&A}, year = {2011}, volume = {536}, pages = {A21} }

1. planck2011-7-7a bibtex=@ARTICLE{planck2011-7.7a,

author = {Planck Collaboration XXII,}, title = {Planck early results. XXII. The submillimetre properties of a sample of Galactic cold clumps}, journal = {A&A}, year = {2011}, volume = {536}, pages = {A22} }

1. planck2011-7-7b bibtex=@ARTICLE{planck2011-7.7b,

author = {Planck Collaboration XXIII,}, title = {Planck early results. XXIII. The Galactic cold core population revealed by the first all-sky survey}, journal = {A&A}, year = {2011}, volume = {536}, pages = {A23} }

1. planck2011-7-12 bibtex=@ARTICLE{planck2011-7.12,

author = {Planck Collaboration XXIV,}, title = {Planck early results. XXIV. Dust in the diffuse interstellar medium and the Galactic halo}, journal = {A&A}, year = {2011}, volume = {536}, pages = {A24} }

1. planck2011-7-13 bibtex=@ARTICLE{planck2011-7.13,

author = {Planck Collaboration XXV,}, title = {Planck early results. XXV. Thermal dust in nearby molecular clouds}, journal = {A&A}, year = {2011}, volume = {536}, pages = {A25} }

1. planck2011-5-1c bibtex=@ARTICLE{planck2011-5.1c,

author = {Planck Collaboration XXVI,}, title = {Planck early results. XXVI. Detection with Planck and confirmation by XMM-Newton of PLCK G266.6-27.3, an exceptionally X-ray luminous and massive galaxy cluster at  $z \approx 1$ }, journal = {A&A}, year = {2011}, volume = {536}, pages = {A26} }

1. planck2011-6-3b bibtex=@BOOK{planck2011-6.3b,

author = {Giommi et al.}, title = {Simultaneous Planck, Swift, and Fermi observations of X-ray and gamma-ray selected blazars}, journal = {Submitted to A&A}, keywords = {Astrophysics}, year = {2011}, publisher = {Submitted to A&A, [arXiv:astro-ph/1108.1114]} }

1. ade2010 bibtex=@ARTICLE{ade2010,

author = {Ade, P. A. R. and Savini, G. and Sudiwala, R. and Tucker, C. and Catalano, A. and Church, S. and Colgan, R. and Desert, F. X. and Gleeson, E. and Jones, W. C. and Lamarre, J.-M. and Lange, A. and Longval, Y. and Maffei, B. and Murphy, J. A. and Noviello, F. and Pajot, F. and Puget, J.-L. and Ristorcelli, I. and Woodcraft, A. and Yurchenko, V.}, title = {Planck pre-launch status: The optical architecture of the HFI}, journal = {A&A}, keywords = {cosmic microwave background, space vehicles: instruments, instrumentation: detectors, instrumentation: polarimeters, submillimeter: general, techniques: photometric}, year = {2010}, month = {sep}, volume = {520}, pages = {A11+}, doi = {10.1051/0004-6361/200913039}, adsurl = {http://adsabs.harvard.edu/abs/2010A%26A..520A..11A}, adsnote = {Provided by the SAO/NASA Astrophysics Data System} }

1. bersanelli2010 bibtex=@ARTICLE{bersanelli2010,

author = {Bersanelli, M. and Mandolesi, N. and Butler, R. C. and Mennella, A. and Villa, F. and Aja, B. and Artal, E. and Artina, E. and Baccigalupi, C. and Balasini, M. and Baldan, G. and Banday, A. and Bastia, P. and Battaglia, P. and Bernardino, T. and Blackhurst, E. and Boschini, L. and Burigana, C. and Cafagna, G. and Cappellini, B. and Cavaliere, F. and Colombo, F. and Crone, G. and Cuttaia, F. and D'Arcangelo, O. and Danese, L. and Davies, R. D. and Davis, R. J. and de Angelis, L. and de Gasperis, G. C. and de La Fuente, L. and de Rosa, A. and de Zotti, G. and Falvella, M. C. and Ferrari, F. and Ferretti, R. and Figini, L. and Fogliani, S. and Franceschet, C. and Franceschi, E. and Gaier, T. and Garavaglia, S. and Gomez, F. and Gorski, K. and Gregorio, A. and Guzzi, P. and Herreros, J. M. and Hildebrandt, S. R. and Hoyland, R. and Hughes, N. and Janssen, M. and Jukkala, P. and Kettle, D. and Kilpiä, V. H. and Laaninen, M. and Lapolla, P. M. and Lawrence, C. R. and Lawson, D. and Leahy, J. P. and Leonardi, R. and Leutenegger, P. and Levin, S. and Lilje, P. B. and Lowe, S. R. and Lubin, P. M. and Maino, D. and Malaspina, M. and Maris, M. and Marti-Canales, J. and Martinez-Gonzalez, E. and Mediavilla, A. and Meinhold, P. and Miccolis, M. and Morgante, G. and Natoli, P. and Nesti, R. and Pagan, L. and Paine, C. and Partridge, B. and Pascual, J. P. and Pasian, F. and Pearson, D. and Pecora, M. and Perrotta, F. and Platania, P. and Pospieszalski, M. and Poutanen, T. and Prina, M. and Rebolo, R. and Roddis, N. and Rubiño-Martin, J. A. and Salmon, M. J. and Sandri, M. and Seiffert, M. and Silvestri, R. and Simonetto, A. and Sjoman, P. and Smoot, G. F. and Sozzi, C. and Stringhetti, L. and Taddei, E. and Tauber, J. and Terenzi, L. and Tomasi, M. and Tuovinen, J. and Valenziano, L. and Varis, J. and Vittorio, N. and Wade, L. A. and Wilkinson, A. and Winder, F. and Zacchei, A. and Zonca, A.}, title = {Planck pre-launch status: Design and description of the Low Frequency Instrument}, journal = {A&A}, archivePrefix = {arXiv}, eprint = {1001.3321}, primaryClass = {astro-ph.IM}, keywords = {cosmic microwave background, cosmology: observations, space vehicles: instruments}, year = {2010}, month = {sep}, volume = {520}, pages = {A4+}, doi = {10.1051/0004-6361/200912853}, adsurl = {http://adsabs.harvard.edu/abs/2010A%26A...520A..4B}, adsnote = {Provided by the SAO/NASA Astrophysics Data System} }

1. lamarre2010 bibtex=@ARTICLE{lamarre2010,

author = {Lamarre, J.-M. and Puget, J.-L. and Ade, P. A. R. and Bouchet, F. and Guyot, G. and Lange, A. E. and Pajot, F. and Arondel, A. and Benabed, K. and Beney, J.-L. and Benoît, A. and Bernard, J.-P. and Bhatia, R. and Blanc, Y. and Bock, J. J. and Bréelle, E. and Bradshaw, T. W. and Camus, P. and Catalano, A. and Charra, J. and Charra, M. and Church, S. E. and Couchot, F. and Coulais, A. and Crill, B. P. and Crook, M. R. and Dassas, K. and de Bernardis, P. and Delabrouille, J. and de Marcillac, P. and Delouis, J.-M. and Désert, F.-X. and Dumesnil, C. and Dupac, X. and Efstathiou, G. and Eng, P. and Evesque, C. and Fourmond, J.-J. and Ganga, K. and Giard, M. and Gispert, R. and Guglielmi, L. and Haissinski, J. and Henrot-Versillé, S. and Hivon, E. and Holmes, W. A. and Jones, W. C. and Koch, T. C. and Lagardère, H. and Lami, P. and Landé, J. and Leriche, B. and Leroy, C. and Longval, Y. and Macías-Pérez, J. F. and Maciaszek, T. and Maffei, B. and Mansoux, B. and Marty, C. and Masi, S. and Mercier, C. and Miville-Deschênes, M.-A. and Moneti, A. and Montier, L. and Murphy, J. A. and Narbonne, J. and Nexon, M. and Paine, C. G. and Pahn, J. and Perdureau, O. and Piacentini, F. and Piat, M. and Plaszczynski, S. and Pointecouteau, E. and Pons, R. and Ponthieu, N. and Prunet, S. and Rambaud, D. and Recouvreur, G. and Renault, C. and Ristorcelli, I. and Rosset, C. and Santos, D. and Savini, G. and Serra, G. and Stassi, P. and Sudiwala, R. V. and

Sygné, J.-F. and Tauber, J. A. and Torre, J.-P. and Tristram, M. and Vibert, L. and Woodcraft, A. and Yurchenko, V. and Yvon, D. }, title = {Planck pre-launch status: The HFI instrument, from specification to actual performance}, journal = {A&A}, keywords = {cosmic microwave background, space vehicles: instruments, submillimeter: general, techniques: photometric, techniques: polarimetric}, year = {2010}, month = {sep}, volume = {520}, pages = {A9+}, doi = {10.1051/0004-6361/200912975}, adsurl = {http://adsabs.harvard.edu/abs/2010A%26A...520A...9L}, adsnote = {Provided by the SAO/NASA Astrophysics Data System} }

1. leahy2010 bibtex=@ARTICLE{leahy2010,

author = {Leahy, J. P. and Bersanelli, M. and D'Arcangelo, O. and Ganga, K. and Leach, S. M. and Moss, A. and Keihänen, E. and Keskitalo, R. and Kurki-Suonio, H. and Poutanen, T. and Sandri, M. and Scott, D. and Tauber, J. and Valenziano, L. and Villa, F. and Wilkinson, A. and Zonca, A. and Baccigalupi, C. and Borrill, J. and Butler, R. C. and Cuttaia, F. and Davis, R. J. and Frailis, M. and Francheschi, E. and Galeotta, S. and Gregorio, A. and Leonardi, R. and Mandolesi, N. and Maris, M. and Meinhold, P. and Mendes, L. and Mennella, A. and Morgante, G. and Prezeau, G. and Rocha, G. and Stringhetti, L. and Terenzi, L. and Tomasi, M. }, title = {Planck pre-launch status: Expected LFI polarisation capability}, journal = {A&A}, keywords = {polarization, instrumentation: polarimeters, space vehicles: instruments, techniques: polarimetric, cosmic microwave background}, year = {2010}, month = {sep}, volume = {520}, pages = {A8+}, doi = {10.1051/0004-6361/200912855}, adsurl = {http://adsabs.harvard.edu/abs/2010A%26A...520A...8L}, adsnote = {Provided by the SAO/NASA Astrophysics Data System} }

1. maffei2010 bibtex=@ARTICLE{maffei2010,

author = {Maffei, B. and Noviello, F. and Murphy, J. A. and Ade, P. A. R. and Lamarre, J.-M. and Bouchet, F. R. and Brossard, J. and Catalano, A. and Colgan, R. and Gispert, R. and Gleeson, E. and Haynes, C. V. and Jones, W. C. and Lange, A. E. and Longval, Y. and McAuley, I. and Pajot, F. and Peacocke, T. and Pisano, G. and Puget, J.-L. and Ristorcelli, I. and Savini, G. and Sudiwala, R. and Wylde, R. J. and Yurchenko, V.}, title = {Planck pre-launch status: HFI beam expectations from the optical optimisation of the focal plane}, journal = {A&A}, keywords = {space vehicles: instruments, submillimeter: general, telescopes, cosmic microwave background, instrumentation: polarimeters, instrumentation: detectors}, year = {2010}, month = {sep}, volume = {520}, pages = {A12+}, doi = {10.1051/0004-6361/200912999}, adsurl = {http://adsabs.harvard.edu/abs/2010A%26A...520A...12M}, adsnote = {Provided by the SAO/NASA Astrophysics Data System} }

1. mandolesi2010 bibtex=@ARTICLE{mandolesi2010,

author = {Mandolesi, N. and Bersanelli, M. and Butler, R. C. and Artal, E. and Baccigalupi, C. and Balbi, A. and Banday, A. J. and Barreiro, R. B. and Bartelmann, M. and Bennett, K. and Bhandari, P. and Bonaldi, A. and Borrill, J. and Bremer, M. and Burigana, C. and Bowman, R. C. and Cabella, P. and Cantalupo, C. and Cappellini, B. and Courvoisier, T. and Crone, G. and Cuttaia, F. and Danese, L. and D'Arcangelo, O. and Davies, R. D. and Davis, R. J. and de Angelis, L. and de Gasperis, G. and de Rosa, A. and de Troia, G. and de Zotti, G. and Dick, J. and Dickinson, C. and Diego, J. M. and Donzelli, S. and Dörl, U. and Dupac, X. and Enßlin, T. A. and Eriksen, H. K. and Falvella, M. C. and Finelli, F. and Frailis, M. and Franceschi, E. and Gaier, T. and Galeotta, S. and Gasparo, F. and Giardino, G. and Gomez, F. and Gonzalez-Nuevo, J. and Górski, K. M. and Gregorio, A. and Gruppuso, A. and Hansen, F. and Hell, R. and Herranz, D. and Herreros, J. M. and Hildebrandt, S. and Hovest, W. and Hoyland, R. and Huppenberger, K. and Janssen, M. and Jaffe, T. and Keihänen, E. and Keskitalo, R. and Kisner, T. and Kurki-Suonio, H. and Lähteenmäki, A. and Lawrence, C. R. and Leach, S. M. and Leahy, J. P. and Leonardi, R. and Levin, S. and Lilje, P. B. and López-Caniego, M. and Lowe, S. R. and Lubin, P. M. and Maino, D. and Malaspina, M. and Maris, M. and Marti-Canales, J. and Martinez-Gonzalez, E. and Massardi, M. and Matarrese, S. and Matthai, F. and Meinhold, P. and Melchiorri, A. and Mendes, L. and Mennella, A. and Morgante, G. and Morigi, G. and Morisset, N. and Moss, A. and Nash, A. and Natoli, P. and Nesti, R. and Paine, C. and Partridge, B. and Pasian, F. and Passvogel, T. and Pearson, D. and Pérez-Cuevas, L. and Perrotta, F. and Polenta, G. and Popa, L. A. and Poutanen, T. and Prezeau, G. and Prina, M. and Rachen, J. P. and Rebolo, R. and Reinecke, M. and Ricciardi, S. and Riller, T. and Rocha, G. and

Roddis, N. and Rohlfs, R. and Rubiño-Martin, J. A. and Salerno, E. and Sandri, M. and Scott, D. and Seiffert, M. and Silk, J. and Simonetto, A. and Smoot, G. F. and Sozzi, C. and Sternberg, J. and Stivoli, F. and Stringhetti, L. and Tauber, J. and Terenzi, L. and Tomasi, M. and Tuovinen, J. and Türlér, M. and Valenziano, L. and Varis, J. and Vielva, P. and Villa, F. and Vittorio, N. and Wade, L. and White, M. and White, S. and Wilkinson, A. and Zacchei, A. and Zonca, A. }, title = {Planck pre-launch status: The Planck-LFI programme}, journal = {A&A}, archivePrefix = {arXiv}, eprint = {1001.2657}, primaryClass = {astro-ph.CO}, keywords = {cosmic microwave background, space vehicles: instruments, instrumentation: detectors, instrumentation: polarimeters, submillimeter: general, telescopes}, year = {2010}, month = {sep}, volume = {520}, pages = {A3+}, doi = {10.1051/0004-6361/200912837}, adsurl = {http://adsabs.harvard.edu/abs/2010A%26A...520A...3M}, adsnote = {Provided by the SAO/NASA Astrophysics Data System }

1. mennella2010 bibtex=@ARTICLE{mennella2010,

author = {Mennella, A. and Bersanelli, M. and Butler, R. C. and Cuttaia, F. and D'Arcangelo, O. and Davis, R. J. and Frailis, M. and Galeotta, S. and Gregorio, A. and Lawrence, C. R. and Leonardi, R. and Lowe, S. R. and Mandolesi, N. and Maris, M. and Meinhold, P. and Mendes, L. and Morgante, G. and Sandri, M. and Stringhetti, L. and Terenzi, L. and Tomasi, M. and Valenziano, L. and Villa, F. and Zacchei, A. and Zonca, A. and Balasini, M. and Franceschet, C. and Battaglia, P. and Lapolla, P. M. and Leutenegger, P. and Miccolis, M. and Pagan, L. and Silvestri, R. and Aja, B. and Artal, E. and Baldan, G. and Bastia, P. and Bernardino, T. and Boschini, L. and Cafagna, G. and Cappellini, B. and Cavaliere, F. and Colombo, F. and de La Fuente, L. and Edgeley, J. and Falvella, M. C. and Ferrari, F. and Fogliani, S. and Franceschi, E. and Gaier, T. and Gomez, F. and Herrerros, J. M. and Hildebrandt, S. and Hoyland, R. and Hughes, N. and Jukkala, P. and Kettle, D. and Laaninen, M. and Lawson, D. and Leahy, P. and Levin, S. and Lilje, P. B. and Maino, D. and Malaspina, M. and Manzato, P. and Marti-Canales, J. and Martinez-Gonzalez, E. and Mediavilla, A. and Pasian, F. and Pascual, J. P. and Pecora, M. and Peres-Cuevas, L. and Platania, P. and Pospieszalsky, M. and Poutanen, T. and Rebolo, R. and Roddis, N. and Salmon, M. and Seiffert, M. and Simonetto, A. and Sozzi, C. and Tauber, J. and Tuovinen, J. and Varis, J. and Wilkinson, A. and Winder, F. }, title = {Planck pre-launch status: Low Frequency Instrument calibration and expected scientific performance}, journal = {A&A}, archivePrefix = {arXiv}, eprint = {1001.4562}, primaryClass = {astro-ph.IM}, keywords = {cosmic microwave background, telescopes, space vehicles: instruments, instrumentation: detectors, instrumentation: polarimeters, submillimeter: general}, year = {2010}, month = {sep}, volume = {520}, pages = {A5+}, doi = {10.1051/0004-6361/200912849}, adsurl = {http://adsabs.harvard.edu/abs/2010A%26A...520A...5M}, adsnote = {Provided by the SAO/NASA Astrophysics Data System }

1. pajot2010 bibtex=@ARTICLE{pajot2010,

author = {Pajot, F. and Ade, P. A. R. and Beney, J.-L. and Bréelle, E. and Broszkiewicz, D. and Camus, P. and Carabétian, C. and Catalano, A. and Chardin, A. and Charra, M. and Charra, J. and Cizeron, R. and Couchot, F. and Coulais, A. and Crill, B. P. and Dassas, K. and Daubin, J. and de Bernardis, P. and de Marcillac, P. and Delouis, J.-M. and Désert, F.-X. and Duret, P. and Eng, P. and Evesque, C. and Fourmond, J.-J. and Fran&ccedil;ois, S. and Giard, M. and Giraud-Héraud, Y. and Guglielmi, L. and Guyot, G. and Haissinski, J. and Henrot-Versillé, S. and Hervier, V. and Holmes, W. and Jones, W. C. and Lamarre, J.-M. and Lami, P. and Lange, A. E. and Lefebvre, M. and Leriche, B. and Leroy, C. and Macias-Perez, J. and Maciaszek, T. and Maffei, B. and Mahendran, A. and Mansoux, B. and Marty, C. and Masi, S. and Mercier, C. and Miville-Deschenes, M.-A. and Montier, L. and Nicolas, C. and Noviello, F. and Perdureau, O. and Piacentini, F. and Piat, M. and Plaszczynski, S. and Pointecouteau, E. and Pons, R. and Ponthieu, N. and Puget, J.-L. and Rambaud, D. and Renault, C. and Renault, J.-C. and Rioux, C. and Ristorcelli, I. and Rosset, C. and Savini, G. and Sudiwala, R. and Torre, J.-P. and Tristram, M. and Vallée, D. and Veneziani, M. and Yvon, D.}, title = {Planck pre-launch status: HFI ground calibration}, journal = {A&A}, keywords = {cosmic microwave background, space vehicles: instruments, submillimeter: general}, year = {2010}, month = {sep}, volume = {520}, pages = {A10+}, doi = {10.1051/0004-6361/200913203}, adsurl = {http://adsabs.harvard.edu/abs/2010A%26A...520A...10P}, adsnote = {Provided by the SAO/NASA Astrophysics Data



System} }

1. rosset2010 bibtex=@ARTICLE{rosset2010,

author = {Rosset, C. and Tristram, M. and Ponthieu, N. and Ade, P. and Aumont, J. and Catalano, A. and Conversi, L. and Couchot, F. and Crill, B. P. and Désert, F.-X. and Ganga, K. and Giard, M. and Giraud-Héraud, Y. and Haïssinski, J. and Henrot-Versillé, S. and Holmes, W. and Jones, W. C. and Lamarre, J.-M. and Lange, A. and Leroy, C. and Macías-Pérez, J. and Maffei, B. and de Marcillac, P. and Miville-Deschênes, M.-A. and Montier, L. and Noviello, F. and Pajot, F. and Perdereau, O. and Piacentini, F. and Piat, M. and Plaszczyński, S. and Pointecouteau, E. and Puget, J.-L. and Ristorcelli, I. and Savini, G. and Sudiwala, R. and Veneziani, M. and Yvon, D.}, title = {Planck pre-launch status: High Frequency Instrument polarization calibration}, journal = {A&A}, archivePrefix = {arXiv}, eprint = {1004.2595}, primaryClass = {astro-ph.CO}, keywords = {space vehicles: instruments, techniques: polarimetric, instrumentation: polarimeters, instrumentation: detectors, cosmic microwave background, submillimeter: general}, year = {2010}, month = {sep}, volume = {520}, pages = {A13+}, doi = {10.1051/0004-6361/200913054}, adsurl = {http://adsabs.harvard.edu/abs/2010A%26A...520A..13R}, adsnote = {Provided by the SAO/NASA Astrophysics Data System} }

1. sandri2010 bibtex=@ARTICLE{sandri2010,

author = {Sandri, M. and Villa, F. and Bersanelli, M. and Burigana, C. and Butler, R. C. and D'Arcangelo, O. and Figini, L. and Gregorio, A. and Lawrence, C. R. and Maino, D. and Mandolesi, N. and Maris, M. and Nesti, R. and Perrotta, F. and Platania, P. and Simonetto, A. and Sozzi, C. and Tauber, J. and Valenziano, L.}, title = {Planck pre-launch status: Low Frequency Instrument optics}, journal = {A&A}, keywords = {cosmic microwave background, space vehicles: instruments, instrumentation: detectors, submillimeter: general, telescopes}, year = {2010}, month = {sep}, volume = {520}, pages = {A7+}, doi = {10.1051/0004-6361/200912891}, adsurl = {http://adsabs.harvard.edu/abs/2010A%26A...520A...7S}, adsnote = {Provided by the SAO/NASA Astrophysics Data System} }

1. tauber2010a bibtex=@ARTICLE{tauber2010a,

author = {Tauber, J. A. and Mandolesi, N. and Puget, J.-L. and Banos, T. and Bersanelli, M. and Bouchet, F. R. and Butler, R. C. and Charra, J. and Crone, G. and Dodsworth, J. and et al.}, title = {Planck pre-launch status: The Planck mission}, journal = {A&A}, keywords = {cosmic microwave background, space vehicles: instruments, instrumentation: detectors, instrumentation: polarimeters, submillimeter: general, radio continuum: general}, year = {2010}, month = {sep}, volume = {520}, pages = {A1+}, doi = {10.1051/0004-6361/200912983}, adsurl = {http://adsabs.harvard.edu/abs/2010A%26A...520A...1T}, adsnote = {Provided by the SAO/NASA Astrophysics Data System} }

1. tauber2010b bibtex=@ARTICLE{tauber2010b,

author = {Tauber, J. A. and Norgaard-Nielsen, H. U. and Ade, P. A. R. and Amiri Parian, J. and Banos, T. and Bersanelli, M. and Burigana, C. and Chamballu, A. and de Chambure, D. and Christensen, P. R. and Corre, O. and Cozzani, A. and Crill, B. and Crone, G. and D'Arcangelo, O. and Daddato, R. and Doyle, D. and Dubruel, D. and Forma, G. and Hills, R. and Huppenberger, K. and Jaffe, A. H. and Jessen, N. and Kletzkine, P. and Lamarre, J. M. and Leahy, J. P. and Longval, Y. and de Maagt, P. and Maffei, B. and Mandolesi, N. and Martí-Canales, J. and Martín-Polegre, A. and Martin, P. and Mendes, L. and Murphy, J. A. and Nielsen, P. and Noviello, F. and Paquay, M. and Peacocke, T. and Ponthieu, N. and Pontoppidan, K. and Ristorcelli, I. and Riti, J.-B. and Rolo, L. and Rosset, C. and Sandri, M. and Savini, G. and Sudiwala, R. and Tristram, M. and Valenziano, L. and van der Vorst, M. and van't Klooster, K. and Villa, F. and Yurchenko, V.}, title = {Planck pre-launch status: The optical system}, journal = {A&A}, keywords = {cosmic microwave background, space vehicles: instruments, instrumentation: detectors, instrumentation: polarimeters, submillimeter: general, telescopes}, year = {2010}, month = {sep}, volume = {520}, pages = {A2+}, doi = {10.1051/0004-6361/200912911}, adsurl = {http://adsabs.harvard.edu/abs/2010A%26A...520A...2T}, adsnote = {Provided by the SAO/NASA Astrophysics Data System} }

1. villa2010 bibtex=@ARTICLE{villa2010,

author = {Villa, F. and Terenzi, L. and Sandri, M. and Meinhold, P. and Poutanen, T. and Battaglia, P. and Franceschet, C. and Hughes, N. and Laaninen, M. and Lapolla, P. and Bersanelli, M. and Butler, R. C. and Cuttaia, F. and D'Arcangelo, O. and Frailis, M. and Franceschi, E. and Galeotta, S. and Gregorio, A. and Leonardi, R. and Lowe, S. R. and Mandolesi, N. and Maris, M. and Mendes, L. and Mennella, A. and Morgante, G. and Stringhetti, L. and Tomasi, M. and Valenziano, L. and Zacchei, A. and Zonca, A. and Aja, B. and Artal, E. and Balasini, M. and Bernardino, T. and Blackhurst, E. and Boschini, L. and Cappellini, B. and Cavaliere, F. and Colin, A. and Colombo, F. and Davis, R. J. and de La Fuente, L. and Edgeley, J. and Gaier, T. and Galtress, A. and Hoyland, R. and Jukkala, P. and Kettle, D. and Kilpia, V.-H. and Lawrence, C. R. and Lawson, D. and Leahy, J. P. and Leutenegger, P. and Levin, S. and Maino, D. and Malaspina, M. and Mediavilla, A. and Miccolis, M. and Pagan, L. and Pascual, J. P. and Pasian, F. and Pecora, M. and Pospieszalski, M. and Roddis, N. and Salmon, M. J. and Seiffert, M. and Silvestri, R. and Simonetto, A. and Sjoman, P. and Sozzi, C. and Tuovinen, J. and Varis, J. and Wilkinson, A. and Winder, F.}, title = {Planck pre-launch status: Calibration of the Low Frequency Instrument flight model radiometers}, journal = {A&A}, archivePrefix = {arXiv}, eprint = {1005.2541}, primaryClass = {astro-ph.IM}, keywords = {cosmic microwave background, space vehicles: instruments, instrumentation: detectors, techniques: miscellaneous}, year = {2010}, month = {sep}, volume = {520}, pages = {A6+}, doi = {10.1051/0004-6361/200912860}, adsurl = {http://adsabs.harvard.edu/abs/2010A%26A...520A...6V}, adsnote = {Provided by the SAO/NASA Astrophysics Data System} }

1. artal2009 bibtex=@ARTICLE{artal2009,

author = {Artal, E. and Aja, B. and de la Fuente, M. L. and Pascual, J. P. and Mediavilla, A. and Martinez-Gonzalez, E. and Pradell, L. and de Paco, P. and Bara, M. and Blanco, E. and García, E. and Davis, R. and Kettle, D. and Roddis, N. and Wilkinson, A. and Bersanelli, M. and Mennella, A. and Tomasi, M. and Butler, R. C. and Cuttaia, F. and Mandolesi, N. and Stringhetti, L.}, title = {LFI 30 and 44 GHz receivers Back-End Modules}, journal = {Journal of Instrumentation}, archivePrefix = {arXiv}, eprint = {1001.4771}, primaryClass = {astro-ph.IM}, year = {2009}, month = {dec}, volume = {4}, pages = {2003-+}, doi = {10.1088/1748-0221/4/12/T12003}, adsurl = {http://adsabs.harvard.edu/abs/2009JInst...4T2003A}, adsnote = {Provided by the SAO/NASA Astrophysics Data System} }

1. battaglia2009 bibtex=@ARTICLE{battaglia2009,

author = {Battaglia, P. and Franceschet, C. and Zonca, A. and Bersanelli, M. and Butler, R. C. and D'Arcangelo, O. and Davis, R. J. and Galeotta, S. and Guzzi, P. and Hoyland, R. and Hughes, N. and Jukkala, P. and Kettle, D. and Laaninen, M. and Leonardi, R. and Maino, D. and Mandolesi, N. and Meinhold, P. and Mennella, A. and Platania, P. and Terenzi, L. and Tuovinen, J. and Varis, J. and Villa, F. and Wilkinson, A.}, title = {Advanced modelling of the Planck-LFI radiometers}, journal = {Journal of Instrumentation}, archivePrefix = {arXiv}, eprint = {1001.4659}, primaryClass = {astro-ph.IM}, year = {2009}, month = {dec}, volume = {4}, pages = {2014-+}, doi = {10.1088/1748-0221/4/12/T12014}, adsurl = {http://adsabs.harvard.edu/abs/2009JInst...4T2014B}, adsnote = {Provided by the SAO/NASA Astrophysics Data System} }

1. cuttaia2009 bibtex=@ARTICLE{cuttaia2009,

author = {Cuttaia, F. and Mennella, A. and Stringhetti, L. and Maris, M. and Terenzi, L. and Tomasi, M. and Villa, F. and Bersanelli, M. and Butler, R. C. and Cappellini, B. and Cuevas, L. P. and D'Arcangelo, O. and Davis, R. and Frailis, M. and Franceschet, C. and Franceschi, E. and Gregorio, A. and Hoyland, R. and Leonardi, R. and Lowe, S. and Mandolesi, N. and Meinhold, P. and Mendes, L. and Roddis, N. and Sandri, M. and Valenziano, L. and Wilkinson, A. and Zacchei, A. and Zonca, A. and Battaglia, P. and De Nardo, S. and Grassi, S. and Lapolla, M. and Leutenegger, P. and Miccolis, M. and Silvestri, R.}, title = {Planck-LFI radiometers tuning}, journal = {Journal of Instrumentation}, archivePrefix = {arXiv}, eprint = {1001.4648}, primaryClass = {astro-ph.IM}, year = {2009}, month = {dec}, volume = {4}, pages = {2013-+}, doi = {10.1088/1748-0221/4/12/T12013}, adsurl = {http://adsabs.harvard.edu/abs/2009JInst...4T2013C}, adsnote = {Provided by the SAO/NASA Astrophysics Data System} }

System} }

1. darcangelo2009a bibtex=@ARTICLE{d'arcangelo2009a,

author = {D'Arcangelo, O. and Figini, L. and Simonetto, A. and Villa, F. and Pecora, M. and Battaglia, P. and Bersanelli, M. and Butler, R. C. and Cuttaia, F. and Garavaglia, S. and Guzzi, P. and Mandolesi, N. and Mennella, A. and Morgante, G. and Pagan, L. and Valenziano, L. }, title = {The Planck-LFI flight model composite waveguides}, journal = {Journal of Instrumentation}, archivePrefix = {arXiv}, eprint = {1001.4711}, primaryClass = {astro-ph.IM}, year = {2009}, month = {dec}, volume = {4}, pages = {2007-+}, doi = {10.1088/1748-0221/4/12/T12007}, adsurl = {http://adsabs.harvard.edu/abs/2009JInst...4T2007D}, adsnote = {Provided by the SAO/NASA Astrophysics Data System} }

1. darcangelo2009b bibtex=@ARTICLE{d'arcangelo2009b,

author = {D'Arcangelo, O. and Simonetto, A. and Figini, L. and Pagana, E. and Villa, F. and Pecora, M. and Battaglia, P. and Bersanelli, M. and Butler, R. C. and Garavaglia, S. and Guzzi, P. and Mandolesi, N. and Sozzi, C.}, title = {The Planck-LFI flight model ortho-mode transducers}, journal = {Journal of Instrumentation}, archivePrefix = {arXiv}, eprint = {1001.4686}, primaryClass = {astro-ph.IM}, year = {2009}, month = {dec}, volume = {4}, pages = {2005-+}, doi = {10.1088/1748-0221/4/12/T12005}, adsurl = {http://adsabs.harvard.edu/abs/2009JInst...4T2005D}, adsnote = {Provided by the SAO/NASA Astrophysics Data System} }

1. davis2009 bibtex=@ARTICLE{davis2009,

author = {Davis, R. J. and Wilkinson, A. and Davies, R. D. and Winder, W. F. and Roddis, N. and Blackhurst, E. J. and Lawson, D. and Lowe, S. R. and Baines, C. and Butlin, M. and Galtress, A. and Shepherd, D. and Aja, B. and Artal, E. and Bersanelli, M. and Butler, R. C. and Castelli, C. and Cuttaia, F. and D'Arcangelo, O. and Gaier, T. and Hoyland, R. and Kettle, D. and Leonardi, R. and Mandolesi, N. and Mennella, A. and Meinhold, P. and Pospieszalski, M. and Stringhetti, L. and Tomasi, M. and Valenziano, L. and Zonca, A.}, title = {Design, development and verification of the 30 and 44 GHz front-end modules for the Planck Low Frequency Instrument}, journal = {Journal of Instrumentation}, archivePrefix = {arXiv}, eprint = {1001.4743}, primaryClass = {astro-ph.IM}, year = {2009}, month = {dec}, volume = {4}, pages = {2002-+}, doi = {10.1088/1748-0221/4/12/T12002}, adsurl = {http://adsabs.harvard.edu/abs/2009JInst...4T2002D}, adsnote = {Provided by the SAO/NASA Astrophysics Data System} }

1. frailis2009 bibtex=@ARTICLE{frailis2009,

author = {Frailis, M. and Maris, M. and Zacchei, A. and Morisset, N. and Rohlf, R. and Meharga, M. and Binko, P. and Türler, M. and Galeotta, S. and Gasparo, F. and Franceschi, E. and Butler, R. C. and D'Arcangelo, O. and Fogliani, S. and Gregorio, A. and Lowe, S. R. and Maggio, G. and Malaspina, M. and Mandolesi, N. and Manzato, P. and Pasian, F. and Perrotta, F. and Sandri, M. and Terenzi, L. and Tomasi, M. and Zonca, A.}, title = {A systematic approach to the Planck LFI end-to-end test and its application to the DPC Level 1 pipeline}, journal = {Journal of Instrumentation}, archivePrefix = {arXiv}, eprint = {1001.4838}, primaryClass = {astro-ph.IM}, year = {2009}, month = {dec}, volume = {4}, pages = {2021-+}, doi = {10.1088/1748-0221/4/12/T12021}, adsurl = {http://adsabs.harvard.edu/abs/2009JInst...4T2021F}, adsnote = {Provided by the SAO/NASA Astrophysics Data System} }

1. herreros2009 bibtex=@ARTICLE{herreros2009,

author = {Herreros, J. M. and Gómez, M. F. and Rebolo, R. and Chulani, H. and Rubiño-Martin, J. A. and Hildebrandt, S. R. and Bersanelli, M. and Butler, R. C. and Miccolis, M. and Peña, A. and Pereira, M. and Torrero, F. and Franceschet, C. and López, M. and Alcalá, C.}, title = {The Planck-LFI Radiometer Electronics Box Assembly}, journal = {Journal of Instrumentation}, archivePrefix = {arXiv}, eprint = {1001.4696}, primaryClass = {astro-ph.IM}, year = {2009}, month = {dec}, volume = {4}, pages = {2008-+}, doi = {10.1088/1748-0221/4/12/T12008}, adsurl = {http://adsabs.harvard.edu/abs/2009JInst...4T2008H}, adsnote = {Provided by the SAO/NASA Astrophysics Data System} }

1. malaspina2009 bibtex=@ARTICLE{malaspina2009,

author = {Malaspina, M. and Franceschi, E. and Battaglia, P. and Binko, P. and Butler, R. C. and D'Arcangelo, O. and Fogliani, S. and Frailis, M. and Franceschet, C. and Galeotta, S. and Gasparo, F. and Gregorio, A. and Lapolla, M. and Leonardi, R. and Maggio, G. and Mandolesi, N. and Manzato, P. and Maris, M. and Meharga, M. and Meinhold, P. and Morisset, N. and Pasian, F. and Perrotta, F. and Rohlfs, R. and Sandri, M. and Tomasi, M. and Türler, M. and Zacchei, A. and Zonca, A.}, title = {LFI Radiometric Chain Assembly (RCA) data handling ``Rachel}}, journal = {Journal of Instrumentation}, archivePrefix = {arXiv}, eprint = {1001.4787}, primaryClass = {astro-ph.IM}, year = {2009}, month = {dec}, volume = {4}, pages = {2017-+}, doi = {10.1088/1748-0221/4/12/T12017}, adsurl = {http://adsabs.harvard.edu/abs/2009JInst...4T2017M}, adsnote = {Provided by the SAO/NASA Astrophysics Data System} }

1. maris2009 bibtex=@ARTICLE{maris2009,

author = {Maris, M. and Tomasi, M. and Galeotta, S. and Miccolis, M. and Hildebrandt, S. and Frailis, M. and Rohlfs, R. and Morisset, N. and Zacchei, A. and Bersanelli, M. and Binko, P. and Burigana, C. and Butler, R. C. and Cuttaia, F. and Chulani, H. and D'Arcangelo, O. and Fogliani, S. and Franceschi, E. and Gasparo, F. and Gomez, F. and Gregorio, A. and Herreros, J. M. and Leonardi, R. and Leutenegger, P. and Maggio, G. and Maino, D. and Malaspina, M. and Mandolesi, N. and Manzato, P. and Meharga, M. and Meinhold, P. and Mennella, A. and Pasian, F. and Perrotta, F. and Rebolo, R. and Türler, M. and Zonca, A.}, title = {Optimization of Planck-LFI on-board data handling}, journal = {Journal of Instrumentation}, archivePrefix = {arXiv}, eprint = {1001.4737}, primaryClass = {astro-ph.IM}, year = {2009}, month = {dec}, volume = {4}, pages = {2018-+}, doi = {10.1088/1748-0221/4/12/T12018}, adsurl = {http://adsabs.harvard.edu/abs/2009JInst...4T2018M}, adsnote = {Provided by the SAO/NASA Astrophysics Data System} }

1. meinhold2009 bibtex=@ARTICLE{meinhold2009,

author = {Meinhold, P. and Leonardi, R. and Aja, B. and Artal, E. and Battaglia, P. and Bersanelli, M. and Blackhurst, E. and Butler, C. R. and Cuevas, L. P. and Cuttaia, F. and D'Arcangelo, O. and Davis, R. and de la Fuente, M. L. and Frailis, M. and Franceschet, C. and Franceschi, E. and Gaier, T. and Galeotta, S. and Gregorio, A. and Hoyland, R. and Hughes, N. and Jukkala, P. and Kettle, D. and Laaninen, M. and Leutenegger, P. and Lowe, S. R. and Malaspina, M. and Mandolesi, R. and Maris, M. and Martínez-González, E. and Mendes, L. and Mennella, A. and Miccolis, M. and Morgante, G. and Roddis, N. and Sandri, M. and Seiffert, M. and Salmón, M. and Stringhetti, L. and Poutanen, T. and Terenzi, L. and Tomasi, M. and Tuovinen, J. and Varis, J. and Valenziano, L. and Villa, F. and Wilkinson, A. and Winder, F. and Zacchei, A. and Zonca, A. }, title = {Noise properties of the Planck-LFI receivers}, journal = {Journal of Instrumentation}, archivePrefix = {arXiv}, eprint = {1001.4608}, primaryClass = {astro-ph.IM}, year = {2009}, month = {dec}, volume = {4}, pages = {2009-+}, doi = {10.1088/1748-0221/4/12/T12009}, adsurl = {http://adsabs.harvard.edu/abs/2009JInst...4T2009M}, adsnote = {Provided by the SAO/NASA Astrophysics Data System} }

1. mennella2009 bibtex=@ARTICLE{mennella2009,

author = {Mennella, A. and Villa, F. and Terenzi, L. and Cuttaia, F. and Battaglia, P. and Bersanelli, M. and Butler, R. C. and D'Arcangelo, O. and Artal, E. and Davis, R. and Frailis, M. and Franceschet, C. and Galeotta, S. and Gregorio, A. and Hughes, N. and Jukkala, P. and Kettle, D. and Kilpiä, V.-H. and Laaninen, M. and Lapolla, P. M. and Leonardi, R. and Leutenegger, P. and Lowe, S. and Mandolesi, N. and Maris, M. and Meinhold, P. and Mendes, L. and Miccolis, M. and Morgante, G. and Roddis, N. and Sandri, M. and Silvestri, R. and Stringhetti, L. and Tomasi, M. and Tuovinen, J. and Valenziano, L. and Zacchei, A. and Varis, J. and Wilkinson, A. and Zonca, A.}, title = {The linearity response of the Planck-LFI flight model receivers}, journal = {Journal of Instrumentation}, archivePrefix = {arXiv}, eprint = {1001.4610}, primaryClass = {astro-ph.IM}, year = {2009}, month = {dec}, volume = {4}, pages = {2011-+}, doi = {10.1088/1748-0221/4/12/T12011}, adsurl = {http://adsabs.harvard.edu/abs/2009JInst...4T2011M}, adsnote = {Provided by the SAO/NASA Astrophysics Data System} }

1. morgante2009 bibtex=@ARTICLE{morgante2009,

author = {Morgante, G. and Pearson, D. and Melot, F. and Stassi, P. and Terenzi, L. and Wilson, P. and Hernandez, B. and Wade, L. and Gregorio, A. and Bersanelli, M. and Butler, C. and Mandolesi, N. }, title = {Cryogenic characterization of the Planck sorption cooler system flight model}, journal = {Journal of Instrumentation}, archivePrefix = {arXiv}, eprint = {1001.4628}, primaryClass = {astro-ph.IM}, year = {2009}, month = {dec}, volume = {4}, pages = {2016-+}, doi = {10.1088/1748-0221/4/12/T12016}, adsurl = {http://adsabs.harvard.edu/abs/2009JInst...4T2016M}, adsnote = {Provided by the SAO/NASA Astrophysics Data System} }

1. terenzi2009a bibtex=@ARTICLE{terenzi2009a,

author = {Terenzi, L. and Lapolla, M. and Laaninen, M. and Battaglia, P. and Cavaliere, F. and De Rosa, A. and Hughes, N. and Jukkala, P. and Kilpiä, V.-H. and Morgante, G. and Tomasi, M. and Varis, J. and Bersanelli, M. and Butler, R. C. and Ferrari, F. and Franceschet, C. and Leutenegger, P. and Mandolesi, N. and Mennella, A. and Silvestri, R. and Stringhetti, L. and Tuovinen, J. and Valenziano, L. and Villa, F.}, title = {Cryogenic environment and performance for testing the Planck radiometers}, journal = {Journal of Instrumentation}, archivePrefix = {arXiv}, eprint = {1001.4644}, primaryClass = {astro-ph.IM}, year = {2009}, month = {dec}, volume = {4}, pages = {2015-+}, doi = {10.1088/1748-0221/4/12/T12015}, adsurl = {http://adsabs.harvard.edu/abs/2009JInst...4T2015T}, adsnote = {Provided by the SAO/NASA Astrophysics Data System} }

1. terenzi2009b bibtex=@ARTICLE{terenzi2009b,

author = {Terenzi, L. and Salmon, M. J. and Colin, A. and Mennella, A. and Morgante, G. and Tomasi, M. and Battaglia, P. and Lapolla, M. and Bersanelli, M. and Butler, R. C. and Cuttaia, F. and D'Arcangelo, O. and Davis, R. and Franceschet, C. and Galeotta, S. and Gregorio, A. and Hughes, N. and Jukkala, P. and Kettle, D. and Laaninen, M. and Leutenegger, P. and Leonardi, R. and Mandolesi, N. and Maris, M. and Meinhold, P. and Miccolis, M. and Roddis, N. and Sambo, L. and Sandri, M. and Silvestri, R. and Tuovinen, J. and Valenziano, L. and Varis, J. and Villa, F. and Wilkinson, A. and Zonca, A.}, title = {Thermal susceptibility of the Planck-LFI receivers}, journal = {Journal of Instrumentation}, archivePrefix = {arXiv}, eprint = {1001.4653}, primaryClass = {astro-ph.IM}, year = {2009}, month = {dec}, volume = {4}, pages = {2012-+}, doi = {10.1088/1748-0221/4/12/T12012}, adsurl = {http://adsabs.harvard.edu/abs/2009JInst...4T2012T}, adsnote = {Provided by the SAO/NASA Astrophysics Data System} }

1. tomasi2009 bibtex=@ARTICLE{tomasi2009,

author = {Tomasi, M. and Mennella, A. and Galeotta, S. and Lowe, S. R. and Mendes, L. and Leonardi, R. and Villa, F. and Cappellini, B. and Gregorio, A. and Meinhold, P. and Sandri, M. and Cuttaia, F. and Terenzi, L. and Maris, M. and Valenziano, L. and Salmon, M. J. and Bersanelli, M. and Binko, P. and Butler, R. C. and D'Arcangelo, O. and Fogliani, S. and Frailis, M. and Franceschi, E. and Gasparo, F. and Maggio, G. and Maino, D. and Malaspina, M. and Mandolesi, N. and Manzato, P. and Meharga, M. and Morgante, G. and Morisset, N. and Pasian, F. and Perrotta, F. and Rohlf, R. and Türler, M. and Zacchei, A. and Zonca, A.}, title = {Off-line radiometric analysis of Planck-LFI data}, journal = {Journal of Instrumentation}, archivePrefix = {arXiv}, eprint = {1001.4642}, primaryClass = {astro-ph.IM}, year = {2009}, month = {dec}, volume = {4}, pages = {2020-+}, doi = {10.1088/1748-0221/4/12/T12020}, adsurl = {http://adsabs.harvard.edu/abs/2009JInst...4T2020T}, adsnote = {Provided by the SAO/NASA Astrophysics Data System} }

1. tomasi2010 bibtex=@ARTICLE{tomasi2010,

author = {Tomasi, M. and Cappellini, B. and Gregorio, A. and Colombo, F. and Lapolla, M. and Terenzi, L. and Morgante, G. and Bersanelli, M. and Butler, R. C. and Galeotta, S. and Mandolesi, N. and Maris, M. and Mennella, A. and Valenziano, L. and Zacchei, A.}, title = {Dynamic validation of the Planck-LFI thermal model}, journal = {Journal of Instrumentation}, archivePrefix = {arXiv}, eprint = {1001.4646}, primaryClass = {astro-ph.IM}, year = {2010}, month = {jan}, volume = {5}, pages = {1002-+}, doi = {10.1088/1748-0221/5/01/T01002}, adsurl = {http://adsabs.harvard.edu/abs/2010JInst...5.1002T}, adsnote = {Provided by the SAO/NASA Astrophysics Data System} }

1. valenziano2009 bibtex=@ARTICLE{valenziano2009,

author = {Valenziano, L. and Cuttaia, F. and De Rosa, A. and Terenzi, L. and Brighenti, A. and Cazzola, G. P. and Garbesi, A. and Mariotti, S. and Orsi, G. and Pagan, L. and Cavaliere, F. and Biggi, M. and Lapini, R. and Panagin, E. and Battaglia, P. and Butler, R. C. and Bersanelli, M. and D'Arcangelo, O. and Levin, S. and Mandolesi, N. and Mennella, A. and Morgante, G. and Morigi, G. and Sandri, M. and Simonetto, A. and Tomasi, M. and Villa, F. and Frailis, M. and Galeotta, S. and Gregorio, A. and Leonardi, R. and Lowe, S. R. and Maris, M. and Meinhold, P. and Mendes, L. and Stringhetti, L. and Zonca, A. and Zacchei, A.}, title = {Planck-LFI: design and performance of the 4 Kelvin Reference Load Unit}, journal = {Journal of Instrumentation}, archivePrefix = {arXiv}, eprint = {1001.4778}, primaryClass = {astro-ph.IM}, year = {2009}, month = {dec}, volume = {4}, pages = {2006-+}, doi = {10.1088/1748-0221/4/12/T12006}, adsurl = {http://adsabs.harvard.edu/abs/2009JInst...4T2006V}, adsnote = {Provided by the SAO/NASA Astrophysics Data System} }

1. varis2009 bibtex=@ARTICLE{varis2009,

author = {Varis, J. and Hughes, N. J. and Laaninen, M. and Kilpiä, V.-H. and Jukkala, P. and Tuovinen, J. and Ovaska, S. and Sjöman, P. and Kangaslahti, P. and Gaier, T. and Hoyland, R. and Meinhold, P. and Mennella, A. and Bersanelli, M. and Butler, R. C. and Cuttaia, F. and Franceschi, E. and Leonardi, R. and Leutenegger, P. and Malaspina, M. and Mandolesi, N. and Miccolis, M. and Poutanen, T. and Kurki-Suonio, H. and Sandri, M. and Stringhetti, L. and Terenzi, L. and Tomasi, M. and Valenziano, L.}, title = {Design, development, and verification of the Planck Low Frequency Instrument 70 GHz Front-End and Back-End Modules}, journal = {Journal of Instrumentation}, archivePrefix = {arXiv}, eprint = {1001.4661}, primaryClass = {astro-ph.IM}, year = {2009}, month = {dec}, volume = {4}, pages = {2001-+}, doi = {10.1088/1748-0221/4/12/T12001}, adsurl = {http://adsabs.harvard.edu/abs/2009JInst...4T2001V}, adsnote = {Provided by the SAO/NASA Astrophysics Data System} }

1. villa2009 bibtex=@ARTICLE{villa2009,

author = {Villa, F. and D'Arcangelo, O. and Pecora, M. and Figini, L. and Nesti, R. and Simonetto, A. and Sozzi, C. and Sandri, M. and Battaglia, P. and Guzzi, P. and Bersanelli, M. and Butler, R. C. and Mandolesi, N.}, title = {Planck-LFI flight model feed horns}, journal = {Journal of Instrumentation}, archivePrefix = {arXiv}, eprint = {1001.4633}, primaryClass = {astro-ph.IM}, year = {2009}, month = {dec}, volume = {4}, pages = {2004-+}, doi = {10.1088/1748-0221/4/12/T12004}, adsurl = {http://adsabs.harvard.edu/abs/2009JInst...4T2004V}, adsnote = {Provided by the SAO/NASA Astrophysics Data System} }

1. zacchei2009 bibtex=@ARTICLE{zacchei2009,

author = {Zacchei, A. and Frailis, M. and Maris, M. and Morisset, N. and Rohlfs, R. and Meharga, M. and Binko, P. and Türler, M. and Galeotta, S. and Gasparo, F. and Franceschi, E. and Butler, R. C. and Cuttaia, F. and D'Arcangelo, O. and Fogliani, S. and Gregorio, A. and Leonardi, R. and Lowe, S. R. and Maino, D. and Maggio, G. and Malaspina, M. and Mandolesi, N. and Manzato, P. and Meinhold, P. and Mendes, L. and Mennella, A. and Morgante, G. and Pasian, F. and Perrotta, F. and Sandri, M. and Stringhetti, L. and Terenzi, L. and Tomasi, M. and Zonca, A.}, title = {Level 1 on-ground telemetry handling in Planck-LFI}, journal = {Journal of Instrumentation}, archivePrefix = {arXiv}, eprint = {1001.4730}, primaryClass = {astro-ph.IM}, year = {2009}, month = {dec}, volume = {4}, pages = {2019-+}, doi = {10.1088/1748-0221/4/12/T12019}, adsurl = {http://adsabs.harvard.edu/abs/2009JInst...4T2019Z}, adsnote = {Provided by the SAO/NASA Astrophysics Data System} }

1. zonca2009 bibtex=@ARTICLE{zonca2009,

author = {Zonca, A. and Franceschet, C. and Battaglia, P. and Villa, F. and Mennella, A. and D'Arcangelo, O. and Silvestri, R. and Bersanelli, M. and Artal, E. and Butler, R. C. and Cuttaia, F. and Davis, R. J. and Galeotta, S. and Hughes, N. and Jukkala, P. and Kilpiä, V.-H. and Laaninen, M. and Mandolesi, N. and Maris, M. and Mendes, L. and Sandri, M. and Terenzi, L. and Tuovinen, J. and Varis, J. and Wilkinson, A.}, title = {Planck-LFI radiometers' spectral response}, journal = {Journal of Instrumentation}, archivePrefix = {arXiv}, eprint = {1001.4589},

primaryClass = {astro-ph.IM}, year = {2009}, month = {dec}, volume = {4}, pages = {2010-+}, doi = {10.1088/1748-0221/4/12/T12010}, adsurl = {http://adsabs.harvard.edu/abs/2009JInst...4T2010Z}, adsnote = {Provided by the SAO/NASA Astrophysics Data System} }

1. holmes2008 bibtex=@ARTICLE{holmes2008,

author = {Holmes, W. A. and Bock, J. J. and Crill, B. P. and Koch, T. C. and Jones, W. C. and Lange, A. E. and Paine, C. G.}, title = {Initial test results on bolometers for the Planck high frequency instrument}, journal = {Appl. Opt}, year = {2008}, month = {nov}, volume = {47}, pages = {5996-+}, doi = {10.1364/AO.47.005996}, adsurl = {http://adsabs.harvard.edu/abs/2008ApOpt..47.5996H}, adsnote = {Provided by the SAO/NASA Astrophysics Data System} }

1. bhandari2004 bibtex=@ARTICLE{bhandari2004,

author = {Bhandari, P. and Prina, M. and Bowman, R. C. and Paine, C. and Pearson, D. and Nash, A.}, title = {Sorption coolers using a continuous cycle to produce 20 K for the Planck flight mission}, journal = {Cryogenics}, year = {2004}, month = {jun}, volume = {44}, pages = {395-401}, adsurl = {http://adsabs.harvard.edu/abs/2004Cryo...44..395B}, adsnote = {Provided by the SAO/NASA Astrophysics Data System} }

1. planck2005-bluebook bibtex=@ARTICLE{planck2005-bluebook,

author = {Planck Collaboration,}, title = {The Scientific Programme of Planck}, journal = {ESA publication ESA-SCI(2005)/01}, eprint = {arXiv:astro-ph/0604069}, keywords = {Astrophysics}, year = {2005}, adsurl = {http://adsabs.harvard.edu/abs/2006astro.ph..4069T}, adsnote = {Provided by the SAO/NASA Astrophysics Data System} }

1. bennett2010 bibtex=@ARTICLE{bennett2010,

author = {Bennett, C. L. and Hill, R. S. and Hinshaw, G. and Larson, D. and Smith, K. M. and Dunkley, J. and Gold, B. and Halpern, M. and Jarosik, N. and Kogut, A. and Komatsu, E. and Limon, M. and Meyer, S. S. and Nolte, M. R. and Odegard, N. and Page, L. and Spergel, D. N. and Tucker, G. S. and Weiland, J. L. and Wollack, E. and Wright, E. L.}, title = {Seven-year Wilkinson Microwave Anisotropy Probe (WMAP) Observations: Are There Cosmic Microwave Background Anomalies?}, journal = {Aps}, archivePrefix = {arXiv}, eprint = {1001.4758}, primaryClass = {astro-ph.CO}, keywords = {cosmic background radiation, cosmological parameters, cosmology: observations, dark matter, early universe, instrumentation: detectors, large-scale structure of universe, space vehicles, space vehicles: instruments, telescopes}, year = {2011}, month = {feb}, volume = {192}, pages = {17-+}, doi = {10.1088/0067-0049/192/2/17}, adsurl = {http://adsabs.harvard.edu/abs/2011ApJS..192...17B}, adsnote = {Provided by the SAO/NASA Astrophysics Data System} }

1. gold2010 bibtex=@ARTICLE{gold2010,

author = {Gold, B. and Odegard, N. and Weiland, J. L. and Hill, R. S. and Kogut, A. and Bennett, C. L. and Hinshaw, G. and Chen, X. and Dunkley, J. and Halpern, M. and Jarosik, N. and Komatsu, E. and Larson, D. and Limon, M. and Meyer, S. S. and Nolte, M. R. and Page, L. and Smith, K. M. and Spergel, D. N. and Tucker, G. S. and Wollack, E. and Wright, E. L.}, title = {Seven-year Wilkinson Microwave Anisotropy Probe (WMAP) Observations: Galactic Foreground Emission}, journal = {Aps}, archivePrefix = {arXiv}, eprint = {1001.4555}, primaryClass = {astro-ph.GA}, keywords = {cosmic background radiation, cosmology: observations, diffuse radiation, Galaxy: halo, Galaxy: structure, ISM: structure}, year = {2011}, month = {feb}, volume = {192}, pages = {15-+}, doi = {10.1088/0067-0049/192/2/15}, adsurl = {http://adsabs.harvard.edu/abs/2011ApJS..192...15G}, adsnote = {Provided by the SAO/NASA Astrophysics Data System} }

1. jarosik2010 bibtex=@ARTICLE{jarosik2010,

author = {Jarosik, N. and Bennett, C. L. and Dunkley, J. and Gold, B. and Greason, M. R. and Halpern, M. and Hill, R. S. and Hinshaw, G. and Kogut, A. and Komatsu, E. and Larson, D. and Limon, M. and Meyer, S. S. and Nolte, M. R. and Odegard, N. and Page, L. and Smith, K. M. and Spergel, D. N. and Tucker, G. S. and Weiland, J. L. and Wollack, E. and Wright, E. L.}, title = {Seven-year Wilkinson Microwave Anisotropy Probe (WMAP) Observations:

Sky Maps, Systematic Errors, and Basic Results}, journal = {Aps}, archivePrefix = {arXiv}, eprint = {1001.4744}, primaryClass = {astro-ph.CO}, keywords = {cosmic background radiation, space vehicles: instruments}, year = {2011}, month = {feb}, volume = {192}, pages = {14-+}, doi = {10.1088/0067-0049/192/2/14}, adsurl = {http://adsabs.harvard.edu/abs/2011ApJS..192...14J}, adsnote = {Provided by the SAO/NASA Astrophysics Data System} }

1. komatsu2010 bibtex=@ARTICLE{komatsu2010,

author = {Komatsu, E. and Smith, K. M. and Dunkley, J. and Bennett, C. L. and Gold, B. and Hinshaw, G. and Jarosik, N. and Larson, D. and Nolta, M. R. and Page, L. and Spergel, D. N. and Halpern, M. and Hill, R. S. and Kogut, A. and Limon, M. and Meyer, S. S. and Odegard, N. and Tucker, G. S. and Weiland, J. L. and Wollack, E. and Wright, E. L.}, title = {Seven-year Wilkinson Microwave Anisotropy Probe (WMAP) Observations: Cosmological Interpretation}, journal = {Aps}, archivePrefix = {arXiv}, eprint = {1001.4538}, primaryClass = {astro-ph.CO}, keywords = {cosmic background radiation, cosmology: observations, dark matter, early universe, space vehicles}, year = {2011}, month = {feb}, volume = {192}, pages = {18-+}, doi = {10.1088/0067-0049/192/2/18}, adsurl = {http://adsabs.harvard.edu/abs/2011ApJS..192...18K}, adsnote = {Provided by the SAO/NASA Astrophysics Data System} }

1. larson2010 bibtex=@ARTICLE{larson2010,

author = {Larson, D. and Dunkley, J. and Hinshaw, G. and Komatsu, E. and Nolta, M. R. and Bennett, C. L. and Gold, B. and Halpern, M. and Hill, R. S. and Jarosik, N. and Kogut, A. and Limon, M. and Meyer, S. S. and Odegard, N. and Page, L. and Smith, K. M. and Spergel, D. N. and Tucker, G. S. and Weiland, J. L. and Wollack, E. and Wright, E. L.}, title = {Seven-year Wilkinson Microwave Anisotropy Probe (WMAP) Observations: Power Spectra and WMAP-derived Parameters}, journal = {Aps}, archivePrefix = {arXiv}, eprint = {1001.4635}, primaryClass = {astro-ph.CO}, keywords = {cosmic background radiation, cosmological parameters, cosmology: observations, dark matter, early universe, space vehicles: instruments}, year = {2011}, month = {feb}, volume = {192}, pages = {16-+}, doi = {10.1088/0067-0049/192/2/16}, adsurl = {http://adsabs.harvard.edu/abs/2011ApJS..192...16L}, adsnote = {Provided by the SAO/NASA Astrophysics Data System} }

1. weiland2010 bibtex=@ARTICLE{weiland2010,

author = {Weiland, J. L. and Odegard, N. and Hill, R. S. and Wollack, E. and Hinshaw, G. and Greason, M. R. and Jarosik, N. and Page, L. and Bennett, C. L. and Dunkley, J. and Gold, B. and Halpern, M. and Kogut, A. and Komatsu, E. and Larson, D. and Limon, M. and Meyer, S. S. and Nolta, M. R. and Smith, K. M. and Spergel, D. N. and Tucker, G. S. and Wright, E. L.}, title = {Seven-year Wilkinson Microwave Anisotropy Probe (WMAP) Observations: Planets and Celestial Calibration Sources}, journal = {Aps}, archivePrefix = {arXiv}, eprint = {1001.4731}, primaryClass = {astro-ph.CO}, keywords = {galaxies: individual: Cygnus A 3C274, ISM: supernova remnants, planets and satellites: general, radio continuum: general, space vehicles: instruments}, year = {2011}, month = {feb}, volume = {192}, pages = {19-+}, doi = {10.1088/0067-0049/192/2/19}, adsurl = {http://adsabs.harvard.edu/abs/2011ApJS..192...19W}, adsnote = {Provided by the SAO/NASA Astrophysics Data System} }

1. hinshaw2009 bibtex=@ARTICLE{hinshaw2009,

author = {Hinshaw, G. and Weiland, J. L. and Hill, R. S. and Odegard, N. and Larson, D. and Bennett, C. L. and Dunkley, J. and Gold, B. and Greason, M. R. and Jarosik, N. and Komatsu, E. and Nolta, M. R. and Page, L. and Spergel, D. N. and Wollack, E. and Halpern, M. and Kogut, A. and Limon, M. and Meyer, S. S. and Tucker, G. S. and Wright, E. L.}, title = {Five-Year Wilkinson Microwave Anisotropy Probe (WMAP) Observations: Data Processing, Sky Maps, and Basic Results}, journal = {Aps}, eprint = {0803.0732}, keywords = {Astrophysics}, year = {2009}, month = {Feb}, volume = {180}, pages = {225-245}, adsurl = {http://adsabs.harvard.edu/abs/2008arXiv0803.0732H}, adsnote = {Provided by the SAO/NASA Astrophysics Data System} }

1. hill2009 bibtex=@ARTICLE{hill2009,



author = {Hill, R. S. and Weiland, J. L. and Odegard, N. and Wollack, E. and Hinshaw, G. and Larson, D. and Bennett, C. L. and Halpern, M. and Page, L. and Dunkley, J. and Gold, B. and Jarosik, N. and Kogut, A. and Limon, M. and Nolta, M.R. and Spergel, D. N. and Tucker, G. S. and Wright, E. L.}, title = {Five-Year Wilkinson Microwave Anisotropy Probe (WMAP) Observations: Beam Maps and Window Functions}, journal = {Aps}, eprint = {0803.0570}, keywords = {Astrophysics}, year = {2009}, month = {Feb}, volume = {180}, pages = {246-264}, adsurl = {http://adsabs.harvard.edu/abs/2008arXiv0803.0570H}, adsnote = {Provided by the SAO/NASA Astrophysics Data System} }

1. gold2009 bibtex=@ARTICLE{gold2009,

author = {Gold, B. and Bennett, C. L. and Hill, R. S. and Hinshaw, G. and Odegard, N. and Spergel, D. N. and Weiland, J. and Dunkley, J. and Halpern, M. and Jarosik, N. and Kogut, A. and Komatsu, E. and Larson, D. and Meyer, S. S. and Nolta, M.R. and Wollack, E. and Wright, E. L.}, title = {Five-Year Wilkinson Microwave Anisotropy Probe (WMAP) Observations: Galactic Foreground Emission}, journal = {Aps}, eprint = {0803.0715}, keywords = {Astrophysics}, year = {2009}, month = {Feb}, volume = {180}, pages = {265-282}, adsurl = {http://adsabs.harvard.edu/abs/2008arXiv0803.0715G}, adsnote = {Provided by the SAO/NASA Astrophysics Data System} }

1. wright2009 bibtex=@ARTICLE{wright2009,

author = {Wright, E. L. and Chen, X. and Odegard, N. and Bennett, C. L. and Hill, R. S. and Hinshaw, G. and Jarosik, N. and Komatsu, E. and Nolta, M. R. and Page, L. and Spergel, D. N. and Weiland, J. L. and Wollack, E. and Dunkley, J. and Gold, B. and Halpern, M. and Kogut, A. and Larson, D. and Limon, M. and Meyer, S. S. and Tucker, G. S.}, title = {Five-Year Wilkinson Microwave Anisotropy Probe (WMAP) Observations: Source Catalog}, journal = {Aps}, eprint = {0803.0577}, keywords = {Astrophysics}, year = {2009}, month = {Feb}, volume = {180}, pages = {283-295}, adsurl = {http://adsabs.harvard.edu/abs/2008arXiv0803.0577W}, adsnote = {Provided by the SAO/NASA Astrophysics Data System} }

1. nolta2009 bibtex=@ARTICLE{nolta2009,

author = {Nolta, M. R. and Dunkley, J. and Hill, R. S. and Hinshaw, G. and Komatsu, E. and Larson, D. and Page, L. and Spergel, D. N. and Bennett, C. L. and Gold, B. and Jarosik, N. and Odegard, N. and Weiland, J. L. and Wollack, E. and Halpern, M. and Kogut, A. and Limon, M. and Meyer, S. S. and Tucker, G. S. and Wright, E.L.}, title = {Five-Year Wilkinson Microwave Anisotropy Probe (WMAP) Observations: Angular Power Spectra}, journal = {Aps}, eprint = {0803.0593}, keywords = {Astrophysics}, year = {2009}, month = {Feb}, volume = {180}, pages = {296-305}, adsurl = {http://adsabs.harvard.edu/abs/2008arXiv0803.0593N}, adsnote = {Provided by the SAO/NASA Astrophysics Data System} }

1. dunkley2009 bibtex=@ARTICLE{dunkley2009,

author = {Dunkley, J. and Komatsu, E. and Nolta, M. R. and Spergel, D. N. and Larson, D. and Hinshaw, G. and Page, L. and Bennett, C. L. and Gold, B. and Jarosik, N. and Weiland, J. L. and Halpern, M. and Hill, R. S. and Kogut, A. and Limon, M. and Meyer, S. S. and Tucker, G. S. and Wollack, E. and Wright, E. L.}, title = {Five-Year Wilkinson Microwave Anisotropy Probe (WMAP) Observations: Likelihoods and Parameters from the WMAP data}, journal = {Aps}, eprint = {0803.0586}, keywords = {Astrophysics}, year = {2009}, month = {Feb}, volume = {180}, pages = {306-376}, adsurl = {http://adsabs.harvard.edu/abs/2008arXiv0803.0586D}, adsnote = {Provided by the SAO/NASA Astrophysics Data System} }

1. komatsu2009 bibtex=@ARTICLE{komatsu2009,

author = {Komatsu, E. and Dunkley, J. and Nolta, M. R. and Bennett, C. L. and Gold, B. and Hinshaw, G. and Jarosik, N. and Larson, D. and Limon, M. and Page, L. and Spergel, D. N. and Halpern, M. and Hill, R. S. and Kogut, A. and Meyer, S. S. and Tucker, G. S. and Weiland, J. L. and Wollack, E. and Wright, E. L.}, title = {Five-Year Wilkinson Microwave Anisotropy Probe (WMAP) Observations: Cosmological Interpretation}, journal = {Aps}, eprint = {0803.0547}, keywords = {Astrophysics}, year = {2009}, month = {Feb}, volume = {180}, pages

= {330-376}, adsurl = {http://adsabs.harvard.edu/abs/2008arXiv0803.0547K}, adsnote = {Provided by the SAO/NASA Astrophysics Data System} }

1. kogut2007 bibtex=@ARTICLE{kogut2007,

author = {Kogut, A. and Dunkley, J. and Bennett, C. L. and Doré, O. and Gold, B. and Halpern, M. and Hinshaw, G. and Jarosik, N. and Komatsu, E. and Nolte, M. R. and Odegard, N. and Page, L. and Spergel, D. N. and Tucker, G. S. and Weiland, J. L. and Wollack, E. and Wright, E. L.}, title = {Three-Year Wilkinson Microwave Anisotropy Probe (WMAP) Observations: Foreground Polarization}, journal = {ApJ}, eprint = {arXiv:0704.3991}, year = {2007}, month = {aug}, volume = {665}, pages = {355-362}, doi = {10.1086/519754}, adsurl = {http://adsabs.harvard.edu/abs/2007ApJ...665..355K}, adsnote = {Provided by the SAO/NASA Astrophysics Data System} }

1. jarosik2007 bibtex=@ARTICLE{jarosik2007,

author = {Jarosik, N. and Barnes, C. and Greason, M. R. and Hill, R. S. and Nolte, M. R. and Odegard, N. and Weiland, J. L. and Bean, R. and Bennett, C. L. and Doré, O. and Halpern, M. and Hinshaw, G. and Kogut, A. and Komatsu, E. and Limon, M. and Meyer, S. S. and Page, L. and Spergel, D. N. and Tucker, G. S. and Wollack, E. and Wright, E. L.}, title = {Three-Year Wilkinson Microwave Anisotropy Probe (WMAP) Observations: Beam Profiles, Data Processing, Radiometer Characterization, and Systematic Error Limits}, journal = {Aps}, eprint = {arXiv:astro-ph/0603452}, year = {2007}, month = {jun}, volume = {170}, pages = {263-287}, doi = {10.1086/513697}, adsurl = {http://adsabs.harvard.edu/abs/2007ApJS..170..263J}, adsnote = {Provided by the Smithsonian/NASA Astrophysics Data System} }

1. hinshaw2007 bibtex=@ARTICLE{hinshaw2007,

author = {Hinshaw, G. and Nolte, M. R. and Bennett, C. L. and Bean, R. and Doré, O. and Greason, M. R. and Halpern, M. and Hill, R. S. and Jarosik, N. and Kogut, A. and Komatsu, E. and Limon, M. and Odegard, N. and Meyer, S. S. and Page, L. and Peiris, H. V. and Spergel, D. N. and Tucker, G. S. and Verde, L. and Weiland, J. L. and Wollack, E. and Wright, E. L.}, title = {Three-Year Wilkinson Microwave Anisotropy Probe (WMAP) Observations: Temperature Analysis}, journal = {Aps}, eprint = {arXiv:astro-ph/0603451}, year = {2007}, month = {jun}, volume = {170}, pages = {288-334}, doi = {10.1086/513698}, adsurl = {http://adsabs.harvard.edu/abs/2007ApJS..170..288H}, adsnote = {Provided by the Smithsonian/NASA Astrophysics Data System} }

1. page2007 bibtex=@ARTICLE{page2007,

author = {Page, L. and Hinshaw, G. and Komatsu, E. and Nolte, M. R. and Spergel, D. N. and Bennett, C. L. and Barnes, C. and Bean, R. and Doré, O. and Dunkley, J. and Halpern, M. and Hill, R. S. and Jarosik, N. and Kogut, A. and Limon, M. and Meyer, S. S. and Odegard, N. and Peiris, H. V. and Tucker, G. S. and Verde, L. and Weiland, J. L. and Wollack, E. and Wright, E. L.}, title = {Three-Year Wilkinson Microwave Anisotropy Probe (WMAP) Observations: Polarization Analysis}, journal = {Aps}, eprint = {arXiv:astro-ph/0603450}, year = {2007}, month = {jun}, volume = {170}, pages = {335-376}, doi = {10.1086/513699}, adsurl = {http://adsabs.harvard.edu/abs/2007ApJS..170..335P}, adsnote = {Provided by the Smithsonian/NASA Astrophysics Data System} }

1. spergel2007 bibtex=@ARTICLE{spergel2007,

author = {Spergel, D. N. and Bean, R. and Doré, O. and Nolte, M. R. and Bennett, C. L. and Dunkley, J. and Hinshaw, G. and Jarosik, N. and Komatsu, E. and Page, L. and Peiris, H. V. and Verde, L. and Halpern, M. and Hill, R. S. and Kogut, A. and Limon, M. and Meyer, S. S. and Odegard, N. and Tucker, G. S. and Weiland, J. L. and Wollack, E. and Wright, E. L.}, title = {Three-Year Wilkinson Microwave Anisotropy Probe (WMAP) Observations: Implications for Cosmology}, journal = {Aps}, eprint = {arXiv:astro-ph/0603449}, year = {2007}, month = {jun}, volume = {170}, pages = {377-408}, doi = {10.1086/513700}, adsurl = {http://adsabs.harvard.edu/abs/2007ApJS..170..377S}, adsnote = {Provided by the Smithsonian/NASA Astrophysics Data System} }

1. nolte2004 bibtex=@Article{nolte2004,

author = {Nolte, M. R. and Wright, E. L. and Page, L. and Bennett, C. L. and Halpern, M. and Hinshaw, G. and Jarosik, N. and Kogut, A. and Limon, M. and Meyer, S. S. and Spergel, D. N. and Tucker, G. S. and Wollack, E.},

title = {First Year Wilkinson Microwave Anisotropy Probe (WMAP) Observations: Dark Energy Induced Correlation with Radio Sources}, journal = {Astrophys. J.}, volume = {608}, year = {2004}, pages = {10-15}, eprint = {astro-ph/0305097} }

1. bennett2003a bibtex=@article{bennett2003a,

author = {Bennett, C. L. and Halpern, M. and Hinshaw, G. and Jarosik, N. and Kogut, A. and Limon, M. and Meyer, S. S. and Page, L. and Spergel, D. N. and Tucker, G. S. and Wollack, E. and Wright, E. L. and Barnes, C. and Greason, M. R. and Hill, R. S. and Komatsu, E. and Nolta, M. R. and Odegard, N. and Peiris, H. V. and Verde, L. and Weiland, J. L.}, title = {First-Year Wilkinson Microwave Anisotropy Probe (WMAP) Observations: Preliminary Maps and Basic Results}, journal = {Aps}, year = {2003}, month = {sep}, volume = {148}, pages = {1-27}, adsurl = {http://adsabs.harvard.edu/cgi-bin/nph-bib\_query?bibcode=2003ApJS..148....1B&db\_key=AST}, adsnote = {Provided by the NASA Astrophysics Data System} }

1. page2003a bibtex=@article{page2003a,

author = {Page, L. and Barnes, C. and Hinshaw, G. and Spergel, D. N. and Weiland, J. L. and Wollack, E. and Bennett, C. L. and Halpern, M. and Jarosik, N. and Kogut, A. and Limon, M. and Meyer, S. S. and Tucker, G. S. and Wright, E. L.}, title = {First-Year Wilkinson Microwave Anisotropy Probe (WMAP) Observations: Beam Profiles and Window Functions}, journal = {Aps}, year = {2003}, month = {sep}, volume = {148}, pages = {39-50}, adsurl = {http://adsabs.harvard.edu/cgi-bin/nph-bib\_query?bibcode=2003ApJS..148...39P&db\_key=AST}, adsnote = {Provided by the NASA Astrophysics Data System} }

1. hinshaw2003a bibtex=@article{hinshaw2003a,

author = {Hinshaw, G. and Barnes, C. and Bennett, C. L. and Greason, M. R. and Halpern, M. and Hill, R. S. and Jarosik, N. and Kogut, A. and Limon, M. and Meyer, S. S. and Odegard, N. and Page, L. and Spergel, D. N. and Tucker, G. S. and Weiland, J. L. and Wollack, E. and Wright, E. L.}, title = {First-Year Wilkinson Microwave Anisotropy Probe (WMAP) Observations: Data Processing Methods and Systematic Error Limits}, journal = {Aps}, year = {2003}, volume = {148}, pages = {63-95}, adsurl = {http://adsabs.harvard.edu/cgi-bin/nph-bib\_query?bibcode=2003ApJS..148...63H&db\_key=AST}, adsnote = {Provided by the NASA Astrophysics Data System} }

1. spergel2003 bibtex=@article{spergel2003,

author = {Spergel, D. N. and Verde, L. and Peiris, H. V. and Komatsu, E. and Nolta, M. R. and Bennett, C. L. and Halpern, M. and Hinshaw, G. and Jarosik, N. and Kogut, A. and Limon, M. and Meyer, S. S. and Page, L. and Tucker, G. S. and Weiland, J. L. and Wollack, E. and Wright, E. L.}, title = {First-Year Wilkinson Microwave Anisotropy Probe (WMAP) Observations: Determination of Cosmological Parameters}, journal = {Aps}, year = {2003}, month = {sep}, volume = {148}, pages = {175-194}, adsurl = {http://adsabs.harvard.edu/cgi-bin/nph-bib\_query?bibcode=2003ApJS..148..175S&db\_key=AST}, adsnote = {Provided by the NASA Astrophysics Data System} }

1. bennett2003b bibtex=@article{bennett2003b,

author = {Bennett, C. L. and Hill, R. S. and Hinshaw, G. and Nolta, M. R. and Odegard, N. and Page, L. and Spergel, D. N. and Weiland, J. L. and Wright, E. L. and Halpern, M. and Jarosik, N. and Kogut, A. and Limon, M. and Meyer, S. S. and Tucker, G. S. and Wollack, E. }, title = {First-Year Wilkinson Microwave Anisotropy Probe (WMAP) Observations: Foreground Emission}, journal = {Aps}, year = {2003}, volume = {148}, pages = {97-117}, adsurl = {http://adsabs.harvard.edu/cgi-bin/nph-bib\_query?bibcode=2003ApJS..148...97B&db\_key=AST}, adsnote = {Provided by the NASA Astrophysics Data System} }

1. barnes2003 bibtex=@article{barnes2003,

author = {Barnes, C. and Hill, R. S. and Hinshaw, G. and Page, L. and Bennett, C. L. and Halpern, M. and Jarosik, N. and Kogut, A. and Limon, M. and Meyer, S. S. and Tucker, G. S. and Wollack, E. and Wright, E. L.}, title = {First-Year Wilkinson Microwave Anisotropy Probe (WMAP) Observations: Galactic Signal Contamination from

Sidelobe Pickup}, journal = {Aps}, year = {2003}, month = {sep}, volume = {148}, pages = {51-62}, adsurl = {http://adsabs.harvard.edu/cgi-bin/nph-bib\_query?bibcode=2003ApJS..148...51B&db\_key=AST}, adsnote = {Provided by the NASA Astrophysics Data System} }

1. peiris2003 bibtex=@article{peiris2003,

author = {Peiris, H. V. and Komatsu, E. and Verde, L. and Spergel, D. N. and Bennett, C. L. and Halpern, M. and Hinshaw, G. and Jarosik, N. and Kogut, A. and Limon, M. and Meyer, S. S. and Page, L. and Tucker, G. S. and Wollack, E. and Wright, E. L.}, title = {First-Year Wilkinson Microwave Anisotropy Probe (WMAP) Observations: Implications For Inflation}, journal = {Aps}, year = {2003}, month = {sep}, volume = {148}, pages = {213-231}, adsurl = {http://adsabs.harvard.edu/cgi-bin/nph-bib\_query?bibcode=2003ApJS..148..213P&db\_key=AST}, adsnote = {Provided by the NASA Astrophysics Data System} }

1. page2003b bibtex=@article{page2003b,

author = {Page, L. and Nolta, M. R. and Barnes, C. and Bennett, C. L. and Halpern, M. and Hinshaw, G. and Jarosik, N. and Kogut, A. and Limon, M. and Meyer, S. S. and Peiris, H. V. and Spergel, D. N. and Tucker, G. S. and Wollack, E. and Wright, E. L.}, title = {First-Year Wilkinson Microwave Anisotropy Probe (WMAP) Observations: Interpretation of the TT and TE Angular Power Spectrum Peaks}, journal = {Aps}, year = {2003}, month = {sep}, volume = {148}, pages = {233-241}, adsurl = {http://adsabs.harvard.edu/cgi-bin/nph-bib\_query?bibcode=2003ApJS..148..233P&db\_key=AST}, adsnote = {Provided by the NASA Astrophysics Data System} }

1. jarosik2003 bibtex=@article{jarosik2003,

author = {Jarosik, N. and Barnes, C. and Bennett, C. L. and Halpern, M. and Hinshaw, G. and Kogut, A. and Limon, M. and Meyer, S. S. and Page, L. and Spergel, D. N. and Tucker, G. S. and Weiland, J. L. and Wollack, E. and Wright, E. L.}, title = {First-Year Wilkinson Microwave Anisotropy Probe (WMAP) Observations: On-Orbit Radiometer Characterization}, journal = {Aps}, year = {2003}, month = {sep}, volume = {148}, pages = {29-37}, adsurl = {http://adsabs.harvard.edu/cgi-bin/nph-bib\_query?bibcode=2003ApJS..148...29J&db\_key=AST}, adsnote = {Provided by the NASA Astrophysics Data System} }

1. verde2003 bibtex=@article{verde2003,

author = {Verde, L. and Peiris, H. V. and Spergel, D. N. and Nolta, M. R. and Bennett, C. L. and Halpern, M. and Hinshaw, G. and Jarosik, N. and Kogut, A. and Limon, M. and Meyer, S. S. and Page, L. and Tucker, G. S. and Wollack, E. and Wright, E. L.}, title = {First-Year Wilkinson Microwave Anisotropy Probe (WMAP) Observations: Parameter Estimation Methodology}, journal = {Aps}, year = {2003}, volume = {148}, pages = {195-211}, adsurl = {http://adsabs.harvard.edu/cgi-bin/nph-bib\_query?bibcode=2003ApJS..148..195V&db\_key=AST}, adsnote = {Provided by the NASA Astrophysics Data System} }

1. kogut2003 bibtex=@article{kogut2003,

author = {Kogut, A. and Spergel, D. N. and Barnes, C. and Bennett, C. L. and Halpern, M. and Hinshaw, G. and Jarosik, N. and Limon, M. and Meyer, S. S. and Page, L. and Tucker, G. S. and Wollack, E. and Wright, E. L.}, title = {First-Year Wilkinson Microwave Anisotropy Probe (WMAP) Observations: Temperature-Polarization Correlation}, journal = {Aps}, year = {2003}, month = {sep}, volume = {148}, pages = {161-173}, adsurl = {http://adsabs.harvard.edu/cgi-bin/nph-bib\_query?bibcode=2003ApJS..148..161K&db\_key=AST}, adsnote = {Provided by the NASA Astrophysics Data System} }

1. komatsu2003 bibtex=@article{komatsu2003,

author = {Komatsu, E. and Kogut, A. and Nolta, M. R. and Bennett, C. L. and Halpern, M. and Hinshaw, G. and Jarosik, N. and Limon, M. and Meyer, S. S. and Page, L. and Spergel, D. N. and Tucker, G. S. and Verde, L. and Wollack, E. and Wright, E. L.}, title = {First-Year Wilkinson Microwave Anisotropy Probe (WMAP) Observations: Tests of Gaussianity}, journal = {Aps}, year = {2003}, month = {sep}, volume = {148}, pages = {119-134}, adsurl = {http://adsabs.harvard.edu/cgi-bin/nph-bib\_query?bibcode=2003ApJS..148..119K&db\_key=AST}, adsnote =

= {Provided by the NASA Astrophysics Data System} }

1. hinshaw2003b bibtex=@article{hinshaw2003b,

author = {Hinshaw, G. and Spergel, D. N. and Verde, L. and Hill, R. S. and Meyer, S. S. and Barnes, C. and Bennett, C. L. and Halpern, M. and Jarosik, N. and Kogut, A. and Komatsu, E. and Limon, M. and Page, L. and Tucker, G. S. and Weiland, J. L. and Wollack, E. and Wright, E. L.}, title = {First-Year Wilkinson Microwave Anisotropy Probe (WMAP) Observations: The Angular Power Spectrum}, journal = {Aps}, year = {2003}, volume = {148}, pages = {135-159}, adsurl = {http://adsabs.harvard.edu/cgi-bin/nph-bib\_query?bibcode=2003ApJS..148..135H&db\_key=AST}, adsnote = {Provided by the NASA Astrophysics Data System} }

1. delabrouille2012 bibtex=@ARTICLE{delabrouille2012,

author = {Delabrouille, J. and Betoule, M. and Melin, J.-B. and Miville-Deschênes, M.-A. and Gonzalez-Nuevo, J. and Le Jeune, M. and Castex, G. and de Zotti, G. and Basak, S. and Ashdown, M. and Aumont, J. and Baccigalupi, C. and Banday, A. and Bernard, J.-P. and Bouchet, F. R. and Clements, D. L. and da Silva, A. and Dickinson, C. and Dodu, F. and Dolag, K. and Elsner, F. and Fauvet, L. and Fa&yuml, G. and Giardino, G. and Leach, S. and Lesgourgues, J. and Liguori, M. and Macias-Perez, J. F. and Massardi, M. and Matarrese, S. and Mazzotta, P. and Montier, L. and Mottet, S. and Paladini, R. and Partridge, B. and Piffaretti, R. and Prezeau, G. and Prunet, S. and Ricciardi, S. and Roman, M. and Schaefer, B. and Toffolatti, L.}, title = {The pre-launch Planck Sky Model: a model of sky emission at submillimetre to centimetre wavelengths}, journal = {ArXiv e-prints}, archivePrefix = {arXiv}, eprint = {1207.3675}, primaryClass = {astro-ph.CO}, keywords = {Astrophysics - Cosmology and Extragalactic Astrophysics}, year = {2012}, month = {jul}, adsurl = {http://adsabs.harvard.edu/abs/2012arXiv1207.3675D}, adsnote = {Provided by the SAO/NASA Astrophysics Data System} }

1. armitage-caplan2009 bibtex=@ARTICLE{armitage-caplan2009,

author = {Armitage-Caplan, C. and Wandelt, B. D.}, title = {PReBeaM for Planck: A Polarized Regularized Beam Deconvolution Map-Making Method}, journal = {Aps}, archivePrefix = {arXiv}, eprint = {0807.4179}, keywords = {cosmic microwave background, cosmology: observations, methods: data analysis}, year = {2009}, month = {apr}, volume = {181}, pages = {533-542}, doi = {10.1088/0067-0049/181/2/533}, adsurl = {http://adsabs.harvard.edu/abs/2009ApJS..181..533A}, adsnote = {Provided by the SAO/NASA Astrophysics Data System} }

1. ashdown2007a bibtex=@ARTICLE{ashdown2007a,

author = {Ashdown, M. A. J. and Baccigalupi, C. and Balbi, A. and Bartlett, J. G. and Borrill, J. and Cantalupo, C. and de Gasperis, G. and Górski, K. M. and Heikkilä, V. and Hivon, E. and Keihänen, E. and Kurki-Suonio, H. and Lawrence, C. R. and Natoli, P. and Poutanen, T. and Prunet, S. and Reinecke, M. and Stompor, R. and Wandelt, B.}, title = {Making maps from Planck LFI 30 GHz data}, journal = {A&A}, eprint = {arXiv:astro-ph/0702483}, keywords = {cosmology: cosmic microwave background, methods: data, analysis, techniques: image processing, cosmology: observations}, year = {2007}, month = {aug}, volume = {471}, pages = {361-380}, doi = {10.1051/0004-6361:20077312}, adsurl = {http://adsabs.harvard.edu/abs/2007A%26A...471..361A}, adsnote = {Provided by the SAO/NASA Astrophysics Data System} }

1. ashdown2007b bibtex=@ARTICLE{ashdown2007b,

author = {Ashdown, M. A. J. and Baccigalupi, C. and Balbi, A. and Bartlett, J. G. and Borrill, J. and Cantalupo, C. and de Gasperis, G. and Górski, K. M. and Hivon, E. and Keihänen, E. and Kurki-Suonio, H. and Lawrence, C. R. and Natoli, P. and Poutanen, T. and Prunet, S. and Reinecke, M. and Stompor, R. and Wandelt, B. and {The Planck CTP Working Group} }, title = {Making sky maps from Planck data}, journal = {A&A}, eprint = {arXiv:astro-ph/0606348}, keywords = {cosmology: cosmic microwave background, methods: data analysis}, year = {2007}, month = {may}, volume = {467}, pages = {761-775}, doi = {10.1051/0004-6361:20065829}, adsurl = {http://adsabs.harvard.edu/abs/2007A%26A...467..761A}, adsnote = {Provided by the SAO/NASA Astrophysics Data System} }

1. ashdown2009 bibtex=@ARTICLE{ashdown2009,

author = {Ashdown, M. A. J. and Baccigalupi, C. and Bartlett, J. G. and Borrill, J. and Cantalupo, C. and de Gasperis, G. and de Troia, G. and Górski, K. M. and Hivon, E. and Hufenberger, K. and Keihänen, E. and Keskitalo, R. and Kisner, T. and Kurki-Suonio, H. and Lawrence, C. R. and Natoli, P. and Poutanen, T. and Prézeau, G. and Reinecke, M. and Rocha, G. and Sandri, M. and Stompor, R. and Villa, F. and Wandelt, B. and {The Planck Ctp Working Group}}, title = {Making maps from Planck LFI 30 GHz data with asymmetric beams and cooler noise}, journal = {A&A}, archivePrefix = {arXiv}, eprint = {0806.3167}, keywords = {cosmology: cosmic microwave background, methods: data analysis, cosmology: observations}, year = {2009}, month = {jan}, volume = {493}, pages = {753-783}, doi = {10.1051/0004-6361:200810381}, adsurl = {http://adsabs.harvard.edu/abs/2009A%26A...493..753A}, adsnote = {Provided by the SAO/NASA Astrophysics Data System} }

1. aumont2010 bibtex=@ARTICLE{aumont2010,

author = {Aumont, J. and Conversi, L. and Thum, C. and Wiesemeyer, H. and Falgarone, E. and Macías-Pérez, J. F. and Piacentini, F. and Pointecouteau, E. and Ponthieu, N. and Puget, J. L. and Rosset, C. and Tauber, J. A. and Tristram, M.}, title = {Measurement of the Crab nebula polarization at 90 GHz as a calibrator for CMB experiments}, journal = {A&A}, keywords = {ISM: supernova remnants, polarization, cosmology: cosmic background radiation}, year = {2010}, month = {may}, volume = {514}, pages = {A70+}, doi = {10.1051/0004-6361/200913834}, adsurl = {http://adsabs.harvard.edu/abs/2010A%26A...514A..70A}, adsnote = {Provided by the SAO/NASA Astrophysics Data System} }

1. cappellini2003 bibtex=@ARTICLE{cappellini2003,

author = {Cappellini, B. and Maino, D. and Albetti, G. and Platania, P. and Paladini, R. and Mennella, A. and Bersanelli, M.}, title = {Optimized in-flight absolute calibration for extended CMB surveys}, journal = {A&A}, eprint = {arXiv:astro-ph/0309317}, keywords = {cosmology: cosmic microwave background, methods: data analysis}, year = {2003}, month = {oct}, volume = {409}, pages = {375-385}, doi = {10.1051/0004-6361:20030927}, adsurl = {http://adsabs.harvard.edu/abs/2003A%26A...409..375C}, adsnote = {Provided by the SAO/NASA Astrophysics Data System} }

1. colombo2009 bibtex=@ARTICLE{colombo2009,

author = {Colombo, L. P. L. and Pierpaoli, E. and Pritchard, J. R. }, title = {Cosmological parameters after WMAP5: forecasts for Planck and future galaxy surveys}, journal = {MNRAS}, archivePrefix = {arXiv}, eprint = {0811.2622}, keywords = {galaxies: statistics , cosmic microwave background , cosmological parameters , large-scale structure of Universe}, year = {2009}, month = {oct}, volume = {398}, pages = {1621-1637}, doi = {10.1111/j.1365-2966.2009.14802.x}, adsurl = {http://adsabs.harvard.edu/abs/2009MNRAS.398.1621C}, adsnote = {Provided by the SAO/NASA Astrophysics Data System} }

1. dupac2005 bibtex=@ARTICLE{dupac2005,

author = {Dupac, X. and Tauber, J.}, title = {Scanning strategy for mapping the Cosmic Microwave Background anisotropies with Planck}, journal = {A&A}, eprint = {arXiv:astro-ph/0409405}, keywords = {cosmic microwave background, methods: observational}, year = {2005}, month = {jan}, volume = {430}, pages = {363-371}, doi = {10.1051/0004-6361:20041526}, adsurl = {http://adsabs.harvard.edu/abs/2005A%26A...430..363D}, adsnote = {Provided by the SAO/NASA Astrophysics Data System} }

1. hanson2009 bibtex=@ARTICLE{hanson2009,

author = {Hanson, D. and Rocha, G. and Górski, K.}, title = {Lensing reconstruction from Planck sky maps: inhomogeneous noise}, journal = {MNRAS}, archivePrefix = {arXiv}, eprint = {0907.1927}, keywords = {gravitational lensing , methods: numerical , cosmic microwave background , cosmology: observations}, year = {2009}, month = {dec}, volume = {400}, pages = {2169-2173}, doi = {10.1111/j.1365-2966.2009.15614.x}, adsurl = {http://adsabs.harvard.edu/abs/2009MNRAS.400.2169H}, adsnote = {Provided by the SAO/NASA Astrophysics Data System} }

1. huffmanberger2010 bibtex=@ARTICLE{huffmanberger2010,

author = {Huffenberger, K. M. and Crill, B. P. and Lange, A. E. and Górski, K. M. and Lawrence, C. R.}, title = {Measuring Planck beams with planets}, journal = {A&A}, archivePrefix = {arXiv}, eprint = {1007.3468}, primaryClass = {astro-ph.CO}, keywords = {cosmic microwave background, cosmological parameters, cosmology: observations}, year = {2010}, month = {feb}, volume = {510}, pages = {A58+}, doi = {10.1051/0004-6361/200913117}, adsurl = {http://cdsads.u-strasbg.fr/abs/2010A%26A...510A...58H}, adsnote = {Provided by the SAO/NASA Astrophysics Data System }

1. leach2008 bibtex=@ARTICLE{leach2008,

author = {Leach, S. M. and Cardoso, J.-F. and Baccigalupi, C. and Barreiro, R. B. and Betoule, M. and Bobin, J. and Bonaldi, A. and Delabrouille, J. and de Zotti, G. and Dickinson, C. and Eriksen, H. K. and González-Nuevo, J. and Hansen, F. K. and Herranz, D. and Le Jeune, M. and López-Caniego, M. and Martínez-González, E. and Massardi, M. and Melin, J.-B. and Miville-Deschênes, M.-A. and Patanchon, G. and Prunet, S. and Ricciardi, S. and Salerno, E. and Sanz, J. L. and Starck, J.-L. and Stivoli, F. and Stolyarov, V. and Stompor, R. and Vielva, P. }, title = {Component separation methods for the PLANCK mission}, journal = {A&A}, archivePrefix = {arXiv}, eprint = {0805.0269}, keywords = {cosmology: cosmic microwave background, methods: data analysis}, year = {2008}, month = {nov}, volume = {491}, pages = {597-615}, doi = {10.1051/0004-6361:200810116}, adsurl = {http://adsabs.harvard.edu/abs/2008A%26A...491..597L}, adsnote = {Provided by the SAO/NASA Astrophysics Data System }

1. massardi2006 bibtex=@INPROCEEDINGS{massardi2006,

author = {Massardi, M.}, title = {Realistic point source maps at Planck frequencies}, booktitle = {CMB and Physics of the Early Universe}, year = {2006}, adsurl = {http://adsabs.harvard.edu/abs/2006cmb.confE..45M}, adsnote = {Provided by the SAO/NASA Astrophysics Data System }

1. mennella2002 bibtex=@ARTICLE{mennella2002,

author = {Mennella, A. and Bersanelli, M. and Burigana, C. and Maino, D. and Mandolesi, N. and Morgante, G. and Stanghellini, G.}, title = {PLANCK: Systematic effects induced by periodic fluctuations of arbitrary shape}, journal = {A&A}, eprint = {arXiv:astro-ph/0111078}, keywords = {COSMOLOGY: COSMIC MICROWAVE BACKGROUND, OBSERVATIONS, INSTRUMENTATION: DETECTORS, MISCELLANEOUS, METHODS: ANALYTICAL}, year = {2002}, month = {mar}, volume = {384}, pages = {736-742}, doi = {10.1051/0004-6361:20020024}, adsurl = {http://adsabs.harvard.edu/abs/2002A%26A...384..736M}, adsnote = {Provided by the SAO/NASA Astrophysics Data System }

1. mennella2003 bibtex=@ARTICLE{mennella2003,

author = {Mennella, A. and Bersanelli, M. and Seiffert, M. and Kettle, D. and Roddis, N. and Wilkinson, A. and Meinhold, P.}, title = {Offset balancing in pseudo-correlation radiometers for CMB measurements}, journal = {A&A}, eprint = {arXiv:astro-ph/0307558}, keywords = {cosmology: cosmic microwave background, observations, instrumentation: detectors, methods: analytical}, year = {2003}, month = {nov}, volume = {410}, pages = {1089-1100}, doi = {10.1051/0004-6361:20031266}, adsurl = {http://adsabs.harvard.edu/abs/2003A%26A...410.1089M}, adsnote = {Provided by the SAO/NASA Astrophysics Data System }

1. natoli2001 bibtex=@ARTICLE{natoli2001,

author = {Natoli, P. and de Gasperis, G. and Gheller, C. and Vittorio, N. }, title = {A Map-Making algorithm for the Planck Surveyor.}, journal = {A&A}, eprint = {arXiv:astro-ph/0101252}, keywords = {COSMIC MICROWAVE BACKGROUND ANISOTROPIES, METHODS: DATA ANALYSIS}, year = {2001}, month = {jun}, volume = {372}, pages = {346-356}, doi = {10.1051/0004-6361:20010393}, adsurl = {http://adsabs.harvard.edu/abs/2001A%26A...372..346N}, adsnote = {Provided by the SAO/NASA Astrophysics Data System }

1. reinecke2006 bibtex=@ARTICLE{reinecke2006,

author = {Reinecke, M. and Dolag, K. and Hell, R. and Bartelmann, M. and Enßlin, T. A.}, title = {A simulation pipeline for the Planck mission}, journal = {A&A}, eprint = {arXiv:astro-ph/0508522}, keywords = {cosmology:

cosmic microwave background, cosmology: large-scale structure of Universe, methods: numerical}, year = {2006}, month = {jan}, volume = {445}, pages = {373-373}, doi = {10.1051/0004-6361:20053413}, adsurl = {http://adsabs.harvard.edu/abs/2006A%26A...445..373R}, adsnote = {Provided by the SAO/NASA Astrophysics Data System} }

1. ricciardi2007 bibtext=@ARTICLE{ricciardi2007,

author = {Ricciardi, S.}, title = {Planck Reference Sky versus WMAP}, journal = {New Astronomy Review}, year = {2007}, month = {mar}, volume = {51}, pages = {310-315}, doi = {10.1016/j.newar.2006.11.054}, adsurl = {http://adsabs.harvard.edu/abs/2007NewAR..51..310R}, adsnote = {Provided by the SAO/NASA Astrophysics Data System} }

1. rocha2009 bibtext=@ARTICLE{rocha2009,

author = {Rocha, G. and Contaldi, C. R. and Bond, J. R. and Gorski, K. M. }, title = {Application of XFaster power spectrum and likelihood estimator to Planck}, journal = {ArXiv e-prints}, archivePrefix = {arXiv}, eprint = {0912.4059}, keywords = {Astrophysics - Cosmology and Extragalactic Astrophysics, Astrophysics - Instrumentation and Methods for Astrophysics}, year = {2009}, month = {dec}, adsurl = {http://adsabs.harvard.edu/abs/2009arXiv0912.4059R}, adsnote = {Provided by the SAO/NASA Astrophysics Data System} }

1. seiffert2002 bibtext=@ARTICLE{seiffert2002,

author = {Seiffert, M. and Mennella, A. and Burigana, C. and Mandolesi, N. and Bersanelli, M. and Meinhold, P. and Lubin, P.}, title = {1/f noise and other systematic effects in the Planck-LFI radiometers}, journal = {A&A}, eprint = {arXiv:astro-ph/0206093}, keywords = {cosmology: cosmic microwave background, observations, instrumentation: detectors, methods: analytical}, year = {2002}, month = {sep}, volume = {391}, pages = {1185-1197}, doi = {10.1051/0004-6361:20020880}, adsurl = {http://adsabs.harvard.edu/abs/2002A%26A...391.1185S}, adsnote = {Provided by the SAO/NASA Astrophysics Data System} }

1. white2006 bibtext=@ARTICLE{white2006,

author = {White, M.}, title = {Cosmological science enabled by Planck}, journal = {New Astronomy Reviews}, eprint = {arXiv:astro-ph/0606643}, year = {2006}, month = {dec}, volume = {50}, pages = {938-944}, doi = {10.1016/j.newar.2006.09.008}, adsurl = {http://adsabs.harvard.edu/abs/2006NewAR..50..938W}, adsnote = {Provided by the SAO/NASA Astrophysics Data System} }

1. buehler1996 bibtext=@INPROCEEDINGS{buehler1996,

author = {Buehler, P. and Desorgher, L. and Zehnder, A.}, title = {Simple Instruments for Continuous Measurement of Trapped Particles}, booktitle = {Environment Modeling for Space-Based Applications}, year = {1996}, series = {ESA Special Publication}, volume = {392}, editor = {T.-D. Guyenne & A. Hilgers}, month = {dec}, pages = {87-+}, adsurl = {http://adsabs.harvard.edu/abs/1996ESASP.392...87B}, adsnote = {Provided by the SAO/NASA Astrophysics Data System} }

1. cantalupo2010 bibtext=@ARTICLE{cantalupo2010,

author = {Cantalupo, C. M. and Borrill, J. D. and Jaffe, A. H. and Kisner, T. S. and Stompor, R.}, title = {MADmap: A Massively Parallel Maximum Likelihood Cosmic Microwave Background Map-maker}, journal = {Aps}, archivePrefix = {arXiv}, eprint = {0906.1775}, primaryClass = {astro-ph.CO}, keywords = {cosmic background radiation, cosmology: observations, methods: data analysis, methods: numerical}, year = {2010}, month = {mar}, volume = {187}, pages = {212-227}, doi = {10.1088/0067-0049/187/1/212}, adsurl = {http://adsabs.harvard.edu/abs/2010ApJS..187..212C}, adsnote = {Provided by the SAO/NASA Astrophysics Data System} }

1. degasperis2005 bibtext=@ARTICLE{degasperis2005,

author = {de Gasperis, G. and Balbi, A. and Cabella, P. and Natoli, P. and Vittorio, N.}, title = {ROMA: A map-making algorithm for polarised CMB data sets}, journal = {A&A}, eprint = {arXiv:astro-ph/0502142}, keywords = {cosmology: cosmic microwave background, methods: statistical, methods: data analysis}, year =



{2005}, month = {jun}, volume = {436}, pages = {1159-1165}, doi = {10.1051/0004-6361:20042512}, adsurl = {http://adsabs.harvard.edu/abs/2005A%26A...436.1159D}, adsnote = {Provided by the SAO/NASA Astrophysics Data System} }

1. finkbeiner1999 bibtex=@ARTICLE{finkbeiner1999,

author = {Finkbeiner, D. P. and Davis, M. and Schlegel, D. J.}, title = {Extrapolation of Galactic Dust Emission at 100 Microns to Cosmic Microwave Background Radiation Frequencies Using FIRAS}, journal = {Ap}, eprint = {arXiv:astro-ph/9905128}, keywords = {ISM: DUST, EXTINCTION, INFRARED: ISM: CONTINUUM, SUBMILLIMETER}, year = {1999}, month = {oct}, volume = {524}, pages = {867-886}, doi = {10.1086/307852}, adsurl = {http://cdsads.u-strasbg.fr/abs/1999ApJ...524..867F}, adsnote = {Provided by the SAO/NASA Astrophysics Data System} }

1. fixsen1997 bibtex=@ARTICLE{fixsen1997,

author = {Fixsen, D. J. and Weiland, J. L. and Brodd, S. and Hauser, M. G. and Kelsall, T. and Leisawitz, D. T. and Mather, J. C. and Jensen, K. A. and Schafer, R. A. and Silverberg, R. F. }, title = {Comparison of the COBE FIRAS and DIRBE Calibrations}, journal = {Ap}, eprint = {arXiv:astro-ph/9707192}, keywords = {COSMOLOGY: COSMIC MICROWAVE BACKGROUND, INFRARED: GENERAL, INSTRUMENTATION: PHOTOMETERS}, year = {1997}, month = {dec}, volume = {490}, pages = {482-+}, doi = {10.1086/304906}, adsurl = {http://cdsads.u-strasbg.fr/abs/1997ApJ...490..482F}, adsnote = {Provided by the SAO/NASA Astrophysics Data System} }

1. gorski2005 bibtex=@ARTICLE{gorski2005,

author = {Górski, K. M. and Hivon, E. and Banday, A. J. and Wandelt, B. D. and Hansen, F. K. and Reinecke, M. and Bartelmann, M.}, title = {HEALPix: A Framework for High-Resolution Discretization and Fast Analysis of Data Distributed on the Sphere}, journal = {Ap}, eprint = {arXiv:astro-ph/0409513}, keywords = {Cosmology: Cosmic Microwave Background, Cosmology: Observations, Methods: Statistical}, year = {2005}, month = {apr}, volume = {622}, pages = {759-771}, doi = {10.1086/427976}, adsurl = {http://adsabs.harvard.edu/abs/2005ApJ...622..759G}, adsnote = {Provided by the SAO/NASA Astrophysics Data System} }

1. keihanen2004 bibtex=@ARTICLE{keihanen2004,

author = {Keihänen, E. and Kurki-Suonio, H. and Poutanen, T. and Maino, D. and Burigana, C.}, title = {A maximum likelihood approach to the destripping technique}, journal = {A&A}, eprint = {arXiv:astro-ph/0304411}, keywords = {methods: data analysis, cosmology: cosmic microwave background}, year = {2004}, month = {dec}, volume = {428}, pages = {287-298}, doi = {10.1051/0004-6361:200400060}, adsurl = {http://cdsads.u-strasbg.fr/abs/2004A%26A...428..287K}, adsnote = {Provided by the SAO/NASA Astrophysics Data System} }

1. keihanen2005 bibtex=@ARTICLE{keihanen2005,

author = {Keihänen, E. and Kurki-Suonio, H. and Poutanen, T. }, title = {MADAM- a map-making method for CMB experiments}, journal = {MNRAS}, eprint = {arXiv:astro-ph/0412517}, keywords = {methods: data analysis, cosmic microwave background}, year = {2005}, month = {jun}, volume = {360}, pages = {390-400}, doi = {10.1111/j.1365-2966.2005.09055.x}, adsurl = {http://cdsads.u-strasbg.fr/abs/2005MNRAS.360..390K}, adsnote = {Provided by the SAO/NASA Astrophysics Data System} }

1. keihanen2010 bibtex=@ARTICLE{keihanen2010,

author = {Keihänen, E. and Keskitalo, R. and Kurki-Suonio, H. and Poutanen, T. and Sirviö, A.-S.}, title = {Making cosmic microwave background temperature and polarization maps with MADAM}, journal = {A&A}, archivePrefix = {arXiv}, eprint = {0907.0367}, primaryClass = {astro-ph.CO}, keywords = {cosmology: cosmic microwave background, methods: data analysis}, year = {2010}, month = {feb}, volume = {510}, pages = {A57+}, doi = {10.1051/0004-6361/200912813}, adsurl = {http://adsabs.harvard.edu/abs/2010A%26A...510A..57K}, adsnote = {Provided by the SAO/NASA Astrophysics Data System} }

1. kurki-suonio2009 bibtex=@ARTICLE{kurki-suonio2009,

author = {Kurki-Suonio, H. and Keihänen, E. and Keskitalo, R. and Poutanen, T. and Sirviö, A.-S. and Maino, D. and Burigana, C.}, title = {Destriping CMB temperature and polarization maps}, journal = {A&A}, archivePrefix = {arXiv}, eprint = {0904.3623}, primaryClass = {astro-ph.IM}, keywords = {methods: data analysis, cosmology: cosmic microwave background}, year = {2009}, month = {nov}, volume = {506}, pages = {1511-1539}, doi = {10.1051/0004-6361/200912361}, adsurl = {http://adsabs.harvard.edu/abs/2009A%26A...506.1511K}, adsnote = {Provided by the SAO/NASA Astrophysics Data System} }

1. macias2007 bibtex=@ARTICLE{macias2007,

author = {Macías-Pérez, J. F. and Lagache, G. and Maffei, B. and Ganga, K. and Bourrachot, A. and Ade, P. and Amblard, A. and Ansari, R. and Aubourg, E. and Aumont, J. and Bargout, S. and Bartlett, J. and Benoît, A. and Bernard, J.-P. and Bhatia, R. and Blanchard, A. and Bock, J. J. and Boscaleri, A. and Bouchet, F. R. and Camus, P. and Cardoso, J.-F. and Couchot, F. and de Bernardis, P. and Delabrouille, J. and Désert, F.-X. and Doré, O. and Douspis, M. and Dumoulin, L. and Dupac, X. and Filliatre, P. and Fosalba, P. and Gannaway, F. and Gautier, B. and Giard, M. and Giraud-Héraud, Y. and Gispert, R. and Guglielmi, L. and Hamilton, J.-C. and Hanany, S. and Henrot-Versillé, S. and Hristov, V. and Kaplan, J. and Lamarre, J.-M. and Lange, A. E. and Madet, K. and Magneville, C. and Marrone, D. P. and Masi, S. and Mayet, F. and Murphy, J. A. and Naraghi, F. and Nati, F. and Patanchon, G. and Perdureau, O. and Perrin, G. and Plaszczynski, S. and Piat, M. and Ponthieu, N. and Prunet, S. and Puget, J.-L. and Renault, C. and Rosset, C. and Santos, D. and Starobinsky, A. and Strukov, I. and Sudiwala, R. V. and Teyssier, R. and Tristram, M. and Tucker, C. and Vanel, J.-C. and Vibert, D. and Wakui, E. and Yvon, D.}, title = {Archeops in-flight performance, data processing, and map making}, journal = {A&A}, eprint = {arXiv:astro-ph/0603665}, keywords = {methods: data analysis, cosmology: cosmic microwave background}, year = {2007}, month = {jun}, volume = {467}, pages = {1313-1344}, doi = {10.1051/0004-6361:20065258}, adsurl = {http://cdsads.u-strasbg.fr/abs/2007A%26A...467.1313M}, adsnote = {Provided by the SAO/NASA Astrophysics Data System} }

1. maino2002 bibtex=@ARTICLE{maino2002,

author = {Maino, D. and Burigana, C. and Górski, K. M. and Mandolesi, N. and Bersanelli, M.}, title = {Removing 1/f noise stripes in cosmic microwave background anisotropy observations}, journal = {A&A}, eprint = {arXiv:astro-ph/0202271}, keywords = {methods: data analysis, cosmology: cosmic microwave background}, year = {2002}, month = {may}, volume = {387}, pages = {356-365}, doi = {10.1051/0004-6361:20020242}, adsurl = {http://cdsads.u-strasbg.fr/abs/2002A%26A...387..356M}, adsnote = {Provided by the SAO/NASA Astrophysics Data System} }

1. melin2006 bibtex=@ARTICLE{melin2006,

author = {Melin, J.-B. and Bartlett, J. G. and Delabrouille, J. }, title = {Catalog extraction in SZ cluster surveys: a matched filter approach}, journal = {A&A}, eprint = {arXiv:astro-ph/0602424}, keywords = {large-scale structure of Universe, galaxies: clusters: general, methods: data analysis}, year = {2006}, month = {nov}, volume = {459}, pages = {341-352}, doi = {10.1051/0004-6361:20065034}, adsurl = {http://adsabs.harvard.edu/abs/2006A%26A...459..341M}, adsnote = {Provided by the SAO/NASA Astrophysics Data System} }

1. poutanen2006 bibtex=@ARTICLE{poutanen2006,

author = {Poutanen, T. and de Gasperis, G. and Hivon, E. and Kurki-Suonio, H. and Balbi, A. and Borrill, J. and Cantalupo, C. and Doré, O. and Keihänen, E. and Lawrence, C. R. and Maino, D. and Natoli, P. and Prunet, S. and Stompor, R. and Teyssier, R. }, title = {Comparison of map-making algorithms for CMB experiments}, journal = {A&A}, eprint = {arXiv:astro-ph/0501504}, keywords = {methods: data analysis, cosmology: cosmic microwave background}, year = {2006}, month = {apr}, volume = {449}, pages = {1311-1322}, doi = {10.1051/0004-6361:20052845}, adsurl = {http://adsabs.harvard.edu/abs/2006A%26A...449.1311P}, adsnote = {Provided by the SAO/NASA Astrophysics Data System} }

1. pratt1978 bibtex=@BOOK{pratt1978,

author = {Pratt, W. K.}, title = {Digital image processing}, booktitle = {A Wiley-Interscience Publication, New York: Wiley, 1978}, year = {1978}, editor = {Pratt, W. K.}, adsurl = {http://adsabs.harvard.edu/abs/1978dip..book.....P}, adsnote = {Provided by the SAO/NASA Astrophysics Data System} }

1. prunet2001 bibtex=@ARTICLE{prunet2001,

author = {Prunet, S. and Ade, P. A. R. and Bock, J. J. and Bond, J. R. and Borrill, J. and Boscaleri, A. and Coble, K. and Crill, B. P. and de Bernardis, P. and De Gasperis, G. and De Troia, G. and Farese, P. C. and Ferreira, P. G. and Ganga, K. and Giacometti, M. and Hivon, E. and Hristov, V. V. and Iacoangeli, A. and Jaffe, A. H. and Lange, A. E. and Martinis, L. and Masi, S. and Mason, P. and Mauskopf, P. D. and Melchiorri, A. and Miglio, L. and Montroy, T. and Netterfield, C. B. and Pascale, E. and Piacentini, F. and Pogosyan, D. and Pongetti, F. and Prunet, S. and Rao, S. and Romeo, G. and Ruhl, J. E. and Scaramuzzi, F. and Sforza, D. and Vittorio, N.}, title = {Noise estimation in CMB time-streams and fast map-making. Application to the BOOMERanG98 data}, journal = {ArXiv Astrophysics e-prints}, eprint = {arXiv:astro-ph/0101073}, keywords = {Astrophysics}, year = {2001}, month = {jan}, adsurl = {http://adsabs.harvard.edu/abs/2001astro.ph..1073P}, adsnote = {Provided by the SAO/NASA Astrophysics Data System} }

1. shoemake1985 bibtex=@inproceedings{shoemake1985,

author = {Shoemake, Ken}, title = {Animating rotation with quaternion curves}, booktitle = {SIGGRAPH '85: Proceedings of the 12th annual conference on Computer graphics and interactive techniques}, year = {1985}, isbn = {0-89791-166-0}, pages = {245--254}, doi = {http://doi.acm.org/10.1145/325334.325242}, publisher = {ACM}, address = {New York, NY, USA}, }

1. shuster1993 bibtex=@ARTICLE{shuster1993,

author = {Shuster, M. D.}, title = {Survey of attitude representations}, journal = {Journal of the Astronautical Sciences}, keywords = {ATTITUDE CONTROL, FLIGHT MECHANICS, KINEMATIC EQUATIONS, SATELLITE ORIENTATION, SATELLITE ROTATION, COVARIANCE, ERRORS, KINEMATICS, TRANSFORMATIONS (MATHEMATICS)}, year = {1993}, month = {oct}, volume = {41}, pages = {439-517}, adsurl = {http://adsabs.harvard.edu/abs/1993JAnSc..41..439S}, adsnote = {Provided by the SAO/NASA Astrophysics Data System} }

1. swinyard2010 bibtex=@ARTICLE{swinyard2010,

author = {Swinyard, B. M. and Hartogh, P. and Sidher, S. and Fulton, T. and Lellouch, E. and Jarchow, C. and Griffin, M. J. and Moreno, R. and Sagawa, H. and Portyankina, G. and Blecka, M. and Banaszkiewicz, M. and Bockelee-Morvan, D. and Crovisier, J. and Encrenaz, T. and Kueppers, M. and Lara, L. and Lis, D. and Medvedev, A. and Rengel, M. and Szutowicz, S. and Vandenbussche, B. and Bensch, F. and Bergin, E. and Billebaud, F. and Biver, N. and Blake, G. and Blommaert, J. and de Val-Borro, M. and Cernicharo, J. and Cavalie, T. and Courtin, R. and Davis, G. and Decin, L. and Encrenaz, P. and de Graauw, T. and Jehin, E. and Kidger, M. and Leeks, S. and Orton, G. and Naylor, D. and Schieder, R. and Stam, D. and Thomas, N. and Verdugo, E. and Waelkens, C. and Walker, H.}, title = {The Herschel-SPIRE submillimetre spectrum of Mars}, journal = {A&A}, archivePrefix = {arXiv}, eprint = {1005.4579}, primaryClass = {astro-ph.EP}, keywords = {instrumentation: spectrographs, space vehicles: instruments, planets and satellites: atmospheres, planets and satellites: individual: Mars, planets and satellites: composition}, year = {2010}, month = {jul}, volume = {518}, pages = {L151+}, doi = {10.1051/0004-6361/201014717}, adsurl = {http://adsabs.harvard.edu/abs/2010A%26A...518L.151S}, adsnote = {Provided by the SAO/NASA Astrophysics Data System} }

1. carvalho2009 bibtex=@ARTICLE{carvalho2009,

author = {Carvalho, P. and Rocha, G. and Hobson, M. P.}, title = {A fast Bayesian approach to discrete object detection in astronomical data sets - PowellSnakes I}, journal = {MNRAS}, archivePrefix = {arXiv}, eprint = {0802.3916}, keywords = {methods: data analysis , cosmic microwave background , cosmology: observations}, year = {2009}, month = {mar}, volume = {393}, pages = {681-702}, doi = {10.1111/j.1365-2966.2008.14016.x}, adsurl

= {http://adsabs.harvard.edu/abs/2009MNRAS.393..681C}, adsnote = {Provided by the SAO/NASA Astrophysics Data System} }

1. colombi2009 bibtex=@ARTICLE{colombi2009,

author = {Colombi, S. and Jaffe, A. and Novikov, D. and Pichon, C. }, title = {Accurate estimators of power spectra in N-body simulations}, journal = {MNRAS}, archivePrefix = {arXiv}, eprint = {0811.0313}, keywords = {methods: analytical , methods: data analysis , methods: N-body simulations , methods: numerical , methods: statistical , large-scale structure of Universe}, year = {2009}, month = {feb}, volume = {393}, pages = {511-526}, doi = {10.1111/j.1365-2966.2008.14176.x}, adsurl = {http://cdsads.u-strasbg.fr/abs/2009MNRAS.393..511C}, adsnote = {Provided by the SAO/NASA Astrophysics Data System} }

1. dame2001 bibtex=@ARTICLE{dame2001,

author = {Dame, T. M. and Hartmann, D. and Thaddeus, P.}, title = {The Milky Way in Molecular Clouds: A New Complete CO Survey}, journal = {ApJ}, eprint = {arXiv:astro-ph/0009217}, keywords = {Galaxy: Structure, ISM: Clouds, ISM: Molecules, Radio Lines: ISM, Galaxy: Solar Neighborhood, Stars: Formation}, year = {2001}, month = {feb}, volume = {547}, pages = {792-813}, doi = {10.1086/318388}, adsurl = {http://cdsads.u-strasbg.fr/abs/2001ApJ...547..792D}, adsnote = {Provided by the SAO/NASA Astrophysics Data System} }

1. ferreira2000 bibtex=@ARTICLE{ferreira2000,

author = {Ferreira, P. G. and Jaffe, A. H.}, title = {Simultaneous estimation of noise and signal in cosmic microwave background experiments}, journal = {MNRAS}, eprint = {arXiv:astro-ph/9909250}, keywords = {COSMIC MICROWAVE BACKGROUND}, year = {2000}, month = {feb}, volume = {312}, pages = {89-102}, doi = {10.1046/j.1365-8711.2000.03108.x}, adsurl = {http://cdsads.u-strasbg.fr/abs/2000MNRAS.312..89F}, adsnote = {Provided by the SAO/NASA Astrophysics Data System} }

1. giorgini1996 bibtex=@INPROCEEDINGS{giorgini1996,

author = {Giorgini, J. D. and Yeomans, D. K. and Chamberlin, A. B. and Chodas, P. W. and Jacobson, R. A. and Keesey, M. S. and Lieske, J. H. and Ostro, S. J. and Standish, E. M. and Wimberly, R. N.}, title = {JPL's On-Line Solar System Data Service}, booktitle = {Bulletin of the American Astronomical Society}, year = {1996}, series = {Bulletin of the American Astronomical Society}, volume = {28}, month = {sep}, pages = {1158-+}, adsurl = {http://ukads.nottingham.ac.uk/abs/1996DPS...28.2504G}, adsnote = {Provided by the SAO/NASA Astrophysics Data System} }

1. mitra2010 bibtex=@ARTICLE{mitra2010,

author = {Mitra, S. and Rocha, G. and Górski, K. M. and Huffenberger, K. M. and Eriksen, H. K. and Ashdown, M. A. J. and Lawrence, C. R. }, title = {Fast Pixel Space Convolution for Cosmic Microwave Background Surveys with Asymmetric Beams and Complex Scan Strategies: FEBeCoP}, journal = {Aps}, archivePrefix = {arXiv}, eprint = {1005.1929}, primaryClass = {astro-ph.CO}, keywords = {cosmic background radiation, methods: data analysis}, year = {2011}, month = {mar}, volume = {193}, pages = {5-+}, doi = {10.1088/0067-0049/193/1/5}, adsurl = {http://adsabs.harvard.edu/abs/2011ApJS..193....5M}, adsnote = {Provided by the SAO/NASA Astrophysics Data System} }

1. onishi2002 bibtex=@ARTICLE{onishi2002,

author = {Onishi, T. and Mizuno, A. and Kawamura, A. and Tachihara, K. and Fukui, Y.}, title = {A Complete Search for Dense Cloud Cores in Taurus}, journal = {ApJ}, keywords = {ISM: Clouds, ISM: Individual: Name: Taurus Cloud Complex, ISM: Molecules, Radio Lines: ISM, Stars: Formation}, year = {2002}, month = {aug}, volume = {575}, pages = {950-973}, doi = {10.1086/341347}, adsurl = {http://cdsads.u-strasbg.fr/abs/2002ApJ...575..950O}, adsnote = {Provided by the SAO/NASA Astrophysics Data System} }

1. rocha2010a bibtex=@ARTICLE{rocha2010a,

author = {Rocha, G. and Pagano, L. and Górski, K. M. and Huppenberger, K. M. and Lawrence, C. R. and Lange, A. E.}, title = {Markov chain beam randomization: a study of the impact of PLANCK beam measurement errors on cosmological parameter estimation}, journal = {A&A}, archivePrefix = {arXiv}, eprint = {0907.5254}, primaryClass = {astro-ph.CO}, keywords = {cosmic microwave background, cosmology: observations, methods: data analysis}, year = {2010}, month = {apr}, volume = {513}, pages = {A23+}, doi = {10.1051/0004-6361/200913032}, adsurl = {http://adsabs.harvard.edu/abs/2010A%26A...513A..23R}, adsnote = {Provided by the SAO/NASA Astrophysics Data System} }

1. rocha2010b bibtex=@ARTICLE{rocha2010b,

author = {Rocha, G. and Contaldi, C. R. and Colombo, L. P. L. and Bond, J. R. and Gorski, K. M. and Lawrence, C. R.}, title = {Performance of XFaster likelihood in real CMB experiments}, journal = {ArXiv e-prints}, archivePrefix = {arXiv}, eprint = {1008.4948}, primaryClass = {astro-ph.CO}, keywords = {Astrophysics - Cosmology and Extragalactic Astrophysics}, year = {2010}, month = {aug}, adsurl = {http://adsabs.harvard.edu/abs/2010arXiv1008.4948R}, adsnote = {Provided by the SAO/NASA Astrophysics Data System} }

1. spencer2010 bibtex=@ARTICLE{spencer2010,

author = {Spencer, L. D. and Naylor, D. A. and Swinyard, B. M.}, title = {Performance evaluation of the Herschel/SPIRE imaging Fourier transform spectrometer through ground-based measurements}, journal = {Measurement Science and Technology}, year = {2010}, month = {jun}, volume = {21}, number = {6}, pages = {065601-+}, doi = {10.1088/0957-0233/21/6/065601}, adsurl = {http://cdsads.u-strasbg.fr/abs/2010MeScT..21f5601S}, adsnote = {Provided by the SAO/NASA Astrophysics Data System} } </biblio>

# Planck Collaboration



The Planck Scientific Collaboration consists of all the scientists which have contributed to the development of the Planck mission, and who participate in the scientific exploitation of the Planck data during the proprietary period, which nominally ends with the release of the scientific products to the community 3.5 yrs after launch, i.e. in January 2013. A complete database of all members of the Planck Collaboration can be searched online<sup>[1]</sup>. Each individual is a member of one or more among four Consortia of scientists:

- The LFI Consortium, Principal Investigator N. Mandolesi of the Istituto di Astrofisica Spaziale e Fisica Cosmica (Bologna, Italy);
- The HFI Consortium, Principal Investigator J.L. Puget of the Institut d'Astrophysique Spatiale (Orsay, France), and co-PI F.R. Bouchet of the Institut d'Astrophysique de Paris (Paris, France);
- The DK-Planck Consortium, led by H.U. Norgaard-Nielsen of the Danish National Space Institute (Copenhagen, Denmark);
- ESA's Planck Science Office, Project Scientist J. Tauber.

The Planck instruments, LFI and HFI were designed, built, tested and delivered to ESA by dedicated teams under the direction of the LFI and HFI Principal Investigators and Project Managers.

The ground operations of the Planck satellite are based on 4 geographically distributed centres:

- The Mission Operations Centre (MOC), located at ESA's Operations Centre in Darmstadt (Germany), is responsible for all aspects of flight control and of the health and safety of the Planck satellite, including both instruments. It plans and executes all necessary satellite activities, including instrument commanding requests by the instrument operations centres. MOC communicates with the satellite using ESA's 35-m antenna located in

New Norcia (Australia) over a daily 3-hour period, during which it uplinks a scheduled activity timeline which is autonomously executed by the satellite, and downlinks the science and housekeeping (HK) data acquired by the satellite during the past 24 hours. The downlinked data are transferred from New Norcia to the MOC over a period of typically 8 hours; at MOC they are put onto a data server from where they are retrieved by the two Data Processing Centres.

- The Planck Science Office (PSO), located at ESA's European Space Astronomy Centre in Madrid (Spain) is responsible for coordinating scientific operations of the Planck instruments, and for planning the sky surveying strategy. It provides to MOC a detailed pointing plan with a periodicity of about 1 month. PSO also develops and operates the archive which stores and distribute the final scientific products to the community.
- The LFI Operations and Data Processing Centre, located at the Osservatorio Astronomico di Trieste (Italy), is responsible for the optimal operation of the LFI instrument, and for the processing of the data acquired by LFI into the final scientific products of the mission.
- The HFI Operations and Data Processing Centres, located respectively at the Institut d'Astrophysique Spatiale in Orsay (France) and at the Institut d'Astrophysique de Paris (France), are similarly responsible for the optimal operation of the HFI instrument, and (with several other institutes in France and the UK) for the processing of the data acquired by HFI into the final scientific products of the mission.

The Planck Science Team (see membership <sup>[2]</sup>) is a formal body set up by ESA at the inception of the project to represent the scientific interests of the mission, which has had a key advisory role to the development of the satellite, payload and ground segment. It is a recognised principle of the mission that the scientific exploitation of Planck during the proprietary period is a joint venture between the involved Consortia, and the Science Team is the body which has taken the role to organise, plan, coordinate, and oversee all the common activities in this respect. All members of the Planck Scientific Collaboration have agreed to abide by the policies set by the Science Team with regard to data access and publication of scientific results.

The scientific activities of the Planck Collaboration within the proprietary period are organised in "Projects", which consist of teams of people who are responsible to write papers on specific scientific topics on behalf of the whole Collaboration. "Working groups" gather Projects in similar areas. Coordinators of Working Groups and Leaders of Projects are nominated by the Planck Science Team. Papers by the Planck Collaboration are based on the scientific programme described in the Planck Bluebook; their authorship is extensive and ordered alphabetically. Individual members who have made important contributions to Planck over many years are referred to as "Planck Scientists" and have the right to co-author all these papers. Other members of the Planck Collaboration are referred to as "Planck Associates" and have the right to co-author papers to which they have contributed. Papers describing technical aspects or very specialized science topics, are prepared by ad-hoc teams and have non-alphabetic author order.

An internal reviewing process ensures that scientific papers submitted for publication by the Planck Collaboration are consistent with each other and of high scientific quality. This process is led by an internal Editorial Board which is led by Planck's Survey Scientists and consists of senior members of the Planck Collaboration. The Editorial Board makes recommendations to the Planck Science Team on the readiness for submission of all Planck papers. The Science Team makes the final decisions.

## Funding

Planck is a project of the European Space Agency - ESA - with instruments provided by two scientific Consortia funded by ESA member states (in particular the lead countries: France and Italy) with contributions from NASA (USA), and telescope reflectors provided in a collaboration between ESA and a scientific Consortium led and funded by Denmark.

ESA has managed the project since its inception in 1993 and funded the development of the satellite, its launch, and its operations.

The Planck LFI project (including instrument development and operation, data processing and scientific analysis) is developed by an international consortium led by Italy and involving Canada, Finland, Germany, Norway, Spain, Switzerland, UK, and USA. The Italian contribution is funded by the Italian Space Agency (ASI) and INAF.

The Planck HFI instrument and associated Data Processing Centre were designed, built, and are operated by an international consortium of laboratories, universities and institutes, with important contributions from industry, under the leadership of the PI institute, the Institut d'Astrophysique Spatiale at Orsay, France. The instrument and associated Data Processing Centre are funded in particular by CNES, CNRS, NASA, STFC, and ASI.

The reflectors of Planck's telescope were developed by a collaboration between ESA and a scientific Consortium (DK-Planck) led and funded by Denmark.

The Planck Collaboration acknowledges the support of: ESA; CNES and CNRS/INSU-IN2P3-INP (France); ASI, CNR, and INAF (Italy); NASA and DoE (USA); STFC and UKSA (UK); CSIC, MICINN and JA (Spain); Tekes, AoF and CSC (Finland); DLR and MPG (Germany); CSA (Canada); DTU Space (Denmark); SER/SSO (Switzerland); RCN (Norway); SFI (Ireland); FCT/MCTES (Portugal); and DEISA (EU).

- European Space Agency <sup>[3]</sup>
- France
  - CNES <sup>[4]</sup>: Centre National des Etudes Spatiales
  - CNRS/INSU-IN2P3-INP: Centre National de la Recherche Scientifique/ Institut National des Sciences de l'Univers- Institut National de Physique Nucleaire et de Physique des Particules- Institut National Polytechnique
- Italy
  - ASI: Agenzia Spaziale Italiana
  - CNR: Consiglio Nazionale della Ricerca
  - INAF: Istituto Nazionale di Astrofisica
- United States of America
  - NASA: National Air and Space Administration
  - DoE: Department of Energy
- United Kingdom
  - STFC: Science and Technology Facilities Council
  - UKSA: UK Space Agency
- Spain
  - CSIC: Consejo Superior de Investigaciones Cientificas
  - MICINN: Ministerio de Ciencia e Innovacion
  - JA: Junta de Andalucia
- Finland
  - Tekes: Finnish Funding Agency for Technology and Innovation
  - AoF: Academy of Finland
  - CSC - IT Center for Science
- Germany



- DLR: Deutsches Zentrum fuer Luft- und Raumfahrt
- MPG: Max-Planck-Gesellschaft zur Foerderung der Wissenschaften
- Canada
  - CSA: Canadian Space Agency
- Denmark
  - DTU Space: Danmarks Tekniske Universitet/Institut for Rumforskning og-teknologi
- Switzerland
  - SER/SSO: State Secretariat for Education and Research/Swiss Space Office
- Norway
  - RCN: Research Council of Norway
  - NSC: Norwegian Space Centre
- Ireland
  - SFI: Science Foundation Ireland
- Portugal
  - FCT/MCTES: Fundacao para a Ciencia e a Tecnologia/ Ministerio da Ciencia, Tecnologia e Ensino Superior
- European Union
  - DEISA: Distributed European Infrastructure for Supercomputing Applications

## References

- [1] <http://www.rssd.esa.int/index.php?project=IDIS&page=people>
- [2] [http://www.rssd.esa.int/index.php?project=PLANCK&page=Science\\_Team](http://www.rssd.esa.int/index.php?project=PLANCK&page=Science_Team)
- [3] <http://www.esa.int>
- [4] <http://www.cnes.fr>

# Article Sources and Contributors

**Main Page** *Source:* <http://www.sciops.esa.int/wikiSI/planckpla/index.php?oldid=3135> *Contributors:* Acoulais, Amoneti, Azacchei, Dmaino, Fbouchet, Jvalivii, Kganga, Lmendes, Lvibert, MediaWiki default, Mfrailis, Rbailey, Rleonard, Xdupac

**Mission overview** *Source:* <http://www.sciops.esa.int/wikiSI/planckpla/index.php?oldid=3115> *Contributors:* Lmendes, Rleonard, Xdupac

**Overview** *Source:* <http://www.sciops.esa.int/wikiSI/planckpla/index.php?oldid=3118> *Contributors:* Lmendes, Rleonard

**The service module** *Source:* <http://www.sciops.esa.int/wikiSI/planckpla/index.php?oldid=3119> *Contributors:* Lmendes, Rleonard

**Common cryogenics** *Source:* <http://www.sciops.esa.int/wikiSI/planckpla/index.php?oldid=3121> *Contributors:* Lmendes

**Thermal design** *Source:* <http://www.sciops.esa.int/wikiSI/planckpla/index.php?oldid=1737> *Contributors:* Lmendes

**Passive cooling** *Source:* <http://www.sciops.esa.int/wikiSI/planckpla/index.php?oldid=1193> *Contributors:* Lmendes

**Sorption cooler** *Source:* <http://www.sciops.esa.int/wikiSI/planckpla/index.php?oldid=650> *Contributors:* Lmendes

**Qualification and performance** *Source:* <http://www.sciops.esa.int/wikiSI/planckpla/index.php?oldid=648> *Contributors:* Lmendes

**HFI design, qualification, and performance** *Source:* <http://www.sciops.esa.int/wikiSI/planckpla/index.php?oldid=3214> *Contributors:* Acoulais, Bcrill, Fpajot, Fpiacent, Jlamarre, Kganga, Lmendes, Lspencer

**LFI design, qualification, and performance** *Source:* <http://www.sciops.esa.int/wikiSI/planckpla/index.php?oldid=2895> *Contributors:* Agregori, Lmendes

**The telescope** *Source:* <http://www.sciops.esa.int/wikiSI/planckpla/index.php?oldid=3110> *Contributors:* Lmendes, Rleonard

**The standard radiation environment monitor** *Source:* <http://www.sciops.esa.int/wikiSI/planckpla/index.php?oldid=1888> *Contributors:* Lmendes, Xdupac

**The fiber optic gyro unit** *Source:* <http://www.sciops.esa.int/wikiSI/planckpla/index.php?oldid=3111> *Contributors:* Lmendes, Rleonard

**Ground segment overview** *Source:* <http://www.sciops.esa.int/wikiSI/planckpla/index.php?oldid=1741> *Contributors:* Lmendes, Xdupac

**Contingencies** *Source:* <http://www.sciops.esa.int/wikiSI/planckpla/index.php?oldid=3112> *Contributors:* Lmendes, Rleonard

**Operational history** *Source:* <http://www.sciops.esa.int/wikiSI/planckpla/index.php?oldid=1743> *Contributors:* Lmendes, Rleonard

**Survey scanning and performance** *Source:* <http://www.sciops.esa.int/wikiSI/planckpla/index.php?oldid=1891> *Contributors:* Lmendes, Xdupac

**Thermal environment** *Source:* <http://www.sciops.esa.int/wikiSI/planckpla/index.php?oldid=1746> *Contributors:* Lmendes, Rleonard

**Radiation environment** *Source:* <http://www.sciops.esa.int/wikiSI/planckpla/index.php?oldid=1745> *Contributors:* Lmendes

**Pointing performance** *Source:* <http://www.sciops.esa.int/wikiSI/planckpla/index.php?oldid=1747> *Contributors:* Lmendes, Xdupac

**Data flow overview** *Source:* <http://www.sciops.esa.int/wikiSI/planckpla/index.php?oldid=1748> *Contributors:* Lmendes, Rleonard

**On-board processing** *Source:* <http://www.sciops.esa.int/wikiSI/planckpla/index.php?oldid=692> *Contributors:* Lmendes

**MOC processing** *Source:* <http://www.sciops.esa.int/wikiSI/planckpla/index.php?oldid=1749> *Contributors:* Lmendes, Rleonard

**The HFI DPC** *Source:* <http://www.sciops.esa.int/wikiSI/planckpla/index.php?oldid=2677> *Contributors:* Fbouchet, Fdesert, Kganga, Lmendes

**Pre-processing** *Source:* <http://www.sciops.esa.int/wikiSI/planckpla/index.php?oldid=3056> *Contributors:* Amoneti, Lmendes, Lvibert

**TOI processing** *Source:* <http://www.sciops.esa.int/wikiSI/planckpla/index.php?oldid=3095> *Contributors:* Crenault, Fdesert, Lmendes

**Pointing&Beams** *Source:* <http://www.sciops.esa.int/wikiSI/planckpla/index.php?oldid=2669> *Contributors:* Ajaffe, Bcrill, Ehivon, Fbouchet

**Map-making** *Source:* <http://www.sciops.esa.int/wikiSI/planckpla/index.php?oldid=3167> *Contributors:* Kganga, Lmendes, Operdere, Xdupac

**PowerSpectra** *Source:* <http://www.sciops.esa.int/wikiSI/planckpla/index.php?oldid=2754> *Contributors:* Fbouchet

**HFI-Validation** *Source:* <http://www.sciops.esa.int/wikiSI/planckpla/index.php?oldid=2794> *Contributors:* Fbouchet, Kganga, Lmontier, Lvibert, Stechene

**Summary** *Source:* <http://www.sciops.esa.int/wikiSI/planckpla/index.php?oldid=2436> *Contributors:* Fbouchet, Kganga, Lvibert

**The LFI DPC** *Source:* <http://www.sciops.esa.int/wikiSI/planckpla/index.php?oldid=2738> *Contributors:* Azacchei, Lmendes

**Pre-processing LFI** *Source:* <http://www.sciops.esa.int/wikiSI/planckpla/index.php?oldid=3051> *Contributors:* Mfrailis

**TOI processing LFI** *Source:* <http://www.sciops.esa.int/wikiSI/planckpla/index.php?oldid=2914> *Contributors:* Pleahy, Pmeinhol, Sgaleott

**TOI-Noise LFI** *Source:* <http://www.sciops.esa.int/wikiSI/planckpla/index.php?oldid=2547> *Contributors:* Dmaino

**Pointing LFI** *Source:* <http://www.sciops.esa.int/wikiSI/planckpla/index.php?oldid=2301> *Contributors:* Sgaleott

**Map-making LFI** *Source:* <http://www.sciops.esa.int/wikiSI/planckpla/index.php?oldid=3063> *Contributors:* Assirvio, Azacchei, Ekeihane, Hkurkis, Jvalivii

**LFI-Validation** *Source:* <http://www.sciops.esa.int/wikiSI/planckpla/index.php?oldid=2660> *Contributors:* Dmaino

**HL** *Source:* <http://www.sciops.esa.int/wikiSI/planckpla/index.php?oldid=2688> *Contributors:* Fbouchet, Joagonza

**Catalogues** *Source:* <http://www.sciops.esa.int/wikiSI/planckpla/index.php?oldid=3100> *Contributors:* Joagonza, Lmendes, Lvibert, Mashdown, Xdupac

**HLcomp** *Source:* <http://www.sciops.esa.int/wikiSI/planckpla/index.php?oldid=2527> *Contributors:* Fbouchet

**C2** *Source:* <http://www.sciops.esa.int/wikiSI/planckpla/index.php?oldid=2709> *Contributors:* Fbouchet

**HL-sims** *Source:* <http://www.sciops.esa.int/wikiSI/planckpla/index.php?oldid=2707> *Contributors:* Fbouchet

**Science** *Source:* <http://www.sciops.esa.int/wikiSI/planckpla/index.php?oldid=2717> *Contributors:* Fbouchet, Lvibert

**PSO processing** *Source:* <http://www.sciops.esa.int/wikiSI/planckpla/index.php?oldid=1750> *Contributors:* Lmendes

**Planck Legacy Archive** *Source:* <http://www.sciops.esa.int/wikiSI/planckpla/index.php?oldid=1875> *Contributors:* Lmendes, Xdupac

**Mission Science products overview** *Source:* <http://www.sciops.esa.int/wikiSI/planckpla/index.php?oldid=1138> *Contributors:* Lmendes

**Timelines** *Source:* <http://www.sciops.esa.int/wikiSI/planckpla/index.php?oldid=2823> *Contributors:* Amoneti, Lmendes

**Single detector maps** *Source:* <http://www.sciops.esa.int/wikiSI/planckpla/index.php?oldid=2210> *Contributors:* Amoneti, Lmendes

**Frequency Maps** *Source:* <http://www.sciops.esa.int/wikiSI/planckpla/index.php?oldid=3106> *Contributors:* Amoneti, Azacchei, Fdesert, Lmendes, Operdere

**Astrophysical component maps** *Source:* <http://www.sciops.esa.int/wikiSI/planckpla/index.php?oldid=3065> *Contributors:* Amoneti, Lmendes

**Spectra** *Source:* <http://www.sciops.esa.int/wikiSI/planckpla/index.php?oldid=1583> *Contributors:* Lmendes, Xdupac

**Likelihood Code** *Source:* <http://www.sciops.esa.int/wikiSI/planckpla/index.php?oldid=2630> *Contributors:* Fbouchet, Lmendes

**The RIMO** *Source:* <http://www.sciops.esa.int/wikiSI/planckpla/index.php?oldid=3093> *Contributors:* Amoneti

**Additional Science products** *Source:* <http://www.sciops.esa.int/wikiSI/planckpla/index.php?oldid=2564> *Contributors:* Lmendes

**Data products** *Source:* <http://www.sciops.esa.int/wikiSI/planckpla/index.php?oldid=2567> *Contributors:* Lmendes

**Specially processed maps** *Source:* <http://www.sciops.esa.int/wikiSI/planckpla/index.php?oldid=2569> *Contributors:* Lmendes

**Additional catalogues** *Source:* <http://www.sciops.esa.int/wikiSI/planckpla/index.php?oldid=2570> *Contributors:* Lmendes

**Additional angular power spectra** *Source:* <http://www.sciops.esa.int/wikiSI/planckpla/index.php?oldid=2572> *Contributors:* Lmendes

**The Planck Sky Model** *Source:* <http://www.sciops.esa.int/wikiSI/planckpla/index.php?oldid=2573> *Contributors:* Lmendes

**Ancillary data** *Source:* <http://www.sciops.esa.int/wikiSI/planckpla/index.php?oldid=2574> *Contributors:* Lmendes

**Scientific data used to generate Planck products** *Source:* <http://www.sciops.esa.int/wikiSI/planckpla/index.php?oldid=2576> *Contributors:* Lmendes

**Simulation data** *Source:* <http://www.sciops.esa.int/wikiSI/planckpla/index.php?oldid=2577> *Contributors:* Lmendes

**Mission history** *Source:* <http://www.sciops.esa.int/wikiSI/planckpla/index.php?oldid=2579> *Contributors:* Lmendes

**Survey history** *Source:* <http://www.sciops.esa.int/wikiSI/planckpla/index.php?oldid=1821> *Contributors:* Lmendes, Xdupac

**Satellite history** *Source:* <http://www.sciops.esa.int/wikiSI/planckpla/index.php?oldid=1753> *Contributors:* Lmendes, Xdupac

**Payload design** *Source:* <http://www.sciops.esa.int/wikiSI/planckpla/index.php?oldid=2581> *Contributors:* Lmendes

**Instrument performance** *Source:* <http://www.sciops.esa.int/wikiSI/planckpla/index.php?oldid=2583> *Contributors:* Lmendes

**Telescope** *Source:* <http://www.sciops.esa.int/wikiSI/planckpla/index.php?oldid=2584> *Contributors:* Lmendes

**Thermal** *Source:* <http://www.sciops.esa.int/wikiSI/planckpla/index.php?oldid=2585> *Contributors:* Lmendes

**FOG** *Source:* <http://www.sciops.esa.int/wikiSI/planckpla/index.php?oldid=2586> *Contributors:* Lmendes

**SREM** *Source:* <http://www.sciops.esa.int/wikiSI/planckpla/index.php?oldid=2587> *Contributors:* Lmendes

**Software utilities** *Source:* <http://www.sciops.esa.int/wikiSI/planckpla/index.php?oldid=2588> *Contributors:* Lmendes

**Appendix** *Source:* <http://www.sciops.esa.int/wikiSI/planckpla/index.php?oldid=2589> *Contributors:* Lmendes

**Acronym list** *Source:* <http://www.sciops.esa.int/wikiSI/planckpla/index.php?oldid=1756> *Contributors:* Lmendes

**References** *Source:* <http://www.sciops.esa.int/wikiSI/planckpla/index.php?oldid=3213> *Contributors:* Lmendes

**Planck Collaboration** *Source:* <http://www.sciops.esa.int/wikiSI/planckpla/index.php?oldid=1719> *Contributors:* Rleonard, Xdupac

---

# Image Sources, Licenses and Contributors

**file:Planck\_Logos.jpg** *Source:* [http://www.sciops.esa.int/wikiSI/planckpla/index.php?title=File:Planck\\_Logos.jpg](http://www.sciops.esa.int/wikiSI/planckpla/index.php?title=File:Planck_Logos.jpg) *License:* unknown *Contributors:* Rleonard

**file:PlanckMissionTimeline.JPG** *Source:* <http://www.sciops.esa.int/wikiSI/planckpla/index.php?title=File:PlanckMissionTimeline.JPG> *License:* unknown *Contributors:* Xdupac

**file:HerschelPlanckLaunch.jpg** *Source:* <http://www.sciops.esa.int/wikiSI/planckpla/index.php?title=File:HerschelPlanckLaunch.jpg> *License:* unknown *Contributors:* Xdupac

**file:PLANCK\_Herschel\_LAUNCH.jpg** *Source:* [http://www.sciops.esa.int/wikiSI/planckpla/index.php?title=File:PLANCK\\_Herschel\\_LAUNCH.jpg](http://www.sciops.esa.int/wikiSI/planckpla/index.php?title=File:PLANCK_Herschel_LAUNCH.jpg) *License:* unknown *Contributors:* Xdupac

**file:Cooldown.jpg** *Source:* <http://www.sciops.esa.int/wikiSI/planckpla/index.php?title=File:Cooldown.jpg> *License:* unknown *Contributors:* Xdupac

**File:381-Herschel\_reflection\_in\_Primary\_Reflector\_H.jpg** *Source:* [http://www.sciops.esa.int/wikiSI/planckpla/index.php?title=File:381-Herschel\\_reflection\\_in\\_Primary\\_Reflector\\_H.jpg](http://www.sciops.esa.int/wikiSI/planckpla/index.php?title=File:381-Herschel_reflection_in_Primary_Reflector_H.jpg) *License:* unknown *Contributors:* Rleonard

**Image:HFI\_2\_4\_1\_JML\_SignalFormation.png** *Source:* [http://www.sciops.esa.int/wikiSI/planckpla/index.php?title=File:HFI\\_2\\_4\\_1\\_JML\\_SignalFormation.png](http://www.sciops.esa.int/wikiSI/planckpla/index.php?title=File:HFI_2_4_1_JML_SignalFormation.png) *License:* unknown *Contributors:* Acoulais

**Image:HFI\_2\_4\_1\_JML\_FeedHorns.png** *Source:* [http://www.sciops.esa.int/wikiSI/planckpla/index.php?title=File:HFI\\_2\\_4\\_1\\_JML\\_FeedHorns.png](http://www.sciops.esa.int/wikiSI/planckpla/index.php?title=File:HFI_2_4_1_JML_FeedHorns.png) *License:* unknown *Contributors:* Acoulais

**Image:HFI\_2\_4\_1\_JML\_beam.png** *Source:* [http://www.sciops.esa.int/wikiSI/planckpla/index.php?title=File:HFI\\_2\\_4\\_1\\_JML\\_beam.png](http://www.sciops.esa.int/wikiSI/planckpla/index.php?title=File:HFI_2_4_1_JML_beam.png) *License:* unknown *Contributors:* Acoulais

**Image:HFI\_2\_4\_1\_JML\_PowerDiff.png** *Source:* [http://www.sciops.esa.int/wikiSI/planckpla/index.php?title=File:HFI\\_2\\_4\\_1\\_JML\\_PowerDiff.png](http://www.sciops.esa.int/wikiSI/planckpla/index.php?title=File:HFI_2_4_1_JML_PowerDiff.png) *License:* unknown *Contributors:* Acoulais

**Image:HFI\_2\_4\_1\_JML\_FarField.png** *Source:* [http://www.sciops.esa.int/wikiSI/planckpla/index.php?title=File:HFI\\_2\\_4\\_1\\_JML\\_FarField.png](http://www.sciops.esa.int/wikiSI/planckpla/index.php?title=File:HFI_2_4_1_JML_FarField.png) *License:* unknown *Contributors:* Acoulais

**Image:HFI\_2\_4\_1\_JML\_FarField2.png** *Source:* [http://www.sciops.esa.int/wikiSI/planckpla/index.php?title=File:HFI\\_2\\_4\\_1\\_JML\\_FarField2.png](http://www.sciops.esa.int/wikiSI/planckpla/index.php?title=File:HFI_2_4_1_JML_FarField2.png) *License:* unknown *Contributors:* Acoulais

**Image:fig3.png** *Source:* <http://www.sciops.esa.int/wikiSI/planckpla/index.php?title=File:Fig3.png> *License:* unknown *Contributors:* Lspencer

**Image:fig4.png** *Source:* <http://www.sciops.esa.int/wikiSI/planckpla/index.php?title=File:Fig4.png> *License:* unknown *Contributors:* Lspencer

**Image:fig1.png** *Source:* <http://www.sciops.esa.int/wikiSI/planckpla/index.php?title=File:Fig1.png> *License:* unknown *Contributors:* Lspencer

**Image:fig2.png** *Source:* <http://www.sciops.esa.int/wikiSI/planckpla/index.php?title=File:Fig2.png> *License:* unknown *Contributors:* Lspencer

**Image:fig5.png** *Source:* <http://www.sciops.esa.int/wikiSI/planckpla/index.php?title=File:Fig5.png> *License:* unknown *Contributors:* Lspencer

**Image:fig6.png** *Source:* <http://www.sciops.esa.int/wikiSI/planckpla/index.php?title=File:Fig6.png> *License:* unknown *Contributors:* Lspencer

**File:HFI\_FilterPlots\_100GHz.png** *Source:* [http://www.sciops.esa.int/wikiSI/planckpla/index.php?title=File:HFI\\_FilterPlots\\_100GHz.png](http://www.sciops.esa.int/wikiSI/planckpla/index.php?title=File:HFI_FilterPlots_100GHz.png) *License:* unknown *Contributors:* Lspencer

**File:HFI\_FilterPlots\_143GHz.png** *Source:* [http://www.sciops.esa.int/wikiSI/planckpla/index.php?title=File:HFI\\_FilterPlots\\_143GHz.png](http://www.sciops.esa.int/wikiSI/planckpla/index.php?title=File:HFI_FilterPlots_143GHz.png) *License:* unknown *Contributors:* Lspencer

**File:HFI\_FilterPlots\_217GHz.png** *Source:* [http://www.sciops.esa.int/wikiSI/planckpla/index.php?title=File:HFI\\_FilterPlots\\_217GHz.png](http://www.sciops.esa.int/wikiSI/planckpla/index.php?title=File:HFI_FilterPlots_217GHz.png) *License:* unknown *Contributors:* Lspencer

**File:HFI\_FilterPlots\_353GHz.png** *Source:* [http://www.sciops.esa.int/wikiSI/planckpla/index.php?title=File:HFI\\_FilterPlots\\_353GHz.png](http://www.sciops.esa.int/wikiSI/planckpla/index.php?title=File:HFI_FilterPlots_353GHz.png) *License:* unknown *Contributors:* Lspencer

**File:HFI\_FilterPlots\_545GHz.png** *Source:* [http://www.sciops.esa.int/wikiSI/planckpla/index.php?title=File:HFI\\_FilterPlots\\_545GHz.png](http://www.sciops.esa.int/wikiSI/planckpla/index.php?title=File:HFI_FilterPlots_545GHz.png) *License:* unknown *Contributors:* Lspencer

**File:HFI\_FilterPlots\_857GHz.png** *Source:* [http://www.sciops.esa.int/wikiSI/planckpla/index.php?title=File:HFI\\_FilterPlots\\_857GHz.png](http://www.sciops.esa.int/wikiSI/planckpla/index.php?title=File:HFI_FilterPlots_857GHz.png) *License:* unknown *Contributors:* Lspencer

**Image:HFI\_2\_4\_1\_FPiacentini\_bolo1.png** *Source:* [http://www.sciops.esa.int/wikiSI/planckpla/index.php?title=File:HFI\\_2\\_4\\_1\\_FPiacentini\\_bolo1.png](http://www.sciops.esa.int/wikiSI/planckpla/index.php?title=File:HFI_2_4_1_FPiacentini_bolo1.png) *License:* unknown *Contributors:* -

**Image:HFI\_2\_4\_1\_FPiacentini\_bolo2.png** *Source:* [http://www.sciops.esa.int/wikiSI/planckpla/index.php?title=File:HFI\\_2\\_4\\_1\\_FPiacentini\\_bolo2.png](http://www.sciops.esa.int/wikiSI/planckpla/index.php?title=File:HFI_2_4_1_FPiacentini_bolo2.png) *License:* unknown *Contributors:* Acoulais

**Image:HFI\_2\_4\_1\_FPiacentini\_table1.png** *Source:* [http://www.sciops.esa.int/wikiSI/planckpla/index.php?title=File:HFI\\_2\\_4\\_1\\_FPiacentini\\_table1.png](http://www.sciops.esa.int/wikiSI/planckpla/index.php?title=File:HFI_2_4_1_FPiacentini_table1.png) *License:* unknown *Contributors:* Acoulais

**Image:HFI\_2\_4\_1\_FPiacentini\_FocalPlaneLayout.png** *Source:* [http://www.sciops.esa.int/wikiSI/planckpla/index.php?title=File:HFI\\_2\\_4\\_1\\_FPiacentini\\_FocalPlaneLayout.png](http://www.sciops.esa.int/wikiSI/planckpla/index.php?title=File:HFI_2_4_1_FPiacentini_FocalPlaneLayout.png) *License:* unknown *Contributors:* Acoulais

**Image:HFI\_2\_4\_1\_FPiacentini\_FocalPlaneGeo.png** *Source:* [http://www.sciops.esa.int/wikiSI/planckpla/index.php?title=File:HFI\\_2\\_4\\_1\\_FPiacentini\\_FocalPlaneGeo.png](http://www.sciops.esa.int/wikiSI/planckpla/index.php?title=File:HFI_2_4_1_FPiacentini_FocalPlaneGeo.png) *License:* unknown *Contributors:* Acoulais

**Image:HFI\_2\_4\_1\_FPiacentini\_table2.jpeg** *Source:* [http://www.sciops.esa.int/wikiSI/planckpla/index.php?title=File:HFI\\_2\\_4\\_1\\_FPiacentini\\_table2.jpeg](http://www.sciops.esa.int/wikiSI/planckpla/index.php?title=File:HFI_2_4_1_FPiacentini_table2.jpeg) *License:* unknown *Contributors:* Acoulais

**File:lfi\_instrument.jpg** *Source:* [http://www.sciops.esa.int/wikiSI/planckpla/index.php?title=File:lfi\\_instrument.jpg](http://www.sciops.esa.int/wikiSI/planckpla/index.php?title=File:lfi_instrument.jpg) *License:* unknown *Contributors:* Agregori

**File:schema.jpg** *Source:* <http://www.sciops.esa.int/wikiSI/planckpla/index.php?title=File:Schema.jpg> *License:* unknown *Contributors:* Agregori

**File:rca\_schematic.jpg** *Source:* [http://www.sciops.esa.int/wikiSI/planckpla/index.php?title=File:Rca\\_schematic.jpg](http://www.sciops.esa.int/wikiSI/planckpla/index.php?title=File:Rca_schematic.jpg) *License:* unknown *Contributors:* Agregori

**File:phase\_switch\_operation.jpg** *Source:* [http://www.sciops.esa.int/wikiSI/planckpla/index.php?title=File:Phase\\_switch\\_operation.jpg](http://www.sciops.esa.int/wikiSI/planckpla/index.php?title=File:Phase_switch_operation.jpg) *License:* unknown *Contributors:* Agregori

**File:groundtest.jpg** *Source:* <http://www.sciops.esa.int/wikiSI/planckpla/index.php?title=File:Groundtest.jpg> *License:* unknown *Contributors:* Agregori

**File:flighttest.jpg** *Source:* <http://www.sciops.esa.int/wikiSI/planckpla/index.php?title=File:Flighttest.jpg> *License:* unknown *Contributors:* Agregori

**file:ESOC.jpg** *Source:* <http://www.sciops.esa.int/wikiSI/planckpla/index.php?title=File:ESOC.jpg> *License:* unknown *Contributors:* Xdupac

**file:ESAC\_6.JPG** *Source:* [http://www.sciops.esa.int/wikiSI/planckpla/index.php?title=File:ESAC\\_6.JPG](http://www.sciops.esa.int/wikiSI/planckpla/index.php?title=File:ESAC_6.JPG) *License:* unknown *Contributors:* Xdupac

**file:GS.jpg** *Source:* <http://www.sciops.esa.int/wikiSI/planckpla/index.php?title=File:GS.jpg> *License:* unknown *Contributors:* Xdupac

**file:GSPlanck.JPG** *Source:* <http://www.sciops.esa.int/wikiSI/planckpla/index.php?title=File:GSPlanck.JPG> *License:* unknown *Contributors:* Xdupac

**file:FocalPlane.png** *Source:* <http://www.sciops.esa.int/wikiSI/planckpla/index.php?title=File:FocalPlane.png> *License:* unknown *Contributors:* Rleonard

**File:ScannStrategy.png** *Source:* <http://www.sciops.esa.int/wikiSI/planckpla/index.php?title=File:ScannStrategy.png> *License:* unknown *Contributors:* Xdupac

**File:Cycloidal\_scanning.JPG** *Source:* [http://www.sciops.esa.int/wikiSI/planckpla/index.php?title=File:Cycloidal\\_scanning.JPG](http://www.sciops.esa.int/wikiSI/planckpla/index.php?title=File:Cycloidal_scanning.JPG) *License:* unknown *Contributors:* Xdupac

**File:Crab\_Nebula.jpg** *Source:* [http://www.sciops.esa.int/wikiSI/planckpla/index.php?title=File:Crab\\_Nebula.jpg](http://www.sciops.esa.int/wikiSI/planckpla/index.php?title=File:Crab_Nebula.jpg) *License:* unknown *Contributors:* Xdupac

**File:Mars.jpg** *Source:* <http://www.sciops.esa.int/wikiSI/planckpla/index.php?title=File:Mars.jpg> *License:* unknown *Contributors:* Xdupac

**File:PlanckMissionTimeline.JPG** *Source:* <http://www.sciops.esa.int/wikiSI/planckpla/index.php?title=File:PlanckMissionTimeline.JPG> *License:* unknown *Contributors:* Xdupac

**file:PointingPerformance2011.JPG** *Source:* <http://www.sciops.esa.int/wikiSI/planckpla/index.php?title=File:PointingPerformance2011.JPG> *License:* unknown *Contributors:* Xdupac

**file:PointingPerformance2011latitude.JPG** *Source:* <http://www.sciops.esa.int/wikiSI/planckpla/index.php?title=File:PointingPerformance2011latitude.JPG> *License:* unknown *Contributors:* Xdupac

**file:PointingPerformanceCorrelation.jpg** *Source:* <http://www.sciops.esa.int/wikiSI/planckpla/index.php?title=File:PointingPerformanceCorrelation.jpg> *License:* unknown *Contributors:* Xdupac

**File:GroundSegment.png** *Source:* <http://www.sciops.esa.int/wikiSI/planckpla/index.php?title=File:GroundSegment.png> *License:* unknown *Contributors:* Rleonard

**File:HFI\_4\_4\_1\_deltatos.png** *Source:* [http://www.sciops.esa.int/wikiSI/planckpla/index.php?title=File:HFI\\_4\\_4\\_1\\_deltatos.png](http://www.sciops.esa.int/wikiSI/planckpla/index.php?title=File:HFI_4_4_1_deltatos.png) *License:* unknown *Contributors:* Lvibert

**File:HFI\_4\_4\_1\_deltatoszoom.png** *Source:* [http://www.sciops.esa.int/wikiSI/planckpla/index.php?title=File:HFI\\_4\\_4\\_1\\_deltatoszoom.png](http://www.sciops.esa.int/wikiSI/planckpla/index.php?title=File:HFI_4_4_1_deltatoszoom.png) *License:* unknown *Contributors:* Lvibert

**File:HFI\_4\_4\_1\_ringduration.png** *Source:* [http://www.sciops.esa.int/wikiSI/planckpla/index.php?title=File:HFI\\_4\\_4\\_1\\_ringduration.png](http://www.sciops.esa.int/wikiSI/planckpla/index.php?title=File:HFI_4_4_1_ringduration.png) *License:* unknown *Contributors:* Lvibert

**File:HFI\_4\_4\_1\_OBTUTC.png** *Source:* [http://www.sciops.esa.int/wikiSI/planckpla/index.php?title=File:HFI\\_4\\_4\\_1\\_OBTUTC.png](http://www.sciops.esa.int/wikiSI/planckpla/index.php?title=File:HFI_4_4_1_OBTUTC.png) *License:* unknown *Contributors:* Lvibert

**File:10\_143\_5\_PBR\_10800RING\_LFER4\_JC.jpg** *Source:* [http://www.sciops.esa.int/wikiSI/planckpla/index.php?title=File:10\\_143\\_5\\_PBR\\_10800RING\\_LFER4\\_JC.jpg](http://www.sciops.esa.int/wikiSI/planckpla/index.php?title=File:10_143_5_PBR_10800RING_LFER4_JC.jpg) *License:* unknown *Contributors:* Fdesert

**File:10\_143\_5\_rcircles\_LFER4\_JC.jpg** *Source:* [http://www.sciops.esa.int/wikiSI/planckpla/index.php?title=File:10\\_143\\_5\\_rcircles\\_LFER4\\_JC.jpg](http://www.sciops.esa.int/wikiSI/planckpla/index.php?title=File:10_143_5_rcircles_LFER4_JC.jpg) *License:* unknown *Contributors:* Fdesert

**File:10\_143\_5\_ft\_LFER4\_JC.jpg** *Source:* [http://www.sciops.esa.int/wikiSI/planckpla/index.php?title=File:10\\_143\\_5\\_ft\\_LFER4\\_JC.jpg](http://www.sciops.esa.int/wikiSI/planckpla/index.php?title=File:10_143_5_ft_LFER4_JC.jpg) *License:* unknown *Contributors:* Fdesert

**File:14\_545\_1\_PBR\_10800RING\_LFER4\_JC.jpg** *Source:* [http://www.sciops.esa.int/wikiSI/planckpla/index.php?title=File:14\\_545\\_1\\_PBR\\_10800RING\\_LFER4\\_JC.jpg](http://www.sciops.esa.int/wikiSI/planckpla/index.php?title=File:14_545_1_PBR_10800RING_LFER4_JC.jpg) *License:* unknown *Contributors:* Fdesert

**File:14\_545\_1\_rcircles\_LFER4\_JC.jpg** *Source:* [http://www.sciops.esa.int/wikiSI/planckpla/index.php?title=File:14\\_545\\_1\\_rcircles\\_LFER4\\_JC.jpg](http://www.sciops.esa.int/wikiSI/planckpla/index.php?title=File:14_545_1_rcircles_LFER4_JC.jpg) *License:* unknown *Contributors:* Fdesert

**File:14\_545\_1\_fft\_LFER4\_JC.jpg** *Source:* [http://www.sciops.esa.int/wikiSI/planckpla/index.php?title=File:14\\_545\\_1\\_fft\\_LFER4\\_JC.jpg](http://www.sciops.esa.int/wikiSI/planckpla/index.php?title=File:14_545_1_fft_LFER4_JC.jpg) *License:* unknown *Contributors:* Fdesert

**File:baseline.jpg** *Source:* <http://www.sciops.esa.int/wikiSI/planckpla/index.php?title=File:Baseline.jpg> *License:* unknown *Contributors:* Fdesert

**File:figIntermPaperGR.jpg** *Source:* <http://www.sciops.esa.int/wikiSI/planckpla/index.php?title=File:FigIntermPaperGR.jpg> *License:* unknown *Contributors:* Fdesert

**File:group10\_143\_5.jpg** *Source:* [http://www.sciops.esa.int/wikiSI/planckpla/index.php?title=File:Group10\\_143\\_5.jpg](http://www.sciops.esa.int/wikiSI/planckpla/index.php?title=File:Group10_143_5.jpg) *License:* unknown *Contributors:* Fdesert

**File:group14\_545\_1.jpg** *Source:* [http://www.sciops.esa.int/wikiSI/planckpla/index.php?title=File:Group14\\_545\\_1.jpg](http://www.sciops.esa.int/wikiSI/planckpla/index.php?title=File:Group14_545_1.jpg) *License:* unknown *Contributors:* Fdesert

**File:T90.jpg** *Source:* <http://www.sciops.esa.int/wikiSI/planckpla/index.php?title=File:T90.jpg> *License:* unknown *Contributors:* Fdesert

**File:10\_143\_5\_4Klines.jpg** *Source:* [http://www.sciops.esa.int/wikiSI/planckpla/index.php?title=File:10\\_143\\_5\\_4Klines.jpg](http://www.sciops.esa.int/wikiSI/planckpla/index.php?title=File:10_143_5_4Klines.jpg) *License:* unknown *Contributors:* Fdesert

**File:14\_545\_1\_4Klines.jpg** *Source:* [http://www.sciops.esa.int/wikiSI/planckpla/index.php?title=File:14\\_545\\_1\\_4Klines.jpg](http://www.sciops.esa.int/wikiSI/planckpla/index.php?title=File:14_545_1_4Klines.jpg) *License:* unknown *Contributors:* Fdesert

**File:jump\_exe.png** *Source:* [http://www.sciops.esa.int/wikiSI/planckpla/index.php?title=File:Jump\\_exe.png](http://www.sciops.esa.int/wikiSI/planckpla/index.php?title=File:Jump_exe.png) *License:* unknown *Contributors:* Fdesert

**File:10\_143\_5\_smooth\_Watt.jpg** *Source:* [http://www.sciops.esa.int/wikiSI/planckpla/index.php?title=File:10\\_143\\_5\\_smooth\\_Watt.jpg](http://www.sciops.esa.int/wikiSI/planckpla/index.php?title=File:10_143_5_smooth_Watt.jpg) *License:* unknown *Contributors:* Fdesert

**File:14\_545\_1\_smooth\_Watt.jpg** *Source:* [http://www.sciops.esa.int/wikiSI/planckpla/index.php?title=File:14\\_545\\_1\\_smooth\\_Watt.jpg](http://www.sciops.esa.int/wikiSI/planckpla/index.php?title=File:14_545_1_smooth_Watt.jpg) *License:* unknown *Contributors:* Fdesert

**File:stddev\_group10\_143\_5.jpg** *Source:* [http://www.sciops.esa.int/wikiSI/planckpla/index.php?title=File:Stddev\\_group10\\_143\\_5.jpg](http://www.sciops.esa.int/wikiSI/planckpla/index.php?title=File:Stddev_group10_143_5.jpg) *License:* unknown *Contributors:* Fdesert

**File:stddev\_group\_14\_545\_1.jpg** *Source:* [http://www.sciops.esa.int/wikiSI/planckpla/index.php?title=File:Stddev\\_group\\_14\\_545\\_1.jpg](http://www.sciops.esa.int/wikiSI/planckpla/index.php?title=File:Stddev_group_14_545_1.jpg) *License:* unknown *Contributors:* Fdesert

**File:23\_353\_TwoLevel.jpg** *Source:* [http://www.sciops.esa.int/wikiSI/planckpla/index.php?title=File:23\\_353\\_TwoLevel.jpg](http://www.sciops.esa.int/wikiSI/planckpla/index.php?title=File:23_353_TwoLevel.jpg) *License:* unknown *Contributors:* Fdesert

**File:HFI\_4\_4\_2\_RTSexample13.jpg** *Source:* [http://www.sciops.esa.int/wikiSI/planckpla/index.php?title=File:HFI\\_4\\_4\\_2\\_RTSexample13.jpg](http://www.sciops.esa.int/wikiSI/planckpla/index.php?title=File:HFI_4_4_2_RTSexample13.jpg) *License:* unknown *Contributors:* Fdesert

**Image:FocalPlane.png** *Source:* <http://www.sciops.esa.int/wikiSI/planckpla/index.php?title=File:FocalPlane.png> *License:* unknown *Contributors:* Rleonard

**File:DX9\_Y3\_consistency.png** *Source:* [http://www.sciops.esa.int/wikiSI/planckpla/index.php?title=File:DX9\\_Y3\\_consistency.png](http://www.sciops.esa.int/wikiSI/planckpla/index.php?title=File:DX9_Y3_consistency.png) *License:* unknown *Contributors:* Stechene

**Image:Glitch\_PowerSpectra\_Expla.png** *Source:* [http://www.sciops.esa.int/wikiSI/planckpla/index.php?title=File:Glitch\\_PowerSpectra\\_Expla.png](http://www.sciops.esa.int/wikiSI/planckpla/index.php?title=File:Glitch_PowerSpectra_Expla.png) *License:* unknown *Contributors:* Lmontier

**File:table.png** *Source:* <http://www.sciops.esa.int/wikiSI/planckpla/index.php?title=File:Table.png> *License:* unknown *Contributors:* Kganga

**File:LFI\_4\_5\_5\_4\_madam\_mask\_1sec\_DB10\_1\_noise\_70GHz\_all\_DX9delta\_nom\_1024outmap.00000.gif** *Source:* [http://www.sciops.esa.int/wikiSI/planckpla/index.php?title=File:LFI\\_4\\_5\\_5\\_4\\_madam\\_mask\\_1sec\\_DB10\\_1\\_noise\\_70GHz\\_all\\_DX9delta\\_nom\\_1024outmap.00000.gif](http://www.sciops.esa.int/wikiSI/planckpla/index.php?title=File:LFI_4_5_5_4_madam_mask_1sec_DB10_1_noise_70GHz_all_DX9delta_nom_1024outmap.00000.gif) *License:* unknown *Contributors:* Hkurkis

**File:LFI\_4\_5\_5\_4\_madam\_mask\_1sec\_DB10\_1\_white\_70GHz\_all\_DX9delta\_nom\_1024binmap.00000.gif** *Source:* [http://www.sciops.esa.int/wikiSI/planckpla/index.php?title=File:LFI\\_4\\_5\\_5\\_4\\_madam\\_mask\\_1sec\\_DB10\\_1\\_white\\_70GHz\\_all\\_DX9delta\\_nom\\_1024binmap.00000.gif](http://www.sciops.esa.int/wikiSI/planckpla/index.php?title=File:LFI_4_5_5_4_madam_mask_1sec_DB10_1_white_70GHz_all_DX9delta_nom_1024binmap.00000.gif) *License:* unknown *Contributors:* Hkurkis

**File:LFI\_4\_5\_5\_4\_madam\_mask\_1sec\_DB10\_1\_rcnoise\_70GHz\_all\_DX9delta\_nom\_1024map.00000.gif** *Source:* [http://www.sciops.esa.int/wikiSI/planckpla/index.php?title=File:LFI\\_4\\_5\\_5\\_4\\_madam\\_mask\\_1sec\\_DB10\\_1\\_rcnoise\\_70GHz\\_all\\_DX9delta\\_nom\\_1024map.00000.gif](http://www.sciops.esa.int/wikiSI/planckpla/index.php?title=File:LFI_4_5_5_4_madam_mask_1sec_DB10_1_rcnoise_70GHz_all_DX9delta_nom_1024map.00000.gif) *License:* unknown *Contributors:* Hkurkis

**file:Archives.JPG** *Source:* <http://www.sciops.esa.int/wikiSI/planckpla/index.php?title=File:Archives.JPG> *License:* unknown *Contributors:* Xdupac

**file:PLA.JPG** *Source:* <http://www.sciops.esa.int/wikiSI/planckpla/index.php?title=File:PLA.JPG> *License:* unknown *Contributors:* Xdupac

**file:PLAview.JPG** *Source:* <http://www.sciops.esa.int/wikiSI/planckpla/index.php?title=File:PLAview.JPG> *License:* unknown *Contributors:* Xdupac

**File:Planck\_Logos.jpg** *Source:* [http://www.sciops.esa.int/wikiSI/planckpla/index.php?title=File:Planck\\_Logos.jpg](http://www.sciops.esa.int/wikiSI/planckpla/index.php?title=File:Planck_Logos.jpg) *License:* unknown *Contributors:* Rleonard